FUNDAMENTAL ASPECTS OF SOLID OXIDE ELECTROLYZER CELL MODELLING AND THE APPLICATION FOR THE SYSTEM LEVEL ANALYSIS

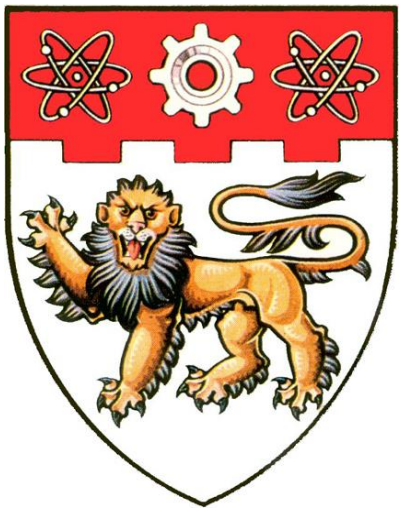

JAN PAWEL STEMPIEN

School of Mechanical and Aerospace Engineering

Nanyang Technological University

2014

FUNDAMENTAL ASPECTS OF SOLID OXIDE ELECTROLYZER CELL MODELLING AND THE APPLICATION FOR THE SYSTEM LEVEL ANALYSIS

JAN PAWEL STEMPIEN

B.Sc.

School of Mechanical & Aerospace Engineering

A thesis submitted to the Nanyang Technological University in partial fulfilment of the requirements for the Degree of Doctor of Philosophy

2014

ACKNOWLEDGEMENTS

Here I would like to express my most sincere appreciation and gratitude to my supervisor, Professor Chan Siew Hwa, for his considerate guidance and encouragement all throughout this PhD project. I have learnt so much from his expertise in the fields of solid oxide electrolyzer cells and mathematical modelling. More than a supervisor, it is his personality, lifestyle, and working philosophy that inspire me all through this three-year odyssey.

I also thank Dr Liu Qinglin for his support and provision of experimental results for this PhD project, without it, it would be impossible to accomplish this thesis. Many thanks go to Dr Ge Xiaoming for the discussions and guidance during the first year of my study. Help from people whose names are not mentioned here is also greatly appreciated.

ABSTRACT

In this work the author discusses the fundamental aspects of modelling Solid Oxide Electrolyzer Cell. The discussion is performed in order to motivate and guide the design of an improved model of SOEC capable of predicting the experimental results in greater accuracy and wider scope. The author proposed a new model including the effects of operating the electrolyzer under the extreme oxygen chemical potential difference, the establishment of equilibrium potential under the co-electrolysis conditions and the effects of electrode's microstructure on cell performance. The proposed model: predicts a new mode of loss if the cell is run with insufficient fuel, i.e. the short-circuiting of the electrolyzer; decreases prediction error of Open-Circuit Voltage from ~20% to <2% and allows for accurate calculation of OCV for co-electrolysis operation; allows to analyse effects of electrode's porosity, tortuosity, pore and grain radiuses, thicknesses and active areas on cell's performance. As defined, the model was applied to analyse several energy conversion systems formulated by the author to address current issues in the energy sector, i.e. mitigation of CO_2 emissions, alleviation of renewable energy intermittency, grid balancing, synthetic hydrocarbon fuel production (major fraction of end-user energy consumption). Formulated systems were analysed and optimized with the use of author's developed model. The systems are divided into two groups, the first designed for CO_2 mitigation and grid balancing and the second purposed for synthetic fuel production from renewable electricity and seawater. The first group of systems included analysis of exhaust gases recycling which is crucial for viable operation of SOEC systems without the need for constant external hydrogen delivery. The systems were predicted to achieve ~50% energy conversion efficiency and ~70% CO_2 conversion potential. The second group of systems was predicted to achieve efficiency from ~60 to ~90% depending on the produced synthetic fuel and 100% of CO_2 conversion. The lower number relates to methanol production and the higher to hydrogen production, other investigated fuels were syngas (89%), methane (81%) and Fischer-Tropsch fuels (67%). The produced Fisher-Tropsch fuels where 31% C1-C4, 36% C5-C17 and the remaining long chained hydrocarbons contributed 33%. The ratio between saturated and unsaturated hydrocarbons for light-distillates was 7.5, for mid-distillates was 11, and for heavy-distillates was 28. The research concluded in this thesis has been disseminated into 7 peer-reviewed journal papers and 1 conference poster.

LIST OF PUBLICATIONS

Journal Articles

[1] JP Stempien, OL Ding, Q Sun, SH Chan. Energy and exergy analysis of Solid Oxide Electrolyser Cell (SOEC) working as a CO_2 mitigation device, International Journal of Hydrogen Energy, 37, 2012, 14518,

[2] JP Stempien, Q Sun, SH Chan. Performance of power generation extension system based on solid-oxide electrolyzer cells under various design conditions, Energy, 55, 2013, 647,

[3] JP Stempien, Q Sun, SH Chan. Solid Oxide Electrolyzer Cell Modeling: A Review, Journal of Power Technologies, 93, 2013, 216,

[4] JP Stempien, Q Sun, SH Chan. Theoretical consideration of Solid Oxide Electrolyzer Cell with zirconia-based electrolyte operated under extreme polarization or with low supply of feedstock chemicals, Electrochimica Acta, 130, 2014, 718,

[5] JP Stempien, Q Liu, M Ni, Q Sun, SH Chan. Physical principles for the calculation of equilibrium potential for co-electrolysis of steam and carbon dioxide in a Solid Oxide Electrolyzer Cell (SOEC), Electrochimica Acta, 147, 2014, 490,

[6] JP Stempien, M Ni, Q Sun, SH Chan. Thermodynamic analysis of combined Solid Oxide Electrolyzer and Fischer-Tropsch processes, Energy, 81, 2015, 682,

[7] JP Stempien, M Ni, Q Sun, SH Chan. Production of sustainable methane from renewable energy and captured CO_2 with use of Solid Oxide Electrolyzer: A thermodynamic assessment, Energy, 81, 2015, 714.

Conference Proceedings

[8] JP Stempien, Q Sun, KA Friedrich, SH Chan. Conceptual analysis of Solid Oxide Electrolyzer integration in energy system, 2nd International Conference on Clean Energy Science, April 2014, Qingdao, China.

TABLE OF CONTENTS

ACKNOWLEDGEMENTS I

ABSTRACT II

LIST OF PUBLICATIONS III

LIST OF TABLES IX

LIST OF FIGURES XI

LIST OF SYMBOLS XVIII

Chapter 1. Introduction 1

1.1 Brief overview of the energy sector 1

1.2 Introduction to electrolysis 7

1.3 Project goals 13

1.4 Objectives of research project 13

1.5 Scope of research project 14

1.6 Thesis layout 15

Chapter 2. Literature review 16

2.1 Cell-level models 16

2.1.1 Chemistry and kinetics of the electrodes' processes 17

2.1.2 Brief overview of Solid Oxide Fuel Cell modelling 21

2.1.3. Modelling of the Solid Oxide Electrolyzer Cell 22

2.1.4. Modelling of impedance spectroscopy 24

2.1.5 Modelling of degradation 25

2.1.6 Modelling of 3D structures and its influence on cell performance 26

2.2 System-level models 26

2.2.1 Economic analysis 27

2.2.2 Technical analysis 28

2.3 Summary 29

Chapter 3. Fundamental aspects of Solid Oxide Electrolyzer Cell operation and modelling 31

3.1 Introduction 31

3.2 Physical fundamentals of the Solid Oxide Electrolyzer Cell 31

3.3 Introduction to modelling 33

3.4 Theory of the Solid Oxide Electrolyzer Cell modelling 35

3.4.1 Classical approach – macro-model. 38

3.4.2 Statistical approach - micro-modelling. 46

3.5 Modelling of the Solid Oxide Electrolyzer Cell operated under extreme oxygen chemical potential difference 51

3.5.1 Introduction 51

3.5.2 Theory 54

3.5.3 Results and discussion 64

3.5.4 Conclusions 72

3.6 Physical principles of establishment of equilibrium potential in a co-electrolysis Solid Oxide Electrolyzer Cell 73

3.6.1 Introduction 73

3.6.2 Theory 75

3.6.3 Experimental 81

3.6.4 Results and discussion 82

3.6.5 Conclusions 100

3.7 Summary of the author’s micro-model and the validation 101

3.7.1 Equilibrium potential 103

3.7.2 Ohmic loss....104

3.7.3 Activation overpotential....105

3.7.4 Concentration overpotential....107

3.7.5 Cell microstructure parameters....107

3.7.6 Validation of model....108

Chapter 4. Carbon dioxide mitigation system based on Solid Oxide Electrolyzer Cell....110

4.1 Energy and exergy analysis of CO_2 mitigation system....111

4.1.1 Introduction....111

4.1.2 Energy and exergy analysis....111

4.1.3 Results and discussions....116

4.1.4 Conclusion....122

4.2 Parametric study of CO_2 mitigation system....123

4.2.1 Introduction....123

4.2.2 Simulation set-up....123

4.2.3 Results and conclusions....125

4.3 Chapter summary....138

Chapter 5. Synthetic, renewable fuel production and energy storage with use of Solid Oxide Electrolyzer Cell....139

5.1 Study of Singapore's electrical grid balancing and surplus energy storage in form of hydrogen, syngas or methanol....145

5.1.1 Introduction....145

5.1.2 SOFC-SOEC model....146

5.1.3 Results....155

5.1.4 Conclusion....164

5.2 Production of renewable and sustainable hydrocarbon fuels in combined Fischer-Tropsch and Solid Oxide Electrolyzer processes 166

5.2.1 Introduction 166

5.2.2 Theory 167

5.2.3 Results and discussion 172

5.2.4 Conclusions 182

5.3 Renewable and sustainable methane production with use of Solid Oxide Electrolyzer 183

5.3.1 Introduction 183

5.3.2 Methane synthesis reactor model 184

5.3.4 Results and discussion 186

5.3.5 Conclusion 193

5.4 Chapter summary 194

Chapter 6. Conclusions, recommendations and outlook for the energy sector 195

6.1 Conclusions 195

6.2 Major achievements 196

6.3 Recommendations 196

6.4 Outlook 197

REFERENCES 198

LIST OF TABLES

Table 1-1 – Comparison of state-of-the-art electrolysis technologies (IEA 2007).

Table 3-1 – Literature (Park & Blumenthal 1989) and fitted conductivity data. The formulae follow the Arrhenius type expression.

Table 3-2 – Summary of the parameters used in the simulation.

Table 3-3 – The values of enthalpy of adsorption and standard adsorption constant reported in the open literature.

Table 3-4 – Non reacting gas composition used in standard model calculations.

Table 3-5 - Values of OCV for selected operating cases of SOEC with Ni-YSZ based fuel electrode.

Table 3-6 – Summary of cell's parameters.

Table 3-7 – Comparison of predicted feedstock conversion efficiency with data from (Graves et al. 2011).

Table 4-1 – Parameters of SOEC for CO_2 mitigation system.

Table 4-2 – Values of temperature, mole flux and EGR used in the parametric study of CO_2 mitigation system.

Table 4-3 – Recommended design conditions of CO_2 mitigation system.

Table 5-1 – Operational parameters at design conditions of hydrogen producing system.

Table 5-2 – Operational parameters at design conditions of syngas producing system.

Table 5-3 – Details of analysis of syngas production case.

Table 5-4 – Operational parameters at design conditions of methanol producing system.

Table 5-5 – Details of analysis of methanol production case.

Table 5-6 – Summary of selectivity parameters for Fischer-Tropsch process.

Table 5-7 – Summary of Fischer-Tropsch process kinetic parameters.

Table 5-8 – SOEC parameters analysed in SOEC-FTS case.

Table 5-9 – FTS parameters analysed in SOEC-FTS case.

Table 5-10 – Parameters of combined process analysed in SOEC-FTS case.

Table 5-11 – Operational parameters of optimized SOEC unit in SOEC-FTS case.

Table 5-12 – Operational parameters of optimized FTS reactor in SOEC-FTS case.

Table 5-13 – Summary of geometric and intrinsic parameters of electrolyzer in SOEC-CH_4 case.

LIST OF FIGURES

Fig. 1-1 – Primary energy demand history and predictions (IAE 2014) compared with GDP per capita (World Bank 2014).

Fig. 1-2 – Relation between carbon dioxide emissions (World Bank 2014) and primary energy demand (IEA 2014).

Fig. 1-3 – Estimated actual global mean temperature (IPCC 2007) and carbon dioxide emissions (World Bank 2014)

Fig. 1-4 – Reserve-to-production ratio of coal, oil and natural gas (British petroleum 2014).

Fig. 1-5 – Prices of fossil fuels in 2014 US$ per GJ of energy (British petroleum 2014).

Fig. 1-6 – Final energy consumption shares in 2012 (IEA 2014).

Fig. 1-7 – Number of new publications in Elsevier and Web of Science with a keyword ‘SOEC’.

Fig. 1-8 – Thermodynamic classification of the fuel cell and the electrolyzer.

Fig. 1-9 – Gibbs energy and enthalpy differences for electrolysis of steam and carbon dioxide as a function of temperature

Fig. 3-1 – Solid Oxide Electrolysis Cell schematic.

Fig. 3-2 – Possible distinctions of modelling

Fig. 3-3 – Black box model

Fig. 3-4 – Classical I-V characteristics of SOEC.

Fig. 3-5 – Experimental data from Schefold et al. and simulation results from YSZ properties extrapolated from reported literature conductivity values (Park & Blumenthal 1989). Temperature was set to 810 °C, pressure 1 bar, oxygen partial pressure on fuel side ~10^{-20} bar and 0.21 bar on air side. Literature conductivity data used to simulate continuous line are reprinted in Table 3-2. Simulated cell parameters are given in Table 3-3.

Fig. 3-6 – Fitting and validation curves as compared to experimental results from Schefold et al., fitting curve obtained at 810°C and validation curve obtained at 895°C.

Fig. 3-7 – On the left axis: Short circuit pressure estimation as a function of 1/RT for literature conductivity data (Park & Blumenthal 1989) and fitted conductivity data. On the right axis: Short circuit voltage, as a function of temperature, observed from experiments (Pham & Glass 1998, Schefold et al. 2009), literature conductivity data (Park & Blumenthal 1989) and fitted conductivity data. Points refer to experimental short circuit voltage.

Fig. 3-8 – Equilibrium oxygen partial pressure of different fuel mixtures at OCV conditions. 827 °C is temperature of equilibrium between hydrogen/steam and CO_2/CO mixture. Line at this temperature would be straight.

Fig. 3-9 – Exemplary calculation of bulk equilibrium oxygen partial pressure of fuel mixture at 700, 800 and 900 °C. Presented results do not consider partial pressure of oxygen at the interface between electrode and electrolyte, and thus cannot be used directly to calculate transport numbers, or Faradic efficiency. The mixture is being balanced with 5% hydrogen. 827 °C is the temperature at which hydrogen/steam and CO_2/CO mixture is at equilibrium, i.e. non-reacting conditions.

Fig. 3-10 – Exemplary results for SOEC operating at 810 °C in the dominant ionic, mixed and dominant electronic conduction modes. The cell was fed with 83% molar H_2O, 13% molar CO_2 and 4% molar H_2. On the left axis: The continuous line represents the cell potential difference. On the right axis: The dashed line represents Faradic efficiency and the dashed-dotted line represents feedstock chemicals' conversion.

Fig. 3-11 – Comparison of experimentally observed OCV values for Pt-cell (dots) and those calculated with the standard model equation (3-105)(lines) (a-c). Prediction error of the standard model (d-f). a and d refer to CO2/H2 mixtures, b and e to H2O/H2 mixtures and c and f to CO2/CO mixtures.

Fig. 3-12 – Comparison of experimentally observed OCV values for Pt-cell (dots) and those calculated with the oxygen partial pressure model equation (3-104) (lines) (a-c). Prediction error of the oxygen partial pressure model (d-f). a and d refer to CO2/H2 mixtures, b and e to H2O/H2 mixtures and c and f to CO2/CO mixtures.

Fig. 3-13 – Comparison of experimentally observed OCV values for Ni-YSZ cell (dots) and those calculated with standard model equation (3-105) and oxygen partial pressure model equation (3-104) (a-c) (lines). Prediction error of the tested models (d-f). a and d refer to H2O/H2 mixtures, b and c to CO2/H2 mixtures and c and f to H2O/CO2/H2 mixtures.

Fig. 3-14 – Comparison of the experimentally observed co-electrolysis OCV values for Ni-YSZ cell (dots) and those calculated by all investigated models (a) (lines). Prediction error for all models (b).

Fig. 3-15 – Comparison of predicted I-V curve for H2O, CO2 and co- electrolysis with data from (Graves et al. 2011) and in house data. Curve-1 steam electrolysis 30% H2O/70%H2 at 800°C, Curve-2 co-electrolysis (Graves et al. 2011) 25%H2O/25%H2/25%CO2/25%CO 850°C, Curve-3 steam electrolysis (Graves et al. 2011) 50%H2O/50%H2 850°C, Curve-4 co-electrolysis (Graves et al. 2011) 45%H2O/45%CO2/10%H2 850°C.

Fig. 4-1 – Schematic of simulated SOEC system.

Fig. 4-2 – Analysis of overpotential losses for model result.

Fig. 4-3 – I-V curves for different recycling ratios at 800 °C.

Fig. 4-4 – I-V curves for different recycling ratios at 700 °C.

Fig. 4-5 – I-V curves for different recycling ratios at 600 °C.

Fig. 4-6 – Relation between the voltage and energy efficiency, exergy efficiency and feedstock conversion for the SOEC operated at 800°C and fed with 18% CO2, 35% H2O and 47% N2, the recycling ratio was set to 0.1 (10%).

Fig. 4-7 – Relation between amount of CO_2 converted and applied voltage for the SOEC operated at 800°C and fed with 18% CO2, 35% H2O and 47% N2, the recycling ratio was set to 0.1 (10%).

Fig. 4-8 – Relation between energy consumption per kg of CO_2 converted and applied voltage for the SOEC operated at 800°C and fed with 18% CO2, 35% H2O and 47% N2, the recycling ratio was set to 0.1 (10%).

Fig. 4-9 – Relation between exergy consumption per mol of CO_2 converted and applied voltage for the SOEC operated at 800°C and fed with 18% CO2, 35% H2O and 47% N2, the recycling ratio was set to 0.1 (10%).

Fig. 4-10 – Schematic of simulated SOEC system #2.

Fig. 4-11 – Efficiency at a constant temperature as a function of voltage, percentage of exhaust gas recycling (EGR) and molar flux – exemplary raw data. F/A stands for flow to cell area (i.e. flux) and R stands for EGR factor.

Fig. 4-12 – Maximum efficiency at 800 °C.

Fig. 4-13 – Maximum efficiency at 700 °C.

Fig. 4-14 – Maximum efficiency at 600 °C

Fig. 4-15 – Maximum efficiency at 500 °C.

Fig. 4-16 – Electricity consumption for thermally balanced cell at 800 °C.

Fig. 4-17 – Electricity consumption for thermally balanced cell at 700 °C.

Fig. 4-18 – Maximum CO_2 removal efficiency at 800 °C

Fig. 4-19 – Maximum CO_2 removal efficiency at 700 °C.

Fig. 4-20 – Maximum CO_2 removal efficiency at 600 °C.

Fig. 4-21 – Maximum CO_2 removal efficiency at 500 °C.

Fig. 4-22 – Maximum H_2O conversion at 800 °C.

Fig. 4-23 – Maximum H_2O conversion at 700 °C.

Fig. 4-24 – Maximum H_2O conversion at 600 °C.

Fig. 4-25 – Maximum H_2O conversion at 500 °C.

Fig. 4-26 – Maximum CO_2 conversion at 800 °C.

Fig. 4-27 – Maximum CO_2 conversion at 700 °C.

Fig. 4-28 – Maximum CO_2 conversion at 600 °C.

Fig. 4-29 – Maximum CO_2 conversion at 500 °C.

Fig. 5-1 – Projected peak demand growth of Singapore's energy system.

Fig. 5-2 – Intermittency of renewable energy sources (IEA 2012). There is in general no correlation between the demand and supply of electrical energy. Therefore, creating rational for energy storage.

Fig. 5-3 – Schematic of the hydrogen production system.

Fig. 5-4 – Schematic of the syngas production system.

Fig. 5-5 – Schematic of the methanol production system.

Fig. 5-6 – Schematic of the SOEC.

Fig. 5-7 – Wind speed graph, hourly over the week 01.03.13 – 07.03.13, hourly average of the week and weekday average (WindFinder.com) measured at ground level. Dotted lines represent wind speed of each separate day during the measurement period.

Fig. 5-8 – Monthly average wind speed (Windfinder.com, Lee et al. 2011).

Fig. 5-9 – Hourly demand for electricity averaged over random weeks of each month between February 2012 and February 2013 (EMA 2012).

Fig. 5-10 – Cumulative probability of wind blowing at particular wind speed.

Fig. 5-11 – Predicted annual electricity production from single off-shore wind turbine in Singapore.

Fig. 5-12 – Derivative of power extraction from wind with respect to wind speed.

Fig. 5-13 – Loading diagram of SOCs working with 1% of Singapore's power plants and yielding syngas.

Fig. 5-14 – Allowable price per cell (in SGD) as function of efficiency gain.

Fig. 5-15 – Loading diagram of SOCs working with 1% of Singapore's power plants and yielding methanol.

Fig. 5-16 – Reduction in CO_2 emissions due to use of SOFC combined with 1% of Singapore's capacity.

Fig. 5-17 – Reduction in CO_2 emissions due to increased combined cycle efficiency.

Fig. 5-18 – Technical summary of proposed systems.

Fig. 5-19 – Scheme of SOEC-FT process.

Fig. 5-20 – Validation of distribution model with the experimental data reported in (van der Laam 1999).

Fig. 5-21 – Optimization of SOEC process for high amount of energy stored in hydrocarbons.

Fig. 5-22 – Optimization of SOEC process for high conversion efficiency.

Fig. 5-23 – Weight distribution of FTS products.

Fig. 5-24 – Optimization of FTS process for high amount of energy stored in hydrocarbons.

Fig. 5-25 – Optimization of FTS process for high conversion efficiency.

Fig. 5-26 – Optimization of FTS process for high yield of heavy paraffins.

Fig. 5-27 – Weight distribution of FTS products.

Fig. 5-28 – Optimization of SOEC-FT process for high amount of energy stored in hydrocarbons.

Fig. 5-29 – Optimization of SOEC-FT process for high conversion efficiency.

Fig. 5-30 – Schematic of the modelled system (Blue arrows indicate combined material and energy streams, red arrows indicate energy streams).

Fig. 5-31 – Representation of the modelled system under Aspen HYSYS® platform (Red arrows represent energy streams, blue arrows correspond to material and energy streams).

Fig. 5-32 – The current-voltage characteristic of the electrolyzer (Green lines: SCR 0.5, red line: SCR 8; Solid lines: 1 bar, dotted lines: 5 bar; and the dash-dot lines: 10 bar).

Fig. 5-33 – Effect of the applied current density and SCR on the maximum electricity to methane conversion efficiency (Green lines: 0.5 A cm^{-2}, blue lines: 1 A cm^{-2}, red lines: 1.5 A cm^{-2}, Solid lines: electrical energy conversion efficiency, dotted lines: overall energy conversion efficiency).

Fig. 5-34 – Effect of applied current and SCR on the maximum energy storage and CO2-to-CH4 conversion (Green lines: 0.5 A cm^{-2}, blue lines: 1 A cm^{-2}, red lines: 1.5 A cm^{-2}; Solid lines: maximum amount of energy stored in methane, dotted lines: maximum CO_2-to-CH_4 conversion).

Fig. 5-35 – Effects of temperature and pressure under the maximum electrical energy conversion efficiency (Green surface: 0.5 A cm^{-2} and SCR 7, Blue surface: 1 A cm^{-2} and SCR 4; Red surface: 1.5 A cm^{-2} and SCR 2.5)

Fig. 5-36 – Effects of temperature and pressure under the maximum amount of energy stored in the methane (Green surface: 0.5 A cm^{-2} and SCR 8, Blue surface: 1 A cm^{-2} and SCR 4, Red surface: 1.5 A cm^{-2} and SCR 2.5)

Fig. 5-37 – Relationship between SCR and applied current density (Red squares: maximum electrical energy conversion efficiency, red line: fitted trend line to red crosses; Green circles: maximum amount of the energy stored in methane, green line: fitted trend line to red circles)

LIST OF SYMBOLS

SUBSCRIPTS & SUPERSCRIPTS

0 – standard or equilibrium

act – activation

an – anode (air electrode)

cat – cathode (fuel electrode)

ch – chemical

con – concentration

e – electron or electronic

eq – equilibrium

eff – effective

eh – electron-hole

gen – generated

h – hole

i – i-th specie or ionic or input

j – j-th specie

L – limiting

max – maximum

min – minimum

o – output

ohm – ohmic

ph – physical

std – standard

th – thermoneutral

LATIN SYMBOLS

a – stoichiometric coefficient of chemical A or electrochemical activity

b – stoichiometric coefficient of chemical B

c - concentration

h – Planck constant or specific enthalpy [m^2 kg s^{-1} or J kg^{-1}]

i – current density [A cm^{-2}]

k – Boltzmann constant or simple reaction rate constant [m^2 kg s^{-2} K^{-1} or *var*]

k_R – pseudo reaction rate constant for olefin re-adsorption

m – selectivity

n – carbon number or number of moles or number of particles per unit volume

n_t – total number of particles per unit volume

n_s – number of available TPB sites

p – partial pressure [atm]

q – charge [C]

r – particle radius [m]

s – specific entropy [$J\ K^{-1}\ kg^{-1}$]

t – time or transport number [s]

t_p – pseudo reaction rate constant of paraffin formation

t_o – pseudo reaction rate constant of olefin formation

x – position along x-axis [m]

y – molar fraction

z – number of electrons per reaction

A – chemical A

B – chemical B

B_g – permeability [m^2]

D – diffusivity [$m^2\ s^{-1}$]

D_p – pore diameters [m]

D_s – grain diameter [m]

E – voltage [V]

F – Faraday constant [$C\ mol^{-1}$]

G – Gibbs free energy [J]

H – enthalpy [J]

I – current [A]

K – reaction equilibrium constant or adsorption constant

N – molar flux [$mol\ s^{-1}\ m^{-2}$]

P – pressure or power or probability of connection between particles [bar or W]

Q – heat or enthalpy of adsorption [J]

R – universal gas constant or LHHW type reaction rate constant [$J\ K^{-1}\ mol^{-1}$]

S – entropy [$J\ K^{-1}$]

S_v – electrochemically active area [$m^2\ m^{-3}$]

T – temperature [K]

W – work [W]

Z – coordination number for conducting particle

GREEK SYMBOLS

α – charge transfer coefficient or probability of hydrocarbon chain growth

γ – pre-exponential factor

δ – thickness [m]

Δ – difference

ε – porosity or specific exergy [J kg^{-1}]

η – overpotential or efficiency [V]

θ – coverage or contact angle between ionic and electronic conducting particles

θ_1 – coverage of alkyl with one carbon atom

μ – chemical potential or dynamic viscosity [J mol^{-1} or m^2 s^{-1}]

$\overline{\mu}$ – electrochemical potential [J mol^{-1}]

ν – frequency of gas molecules vibration

ξ – tortuosity

ϕ – electrical potential [V]

Φ - volumetric fraction of electronic conductors in porous electrode

ρ – resistance [ohm]

σ – conductivity or sticking probability [S]

χ – conversion

ψ – flux of gas molecules [mol s^{-1} m^{-2}]

ABBREVIATIONS

ASF – Anderson-Schulz-Flury distribution

ASR – Area Specific Resistance

B-V – Butler-Volmer equation

CCPP – Combined Cycle Power Plant

CFD – Computational Fluid Dynamics

DFT – Density Functional Theory

DGM – Dusty-Gas Model

EEET – Efficiency of Electrical Energy Transformation

EGR – Exhaust Gas Recycling

FT – Fischer-Tropsch process

FTS – Fischer-Tropsch Synthesis

GDP – Gross Domestic Product

HHV – Higher Heating Value

IPCC – International Panel on Climate Change

LCA – Life-Cycle Assessment

LHV – Lower Heating Value

MPT – Mixed Potential Theory

NASA – National Aeronautics and Space Administration

OCV – Open Circuit Voltage

OECD – Organisation for Economic Co-operation and Development

PEM – Proton Exchange Membrane

PEN – Positive electrode – Electrolyte – Negative electrode assembly

PM – Particulate Matter

PV – Photo Voltaic cell

R&D – Research and Development

R-to-P – reserve to product

RWGS – Reverse Water-Gas Shift reaction

SCR – Steam to Carbon Ratio

SCV – Short Circuit Voltage

SMR – Steam Methane Reforming

SOC – Solid Oxide Cell

SOEC – Solid Oxide Electrolyzer Cell

SOFC – Solid Oxide Fuel Cell

STP – Standard Temperature and Pressure

TPB – Triple Phase Boundary

TPD – Temperature Programmed Desorption

WGS – Water-Gas Shift reaction

CHEMICALS

(g) – gaseous state

Bi_2O_3 – dibismuth trioxide

$C_{12}H_{26}$ – dodecane

CO – carbon monoxide

Co – cobalt

CO_2 – carbon dioxide

Cu – copper

e^- – electron

GDC – Gadolinium-doped Ceria

$h^{\bullet}$ – single charged hole

H_2 – hydrogen

H_2O – dihydrogen oxide, water

H_2S – dihydrogen sulfide

LSCF – Lanthanum Strontium Cobalt Ferrite

LSM – Lanthanum Strontium Manganite

N_2 – nitrogen

Ni – nickel

NO_x – nitrogen oxides

$O^{=}$ – double negatively charged oxygen ion

O_2 – oxygen

O_O^x – neutral oxygen on oxygen site

Pt – platinum

SO_x – sulphur oxides

$V_O^{\bullet\bullet}$ – doubly charged oxygen vacancy

Y’’’ – yttrium ion

$Y_{Zr}^{\bullet}$ – single charged yttrium ion on zirconium site

Y_2O_3 – diyttrium trioxide

YSZ – Yttria-Stabilized Zirconia

Zr’’’’ – zirconium ion

ZrO_2 – zirconium dioxide

Chapter 1. Introduction

1.1 Brief overview of the energy sector

Growing demand for energy, environmental concerns and the finite amount of fossil fuels are major elements shaping the future energy sector. The increase in energy consumption is following the growth in population and economic progress of the world (Fig. 1-1). In 2012, the average energy consumption per capita in the member states of Organisation for Economic Co-operation and Development (OECD) was 120.49 GJ, whereas in non-OECD countries it was only 39.28 GJ (IEA 2014), thus suggesting that indeed the human progress is requiring increasing amount of energy. This trend is especially dangerous in developing countries, where state-of-the-art technologies are often unavailable and are substituted by older and more energy intensive and polluting ones. Populous countries, like China, India or Indonesia, have experienced rapid growth in their Gross Domestic Product (GDP), this was followed by the quick decline in air, water and soil quality. Economic growth based on fossil fuels has pulled millions out of poverty, however created new problems linked to the environment and climate change. Carbon dioxide (CO_2) emissions trend closely follow that of energy demand (Fig. 1-2). This is not surprising given that current energy sources are mostly of fossil origin (89.1%, IEA 2014). Atmospheric concentration of carbon dioxide is closely related to the amount of heat trapped in earth atmosphere and thus leads to the global average temperature rise. According to the recent report by Intergovernmental Panel on Climate Change (IPCC) (IPCC 2013), the anthropogenic generation of CO_2 can be considered as a driving force behind increased rate of the temperature rise (Fig. 1-3) observed over the past few decades (IPCC 2007).

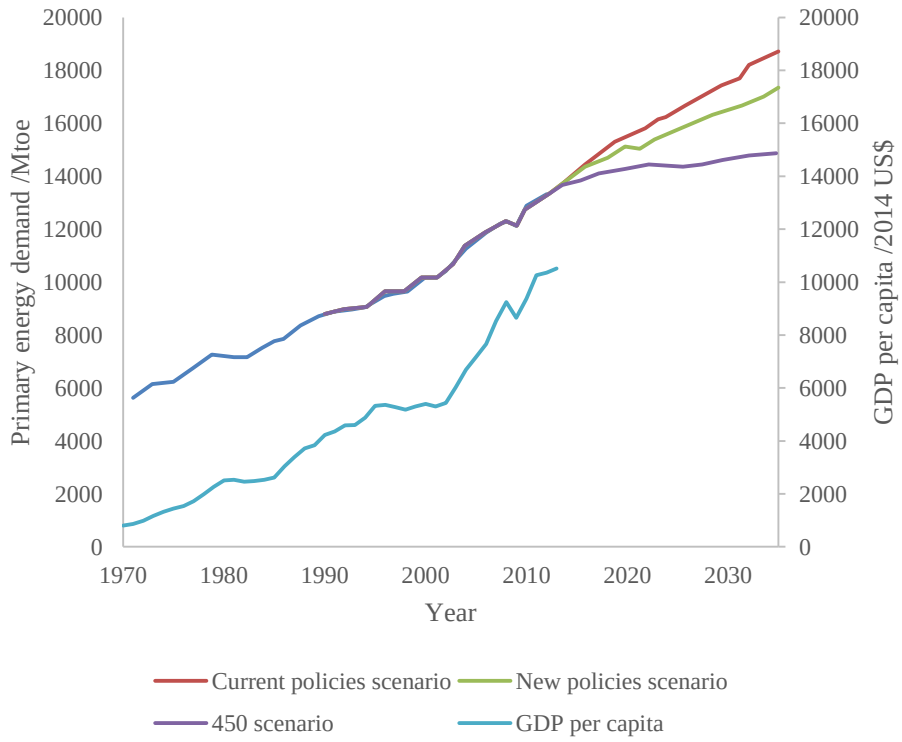

Fig. 1-1 – Primary energy demand time-series and forecast (IAE 2014) compared with GDP per capita (World Bank 2014). Close correlation can be observed between the data suggesting causality between economic and population growth and energy demand.

The consequences of the temperature rise are (IPCC 2014):

- Altered hydrological systems affecting quantity and quality of water resources,
- Shifting geographical ranges, abundance, migration patterns and species interactions of terrestrial and freshwater species. Few recent species extinctions are attributed to anthropogenic climate change,
- Negative impact on crop yield,
- Increase in heat-related mortality in some regions,
- Higher vulnerability to climate change of people who are socially, economically, culturally, politically institutionally, or otherwise marginalized,
- Very high vulnerability to climate extremes of some ecosystems and many human systems.

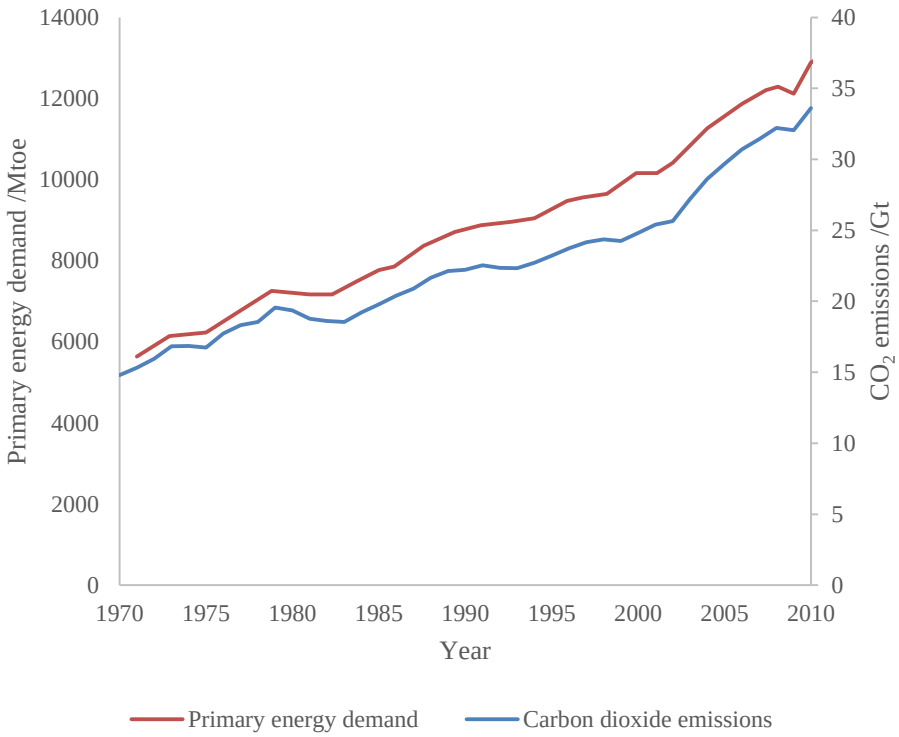

Fig. 1-2 – Relation between carbon dioxide emissions (World Bank 2014) and primary energy demand (IEA 2014).

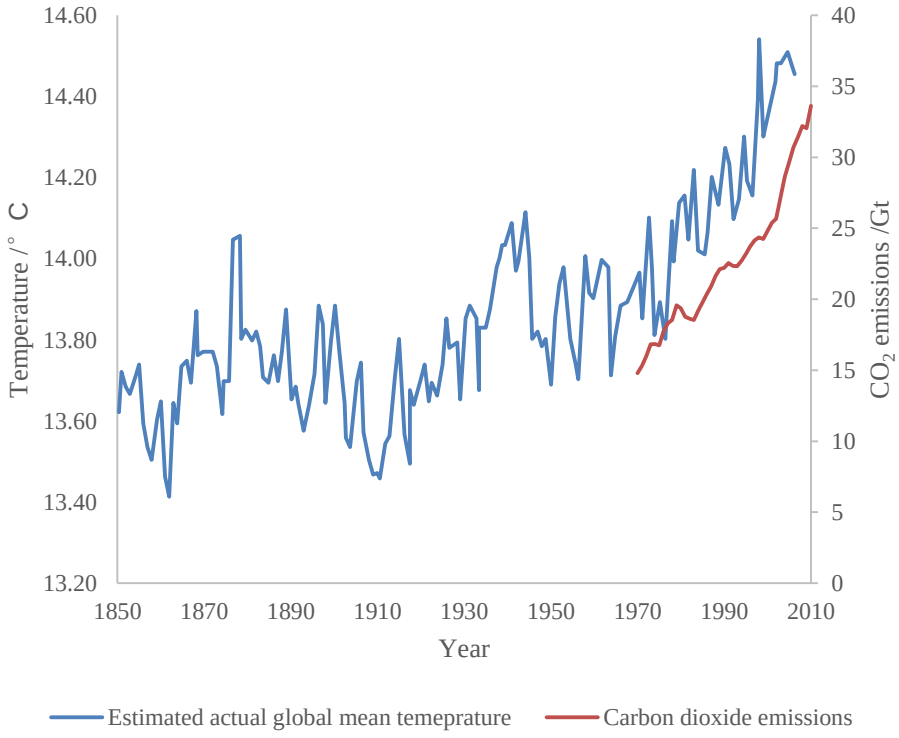

Fig. 1-3 – Estimated actual global mean temperature (IPCC 2007) and carbon dioxide emissions (World Bank 2014).

Needless to say, it is imperative to mitigate the consequences of the climate change. One of the ways of doing so is by limiting CO_2 concentration in the atmosphere. Moving from wood burning to coal, oil and finally natural gas can limit the amount of emitted CO_2 and other pollutants. However, these resources are finite and cannot be relayed upon indefinitely.

Despite the ratio of reserve-to-product (R-to-P) for fossil resources remained relatively constant over past 30 years, these are the finite resources and are deemed to be supplanted by more advanced, sustainable energy sources. The number for R-to-P for natural gas remained relatively constant, slightly increased for oil and dramatically decreased for coal over the surveyed period (British Petroleum 2014). Current estimates indicate reserve for 53 years, at current consumption level, for oil, 57 for natural gas and 112 for coal (Fig. 1-4). Nevertheless, the emissions following from the combustion of all the available resources would amount to a temperature rise above the safe levels, thus is undesirable.

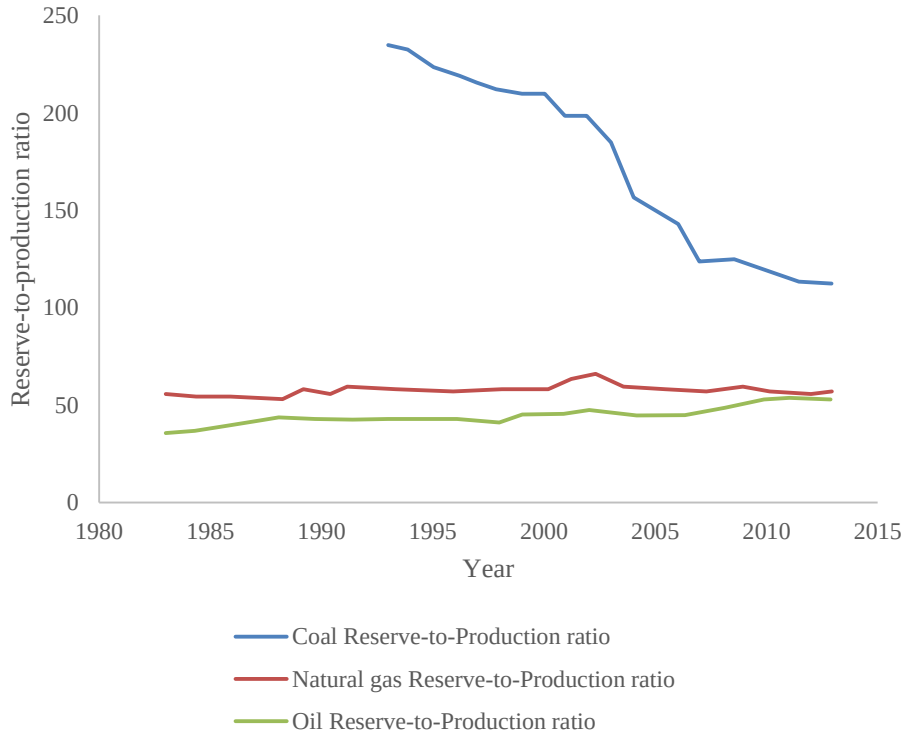

Fig. 1-4 – Reserve-to-production ratio of coal, oil and natural gas (British petroleum 2014).

Besides the environmental concerns and availability of the resources, the energy cost is an important socio-economic factor in energy future considerations. According to the historical data the prices of oil and natural gas are constantly growing for the past twenty

years (Fig. 1-5).

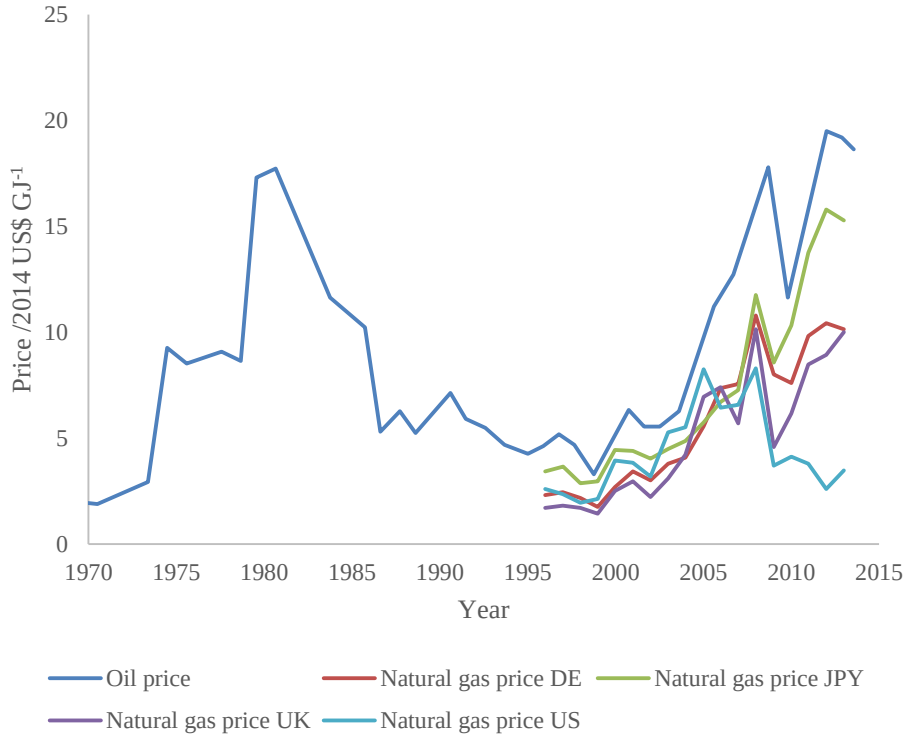

Fig. 1-5 – Prices of fossil fuels in 2014 US$ per GJ of energy (British petroleum 2014).

These trends can be summed up in three bullet points creating the broader context of this PhD thesis:

- The fossil fuel based economy growth model is resulting in undesirable consequences of the climate change,
- The amount of fossil fuels is limited and currently estimated to suffice for the next 50 – 150 years, the lower number is for oil and natural gas, whereas the higher is for coal,
- The price of fossil fuels (ergo, energy price and progress in general price) is difficult to forecast and subjected to large number of complex factors and constantly growing over the past 20 years.

The future energy system is required to meet a list of criteria:

- Low cost of end-user energy,
- Instant availability of required quality and quantity of energy,
- Environmental sustainability and benignity.

Only two of the above criteria are partially met by the current, fossil based energy system. Current research efforts are focused on energy sources that are essentially infinite and

free, these include the energy of solar radiation, the gravitational energy of the solar system and the geothermal energy. The amount of energy available on earth from these three sources exceeds current and projected needs, thus, being free can in principle satisfy the first criteria posed to the future energy system. Second criteria can only be met on small scale by certain renewable technologies, i.e. hydro electricity, geothermal heat, etc. Other investigated technologies require energy storage to be employed in order to be instantly available. Third point can be in principle secured by renewable technologies, if certain precautionary steps are taken, e.g. limit of the hydropower retention tank capacity, clean manufacturing technology, etc.

Technologies able to harvest renewable energy include photovoltaic cells, wind turbines, solar-thermal cells, biomass, hydro power, etc. The most popular ones are the photovoltaic cells and wind turbines, which can produce electricity via photo-electrochemical reaction and mechanical energy conversion respectively. Except biomass-related processes, geothermal and solar-thermal, the product of these technologies is an intermittent electricity.

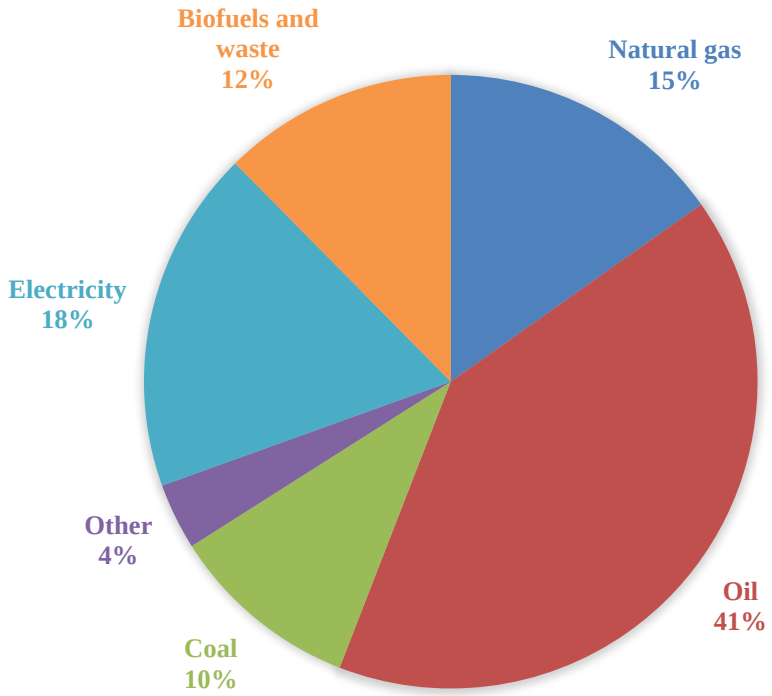

Fig. 1-6 – Final energy consumption shares in 2012 (IEA 2014).

However, according to International Energy Agency (IEA) (IEA 2014), only 18.1% of

the final energy consumption is in the form of electricity (Fig. 1-6). This, combined with energy intermittency and lack of required infrastructure causes a major obstruction in the introduction of renewable energy to the global energy mix. The amount of electricity generated by renewable sources was only 21.2% in 2012 (IEA 2014), that is 3.9% of final energy consumption came from a renewable electricity source. The number for bio-derived fuels is slightly larger, at <7% in 2012 (IEA 2014). This sums up to a contribution from renewable resources at <10.9%.

There are several ways to tackle the existing issues preventing introduction of renewable energy. These must address the problems of supply intermittency, final energy consumption structure and infrastructure requirements. Currently the researchers focus on biofuels production, introduction of electrical and fuel cell cars, energy storage, etc. Another, alternative way is the introduction of renewable, sustainable synthetic fuels.

The synthetic fuel pathway carries the benefits of retaining the current energy infrastructure, does not compete with the food industry, is industrially proven technology and can be used as energy storage technology. The issue connected with the synfuel production is the emission of CO_2, thus modifying the traditional process by CO_2 recycling and use of renewable energy to drive the electrolysis is a closed cycle and no new emissions are created. Synthetic fuel production technologies are currently based on transformation of solid or gaseous fossil energy sources to liquid transportation fuels. It is, however, possible to use sequestrated CO_2 and seawater to produce liquid or gaseous fuels. In the long term, it is possible to exclude carbon from the loop and produce renewable hydrogen out of seawater.

1.2 Introduction to electrolysis

The technology making the synfuel production a renewable process is called the electrolysis. The electrochemical reaction transforming electrical energy into chemical energy in an environmentally benign way. The history of electrolysis dates back to 1800 (Nicholson & Carlisle 1800) when Nicholson and Carlisle performed water electrolysis for the first time, decomposing it to its constituent elements of hydrogen and oxygen. Over the past two hundred years the technology was developed tremendously, however, it is still used only in marginal cases for the production of hydrogen (4% of total production, rest from fossil resources). The reason behind this is the much lower cost of production in large scale plants and without the use of electricity (IEA 2007).

Currently available electrolysis technologies include Alkaline electrolyzers, Proton Exchange Membrane (PEM) electrolyzers and Solid Oxide Electrolysis Cells (SOEC). Only the first device is commercially available, whereas the PEM electrolyzer is in precommercial stage and SOEC is in R&D stage. Summary of the technologies is presented in Table 1-1.

Table 1-1 – Comparison of state-of-the-art electrolysis technologies (IEA 2007).

Technology	Alkaline large-scale	Alkaline high-pressure	Advanced Alkaline	PEM	SOEC
Status	Commercial	Commercial	Precommercial	Precommercial	R&D
Temp °C	70 - 90	70 - 90	80 - 140	80 - 150	600 - 1000
Press bar	Up to 25	Up to 690	Up to 120	Up to 400	Up to 30
Hydrogen-to-Electrical energy ratio [%]	55 - 70	55 - 60	70 - 79	55 - 83	85 - 119

The beginning of Solid Oxide Electrolyzer Cell technology can be traced back to 1899, when Nernst (Nernst 1899) reported on the possibility of enhancing ionic conductivity at high temperatures by doping certain oxides. The material was called the Nernst mass and in 1962 was used by American scientists to construct the reverse of the electrolyzer, the Solid Oxide Fuel Cell (Weissbart & Ruka 1962). Later R&D efforts came from Germany in the 1980's under the project Hot Elly (Doenitz et al. 1980, 1988, Doenitz & Schmidberger 1982, Doenitz & Erdle 1985, Erdle et al. 1986, Erdle et al. 1990, Doenitz et al. 1990). However, the project was shut down due to low prices of oil in the 1990's. Currently, the area is experiencing considerable attention both from science and industry due to increasing fossil fuels prices and environmental concerns (Fig. 1-7). Materials typically used for SOEC are YSZ for electrolyte, Ni-YSZ cermet fuel electrode and perovskite based air electrode, typically LSM or LSCF. Some popular alternatives include GDC for the electrolyte and other La-based perovskites. Good review on materials used in SOEC was given by Ni et al. (Ni et al. 2008). Using ceramics is a distinct feature of SOEC technology, compared to other electrolyzer technologies. It brings a benefit of rigidity and allows to produce cells of various form. However, the problem with ceramics is its underdeveloped production techniques. Majority of the

materials are still being prepared inside R&D labs only on a small scale. Some of the research groups see future of large scale SOEC production in additive manufacturing.

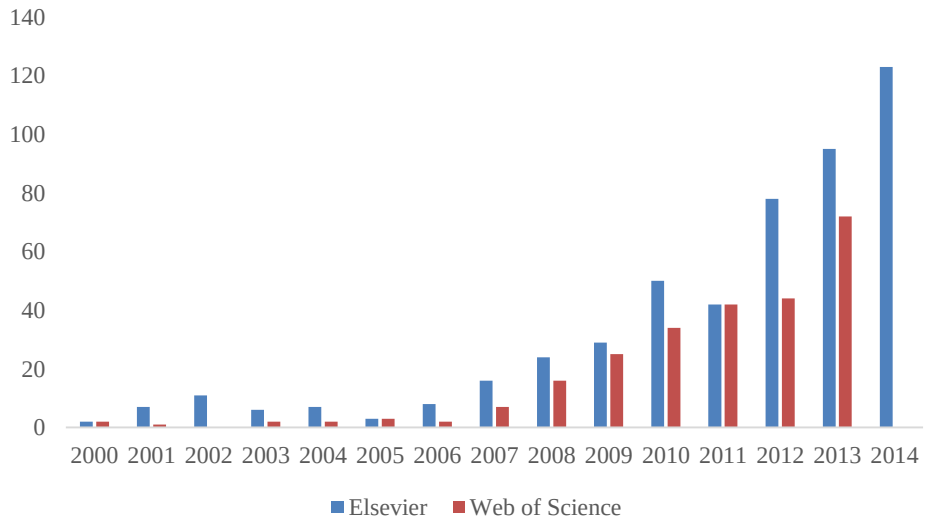

Fig. 1-7 – Number of new publications in Elsevier and Web of Science with a keyword 'SOEC'.

A keen reader will notice that over 100% efficiency is claimed for the SOEC, the large number of conversion efficiency is due to its ability to operate in endothermic mode, where part of the energy required for the electrolysis is supplied in form of heat (not part of efficiency calculation). In this view, it is important to stress that the electrolyzer is an equivalent of a heat pump, not a heat engine. Thus, the *conversion efficiency* can be in principle higher than 100% (Fig. 1-8).

There are, of course, other technologies offering hydrogen production. These include natural gas reforming, coal gasification, thermal water-splitting, biomass processes (pyrolysis, gasification, anaerobic digestion, etc.), photo-electrolysis, biological processes involving microalgae or bacteria. Natural gas reforming is the most popular process of hydrogen production, however it is based on non-renewable resource, hence it is not desirable for application in the future energy system. The same reason disqualifies coal gasification. Thermal water-splitting was investigated extensively in the past, however, no commercially available technology arose. Biomass related processes carry the same limitations as biofuels and other biomass based technologies, i.e. they compete with the food market, are generally limited to small scale applications and are heavily dependent on the supply chain of the biomass. Photo-electrolysis and

biological processes are very interesting alternatives, however, still require large R&D efforts. Thus, electrolysis seems to be the sole process able to produce renewable hydrogen or synthetic fuels when combined with renewable energy source. In the future it should be supplanted by the photo-electrolysis and biological processes. Out of possible technologies, SOEC can provide the highest conversion efficiency and high energy density. Moreover, it is the only technology which allows the co-electrolysis of steam and carbon dioxide, a very important factor in the view of production of synfuels, resulting in process simplification. The product of co-electrolysis is the mixture of hydrogen and carbon monoxide, i.e. the syngas, an important reagent gas for synthetic fuel production. Another benefit of high temperature operation is that the hydrogen/syngas generation rate is higher and combination with other industrial processes is more attractive.

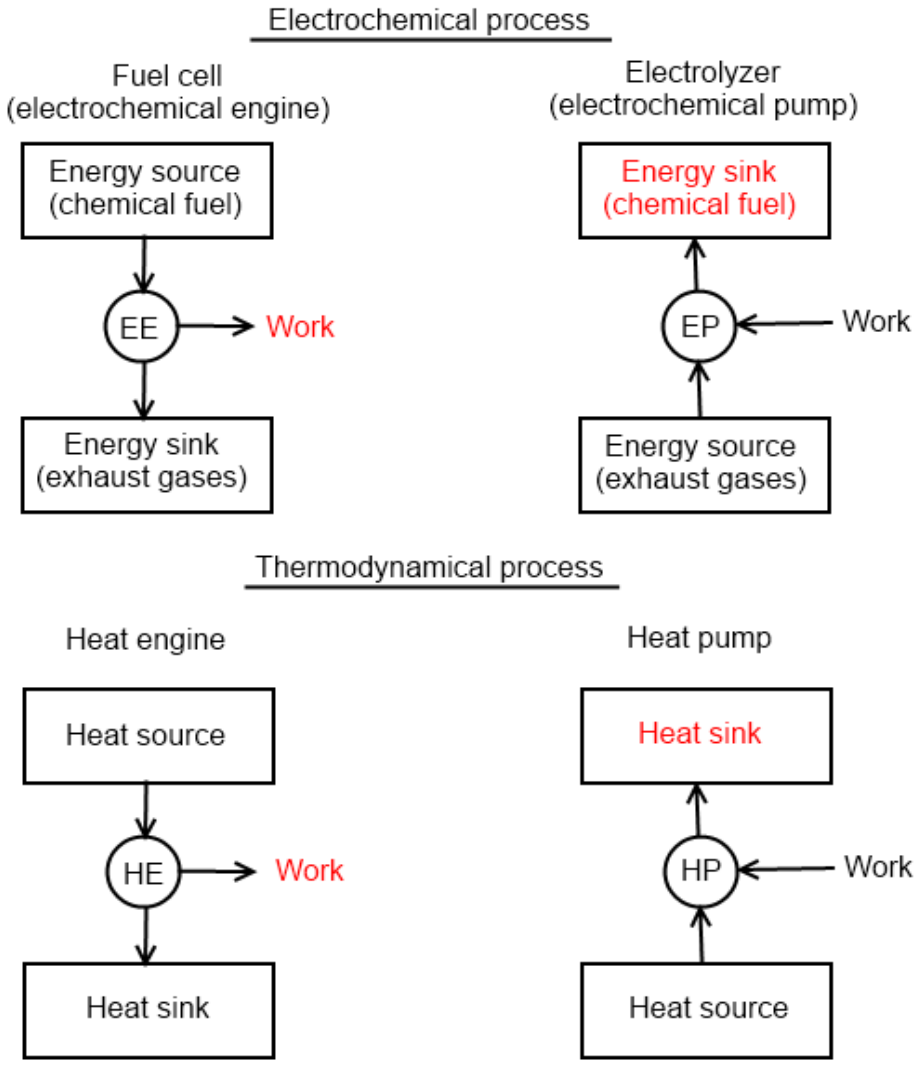

Fig. 1-8 – Thermodynamic classification of the fuel cell and the electrolyzer.

The minimum amount of energy to electrochemically convert steam and/or carbon dioxide to hydrogen and/or carbon monoxide can be estimated from the Nernst equation (Nernst 1899) which for the general reaction

$$a_1A_1 + a_2A_2 + \cdots + a_iA_i \rightarrow b_1B_1 + b_2B_2 + \cdots + b_jB_j \quad (1\text{-}1)$$

can be written as

$$E_0 = -\frac{\Delta G_0}{zF} - \frac{RT}{zF} ln\left(\frac{\prod_j B_j^{b_j}}{\prod_i A_i^{a_i}}\right) \quad (1\text{-}2)$$

where a_i is the stoichiometric coefficient of reagent A_i and b_j is the stoichiometric coefficient of the product B_j, z is the number of electrons transferred in the electrochemical reaction, F is the Faraday constant (96485,337 C mol^{-1}), ΔG_o is the Gibbs free energy change of the electrochemical reaction, R is the universal gas constant (8.314 J K^{-1} mol^{-1}) and T is the temperature.

The actual operation of an electrolyzer is always at a voltage difference higher than the one following from the Nernst equation. The additional energy requirement is dictated by several losses occurring during the operation of the cell. More detailed description of the physical basics of SOEC operation will be provided in Chapter 3.

Another important parameter of the cell is its thermoneutral voltage. It describes the theoretically required voltage to operate the electrolyzer in energy self-sufficient mode, i.e. with no heat leaving or entering the cell, i.e. with 100% efficiency. It can be calculated from following formulae

$$E_{th} = \frac{\Delta H}{zF} \quad (1\text{-}3)$$

where ΔH is the enthalpy change of the electrochemical reaction.

The reactions occurring in a typical SOEC are those of dissociation of steam and carbon dioxide, they can be written in the net form as

$$H_2O + \text{electricity} \rightarrow H_2 + \frac{1}{2}O_2 \quad (1\text{-}4)$$

$$CO_2 + \text{electricity} \rightarrow CO + \frac{1}{2}O_2 \quad (1\text{-}5)$$

The enthalpy of the above reactions and the change of the Gibbs energy is depicted in

(Fig. 1-9) as a function of temperature. As follows from equation (1-2) the electrical energy to perform the dissociation reactions is dropping with the increase in temperature. This is the physical basis behind the higher conversion efficiency of high temperature cells.

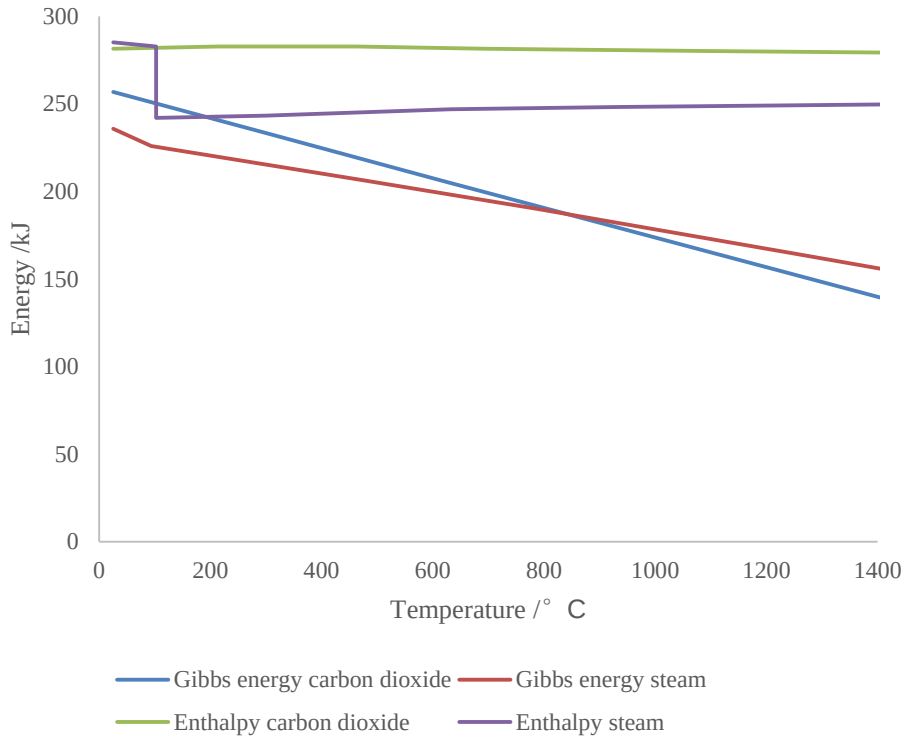

Fig. 1-9 – Gibbs energy and enthalpy differences for electrolysis of steam and carbon dioxide as a function of temperature.

Having the expressions for thermoneutral voltage and Nernst voltage, one can define two more parameters, i.e. theoretical conversion efficiency of the cell and the maximum of this parameter. The first indicator can be written as

$$EEET = \frac{E_{th}}{E} \tag{1-6}$$

where *EEET* stands for Efficiency of Electrical Energy Transformation and *E* is the voltage applied to the cell.

The maximum conversion efficiency can be calculated from

$$EEET_{max} = \frac{E_{th}}{E_0} \tag{1-7}$$

and is only the function of temperature and composition.

1.3 Project goals

Current situation in the energy sector and the great interest of social benefit of the sustainable energy future, calls for developing methods for energy conversion that will provide cheap, easy to store, accessible and desired quality energy that is benign to the environment. One of the pathways towards this future is using the Solid Oxide Electrolyzer Cells combined with other upstream technologies.

Prospects of using SOEC include hydrogen production, renewable energy intermittency mitigation, energy storage, CO_2 mitigation, CO_2 recycling, synthesis of sustainable hydrocarbon fuels, refinery waste upgrading or water desalination. However, much research is still needed to allow commercialization of this technology. Many phenomena, especially those connected with co-electrolysis are still not entirely understood.

In this work the author investigates possible applications of SOEC in different energy systems aimed at reducing the CO_2 emissions from power plant and production of synthetic fuels. To this end the author explores fundamental, physical understanding of co-electrolysis process and provide with an accurate model able to simulate the SOEC working in such systems.

Proposed micro-level model is used on a system-level scale to analyse a few systems aimed at providing energy systems for the future generations.

1.4 Objectives of research project

The motivation for this research is the need for multi-scale model allowing engineers to design and optimize energy systems which are environmentally friendly. Currently available models allow for accurate prediction of cell performance on a macro or micro level, additionally only for well investigated experimentally conditions. The applicability of the available models for the analysis of co-electrolysis is imperfect. To improve this limitations model must allow: to be applied for scales ranging from micro to system level; to be able to investigate industrially relevant systems; include the accurate description of co-electrolysis process.

Objectives of this research can be summarized as follows:

1. Micro model enhanced thermodynamic analysis of co-electrolysis Solid Oxide Cell (SOC).

Physical co-electrolysis model based on thermodynamics and electrochemistry considerations validated with in-house data is provided to assess influence of changes in macro- and micro-scale design of system on its overall performance. System level considerations are to be easily performed with availability to change: materials used in the model; electrodes and electrolyte thicknesses; electrodes ionic and electronic particles sizes; operating temperature; pressure; inlet gas composition; product stream recycling; and more. Simulation also provides possibility to investigate behaviour of a cell in both SOEC and SOFC modes.

2. Design structure optimization of a system aimed at limiting the industrial CO_2 emissions,

   Formulate, design and optimize a comprehensive solution in the form of robust design of system capable of limiting emissions of CO_2 by transforming it to usable syngas fuel. System is also applicable with the intermittent energy sources, i.e. wind and solar energy.

3. Design structure optimization of a system aimed at producing a range of synthetic fuels and balancing the grid demand fluctuations.

   Formulate, design and optimize the operational parameters of a system composed of the SOEC and a catalytic conversion reactor producing hydrogen, syngas, methanol, methane or the Fischer-Tropsch fuels (gasoline, diesel, kerosene). The system can simultaneously recycle transportation-generated CO_2 back to usable hydrocarbon fuels and stabilize energy production curve by using surplus electricity to produce fuel and transforming it back to electricity in peak hours.

1.5 Scope of research project

- To perform thorough literature review,
- To prepare and validate adequate model for the co-electrolysis electrolyzer system,

- To provide with thorough analysis of designed systems,
- To suggest future solutions for sustainable growth.

1.6 Thesis layout

Chapter 2 provides the reader with the literature review on topics associated with SOEC modelling for different purposes and on various levels.

Chapter 3 presents fundamental theoretical aspects of operating SOEC in the co-electrolysis mode. Based on the physical principles, a model is developed and proposed allowing the multi-level modelling of SOEC.

In chapter 4 results of analysis and optimization of a proposed system aimed at CO_2 mitigation with use of SOEC are presented.

In chapter 5, proposed systems aimed at synthetic hydrocarbon fuel production, grid balancing and energy storage are analysed.

Chapter 6 concludes, recommends and gives outlook for the future energy system.

Chapter 2. Literature review

Solid Oxide Electrolyzer Cells have many potential applications, ranging from production of hydrogen, production of carbon monoxide, production of syngas, production of oxygen through utilization of CO_2, water desalination to energy storage, synthetic fuels production, renewable energy intermittency mitigation, etc. Studies of such predestined systems include experimental investigations of new materials as well as different operational set-ups, mathematical investigation of possible mechanisms of operation, computational optimization of cell structure ranging from nano- to macro-scale analysis of systems involving these cells.

After discovery by Nernst (Nernst 1899) of ionic conductivity of doped oxides the material was proposed to use as a base for oxygen generator and CO_2 utilization during extra-terrestrial missions (Weissbart & Smart 1967). The research at NASA continues until today (McKellar et al. 2010). First report aimed at commercial use of the SOEC was followed shortly after the initial NASA report and was prepared by researchers from General Electric R&D department (Spacil & Tedmon Jr. 1969). The paper investigated the SOEC as a potential technology for cheap and pure hydrogen production.

Several reviews are available on progress in the SOEC technology (Ebbesen et al. 2014, Ni et al. 2008, Laguna-Bercero 2012, Uhm & Kim 2014, Nechache et al. 2014), thus in this chapter the author only focuses on the review of modelling of cell and systems. The first published review on the modelling is the early version of this chapter (Stempien et al. 2013), it is the only published review focusing on the modelling of SOEC. The models of SOEC are most often based on the available models of SOFC, a review of modelling techniques of SOFC was performed by Kakac et al. (Kakac et al. 2007).

In this review the author focuses on cell modelling in the first subsection of this chapter and on the system level modelling in the second subsection of the chapter.

2.1 Cell-level models

It was briefly mentioned in chapter 1, that major research effort in Solid Oxide Electrolyzer Cell technology came mostly in recent decade. This may seem strange, given that the technology was investigated as early as in 1960's. The reason for this is that the low prices of fossil fuel at a time were not very favourable for further exploring

of this technology. The progress in SOEC technology was nevertheless made, however, under the domain of Solid Oxide Fuel Cells. As mentioned already, the models of SOEC a largely based on those developed for SOFC, thus it is important to briefly mention major areas and contributions made in the field before moving on to the more detailed review of models dedicated to SOEC.

The first part of chapter 2.1 will deal with modelling of electrode electrochemistry. The progress made in this area is directly applicable to SOEC. Moreover, it is still an active research topic, with most recent publications appearing just at the year of this writing. Second subsection of the review deals directly with the models of SOFC and is just a short mention of most important contributions.

The third section is dealing with the modelling of SOEC and is given in more detail in order to identify and highlight the research gaps and directions.

The last part focuses on few less popular areas of research in modelling of Solid Oxide Cells, including impedance spectroscopy modelling, degradation modelling and composite electrode microstructure modelling.

2.1.1 Chemistry and kinetics of the electrodes' processes

Multiple authors have proposed different mechanisms of the reaction occurring on the cell's electrodes. Thus far, there is no agreement on what is the actual mechanism of SOEC operation. Schouler (Schouler 1983) suggested electrocatalytic effect of the electrolyte surface as an important phenomena dictating the rate of electrochemical reactions. The author suggested that the concentration of oxygen vacancies and electronic conductivity of the interface are directly proportional to the reaction rate. Mizusaki et al. (Misuzaki et al. 1994) proposed to use the patterned electrodes with well-defined Triple Phase Boundary (TPB) in order to elucidate the mechanism of the reaction on the nickel electrode. The authors suggested that the rate of anodic reaction is limited by reaction between adsorbed oxygen on the nickel surface and gaseous hydrogen (fuel cell operation), whereas the cathodic reaction is limited by either surface diffusion of adsorbed hydrogen or the first order reaction of the hydrogen. Primdahl and Mogensen (Primdahl & Mogensen 1997) studied the oxidation of hydrogen on cermet Ni/YSZ electrode by means of impedance spectroscopy suggesting that the reaction is limited by three different processes depending on gas composition and cermet microstructure, also they proposed that the reaction zone spreads to 20 μm or less from

the interface. Jiang and Badwal (Jiang & Badwal 1997, 1999) also studied the hydrogen oxidation by means of spectroscopy. The first study was conducted on metal electrodes, the second on cermets. Similarly, they concluded that there are at least two processes controlling the reaction. The first is the adsorption/decomposition of hydrogen and the second being spillover of hydrogen followed by charge transfer at the YSZ surface. Holtappels et al. (Holtappels et al. 1999, 1999) studied the hydrogen oxidation on cermet electrodes at different temperatures and applied potentials, concluding that charge transfer is the rate limiting step at low temperatures and adsorption and chemical reaction of adsorbed species is dominant at high temperatures. Important contribution to understanding of the reaction mechanism was contributed by Mitterdorfer and Gauckler in a series of three papers (Mitterdorfer & Gauckler 1999, 1999, 1999). The authors proposed a model derived from a system and control theory to investigate the mechanism of oxygen reaction on Pt air electrode. The model is referred to in the literature as the space-state model. The resulting mechanism was limited by charge-transfer and surface diffusion for temperatures above 800°C and high oxygen partial pressure, whereas at lower temperatures and/or partial pressures the surface diffusion takes on more determinant role. Bieberle et al. continued the work with the space-state model analysing the reaction on the Ni patterned fuel electrodes (Bieberle et al. 2001, Bieberle & Gauckler 2002,) proposing that the reaction rate is limited by one process only at low overpotential and by two at high. The water was found to have a catalytic effect on the cell performance. However, no clear mechanism was found in the study. Williford and Chick (Williford & Chick 2003) used a simulation technique to question the common assumption that the electrochemical reaction is localized at the TPB, contrary, they proposed that the oxygen spillover on Ni surface is limiting the cell's performance. Goodwin et al. (Goodwin et al. 2009) explained experimental results of Mizusaki et al. (Mizusaki et al. 1994) to prove the hydrogen spillover as the mechanism of hydrogen oxidation on the patterned electrode. Large volume of research in reaction mechanism came from Germany (Bessler 2005, Bessler et al. 2007, Bessler et al. 2007, Gewies et al. 2007, Bessler et al. 2007, Rossmeisl & Bessler 2008, Vogler et al. 2009, Vogler & Bessler 2009, Bessler et al. 2010, Yurkiv et al. 2011, Bertei et al. 2012, Yurkiv et al. 2012, Yurkiv et al. 2012). The authors proposed to simulate the impedance spectroscopy based on the reaction kinetics and surface diffusion. The model was an alternative to state-space model. It was later expanded to allow of modelling I-V characteristics without the need of using Nernst equation, or Butler-Volmer equation.

The authors suggested that previously reported 'catalytic' effect of water is barely due to water concentration impact on the equilibrium potential, rather than any special catalytic or kinetic effect. Moreover, by comparing the standard equivalent-circuit impedance model with the proposed kinetic-diffusion model the authors linked the impedance features with their physical origins. The authors, performed quantum mechanical simulations to identify preferred materials for SOFC electrode and confirming the limiting character of oxygen spillover on the cell performance. However, in further publication the authors claim that the two hydrogen spillover steps are more plausible as rate determining, this was further confirmed in later publications for patterned electrodes. The authors also analysed a pathway of interstitial hydrogen, suggesting that it may be possible if there are some impurities in the electrode material. The authors analysed the mechanism of CO/CO_2 reaction on Ni/YSZ electrode suggesting that it follows two charge transfer processes and oxygen spillover step, later the authors suggested two different mechanism depending on the ratio of CO to CO_2. These findings were checked against the DFT simulation and suggested that it is possible to oxidize CO on bare YSZ surface without the metallic catalyst, given enough concentration of oxygen atoms on YSZ surface. The authors also proposed a model for mixed ionic conductor fuel cell, performing structure optimization of the cell.

More DFT study on hydrogen oxidation was contributed by Anderson and Vayner (Anderson & Vayner 2006). The authors suggest the mechanism based on hydrogen spillover from Ni to YSZ and later charge transfer as the limiting step. Mukherjee and Linic (Mukherjee & Linic) investigated the reaction on Cu, Co and Ni suggesting the oxygen spillover path. Alternative mechanism was proposed by Shishkin and Ziegler (Shishkin & Ziegler 2010) including the oxidation of hydrogen by an oxygen atom bound to both, the metal and zirconium (or yttrium). The proposed mechanism was later validated via experimental/kinetic modelling study by Yao and Croiset (Yao & Croiset 2014). Gorski et al. (Gorski et al. 2011) used DFT and temperature-programmed desorption (TPD) to analyse the reaction. The authors proposed refined adsorption/desorption and surface reaction kinetics data based on oxygen spillover mechanism.

Interesting modelling tool was used by Dar et al. (Dar et al. 2012) to investigate the oxidation of hydrogen on the cermet electrode. The authors used reaction route method to elucidate the reaction mechanism. The method is different to previously used, as it is not comparing different pathways (i.e. rate determining step is not apriori assumed),

rather it assumes that all of them are possible and later investigate which one has the lowest resistance. The authors suggest two hydrogen spillover mechanism and hydrogen spillover to oxide ion as the rate determining step.

Matsuzaki and Yasude (Matsuzaki & Yasuda 2000) where the first to analyse the mechanism of syngas oxidation on cermet electrode. The study was conducted at 800 °C and 1000 °C. The authors observed much faster kinetics (1.9 – 3.1 times faster) for hydrogen oxidation, than for CO oxidation. Much slower diffusion of CO and slower charge transfer were suggested as possible explanations. This research direction was later motivated by the ability to feed SOFC with natural gas. Zhu et al. (Zhu et al. 2005, 2006, 2012), proposed a model able to predict the performance of cell operated on gas mixture undergoing chemical reaction. Later, the authors extended the model to allow for modelling of the impedance spectra and analysed the effects of the surface chemistry on behaviour of impedance spectra. Hecht et al. (Hecht et al. 2005) investigated the kinetics of internal methane reforming within the cermet electrode support. Sukeshini et al. (Sukeshini et al. 2006) analysed the mechanism of syngas oxidation on patterned Ni electrodes suggesting that adding water to the mixture can lower the overpotential for CO oxidation. Janardhanan and Deutschmann (Janardhanan & Deutschmann 2006) performed a CFD analysis of SOFC including the electrochemical and catalytic processes. Shishkin and Ziegler (Shishkin & Ziegler 2008, 2009) performed a DFT study of the process. The authors found that hydrogen and methane can be oxidized on YSZ surface only if it is enriched by oxygen. The authors suggested that the reaction can occur either by spillover of hydrogen atoms from nickel to YSZ or by direct adsorption on oxygen enriched YSZ, contrary to previous findings suggesting oxygen spillover. Kleis et al. (Kleis et al. 2009) conducted DFT study of hydrogen, CO and methane oxidation over several transition metals. The authors suggested oxygen spillover as the mechanism of the oxidation and judge the performance of different materials by its adsorption energies towards the oxygen. Alternatively, they correlated the performance to the carbon adsorption energy. A group from Tsinghua University is the most recent contributor to the topic (Li et al. 2010, Shi et al. 2011, 2013). The authors proposed elementary reaction kinetics model for SOFC fuelled with syngas and CO/CO_2 mixture. They also proposed a model of reduction of CO_2 in SOEC. Xie and Xue (Xie & Xue 2012, 2012) proposed two models based on multi-scale electrochemical reaction model. The first model is used to predict the performance of hydrogen fuelled SOFC, later authors use the same model to predict the syngas production performance of SOEC.

2.1.2 Brief overview of Solid Oxide Fuel Cell modelling

One of the most profound early contributions to modelling of the SOFC was done by Achenbach (Achenbach 1994). In his paper, the author presented three-dimensional, time-dependent model of the SOFC stack. The model was aimed at optimizing the flow arrangement, gas recycling and heat interaction with surroundings. Another milestone was achieved by Costamagna at el. (Costamagna et al. 1998, 1998) with the first model of the cells composite electrode. The authors used the theory of the particle coordination number in random packing of spheres and percolation theory to investigate the optimum composition of the composite and the effects of electrode's microstructure on the cell's performance. Chan et al. (Chan 2001, 2001, 2002, 2004, Chen et al. 2004) proposed a complete polarization model based on Butler-Volmer equation, as well as Fickian and Knudsen diffusion. The proposed model is to date the most widely cited and forms the base of current state-of-the-art modelling. In later work, the authors combine their model with the technique proposed by Costamagna et al. and developed micromodels of anode and cathode. The authors also contributed an electrolyte model based on Nernst-Planck equation, rather than typically used Ohm's equation. The authors also analysed the mechanism of oxygen reduction on YSZ-LSM composite air electrode including two charge transfers and ion spillover to the YSZ. Zhu and Kee (Zhu & Kee 2003) extended the model proposed by Chan et al. to analyse performance of fuel cell's designed for direct oxidation of hydrocarbons. Suwanwarangkul et al. (Suwanwarangkul et al. 2003) compared available models for concentration overpotential of fuel electrode (the SOFC's anode) concluding that the Dusty-Gas Model is the most accurate model, however, can be supplanted by mathematically simpler Fick's law or Stefan-Maxwell law in some cases of simple H_2/H_2O or CO/CO_2 operation. Hernandez-Pacheco et al. (Hernandez-Pacheco et al. 2004) performed similar comparison of available activation overpotential and concentration overpotential models. The authors suggest the use of Butler-Volmer equation to predict the activation loss, however they note that Tafel or linear expression give only 5% error. The Dusty-Gas Model was suggested for concentration overpotential calculation. Noren and Hoffman (Noren & Hoffman 2005) further clarified the use of appropriate activation overpotential model suggesting that the Butler-Volmer equation should be used in modern cells operated at temperatures <800 °C. Deng and Petric (Deng & Petric 2005) proposed a model connecting the electrode's microstructure with the resulting Triple-Phase Boundary (TPB), the model

was based on that by Costamagna et al.. Nam and Jeon (Nam & Jeon 2006) combined the micromodel developed by Costamagna et al. and Chan et al. with the chemical kinetic models to comprehensively analyse intermediate temperature SOFC. Jeon (Jeon 2009) later implemented his model into commercial CFD package, Comsol. Ni et al. (Ni et al. 2007) proposed a simplified micromodel of SOFC by incorporation of Deng and Petric relation into exchange current density model, thus linking its value directly with electrode's microstructure. Ni et al. (Ni et al. 2007) later proposed the use of micro-structurally graded electrodes based on the results of their micromodel. Similar idea was analysed by Andersson et al. (Andersson et al. 2013). The authors used CFD approach to investigate the performance of SOFC with graded amount of electrochemical active sites along the flow direction. Shi and Xue (Shi & Xue 2011) proposed an algorithm to extract properties of porous electrodes from cell's polarization curve. Recently, Henke et al. (Henke et al. 2013) proposed a model for SOFC stack operated at elevated pressure.

2.1.3. Modelling of the Solid Oxide Electrolyzer Cell

The first modelling study on Solid Oxide Electrolyzer Cell was conducted at the end of 1960's when Spacil and Tedmon Jr (Spacil & Tedmon Jr. 1969) simulated the cell behaviour considering the ohmic and concentration losses. The authors suggested to connect the cells in series in order to limit the heat loss from the electric connection ending. Developments in the 70's and 80's were focused on experimental side, whereas the modelling effort of 90's was focused on the fuel cell. The next major contributions in SOEC modelling came only in 2000's. Hawkes et al. (Hawkes at al. 2005, 2009) implemented an electrochemical model of SOEC stack into commercial CFD package, Fluent. Later, O'Brien et al. (O'Brien 2005) compared the 3D results with 1D model concluding only small deviations in accuracy of predicted characteristics. The same group reported a syngas production equilibrium model (Stoots et al. 2009).

Ni et al. (Ni et al. 2006, 2006, 2007, 2007, 2007, Ni 2010, 2012, 2012) contributed largely to modelling of SOEC and is one of the most cited authors in the field. In 2006 the authors published a study on concentration overpotential in the SOEC developing formulae for use in both, the fuel cell and the electrolyzer. Between 2006 and 2007 the authors developed electrochemical model for hydrogen production, coupled it with the mass transport model suggested by Costamagna et al. (Costamagna et al. 1998) and Chan et al. (Chan et al. 2001) for fuel cells. They later performed the optimization of the

cell structure and energy and exergy analysis of hydrogen production system. Ni then proposed an electrochemical model of CO_2 electrolysis and later combined it with the H_2O electrolysis to report first electrochemical model for co-electrolysis in 2012. The model was later implemented in a CFD in-house developed code.

Another important contribution comes from Imperial Collage London group of N. P. Brandon (Udagawa et al. 2007, 2008, 2008, Cai et al. 2010, Iora et al. 2009, 2012). Udagawa et al. proposed a dynamic model for steam electrolysis and used it to propose a control strategy for heat management of the cell. The results of the dynamic model were compared with the steady-state model. This research was later continued by Cai et al. who performed a parametric study of the system. Iora et al. extended the proposed cell model to the stack level including detailed heat transfer modelling and used it to study a system for high purity oxygen production. Similar study was conducted by Dillig and Karl (Dillig & Karl 2012) who analysed heat management of SOEC/SOFC system with integrated heat pumps in order to thermally balance the cell. The authors concluded that integration of heat pipes can dramatically improve the temperature distribution throughout the stack.

Several modelling papers were published in Franco-German cooperation (Grondin et al. 2010, 2011, 2013 Laurencin et al. 2011, Lay-Grindler et al. 2013). Grondin et al. proposed a model based on Butler-Volmer equation to predict the polarisation characteristics of the cell, however, the estimated values of exchange current densities are much higher than usually reported. In the later research the authors substituted the use of Butler-Volmer equation with the chemical kinetic equations. The substitution resulted in better reproduction of polarisation characteristics. In their next paper the authors proposed to use artificial neural network to describe the surface chemistry on fuel electrode of SOEC. Laurencin et al. proposed a 2D model with the use of the Dusty-Gas model for diffusion and focused on thermal aspects of the cell's operation. Lay-Grindler et al. combined percolation and coordination number theory based micromodel with surface chemistry of oxygen formation on LSM-YSZ cermet electrode. The authors analysed several possible degradation mechanisms by manipulating respective conductivities and electrode microstructure to assess their impact on the performance drop.

Dumortier et al. (Dumortier et al. 2012, 2012, 2014) proposed a CFD model of SOEC/SOFC. The proposed model included the effects of gas velocity, suggested using the gas composition in calculation of activation overpotential, and use of cermet surface

ratios rather than volumetric ratios. The authors also analysed the effects of electrode parameters and energy transport on parameters distribution. The authors, later linearized their model to predict the thickness of reaction layer inside the cermet electrode.

The group from Tsinghua University contributed several papers (Li et al. 2013, 2014, Luo et al. 2014). Li et al. proposed elementary kinetics model of co-electrolysis cell based on reaction model developed by Janardhanan and Deutschmann. The authors proposed a micromodel of co-electrolysis based on percolation and coordination number theories and adopted it to be utilized for both SOEC and SOFC simulations. Luo et al. proposed a 2D model for co-electrolysis in tubular SOEC.

Kazempoor and Braun (Kazempoor & Braun 2014, 2014) proposed an electrochemical model of SOEC/SOFC operated in co-electrolysis or fed with natural gas, respectively.

Demin et al. (Demin et al. 2007) proposed a simple model for co-ionic electrolyte based SOEC. The authors later analysed the performance of the cell operated in co- and counter-flow as well as the impact of the electrolyte proton transfer number. Jin and Xue reported a dynamic 2D model of SOEC/SOFC and analysed the switching between the modes. Garcia-Camprubi et al. (Garcia-Camprubi et al. 2014) utilized CFD model of SOEC/SOFC to compare different techniques of fitting the parameter values for exchange current density and charge transfer coefficients.

2.1.4. Modelling of impedance spectroscopy

One of the most utilized experimental technique to investigate the performance of the Solid Oxide Cells is the impedance spectroscopy. However, the use of this method can only provide a qualitative analysis. In order to quantify the resistance of the processes influencing the impedance spectra it is necessary to use the model systems. A review of the proposed models was done by Sunde (Sunde 2000), Fleig (Fleig 2003) and most recently by Nielsen and Hjelm (Nielsen & Hjelm 2014).

Modelling of impedance spectra is not very popular method in SOC modelling, however few works require to be mentioned. Sunde (Sunde 1997) was one of the first authors to take on the topic of impedance modelling. The author used artificially generated three-dimensional impedance network consisting of electrode and electrolyte particles and then applied Kirchhoff's current law to calculate the impedance of the created networks. More recently Mortensen et al. (Mortensen et al. 2014) proposed an analytical 1D model of impedance of composite fuel cell cathode. The authors succeeded in reproducing large

amount of impedance spectra covering impressively wide range of conditions.

2.1.5 Modelling of degradation

Solid Oxide Cells degradation is the most serious barrier preventing the technology from the commercialization. Several mechanism of degradation have been successfully identified and efforts are being put to develop new generation of cells resistant to degradation (Kim et al. 2013, Mocoteguy & Brisse 2013, Hjalmarsson et al. 2014, Keane et al. 2014).

Most of the modelling work investigates the reason for critical cell failure by means of air electrode delamination. The largest contribution in this area can be attributed to Virkar et al. (Virkar 2007, 2010, Virkar et al. 2014) who suggested that the delamination is a result of developing of extremely high pressure in the cavities between the air electrode and the electrolyte. In his first paper, he suggested this mode of degradation for fuel cells operated in stack and derived all the basic formulae relating the oxygen pressure with the applied voltage. This theory was criticized by Jacobsen and Mogensen (Jacobsen & Mogensen 2008) who misinterpreted some assumptions and actually ended up supporting the Virkar's theory and proposing this mechanism to occur in SOEC. Virkar later applied his qualitative model to analyse the delaminations in electrolyzers, however, due to lack experimental parameters no solid proof was given. Moreover, for the mechanism to be valid, certain degree of electronic conductivity in YSZ was essential. A requirement usually dismissed as negligible. Recently, Virkar et al. have presented the validation of Virkar's theory with experimental data. Jin and Xue (Jin & Xue 2010) performed simplified CFD study analysing operation of the SOEC with crack between the air electrode and the electrolyte. The authors suggest that the delamination may occur due to thermal expansion mismatch between the air electrode and the electrolyte. Rashkeev and Glazoff (Rashkeev & Glazoff 2012) performed a DFT study of LSM/YSZ interface suggesting that high temperature atomic migration across the interface can significantly affect its structural stability, thus allowing for delamination due to oxygen pressure build up.

Jensen et al. (Jensen et al. 2013) modelled degradation in SOEC's impedance spectra and concluded that the long term degradation only occurs in Ni-YSZ electrode and relates to electrochemical reaction resistance evolution at the TPB.

2.1.6 Modelling of 3D structures and its influence on cell performance

The use of complex composite electrodes greatly enhances the performance of the Solid Oxide Cells, mostly because of densification of the Triple Phase Boundary (i.e. the reaction zone). However, the use of composite electrodes introduces the modelling problem, as it is very difficult to reproduce those complex geometries, moreover they tend to vary from case to case. Recent advances (Grew et al. 2010, Cumming et al. 2013, Kennouche et al. 2013) in 3D imagining techniques promises interesting prospects in the modelling of the composite electrodes, however this branch of research is still in its infancy. Hertz and Tuller (Hertz & Tuller 2007) proposed a model for constriction of current due to narrowing of the current passage path at the Triple Phase Boundary of the ionically-blocking electrodes. Choi et al. (Choi et al. 2011) proposed an algorithm to calculate effective transport properties from 3D reconstructed image of the SOC electrode. Holzer et al. (Holzer et al. 2013) also combined the effort of Hertz and Tuller and Choi et al. by developing an algorithm linking effective transport properties with the constrictivity, tortuosity and volume fraction of electrode's constituent materials. Nelson et al. (Nelson et al. 2011, 2012) analysed the effects of varying cross-section of charge transfer path on the charge transfer resistance by means of model derived from heat transfer's fin approximation model. The authors performed 1D and 2D analysis of different designs giving a handy tool to judge the quality of sintering process and suggested using it instead of generally used approach of effective parameters. Synodis et al. (Synodis et al. 2013) performed similar analysis on recently popular infiltrated electrodes to link the percolation threshold and effective conductivity with infiltrate size, pore size and porosity. More recently Usseglio-Viretta et al. (Usseglio-Viretta et al. 2014) used microstructure description derived from 3D reconstruction to simulate Ni-YSZ electrode polarization. The authors demonstrated the usability of the 3D reconstruction in extraction of effective parameters for micro-level models.

2.2 System-level models

Cell-level models are aimed at understanding the principles of operation, optimizing the microstructure and materials choice or testing different configurations of cells. The system-level models can provide information on how the cell can be used, what benefits can it bring or simply how much money a system composing of those devices can earn.

The papers published on Solid Oxide Cells usually focus on analysing new possible applications, comparing the technology against its competitors or to evaluate the economics of a system composing of the SOCs.

2.2.1 Economic analysis

Damen et al. (Damen et al. 2006) compared several electricity and hydrogen production systems with CO_2 capture and storage. They included analysis of SOFC as a potential electricity generation device in two variants. The first assumed combining the fuel cell with a gas turbine and feeding it with gas produced from coal gasification, the second considered combining SOFC with a gas turbine and feeding it with natural gas. The authors performed economic analysis and predicted that the coal gasification variant could be price competitive with existing technologies. The variant with natural gas feed was predicted to be the most expensive among the electricity generation variants. The authors did not analyse the production of hydrogen via SOEC. Gahleitner (Gahleitner 2013) envisaged a production of renewable hydrogen and focused on reviewing existing pilot plants of power-to-gas. The report covers all existing and planned plants based on utilizing renewable electricity in conjunction with electrolyzer technology. The majority of analysed systems were based on alkaline and PEM electrolyzers. None of the investigated system utilized the SOEC thus far, however, the author mentions in the outlook the benefits of storing renewable energy in form of synthetic hydrocarbons. In such scenario, SOEC carry an advantage over other technology due to its ability to produce syngas, a feed in most hydrocarbon synthesis processes. Ridjan et al. (Ridjan et al. 2013, 2014) analysed the feasibility of synthetic fuels in 100% renewable energy system with special focus on fuels production by means of the SOEC. The authors compared the prices of producing methanol and methane in SOEC with prices of production of biofuels. The conclusion was that the production cost of synthetic fuels is comparable to that of petrol production cost if the cost of CO_2 emissions is included in the price of petrol. Ferrero et al. (Ferrero et al. 2013) compared the production of hydrogen via the SOEC and PEM electrolyzer. The authors performed energy and exergy analysis concluding that SOEC is better choice if operated at current densities over 0.25 A cm^{-2} and that the efficiency is increased up by 14% in the case of SOEC. Fu et al. (Fu et al. 2010) assessed the economics of syngas production via the SOEC concluding that the process is economically competitive with biomass-to-liquid

processes given the source of electricity to drive the electrolyzer is nuclear energy or the surplus wind energy. Manage et al. (Manage et al. 2011) conducted a techno-economic analysis of hydrogen production linking the price of electricity and efficiency of hydrogen generation to resulting price of hydrogen. The authors predict that if SOEC is operated at 100% efficiency and coupled with nuclear power source it can be already competitive with steam-methane reforming technology. Patyk et al. (Patyk et al. 2013) performed a life cycle assessment of hydrogen generation from the SOEC and compared it with large scale steam-methane reforming (SMR). The author predicts that in all analysed cases of electricity source to the electrolyzer the life cycle emission of CO_2 is lower than for the SMR. However, only coupling with the wind power gives lower overall energy requirement for the process. The results were most sensitive to manufacturing cost of the SOEC and cost of electricity supply to the electrolyzer. Becker et al. (Becker et al. 2012) provided a techno-economic analysis of combined Fischer-Tropsch and SOEC systems. The authors utilized a simplified model of both processes to predict an overall system efficiency of 51% and possible price of liquid fuel at 4.4 $ per gallon of gasoline equivalent.

2.2.2 Technical analysis

First purely technical system analysis of SOEC systems was performed for NASA by Sridhar et al. (Sridhar et al. 2004). The authors analysed the possibility of resource utilization for Mars missions. They compared the SOEC-based system with other able to perform similar functions and concluded that the Solid Oxide system has the highest power density and is easy to scale. O'Brien et al. (O'Brien et al. 2009) used simple linear model of co-electrolysis to evaluate a large scale syngas production plant. The authors predicted overall power efficiency of up to 55% when combining SOEC with a nuclear reactor. McKellar et al. (McKellar et al. 2010) compared three closed-loop atmosphere revitalization systems for application in space exploration missions. The authors concluded that incorporation of co-electrolysis into existing processes based on Sabatier and Bosch reaction can reduce the requirement for energy. They identified the combined hydrogenation and co-electrolysis as the best candidate for NASA application. Perdikaris et al. (Perdikaris et al. 2010) analysed a tri-generation system producing electricity, heat and hydrogen in a carbon free manner via combined SOEC/SOFC fed with natural gas. The authors used linear model of the electrochemical cell and predicted

efficiency of ~28% for electricity, ~18% for hydrogen and ~26% for heat generation, i.e. overall natural gas conversion efficiency of ~72%. A similar system was proposed by Iora et al. (Iora et al. 2010), the authors reported the value of overall efficiency which is almost identical with that reported by Perdikaris et al.. Zhang et al. (Zhang et al. 2013, 2013) used a simple overpotential model of SOEC to investigate the efficiency of two systems, the first combining solar energy with the SOEC to produce hydrogen, the second aimed at reducing the CO_2. In the first study authors predict the overall efficiency of solar hydrogen system at ~45%. In the second study authors proposed five systems aimed at CO_2 reduction based on the amount of heat generated in the cell, no efficiency number was reported, however. Peters et al. (Peters et al. 2013) analysed SOFC system concepts including anode gas recycling in order to increase the fuel efficiency and the water requirement for reforming. The authors used simple thermodynamic model and concluded that recycling is a viable option resulting in overall energy efficiency of 50 – 66% depending on configuration. The fuel electrode gas recycling is also important in the electrolyzer in order to provide sufficient amount of hydrogen to prevent the electrode reduction. Petipas et al. (Petipas et al. 2013) analysed operation of SOEC at various loads. The authors used simple thermodynamic model and predicted that the system can achieve constant 91% efficiency (HHV) of hydrogen production for loading above 60% and thermoneutral operation. Below that utilization, external heating is required. The authors also analysed the case of supplying steam to the electrolyzer, rather than water (Petipas et al. 2014). The modification resulted in jump of efficiency to ~110% vs hydrogen (HHV).

2.3 Summary

To summarize the trends in modelling of Solid Oxide Cells, a few points are brought forward:

- Models making use of 3D reconstruction of electrodes have started to appear in open literature. This method can disambiguate the actual chemical, electrochemical and surface reactions occurring inside the cell's electrodes,
- Analytical solutions of transport and electrochemical phenomena have enhanced the understanding of complex impedance spectra and its evolution during the cell's lifetime,
- First-principle studies are used to identify the possible future materials for cell's

electrode and to clarify the reaction mechanisms. However, ambiguity still exist in modelling electrostatically polarized materials.

- Non-linear models linking the gas composition, operating temperature and pressure, etc. are more commonly used in system level studies, making it viable to optimize systems for desired performance.

Future direction in modelling of SOEC may include, first-principle models including externally applied electric field, reaction mechanism investigation under the electrical bias, use of 3D reconstructions with elementary physical equations and highly non-linear system level models.

The research gaps identified and filled by the author include:

- co-electrolysis micro-model of SOEC,
- extreme oxygen electrochemical potential difference model and its consequences,
- investigation of fuel electrode gas recycling effects on SOEC performance,
- complex multi-level models of CO_2 mitigation, load balancing/energy storage and sustainable fuels production systems.

Chapter 3. Fundamental aspects of Solid Oxide Electrolyzer Cell operation and modelling

3.1 Introduction

In this chapter the author briefly introduces fundamentals of operation of SOEC and its mathematical modelling based on these fundamental physical principles. In sections 3.2 to 3.4 state-of-the-art modelling approach is presented as reported in the open literature and most commonly used. Sections 3.5, 3.6 and 3.7 are the author's own input to modelling.

The author's contribution includes analysing the operation of electrolyzer under extreme oxygen potential difference and proposal of appropriate modelling approach (chapter 3.5). The author of this thesis also analysed the physical principles behind establishment of equilibrium potential in SOEC operated in co-electrolysis mode and proposed a physically based model of the phenomena (chapter 3.6). The author also proposed modelling of activation overpotential with inclusion of electrode's microstructure (chapter 3.7). The contents of chapters 3.5 and 3.6 were published as two international, peer-reviewed journal papers. The model from chapter 3.7 has been first reported in two system level peer reviewed journal papers on CO_2 mitigation system.

3.2 Physical fundamentals of the Solid Oxide Electrolyzer Cell

Solid Oxide Electrolyzer Cell (SOEC) or Solid Oxide Steam Electrolyzer (SOSE) (Fig. 3-1) is an electrochemical energy conversion cell which allows transforming electrical energy of passing current to chemical energy of fuel. Typical SOEC is capable of producing carbon monoxide, hydrogen and mixture of both by electrochemical reactions. It continues to deliver the fuel as long as steam and/or carbon dioxide and electrical energy are supplied.

In reality lifetime of the cell is limited by degradation of its components (see chapter 2.1.5). Cell is based on semi-permeable properties of mixed (doped) solid oxides. The most commonly used is Yttrium Stabilized Zirconium (YSZ), which allows transporting oxygen ions when polarized with electrical field. There are also other, less popular kinds of SOEC: i.e. co-ionic cells and proton conducting cells, where both oxygen and

hydrogen ions or only hydrogen ions are transported through the membrane. This work is limited to oxygen ion conducting cells (not necessarily based on YSZ). Aforementioned doped oxide is playing the role of electrolyte, which is sandwiched between two electrically connected porous electrodes and thus creates closed electrical circuit. Beside Positive Electrode-Electrolyte-Negative electrode (PEN) assembly, cell consists of interconnects and gas channels. Present design of the cell follows directly from that of solid oxide fuel cells, thus description of it is omitted in this work and reader is referred to any review article or book on SOFC available on the market (e.g. Milewski et al. 2011). It is worth mentioning, though, that since the cell is made of solid components, it is possible to shape it according to desired specification.

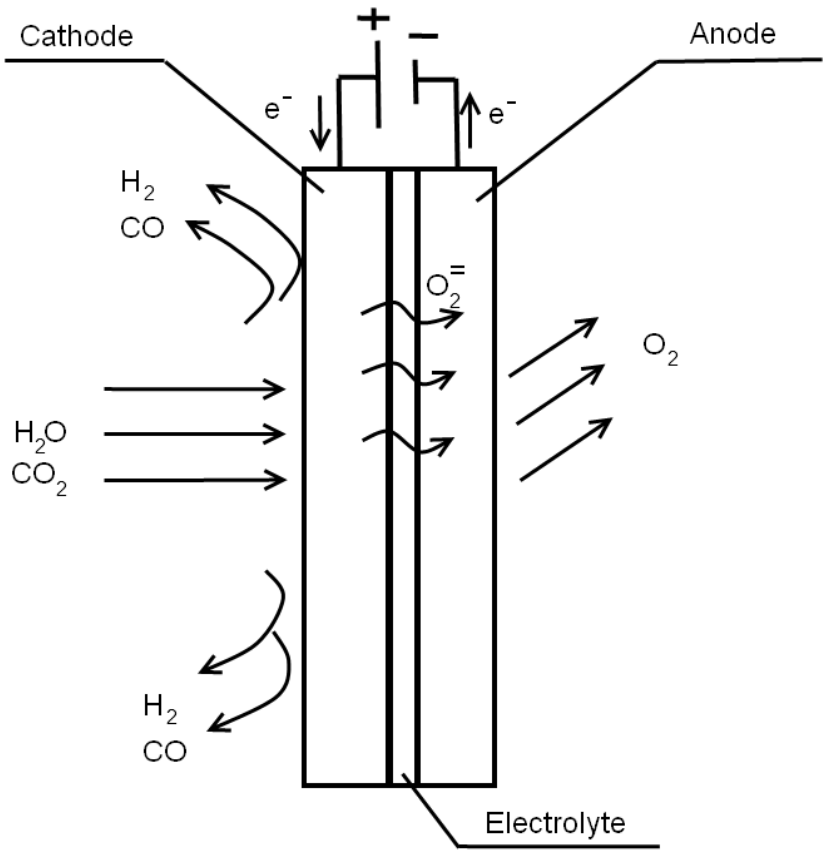

Fig. 3-1 – Solid Oxide Electrolysis Cell schematic.

Like SOFC, electrolysis cells can be connected in series to form a stack. SOEC shares design flexibility and high operational efficiency with SOFC. Current status of cell development allows using one cell both, as SOEC and SOFC, depending on polarization. This presents interesting possibilities of application of the Solid Oxide Cell (SOC).

Operation of SOEC, as complicated as it is in detail, is relatively simple to explain in general. On cathode side of the cell steam and/or carbon dioxide is delivered, mixture of gases penetrates through porous electrode to reach triple phase boundary where it reacts with electrons to split to hydrogen and/or carbon monoxide and oxygen ions. Oxygen ions, then, are being transferred to the anode side through an electrolyte, where another Faradic reaction occurs splitting anions to electrons and oxygen molecules. Oxygen permeates to the anode gas channel and out of the cell, while electrons follow the electrical circuit back to the cathode, thus closing the cycle. If the cell is operated with high enough voltages (over the thermoneutral threshold, Equation 1-3) it produces not only synthetic fuel, but also heat. The cell can operate in temperature range from 450 °C to 1000 °C, with atmospheric or elevated pressures.

While the exact steps of the reaction are under speculation (see chapter 2.1.1), scientists have been using several relatively uncomplicated laws to predict behaviour and performance of the single cell or stack design.

3.3 Introduction to modelling

Modelling of any physical process can be done in several ways (Fig. 3-2) depending on the purpose of the simulation. One of the basic distinctions is between empirical and phenomenological modelling. Empirical modelling has developed recently alongside with rise of computer capabilities. It does not require full understanding of the physics behind the process. It is even possible to model a phenomenon without any knowledge of its mechanism. Such models are called “black boxes”, they are based on artificial intelligence, genetic programming, etc. Process or device is recognized literally as a box with i-th number of inputs and j-th number of outputs (Fig. 3-3). Large amounts of experimental data are necessary to calibrate them. Phenomenological models are based on laws of physics and they provide good explanation to why process behaves the way it does. All of the parameters in such models have physical meaning, unlike in empirical or semi empirical models.

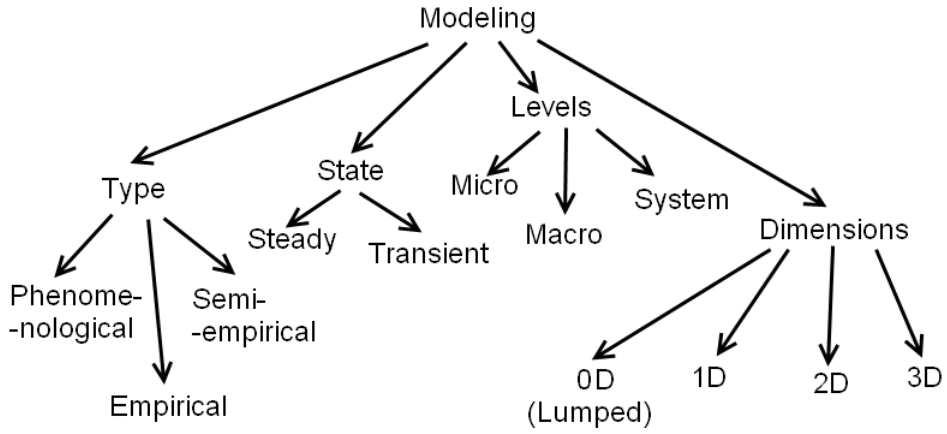

Fig. 3-2 – Possible distinctions of modelling.

Nowadays, due to low availability of material properties, combinations of both models are used. To authors best knowledge there has not been fully empirical model of SOEC developed to date. It is worth mentioning that there are few empirical models of SOFC available (Grondin et al. 2013). Nevertheless, they did not gain any popularity, probably due to in significant contribution towards understanding of the physical fundamentals of the electrolysis phenomena.

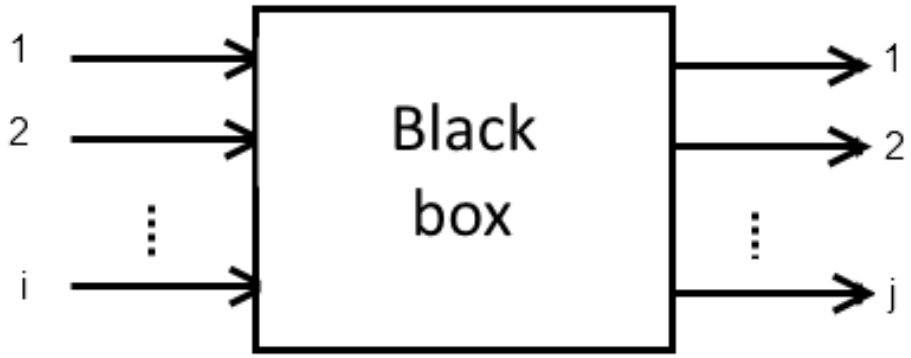

Fig. 3-3 – Black box model.

Modelling study in the early stages of device development is usually done in steady state, meaning time independent. These kinds of models are used to evaluate general, design parameters of the process. Transient, time dependent models are useful for safety considerations, control strategy design and any other system dynamic properties or responses.

Another way to divide models is by scale used. When energy processes are being

considered a system level scale is very important, where SOEC is just small part of a bigger plant. If optimization of design is considered, then macro- and micro-scale models are used. Available literature is either on one or the other scale. There is in general no universal model combining two or more scales, thus allowing speculation on performance of SOEC in some abstract, far from experimentally studied, plant.

When system level modelling is considered SOEC electrochemistry is usually modelled by one linear equation combining voltage with current. In general performance of cell is fixed and independent of operating conditions. Such models can be used for some basic feasibility studies, however with a limited applicability.

Macro- and micro-level models are much more sophisticated. In micro-level simulations complex statistical theories are used to assess the performance of cermet electrodes. Macro-level models are in between system and micro-level, they are most commonly used. They provide decent trade-off between choice of control parameters and computational efficiency.

The last type of distinction proposed in this work is by number of analysed dimensions. This division can be associated with previous one, system-level models are usually zero dimensional, macro-level models are 1D, 2D or 3D. Micro-level models are usually 1D or 2D. In general, the lower the number of dimensions involved, the faster the calculations. Considering geometry of the cell one can easily notice that one of the dimensions, i.e. thickness, of the cell is much smaller than all others, hence one-dimensional models should be effective for cell modelling. Three dimensional models are usually used for stack configuration design and thermal balance studies.

Vast majority of available models aim at predicting electrical performance of the cell, fuel conversion & output and cell/system efficiency, thus are electrochemistry-based.

It is generally advised to become acquainted with a review paper or a book on SOFC modelling before approaching this work (Kakac et al. 2007, Milewski et al. 2011).

3.4 Theory of the Solid Oxide Electrolyzer Cell modelling

Performance of Solid Oxide Electrolysis Cell depends largely on reaction rates occurring on Triple Phase Boundary, operating temperature and pressure, applied potential difference, and microstructure of the cell. These need to be included in the modelling. Net reactions for the cathode are

$$H_2O(g) + 2e^- \rightarrow H_2(g) + O^= \quad (3\text{-}1)$$

$$CO_2(g) + 2e^- \rightarrow CO(g) + O^= \quad (3\text{-}2)$$

whereas for the anode

$$O^= \rightarrow \frac{1}{2}O_2 + 2e^- \quad (3\text{-}3)$$

The overall co-electrolysis reaction can be written as

$$H_2O + CO_2 \rightarrow H_2 + CO + O_2 \quad (3\text{-}4)$$

In reference to electrolyte process mechanism, these reactions can be written in the following form. For the cathode:

$$H_2O(g) + 2e^- + V_O^{\cdot\cdot} \rightarrow H_2(g) + O_o^x \quad (3\text{-}5)$$

$$CO_2(g) + 2e^- + V_O^{\cdot\cdot} \rightarrow CO(g) + O_o^x \quad (3\text{-}6)$$

whereas for the anode:

$$O_o^x + 2\dot{h} \rightarrow \frac{1}{2}O_2(g) + V_O^{\cdot\cdot} \quad (3\text{-}7)$$

For electron – electron hole pair:

$$2\left(e^- + \dot{h}\right) \leftrightarrow 0 \quad (3\text{-}8)$$

As already mentioned real reactions mechanisms are complex and still not well investigated, above reactions are used as simulation simplifications. Reaction rates depend on temperature, pressure, concentration of products, time in the reaction zone and catalyst used. Unfortunately, models developed to date lack the sufficient consideration of kinetics of reaction. They are based on assumed, constant value of product conversion. Such models are unable to predict performance of the cell for conditions which were not investigated experimentally.

Limiting processes involved in cell operation are discussed to be:

- Porous Gas Diffusion.
- Adsorption/Desorption.
- Surface Diffusion.
- Reaction Kinetics.
- Charge Transfer.
- Electrolyte Transport.

These processes, excluding adsorption/desorption, surface diffusion and reaction kinetics, are usually modelled with use of Butler-Volmer equation, Ohm's law, Faraday's law and one of several gas transport laws.

Modelling of SOEC focuses on predicting current-voltage curves, electrical losses sources, fuel production yield and several thermodynamic parameters of operation, i.e. efficiencies, fuel conversion, etc. Typically, different level models are capable of predicting different data and accuracy of predictions usually drops with increasing the scale of model.

In this section two most popular types of models will be discussed, micro- and macro-level models. System-level design is skipped due to its simplicity.

Macro-model design is based on Faraday law, Butler-Volmer equation, Ohm's law and gas transport equations. Faraday law is connecting applied current to flow of oxygen ions through the electrolyte. Ohm's law corresponds to the loss associated with the flow of oxygen ions in between triple phase boundaries on each side of electrolyte (often assumed electrolyte thickness). Most commonly it is assumed that electrodes have negligible electronic resistance, thus Ohm's law is limited to electrolyte. Butler-Volmer equation is modelling the increase in potential to activate the reaction on each of the electrodes. Gas transport law links drop of performance with concentration gradients across electrode gas channel and Triple Phase Boundary (often assumed thickness of electrode). Dusty gas model has been proved as the most appropriate and is most widely used to model diffusion process. Other applied models are Fick's law and Stefan-Maxwell's law.

Micro-models additionally use percolation theory to describe processes occurring on cermet electrodes.

Due to compactness of the following work all derivations are limited and reader is being introduced mostly only with results, necessary assumptions and boundary conditions where applicable.

3.4.1 Classical approach – macro-model.

The most common way to model SOEC is when limiting processes mentioned in previous section are described by introduction of overpotentials. This nomenclature follows from electrochemistry and can be categorized in few subgroups. Namely: concentration overpotentials occurring in both electrodes, activation overpotentials occurring in both electrodes and Ohmic overpotentials occurring in all electrolyte and both electrodes (Fig. 3-4).

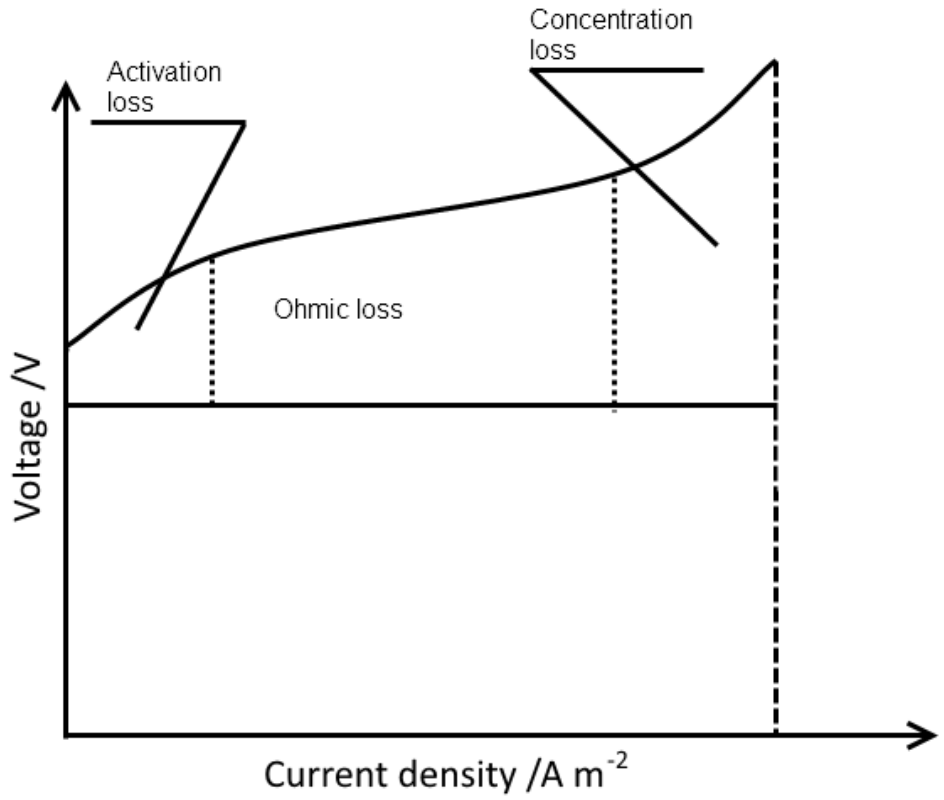

Fig. 3-4 – Classical I-V characteristics of SOEC.

Some researchers also considered so-called offset overpotential which is assumed mainly due to contact resistance and is constant. All other overpotentials are functions of operating conditions. In this approach potential difference at the cell electrical terminal is expressed as follows

$$E = E_0 + \eta_{act,an} + \eta_{act,cat} + \eta_{ohm,an} + \eta_{ohm,cat} + \eta_{ohm,elec} + \eta_{con,an} + \eta_{con,cat} + \eta_{offset} \quad (3\text{-}9)$$

where E_0 is the electrochemical potential or electromotive force equation (1-2).

3.4.1.1 Open circuit voltage

At the open circuit, electrochemical potential is the minimum potential difference required to split steam/carbon dioxide, or in SOFC mode maximum electromotive force possible to obtained from converting the fuel gases. It can be calculated by considering minimum work concept of thermodynamics. For an open system operating in steady state first law of thermodynamics implies following:

$$0 = H_i - H_o + Q - W \tag{3-10}$$

The second law can be expressed as:

$$0 = S_i - S_o + \frac{Q}{T} + S_{gen} \tag{3-11}$$

The concept of minimum work requires assumption of reversible operation, hence S_{gen} is equal zero and heat from Equation 3-11 can be written as:

$$Q = T(S_o - S_i) \tag{3-12}$$

Now substituting Equation 3-12 into Equation 3-10 and realizing that reversible system requires minimum work input to operate:

$$0 = H_i - H_o + T(S_o - S_i) - W_{min} \tag{3-13}$$

Realizing the definition of Gibbs function, one can write

$$W_{min} = -\Delta G \tag{3-14}$$

To calculate the minimum work input to the system, change in Gibbs potential for overall reaction is needed.

Minimum work can also be written as the integral over time of power consumed:

$$W_{min} = \int_0^t E(t)I(t)dt \tag{3-15}$$

If the applied voltage is constant (*E(t)=const*), then Equation 3-15 can be written as:

$$W_{min} = E_0 \int_0^t I(t)dt = E_0 q \tag{3-16}$$

Amount of charged transferred for 1 mole of fuel can be expressed as:

$$q = zF \tag{3-17}$$

Putting Equation 3-17 into Equation 3-16 and back to Equation 3-13 yields basic electrochemistry relation:

$$E_0 = -\frac{\Delta G}{zF} \tag{3-18}$$

Gibbs potential for ideal gas mixtures can be calculated using:

$$G_i = G_i^0 + n_i RT ln\left(\frac{p_i}{p_{std}}\right) \tag{3-19}$$

Where, n_i is the number of moles of gas species *i*
From the definition of chemical potential:

$$\mu_i = \left(\frac{\partial G}{\partial n_i}\right)_{T=const,P=const,n_j=const} \tag{3-20}$$

One can obtain relation for standard Gibbs potential $G^0=n\mu^0$, using this Equation 3-19 can be written in the following form

$$G_i = n_i \mu_i^0 + n_i RT ln\left(\frac{p_i}{p_{std}}\right) \tag{3-21}$$

If the reaction of ideal gases in the ideal mixture is considered, the change in Gibbs potential can be expressed as:

$$\Delta G = \sum G_i(products) - \sum G_j(reactants) \tag{3-22}$$

In the simplest case, when the cell is fed with steam the overall reaction follows

$$\mathrm{H_2O} \rightarrow \mathrm{H_2} + \frac{1}{2}\mathrm{O_2} \tag{3-23}$$

Using Equations 3-21 and 3-22 change of Gibbs potential can be written as:

$$\Delta G = \mu^0_{H_2} + RTln\left(\frac{p_{H_2}}{p_{std}}\right) + \frac{1}{2}\mu^0_{O_2} + \frac{1}{2}RT\,ln\left(\frac{p_{O_2}}{p_{std}}\right)$$
$$-\mu^0_{H_2O} - RTln\left(\frac{p_{H_2O}}{p_{std}}\right) \tag{3-24}$$

At equilibrium it can be written in the form:

$$\Delta G^0 = \mu^0_{H_2} + \frac{1}{2}\mu^0_{O_2} - \mu^0_{H_2O} \tag{3-25}$$

Putting Equation 3-25 into 3-24 gives:

$$\Delta G = \Delta G^0 + RTln\left[\frac{p_{H_2}p_{O_2}^{\frac{1}{2}}}{p_{H_2O}p_{std}^{\frac{1}{2}}}\right] \tag{3-26}$$

Similar derivation can be applied to the reaction of carbon dioxide electrolysis and then substituting Equation 3-26 into 3-18 and using the relation between partial pressure and molar fraction yields:

$$E_o^{H_2O} = -\frac{\Delta G_{f,H_2O}(T)}{2F} - \frac{RT}{2F}ln\left[\left(\frac{y_{H_2O}}{y_{H_2}y_{O_2}^{\frac{1}{2}}}\right)\left(\frac{P}{P_{std}}\right)^{-\frac{1}{2}}\right] \text{ or}$$
$$E_o^{CO_2} = -\frac{\Delta G_{f,CO_2}(T)}{2F} - \frac{RT}{2F}ln\left[\left(\frac{y_{CO_2}}{y_{CO}y_{O_2}^{\frac{1}{2}}}\right)\left(\frac{P}{P_{std}}\right)^{-\frac{1}{2}}\right] \tag{3-27}$$

Note that Equation 3-27 is only valid for non-reacting gas mixtures, hence for co-

electrolysis mixture must be brought to the chemical equilibrium or to quasi-equilibrium before applying the equation. Moreover, as will be shown in chapter 3.6 a superposition of above potential differences is actually observed. Reaction occurring in steam/carbon dioxide mixture is the Water Gas Shift Reaction (WGS) or the Reversed Water Gas Shift (RWGS) reaction depending on the temperature of mixture. Equilibrium temperature is about 827 °C. Below this temperature the former reaction proceeds, above it the later. Reaction follows formula according to Equation 3-28. One may wonder why there is hydrogen in the feed mixture of SOEC. The reason for that is to prevent Nickel particle in the cathode from oxidation. By adding the hydrogen, the resulting oxygen partial pressure of the mixture, ergo ability to oxidize, is greatly reduced.

$$\mathrm{CO} + \mathrm{H_2O} \rightleftarrows \mathrm{CO_2} + \mathrm{H_2} \tag{3-28}$$

3.4.1.2 Activation overpotential

Activation overpotential on both electrodes is due to two phenomena. First one is chemical, the chemical equilibrium state of ions at the electrode-electrolyte interface. The second is electrical, overcoming of the electric field due to the transfer of charged particles across interface by ions. Free energy of activation has two constituents: chemical energy of activation (Gibbs energy) and electrical contribution to it (electrical bias). Activation overpotential can be mitigated with increased temperature, active surface area and activity of catalyst used. Free activation energies of electrodes can be written as:

$$E^{-} = G^{0} + \alpha F \Delta\phi \tag{3-29}$$

and

$$E^{+} = G^{0} - (1 - \alpha) F \Delta\phi \tag{3-30}$$

where, $\alpha F \Delta\phi$ is the electrical contribution, which amounts to lowering the energy barrier towards electrode-to-ion transfer (for SOEC, SOFC it is ion-to-electrode).
Electronation is the process of transferring electrons (charge transfer) from electrode to oxygen to form ions. Electronation current density can be expressed as follows:

$$\vec{\imath} = \frac{FkT}{h} c_m e^{-\frac{G^0}{RT}} e^{-\frac{\alpha F \Delta\phi}{RT}} \tag{3-31}$$

where, *k* is the Boltzmann's constant, *h* is the Planck's constant, *F* is the Faraday's constant, *R* is the universal gas constant.

De-electronation is process opposite to the electronation and describes process of transferring electrons from oxygen ions to electrode. De-electronation current density can be expressed as:

$$\overleftarrow{\imath} = \frac{FkT}{h} c_j e^{-\frac{G^0}{RT}} e^{\frac{(1-\alpha) F \Delta\phi}{RT}} \tag{3-32}$$

At the equilibrium electronation and de-electronation current densities are equal representing the rate of charge transfer reaction and they are called exchange current density i_0. This value varies with temperature, electrode materials, gas composition, etc. Difference between Equation 3-31 and 3-32 represents net current flow. Defining overpotential as difference between non-equilibrium and equilibrium potentials

$$\eta = \Delta\phi - \Delta\phi_{eq} \tag{3-33}$$

one can arrive with following expression:

$$i = \frac{FkT}{h} \left[\left(c_j e^{-\frac{G^0}{RT}} e^{\frac{(1-\alpha) F \Delta\phi}{RT}} \right) e^{\frac{(1-\alpha) F \eta}{RT}} - \left(c_m e^{-\frac{G^0}{RT}} e^{-\frac{\alpha F \Delta\phi}{RT}} \right) e^{-\frac{\alpha F \eta}{RT}} \right] \tag{3-34}$$

Utilizing definition of exchange current density more compact expression can be obtained:

$$i = i_{0,i} \left[exp\left(\frac{\alpha z F \eta_{act,i}}{RT} \right) - exp\left(-\frac{(1-\alpha) z F \eta_{act,i}}{RT} \right) \right] \tag{3-35}$$

This equation is called Butler-Volmer equation. Often used in modelling is assumption of charge transfer coefficient equal to half (i.e. electronation and de-electronation rates are equal), and then following form can be used:

$$i = 2i_{0,i}\, sinh\left(\frac{F\eta_{act,i}}{zRT}\right) \tag{3-36}$$

When the overpotential is large the linear approximation is valid and can be written as:

$$\eta_{act.i} = \frac{RTi}{zFi_{0,i}} \tag{3-37}$$

where i = {anode, cathode}, the exchange current density has been confirmed to obey Arrhenius exponential dependence on temperature

$$i_{0,i} = \gamma_i\, exp\left(-\frac{E_{act,i}}{RT}\right) \tag{3-38}$$

3.4.1.3 Ohmic overpotential

Ohmic overpotential of the cell can be computed using following formulation of the Ohm's law

$$\eta_{ohm} = \frac{i\delta}{\sigma} \tag{3-39}$$

where σ is combined ionic conductivity of the cell and δ is the electrolyte thickness. Most commonly only ionic resistance of the electrolyte is considered, other resistances are assumed to be orders of magnitude lower.

3.4.1.4 Concentration overpotential

Concentration overpotential is the last from the three major constituents of cell polarization. It is modelled in several different ways in the literature. In general, it follows from the mass transfer limitations of the porous electrodes. Concentration of species in the electrodes is the same as concentration in free stream only when no current is passing through the cell. Naturally when current starts to pass concentration of fuel species at the interface, c_x=0, is decreasing from free stream value, c_0. Due to this concentration decrease respective voltage drop is present.

$$\eta_{concentration} = \Delta\phi - \Delta\phi_{eq} \tag{3-40}$$

For the equilibrium state Nernst equation for the electrode states:

$$\Delta\phi_{eq} = \Delta\phi^0 + \frac{RT}{zF} ln(c^0) \tag{3-41}$$

Respectively, when current flows through the cell Nernst potential can be written as:

$$\Delta\phi = \Delta\phi^0 + \frac{RT}{zF} ln(c_{x=0}) \tag{3-42}$$

Combining Equations 3-41 and 3-42 yields:

$$\eta_{concentration} = \Delta\phi - \Delta\phi_{eq} = \frac{RT}{zF} ln\left(\frac{c_{x=0}}{c^0}\right) \tag{3-43}$$

To calculate the concentration at the interface several methods can be applied: Fick's model, Stefan-Maxwell's model or Dusty Gas Model (Suwanwarangkul et al. 2003).
In this section only Dusty Gas Model (DGM) is highlighted since it has been proved as the most appropriate for multi-component gas transport (Suwanwarangkul et al. 2003). Nevertheless, it is important to note that for many applications simpler models are accurate enough.
According to DGM transport of the species can be summarized in Equations 3-44 and 3-45.

$$\frac{\mu}{RT}\frac{\partial p_i}{\partial t} = -\nabla N_i + R_i \tag{3-44}$$

$$\frac{N_i}{D_{i,k}^{eff}} + \sum_{j=1, j\neq i}^{n} \frac{y_j N_i - y_i N_j}{D_{ij}^{eff}} = -\frac{P}{RT}\frac{dy_i}{dx} \tag{3-45}$$

Solutions to these equations are partial pressures (concentrations) of involved gases at electrode-electrolyte interface. Concentration losses for each of electrodes is later calculated using Equations 3-46 and 3-47.

$$\eta_{con,i} = \frac{RT}{2F} ln \left[\frac{p^I_{H_2} \left(p^I_{O_2}\right)^{\frac{1}{2}}}{p^I_{H_2O}} \right] \tag{3-46}$$

$$\eta_{con,i} = \frac{RT}{2F} ln \left[\frac{p^I_{CO} \left(p^I_{O_2}\right)^{\frac{1}{2}}}{p^I_{CO_2}} \right] \tag{3-47}$$

Another approach to predict concentration overpotential is by combining electrochemistry, mass transfer and boundary layer theory. This consideration results in introduction of limiting current density. It can be shown that:

$$\frac{i}{zF} = -D \left(\frac{dc}{dx}\right)_{x=0} = -D \left(\frac{c^0 - c_{x=0}}{\delta}\right) \tag{3-48}$$

where, *D* is the diffusivity
Current density from the above relation will be equal to the limiting current density when c_x=0 is equal to zero:

$$\frac{i_L}{zF} = \lim_{c_{x=0} \to 0} \left[-D \left(\frac{c^0 - c_{x=0}}{\delta}\right) \right] = -D \frac{c^0}{\delta} \tag{3-49}$$

Substituting Equation 3-48 and 3-49 to 3-43 yields:

$$\eta_{concentration} = \frac{RT}{zF} ln \left(1 - \frac{i}{i_L}\right) \tag{3-50}$$

Calculation of limiting current density follows from mass transfer analysis, several formulae are used to derive this value.

3.4.2 Statistical approach - micro-modelling.

When micro-modelling is considered, slightly different approach is utilized. Overpotentials are not divided between activation, concentration and Ohmic. Rather than that, balances of charge, Ohm's law and the mass balance are evaluated for each electrode and Ohm's law is applied for electrolyte.
Therefore, one can write Ohm's law for electronic conductor as:

$$\nabla \varphi_{el} = \rho_e^{eff} i_e \tag{3-51}$$

Respectively for ionic conductor:

$$\nabla \varphi_i = \rho_i^{eff} i_i \tag{3-52}$$

Since both electrodes are mixed conductors charge balance must incorporate both ionic and electronic current densities

$$\nabla j_e = -S_v i = -\nabla i_i \tag{3-53}$$

i is the transfer current density calculated from Butler-Volmer equation as in classical model (A m^{-2}), ∇j_e is given in A m^{-2}. S_v is electrochemically active area per unit volume of the electrode (m^{-2} m^{-3}), it is computed according to statistical consideration

$$S_V = \pi \sin^2 \theta r_e^2 n_t n_e n_i \frac{Z_e Z_i}{6} P_e P_i \tag{3-54}$$

For the meaning of all the symbols reader is asked to check the nomenclature. Following formulae are based on theory of particle coordination number in random packing of spheres and percolation theory firstly used by Costamagna et al. (Costamagna et al. 1998) and further enhanced to use in a complete cell model by Chan and Xia (Chan and Xia 2001).

Total number of particles per unit volume can be considered as:

$$n_t = \frac{1-\varepsilon}{\frac{4}{3}\pi r_e^3 \left[n_e + (1-n_e)\left(\frac{r_i}{r_e}\right)^3 \right]} \tag{3-55}$$

Note that only allowable particles are ionic or electronic conductors, hence:

$$n_i = 1 - n_e \tag{3-56}$$

Number of electron conducting particles can be obtained from:

$$n_e = \frac{\Phi}{\Phi+(1-\Phi)\left(\frac{r_i}{r_e}\right)^3} \tag{3-57}$$

Coordination number for electronic conductor can be expressed as:

$$Z_e = 3 + \frac{3}{n_e+(1-n_e)\left(\frac{r_i}{r_e}\right)^2} \tag{3-58}$$

Respectively, coordination number for ionic conductor can be written as:

$$Z_i = 3 + \frac{3\left(\frac{r_i}{r_e}\right)^2}{n_i+(1-n_i)\left(\frac{r_i}{r_e}\right)^2} \tag{3-59}$$

Probability for the connections between the same type particles can be calculated for electronic conductors and ionic conductors respectively, from Equations 3-60 and 3-61:

$$P_e = \left[1 - \left(\frac{4.236-Z_{e-e}}{2.472}\right)^{2.5}\right]^{0.4} \tag{3-60}$$

$$P_i = \left[1 - \left(\frac{4.236-Z_{i-i}}{2.472}\right)^{2.5}\right]^{0.4} \tag{3-61}$$

Average coordination number of electronic to electronic particles and ionic to ionic particles can be written as

$$Z_{e-e} = \frac{6n_e}{n_e+(1-n_e)\left(\frac{r_i}{r_e}\right)^2} \tag{3-62}$$

$$Z_{i-i} = \frac{6n_i}{n_e+(1-n_i)\left(\frac{r_i}{r_e}\right)^{-2}} \tag{3-63}$$

At this stage it is necessary to mention that most of the parameters in this model are difficult to obtain, thus often require fitting.

3.4.2.1 Cathode model

Cathode overpotential can be expressed by

$$\eta_c = (\phi_i^0 - \phi_e^0) - (\phi_i - \phi_e) \tag{3-64}$$

Potentials can be evaluated using Ohm's law Equation 3-51 and 3-52 for both types of conductors. Effective resistivity can be obtained by applying Equation 3-65 for electronic and 3-66 for ionic conductors.

$$\rho_e^{\text{eff}} = \frac{\xi}{\Phi(1-\varepsilon)\sigma_e} \tag{3-65}$$

$$\rho_i^{eff} = \frac{\xi}{(1-\Phi)(1-\varepsilon)\sigma_i} \tag{3-66}$$

Next step is to take second derivative of Equation 3-64, which results in following expression

$$\frac{d^2\eta_c}{dx^2} = S_v i_{0,c}\left(\rho_i^{eff} + \rho_e^{eff}\right) i \tag{3-67}$$

where i is calculated according to Equation 3-35. Boundary conditions are defined as follows

$$\begin{cases} i_{i,c}=0 \; at \; x=0 \\ i_{e,c}=i_{total} \; at \; x=0 \\ \frac{d\eta_c}{dx}=-\rho_{e,c}^{eff} i_{total} \; at \; x=0 \\ i_{i,c}=t_{total} \; at \; x=\delta_c \\ i_{e,c}=0 \; at \; x=\delta_c \\ \frac{d\eta_c}{dx}=-\rho_{i,c}^{eff} i_{total} \; at \; x=\delta_c \end{cases} \tag{3-68}$$

Last step of derivation is conservation of species. Since DGM model was already decided to be most appropriate, only resulting equation is provided.

$$\frac{d^2 y_i}{dx^2} + \frac{\beta}{D_{i,j}^{eff}}\left(\frac{1}{D_{i,k}^{eff}} + \frac{1-\beta y_i}{D_{i,j}^{eff}}\right)^{-1}\left(\frac{dy_i}{dx}\right)^2 - \frac{S_v i RT}{2FP}\left(\frac{1}{D_{i,k}^{eff}} + \frac{1-\beta y_i}{D_{i,j}^{eff}}\right) = 0 \tag{3-69}$$

Boundary conditions are defined as follows

$$\begin{cases} y_i = y_i^0 \ at \ x = 0 \\ \frac{dy_i}{dx} = -\frac{RTi_{total}}{2FP}\left(\frac{1}{D_{i,k}^{eff}} + \frac{\sqrt{\frac{M_i}{M_j}}y_i}{D_{i,j}^{eff}}\right) at \ x = 0 \end{cases} \quad (3\text{-}70)$$

Solving Equation 3-67 and 3-69 with respect to appropriate boundary conditions yield total cathode overpotential.

3.4.2.2 Anode model

For the anode similar reasoning can be applied to obtain equation in same form as Equation 3-67.

The difference between modelling of anode and cathode lies in the choice of model equation for species conservation. In the anode, only a binary gas mixture of nitrogen and oxygen exist. Moreover, the physical phenomena occurring in the anode regards only one of the gases in the mixture, the oxygen. In the negative electrode, one observes oxygen permeation, rather than non-binary diffusion of three or more species. As a result, instead of using DGM equation to solve Equation 3-44, much simpler Darcy law can be applied, Equation 3-71.

$$N_{O_2} = -\frac{P_{O_2}B_g}{RT\mu}\nabla p_{O_2} \quad (3\text{-}71)$$

The resulting governing equation is

$$\frac{d^2p_{O_2}}{dx^2} + \frac{1}{P_{O_2}}\left(\frac{dp_{O_2}}{dx}\right)^2 + \frac{S_v iRT\mu}{4FB_g P_{O_2}} = 0 \quad (3\text{-}72)$$

Appropriate boundary conditions are:

$$\begin{cases} y_{O_2} = y_{O_2}^2 \ at \ x = 0 \\ \frac{dp_{O_2}}{dx} = -\frac{RTi_{total}\mu}{2FP_{O_2}B_g} \ at \ x = 0 \end{cases} \quad (3\text{-}73)$$

3.4.2.3 Electrolyte model

Electrolyte is modelled with use of Ohm's law Equation 3-39.

3.5 Modelling of the Solid Oxide Electrolyzer Cell operated under extreme oxygen chemical potential difference

This chapter has been published in a modified form as JP Stempien, Q Sun, SH Chan. Theoretical consideration of Solid Oxide Electrolyzer Cell with zirconia-based electrolyte operated under extreme polarization or with low supply of feedstock chemicals, Electrochimica Acta, 130, 2014, 718.

3.5.1 Introduction

Pure Zirconium oxide (ZrO_2) is an amphoteric semiconductor with transition from n-type to p-type conductivity under decreasing oxygen partial pressure difference (Vest et al. 1964). The conductivity in ZrO_2 is due to defects in its lattice structure (Kingery et al. 1959). Doubly charged oxygen vacancies allow an ionic transport of oxygen, whereas electrons and holes allow an electronic transport. Altering the defect concentration influences conductivity of a given type. It is known that substituting ions in a semiconductor changes the defect concentration (Wagner 1933). Adding higher valence cations to an n-type semiconductor causes a decrease in the ionic defect concentration and increase in the electronic defect concentration. The opposite is true for a p-type semiconductor. Doping Zirconium oxide with Yttrium oxide replaces Zr`````` cation with Y``` cation and thus increases the ionic conductivity.

Yttria-doped Zirconia, or Yttria-stabilized Zirconia (YSZ), membranes are most commonly used in oxygen sensors (Akbar et al. 2006), oxygen pumps or separators (Yuan & Kroeger 1969), solid oxide fuel cells (Singhal & Kendall 2003) and solid oxide electrolyzer cells (Elikan et al. 1972). Apart from changing the oxygen partial pressure difference across the membrane, the lattice defect concentration of YSZ can be also altered by variation of electrostatic potential difference, thus it can be used to relate oxygen partial pressure difference[1] with the electrostatic field, given constant doping

[1] Throughout the text the author uses oxygen partial pressure as a traditional approach. However, sometimes oxygen chemical potential when referring to SOEC is used. SOEC is essentially

level. In the oxygen sensors, concentration of oxygen in investigated gas mixture is estimated from the observed open circuit voltage across the YSZ membrane. Fuel cells generate electrostatic potential difference and current flow, when exposed to difference in chemical potentials of oxygen. Oxygen pump or electrolyzer works reverse to the fuel cell. When exposed to high enough electrostatic potential difference, they generate oxygen partial pressure difference or chemical potential difference, respectively. An electrolyzer additionally facilitates chemical and electrochemical reactions to create oxygen (i.e. hydrogen evolution).

Solid Oxide Electrolyzer Cells (SOEC) attracted an increased attention in recent years due to their ability to recycle combustion products back into usable fuels (Xie et al. 2011, Fu et al. 2010, Wachsman et al. 2012, Zhan et al. 2009). YSZ electrolyte is the most common choice for high temperature electrochemical cells or sensors. Fuel cells and electrolyzer, regardless still being in the development stage, pose great opportunities for the energy security and sustainability. However, due to the nature of their operation, it is possible to run them in abnormal conditions characterized by extremely high oxygen partial pressure difference (Mendybaev et al. 1998, Sridhar & Blanchard 1999, Pham & Glass 1988, Schefold et al. 2009). Specifically, this refers to the oxygen pumps and the electrolyzers, moderately to the fuel cells. It is hypothesized here that such conditions may occur in SOEC if it is designed incorrectly.

In the SOEC it is traditionally assumed that YSZ is a pure ionic conductor (Stempien et al. 2012, 2013, 2013, Petipas et al. 2013, Ni 2012, Cai et al. 2010), thus its Faradic efficiency is always 100%. This assumption is often true in fuel cell mode of operation. However, when operating electrolyzer or oxygen pump[2] with either high electrostatic potential difference or low feedstock chemicals' supply, one can create extremely high oxygen partial pressure difference across the cell. Consequently, switching to mixed or dominantly electronic conduction mode and hence running on low or zero Faradic efficiency. This can be due to the improper design, or when SOEC is coupled with an intermittent energy source without proper safety measures against rapid surges in generated power.

creating oxygen chemical potential difference, rather than partial pressure difference.

[2] Electrochemical pump refers to oxygen pumps and electrolyzers, as from electrolyte point of view they are the same device.

Most representative works investigating either running on low feedstock supply or extreme polarization were published by two independent groups in 1998 and 2009. The first group, Pham and Glass (Pham & Glass 1998), investigated the operational characteristics of an oxygen pump based on 8YSZ (zirconium oxide doped with 8-moles of yttrium oxide). The experimental setup considered pumping oxygen from an enclosed volume of gas mixture with low initial oxygen partial pressure. Due to the experiment arrangement, authors arrived in a region of mixed and dominantly electronic conductivity. The second group, Schefold et al. (Schefold et al. 2009), performed experiments on several 8YSZ-based SOECs. The group presented that it is possible to operate SOEC fed with steam with the injected electric current exceeding theoretical value required to convert 100% of the steam, thus with Faradic efficiency < 100%. Moreover, the group showed that it is even possible to run the cell with no steam or CO_2 supply at all (Faradic efficiency equal zero). They investigated cases of excessive polarization and insufficient feedstock supply. Both groups indicated existence of a short circuit voltage (SCV) in all of the experiments. The values were in the same range of 1.6 – 1.8 V. Similarly, our in-house experiments showed possibility of injecting electric currents larger than that required for 100% electrochemical conversion of feedstock chemicals, though, no saturation potential difference was observed. Up to date literature investigated probability of electrochemical decomposing of the electrolyte, however, arriving at mixed conclusions. None of the efforts examined consequences of running the cell under mildly mixed conduction mode. Such effort is made here.

Few models are available in the open literature, describing the transport in a mixed conducting electrolyte. Naefe (Naefe 1997) authored a good review of modelling mixed ionic-electronic conductors. Chan et al. (Chan et al. 2002) proposed an electrolyte model for oxygen pump and a solid oxide fuel cell. They analysed the effects of multiple parameters on oxygen permeation in YSZ and doped Bi_2O_3 electrolytes. Jacobsen and Mogensen (Jacobsen & Mogensen 2008) analysed the course of oxygen partial pressure across the electrolyte in view of delamination process occurring in the solid oxide fuel cells. The above models focused solely on electrolyte processes. Modelling studies on complete cells based on mixed conducting membranes are only handful and limited to membranes conducting protons and ions, not electrons (Virkar 2012, Demin et al. 2007, Bertei et al. 2012). An interesting approach was undertaken by Milewski et al. (Milewski et al. 2012). In their book, the authors proposed an equivalent circuit model for SOFC based on an assumption that YSZ has small electronic conductivity. Nevertheless, after

close inspection, the model simplifies to a linear equation when electronic resistance is set to infinity. This makes the model non generic, and thus limits its applicability.

In the following chapter the author theoretically confirms that operating an SOEC in extreme polarization conditions or insufficient feedstock supply results in switching from dominantly ionic to dominantly electronic conduction mode, consequently lowering the Faradic efficiency to near 0%. The author proposes a theoretical framework for the prediction of polarization curves, calculation of OCV and feedstock chemicals' conversion in such conditions. Proposed model is reducible to a widely accepted form for the pure ionic conduction and, thus, is proved generic. The author concludes that the assumption used to derive the relation between oxygen partial pressure and electrolyte's conductivity is not valid for extremely low oxygen partial pressure (or extremely high oxygen partial pressure/chemical potential difference). Furthermore, the common practice of estimating hydrogen, carbon monoxide or syngas production rate in SOEC using the Faraday's law is questioned. Lastly, the author suggests that the proposed mechanism of switching to electronic conduction may occur in all pumping electrochemical cells, not only in those based on 8YSZ electrolyte. Proposed model is expected to be able to model such cells reliably.

3.5.2 Theory

3.5.2.1 Electrolyte material properties

The detailed mechanism of conduction in YSZ is well studied (Park & Blumenthal 1989) and will not be discussed. Here only the main points are briefly presented.

Using the Kröger–Vink notation the following defect reaction holds for doping of ZrO_2 with Y_2O_3:

$$Y_2O_3 \rightarrow 2Y'_{Zr} + V_O^{\cdot\cdot} + 3O_O^x \tag{3-74}$$

Where Y'_{Zr} is a charged Yttrium atom on a Zirconium site, $V_O^{\cdot\cdot}$ is a doubly negatively charged oxygen vacancy and O_O^x is a neutral oxygen on an oxygen site.

It can be written in a nonstoichiometric form for low oxygen partial pressure (Patterson et al. 1971):

$$O_O^x \rightarrow 2e' + V_O^{\cdot\cdot} + \frac{1}{2}O_2(g) \tag{3-75}$$

where $e^{\cdot}$ is a negatively charged electron and $O_2(g)$ is an oxygen molecule in gaseous form.

Reaction equation (3-75) is used to derive the reaction constant from the law of mass action.

$$K = [V_O^{\cdot\cdot}][e^{\cdot}]^2[O_2(g)]^{\frac{1}{2}} \tag{3-76}$$

Gaseous oxygen concentration may be replaced with oxygen partial pressure[3],$p_{O_2} = p_{mixture}[O_2(g)]$, or fugacity[4]. It is assumed that the concentration of oxygen vacancies is constant (Brook et al. 1981) and therefore, electron concentration is only a function of oxygen partial pressure. This assumption holds when $[V_O^{\cdot\cdot}] \gg [e^{\cdot}]$. This assumption will be revisited later in this section.

From Equation 3-76 the electron concentration can be written as:

$$[e^{\cdot}] = K[V_O^{\cdot\cdot}]^{-1}p_{O_2}^{-\frac{1}{4}} \tag{3-77}$$

Using the well-known relation, electron conductivity can be calculated if mobility of the carriers does not depend upon its concentration (Patterson et al. 1971, Minh & Takahashi 1995).

$$\sigma_e = [e^{\cdot}]|q|\mu_e = K|q|\mu_e[V_O^{\cdot\cdot}]^{-1}p_{O_2}^{-\frac{1}{4}} \tag{3-78}$$

where μ_e is the carrier mobility and it can be calculated from diffusivity using the Nernst-Einstein relation (Van Zeghbroeck 2011), while the diffusivity can be obtained

[3] The reaction constant and following conductivities are function of pressure ratio across the membrane, rather than absolute pressure. However, it is conveniently assumed that pressure on the air side of YSZ membrane is constant and equal to 0.21 atm. In real electrolytic cell this is true given sufficiently large air flux on the air electrode side.

[4] Despite that fugacity is the proper parameter in most of the formulae presented, the author decides to use oxygen partial pressure as is traditionally accepted.

experimentally (Park & Blumenthal 1989). Following similar treatment hole conductivity is proportional to the oxygen partial pressure via power law with exponent ¼.

$$\sigma_h \propto p_{O_2}^{\frac{1}{4}} \tag{3-79}$$

From the assumption of the constant oxygen vacancy concentration arises the constant, independent of p_{O_2}, ionic conductivity.

One may expect the air side of the electrolyte, due to high concentration of oxygen from air, to be permanently in ionic conduction mode. However, as seen from Equation 3-76 and due to equilibrium of Fermi level at electrode/electrolyte interface, any electrolytic bias will affect conductivity four times stronger than oxygen partial pressure.

Above assumptions are experimentally confirmed for oxygen partial pressures in the range $1 – 10^{-20}$ atm, temperature 600 – 900 °C and ZrO_2 doped with 8 mol Y_2O_3 (8YSZ) (Park & Blumenthal 1989). Literature reported conductivity data are presented in the second column of Table 3-1.

Table 3-1 – Literature (Park & Blumenthal 1989) and fitted conductivity data. The formulae follow the Arrhenius type expression.

Parameter	Literature data	Fitted data
Ionic conductivity $\Omega^{-1}cm^{-1}$	$1.63x10^2exp(-0.79eV/kT)$	$1.31x10^2exp(-0.79eV/kT)$
Electron conductivity $\Omega^{-1}cm^{-1}$ [a]	$1.31x10^7exp(-3.88eV/kT)p_{O_2}^{-\frac{1}{4}}$	$9x10^{12}exp(-3.88eV/kT)p_{O_2}^{-\frac{1}{8}}$
Hole conductivity $\Omega^{-1}cm^{-1}$ [a]	$2.35x10^2exp(-1.67eV/kT)p_{O_2}^{\frac{1}{4}}$	$2.35x10^2exp(-1.67eV/kT)p_{O_2}^{\frac{1}{8}}$
Electron diffusivity $cm^2\,s^{-1}$	$2.30x10^2exp(-2.00eV/kT)$	$2.30x10^2exp(-2.00eV/kT)$
Hole diffusivity $cm^2\,s^{-1}$	$0.23\,exp(-1.15eV/kT)$	$0.23\,exp(-1.15eV/kT)$
Electron mobility $cm^2\,s^{-1}\,V^{-1}$	$8.02x10^2exp(-1.89eV/kT)$	$8.02x10^2exp(-1.89eV/kT)$

Table 3-1 continued

Parameter	Literature data	Fitted data
Hole mobility $cm^2\ s^{-1}\ V^{-1}$	0.85 exp(-1.05eV/kT)	0.85 exp(-1.05eV/kT)
Electron concentration in the simulated electrolyte [a]	$1.04 \times 10^{23} \exp(-1.99eV/kT) p_{O_2}^{-\frac{1}{4}}$	$7 \times 10^{28} \exp(-1.99eV/kT) p_{O_2}^{-\frac{1}{8}}$
Hole concentration in the simulated electrolyte [a]	$1.72 \times 10^{21} \exp(-0.62eV/kT) p_{O_2}^{\frac{1}{4}}$	$1.72 \times 10^{21} \exp(-0.62eV/kT) p_{O_2}^{\frac{1}{8}}$

[a] oxygen partial pressure is given in atm

One of important characteristics of an electrolyte is a ratio of ionic/electronic conductivity to total conductivity. It is a definition of transference or transport number.

$$t_k = \frac{\sigma_k}{\sigma_i + \sigma_e + \sigma_h} \tag{3-80}$$

In the case of YSZ it is most often assumed that t_i is equal to 1 and t_{eh} is 0 (Stempien et al. 2012, 2013, 2013, Petipas et al. 2013, Ni 2012, Cai et al. 2010), where subscript *i* stands for ionic and *eh* for electronic. However, as shown in the experiments (Pham & Glass 1998, Schefold et al. 2009), it is possible to operate the cell with $t_i<1$.

The experimental results of Schefold et al. (Fig. 3-5), Pham and Glass, and our in-house experimental data all present the same sigmoidal shape indicating existence of three distinctive processes. In the low current region, the cell works in the dominant ionic conduction mode, a slight increase in potential difference is observed with increasing current. In the mid current region, a sharp increase of current is observed, this is related to transition between $t_i \approx 1$ to $t_i \approx 0$. When t_i goes below 1 an increase in total current is needed to sustain the ionic current equal to the number resulting from established electrolysis rate. The third region features only a small increase in the potential difference with the increasing current, it is related to a dominant electronic conduction and the potential difference increase is due to an ohmic loss and a concentration overpotential. Sharp increase in potential difference at high current densities is typically assigned to mass transport limitation. However, use of modern electrodes is expected to minimize such loss. It seems reasonable to explain the commonly observed potential difference surge by a combination of drop of ionic transport number and mass transport

loss, rather than the later alone.

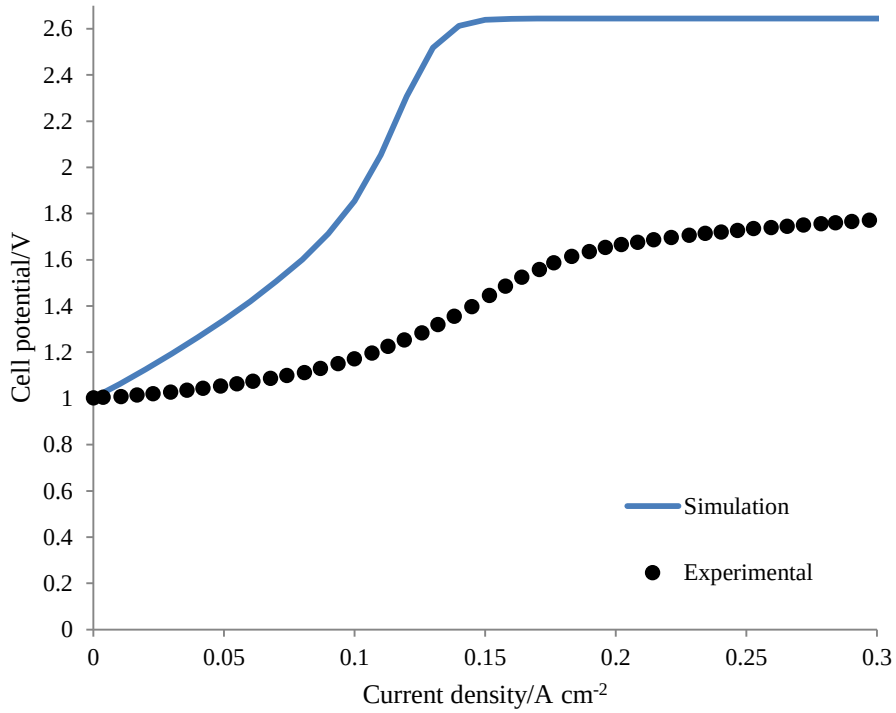

Fig. 3-5 – Experimental data from Schefold et al. and simulation results from YSZ properties extrapolated from reported literature conductivity values (Park & Blumenthal 1989). Temperature was set to 810 °C, pressure 1 bar, oxygen partial pressure on fuel side ~10^{-20} bar and 0.21 bar on air side. Literature conductivity data used to simulate continuous line are reprinted in Table 3-2. Simulated cell parameters are given in Table 3-3.

Fig. 3-5 shows experimental data of Schefold et al. and simulation based on the conductivities reported in the literature (Park & Blumenthal 1989) (Table 3-2). Used model equations are derived and described in a later section. Large discrepancies are observed between the experimental and simulation data. This indicates inapplicability of the conductivity data. Quick analysis of the reported open circuit voltage reveals that initial pressure on the fuel electrode side is of the order of magnitude 10^{-20} atm, therefore the cell was operated in the region outside the confirmed dominant ionic conduction. Conductivity data for oxygen partial pressure below 10^{-20} atm is required. Due to the lack of such data in the open literature it is here fitted for the purpose of further analysis. The sigmoidal shape of the I-V curve is influenced by two parameters. The power exponent of the pressure in conductivity data controls the slope of the transition or medium current part. The pre-exponential constants of all three conductivities influence

the magnitude of maximum potential difference (short circuit voltage, SCV). Such dependence allows for relatively easy fitting of extrapolated conductivity data.

After conductivity data adjustment, defect concentrations must also be amended. It is assumed that diffusivity of the charge carries is unaffected. It is worth revisiting assumptions regarding the power exponent of pressure term in conductivity data. From the theoretical point of view, increased electron conductivity means that the condition $[V_O^{\cdot\cdot}] \gg [e^{\cdot}]$ is no longer valid at the extremely low oxygen partial pressures. Therefore, the power exponent of the pressure term should be changed. From the experimental results, it follows that the absolute value of the power exponent should be decreased in order to stretch the transition between dominant ionic and dominant electronic conduction. Indeed, recent results by Pietrowski et al. (Pietrowski et al. 2013) showed that diffusivity of oxygen isotope is constant with oxygen partial pressure. However, surface exchange coefficient showed power law dependence on oxygen partial pressure with exponent of 0.1 and 0.7 for two different YSZ faces. Later the author showed that the first value is closer to value fitted for experiments of Schefold et al..

In the above formulations and in the conductivity data oxygen partial pressure is a ubiquitous parameter. However, some readers may be confused as there should be no oxygen on fuel side of the cell. The values used for calculations are derived from thermodynamic equilibrium of the feedstock chemicals. It is obtained by minimizing the Gibbs function of a given gas mixture at a given temperature and pressure (i.e. the chemical potentials of mixture constituents are equilibrated).

Such universality of one parameter suggests using it as an indicator of design performance. Therefore, a map can be created to relate the oxygen partial pressure of the feedstock chemicals with their conversion (an equivalent of fuel utilization in fuel cells). Such a map can be used to judge if any given design conditions meet requirement for operation with 100% Faradic efficiency and therefore, the use of simplified SOEC model to calculate the electrolysis yield and polarization curve.

3.5.2.2 Electrolyte modelling

A current injected into an electrolyte can be divided into an electronic (electrons and holes) and an ionic part.

$$I = I_i + I_{eh} \tag{3-81}$$

The ionic and the electronic contributions to the total current can be calculated by multiplying the current with respective transport number, i.e.:

$$I_i = t_i I \quad I_{eh} = t_{eh} I \tag{3-82}$$

The ionic current is due to a movement of oxygen ions through the YSZ membrane, whereas the electronic current is due to a movement of electrons and holes. In the fuel cell mode oxygen ions' flux is in the opposite direction to the electrons' flux, while in the electrolyzer and the oxygen pump contrary is true. When respective molar flux is multiplied by the charge it carries and Faraday constant (charge of a mole of particles), a current term can be obtained.

$$I = z_h F N_h + z_e F N_e + z_i F N_i \tag{3-83}$$

where F is the Faraday constant (96485.33 C mol^{-1}), I is current A, N_k is a molar flux mol s^{-1}. Charge, z, of a hole is equal to 1, an electron is equal to -1 and an oxygen anion is equal to -2. A molar flux of the carriers can be calculated by Nernst-Planck equation with the convective terms omitted (Naefe 1997, Chan et al. 2002).

$$N_k = -\frac{D_k}{RT} c_k \nabla \overline{\mu_k} \tag{3-84}$$

where D_k is diffusivity of charge carriers m^2 s^{-1}, R is the universal gas constant (8.31 J K^{-1} mol^{-1}), T is the temperature K, c_k is concentration of charge carriers and $\overline{\mu}_k$ is electrochemical potential of charge carriers. Diffusivity of charge carriers can be obtained experimentally by a time lag method (Park & Blumenthal 1989). The concentration of charge carriers can be obtained by comparing the steady state conductivity measurements with the non-steady state time lag mobility measurement, Equation 3-76 (Park & Blumenthal 1989). By splitting the electrochemical potential into chemical and electrical term, $\overline{\mu}_k = \mu_k + \phi/F$ (Broensted & Laerebog 1943), one can obtain a flux expression in terms of concentration gradient and applied electrostatic potential difference.

$$N_k = -D_k \nabla c_k - \frac{z_k F}{RT} D_k c_k \nabla \varphi \tag{3-85}$$

where φ is the applied electrostatic potential.

Equation 3-85 can be used to calculate electronic current through the electrolyte. To do so, it must be put into an equivalent form of Equation 3-83 for the electronic current (last term is omitted). Presented solution follows the one given by Jacobsen and Mogensen (Jacobsen & Mogensen 2008), alternative solutions were reviewed by Naefe (Naefe 1997) or proposed by Chan et al. (Chan et al. 2002).

$$i_{eh} = -F(D_h \nabla c_h - D_e \nabla c_e) - \frac{F^2}{RT}(D_h c_h - D_e c_e) \nabla \varphi \tag{3-86}$$

Assuming that the oxygen reaction occurs only outside of the electrolyte in its vicinity (only partially applicable to modern cermet and composite electrodes), follows that the ionic current must be constant throughout the electrolyte.

$$i_i = -\sigma_i \nabla \varphi = const \tag{3-87}$$

The above is not true for electron current and hole current. However, due to the electroneutrality condition, their sum must remain constant within the electrolyte (above assumption is not valid if an electronic double layer develops near electrode/electrolyte interface). Moreover, the product of electron and hole concentration must be constant within the electrolyte.

$$K = c_e c_h \tag{3-88}$$

With the above assumptions, equation (3-86) has an implicit 1D solution for the electrons concentration along the location within the electrolyte (x) in the form taken from Jacobsen and Mogensen (Jacobsen & Mogensen 2008).

$$x = \frac{RT}{F \nabla \varphi} \left\{ ln \frac{c_e(x)}{c_e(0)} + \frac{1}{\sqrt{1 - \frac{4 D_k K}{D_e} \left(\frac{F \nabla \varphi D_e F}{RT i_{eh}} \right)^2}} \times \right.$$

$$ln\left[\frac{2\frac{F\nabla\varphi D_e F}{RTi_{eh}}c_e(x)+1+\sqrt{1-\frac{4D_h K}{D_e}\left(\frac{F\nabla\varphi D_e F}{RTi_{eh}}\right)^2}\,2\frac{F\nabla\varphi D_e F}{RTi_{eh}}c_e(0)+1+\sqrt{1-\frac{4D_h K}{D_e}\left(\frac{F\nabla\varphi D_e F}{RTi_{eh}}\right)^2}}{2\frac{F\nabla\varphi D_e F}{RTi_{eh}}c_e(0)+1-\sqrt{1-\frac{4D_h K}{D_e}\left(\frac{F\nabla\varphi D_e F}{RTi_{eh}}\right)^2}\,2\frac{F\nabla\varphi D_e F}{RTi_{eh}}c_e(x)+1-\sqrt{1-\frac{4D_h K}{D_e}\left(\frac{F\nabla\varphi D_e F}{RTi_{eh}}\right)^2}}\right] \quad (3\text{-}89)$$

where x is 0 at the fuel electrode interface and δ (electrolyte thickness) at the air electrode interface. The method for solving this equation is described by Jacobsen and Mogensen. Originally, Jacobsen and Mogensen proposed to assume a value for $c_{e(0)}$, as it is not, in principle, known. However, the total concentration of the electrons is reported in literature (Park & Blumenthal 1989). An extra iteration step is required in order to get real values of $c_{e(x)}$. After obtaining $c_{e(x)}$, it is integrated over the thickness of the electrolyte in order to get the total concentration of electrons. This value is compared against experimentally obtained electron concentration. Adjustment is made to $c_{e(0)}$ until satisfied convergence is obtained.

The above approach shows the method for simulating Solid Oxide Cell's (SOC) or oxygen pump's electrolyte without the assumption of pure ionic conductivity. Despite the electron and hole distributions are calculated in all simulation cases, they are not presented in this chapter for the sake of reporting clarity. In the remaining of this chapter, the author models the whole cell operated in all conductivity modes and with Faradic efficiency lower than 100%. To the best of author's knowledge such model was never reported in the literature.

3.5.2.3 Solid Oxide Electrolyzer cell modelling

In the case of operating SOEC in a mixed conduction mode classical formulae should be evaluated for ionic current only. Extra terms are required to account for electronic transport. These terms take an equivalent form to the previously discussed.

The equilibrium potential difference no longer consists only the open circuit term, but also a short circuit term (due to an electronic conductivity and electrostatic potential difference). To calculate the short circuit voltage, one must realize that the full short circuiting of the cell occurs when $t_i \approx 0$, i.e. electronic transport is dominant. From the conductivity data, it is possible to estimate oxygen partial pressure, p_{SCV}, at which $t_i \approx 0$ and this pressure must be used in the denominator of the short circuit voltage expression.

$$p_{SCV} \approx \lim_{t_i \to 0}\left(\frac{\sigma_i(1-t_i)}{t_i\gamma_e}\right)^{\frac{1}{m}} \quad (3\text{-}90)$$

where m is the power exponent of conductivity and γ_e is thermally activated pre-exponential factor for conductivity. The above formula is valid only at low oxygen partial pressures. Rigorous form of the equilibrium potential difference is given as:

$$E_0 = t_i OCV + t_{eh} SCV = t_i \frac{RT}{4F} ln\left(\frac{p_{air\ electrode}}{p_{fuel\ electrode}}\right) + t_{eh} \frac{RT}{4F} ln\left(\frac{p_{air\ electrode}}{p_{SCV}}\right) \quad (3\text{-}91)$$

The concentration loss due to the flow of electrons from electrolyte/electrode interface to current collector is calculated from Ohm's law and is assumed negligible. Conversely, one must consider the concentration loss due to oxygen transport in the fuel electrode. It can be conveniently described by Darcy's law or Fick's law.

The activation loss for the electrodes can be adequately described with Butler-Volmer equation for electron transfer. Though, due to transferring the charge in form of an electron, it can be neglected.

The ohmic loss should be calculated for ionic and electronic currents respectively:

$$\eta_{ohm} = \frac{i_i \delta}{\sigma_i} + \frac{i_{eh} \delta}{\sigma_{eh}} \quad (3\text{-}92)$$

Following the above treatment, the equation for the total cell's voltage takes the form:

$$E = E_0 + \eta_{ohm} + t_i \eta_{act\ electrodes} + t_{eh} \eta_{con\ oxygen} \quad (3\text{-}93)$$

where the first term describes equilibrium potential difference, which includes OCV and SCV, the second term describes ohmic loss in the electrolyte due to ionic and electronic carriers, the third and fourth describe concentration and activation loss due to ionic transport, the fifth term describes concentration loss due to oxygen transport in the fuel electrode.

When ti is equal to one and the t_{eh} is equal to zero Equation 3-93 is reduced to classical and represents the case for pure ionic conduction. In the opposite case, Equation 3-93 represents the case of pure electronic conduction. Such feature makes the proposed model generic.

The Faradic efficiency indicates how much current injected into the cell is actually used

to mobilize oxygen ions, and thus convert the chemicals. It can be calculated directly from the ionic transport number with the following equation.

$$\eta_{Faradic} = \frac{I_{ionic}}{I_{total}} \times 100\% = \frac{t_i I_{total}}{I_{total}} \times 100\% = t_i \times 100\% \quad (3\text{-}94)$$

In the present study conductivity data from the literature is used in the p_{O_2} range of 0.21 – $5x10^{-20}$ atm and fitted data is used for partial pressure corresponding to $t_{eh}\approx 1$. In the gap between above regions linear interpolation is used to calculate t_i and t_{eh}. It is worth noting that an alternative approach would consider fitting the transport numbers, rather than the conductivity. The benefit of such approach would be a much simpler fitting and solution for the problem. Nonetheless, exact distributions of charge carriers within the electrolyte would be more difficult to obtain.

In (Nasarallah & Douglass 1974), Nasarallah and Douglass proposed a model for ionic transport number in low oxygen partial pressure region with the following expression.

$$t_i = \frac{1}{1+const\times p_{O_2}^{-\frac{1}{4}}[Y_2O_3]^{-\frac{3}{2}}} \quad (3\text{-}95)$$

where the constant is thermally activated with activation energy equal to 21.8 kcal mol^{-1}.

3.5.3 Results and discussion

The above equations were solved using Aspen HYSYS® V7.2 (Aspen HYSYS) with Peng-Robinson's equation of state (Robinson et al. 1985). The summary of the simulated cell's parameters is presented in Table 3-2. In the simulation it is assumed that both steam and carbon dioxide undergo electrolysis and additionally both inlet and outlet gas compositions are brought to chemical equilibrium. The electrolysis reactions are assumed to be simple and to follow Arrhenius type kinetic constants. Pre-exponential factor, γ, refers to frequency of molecules' collisions and typically decrease with increase of molecules mass. Energy of activation, E_{act}, refers to probability of reaction's occurrence and this probability typically decreases with the strength of chemical bonds, resulting in increased energy of activation. The reaction volume is calculated as a triple phase boundary (TPB) volume (assuming the TPB area of 2 $Å^2$, the value is based on an

average size of involved atoms, i.e. Nickel, Yttrium and Zirconium). TPB length density is taken from 3D imaging study (Guan et al. 2011).

Table 3-2 – Summary of the parameters used in the simulation.

Parameter	Value
Electrolyte material	ZrO_2 doped with 8 mole of Y_2O_3 (YSZ)
Fuel electrode material	Ni-YSZ cermet
Air electrode material	LSM-YSZ composite
Operational pressure	1 bar
Operational temperature	810, 895 °C
Cell active area	45 cm^2
Fuel flow rate	230 sccm (validation), 5 sccm (simulation)
Air flow rate	1500 sccm (secures constant composition on air side) (validation), 5 sccm (simulation)
Electrolyte thickness	10 μm
Fuel electrode thickness (+ support)	200 μm
Air electrode thickness	35 μm
Porosity	30 %
Tortuosity	5
Average pore radii	0.5 μm
TPB length density	$4x10^6$ m cm^{-3}
TPB area	2 $Å^2$
H_2O electrolysis kinetic data	γ=$1.2x10^6$, E_{act}=1.2 kJ $mole^{-1}$
CO_2 electrolysis kinetic data	γ=$5x10^5$, E_{act}=1.3 kJ $mole^{-1}$

3.5.3.1 Validation of the electrolyte properties at $p_{O_2} < 10^{-20}$

The experimental results of Schefold at al. were used to fit and validate the electrolyte properties. The experimental results obtained by the group are most representative to the case discussed in this section. The operation of the SOEC with a feedstock of hydrogen and nitrogen was reported at two temperatures, 810 °C and 895 °C. The first set of the results was used to fit the electrolyte properties, while the second one was used to validate it (Fig. 3-6).

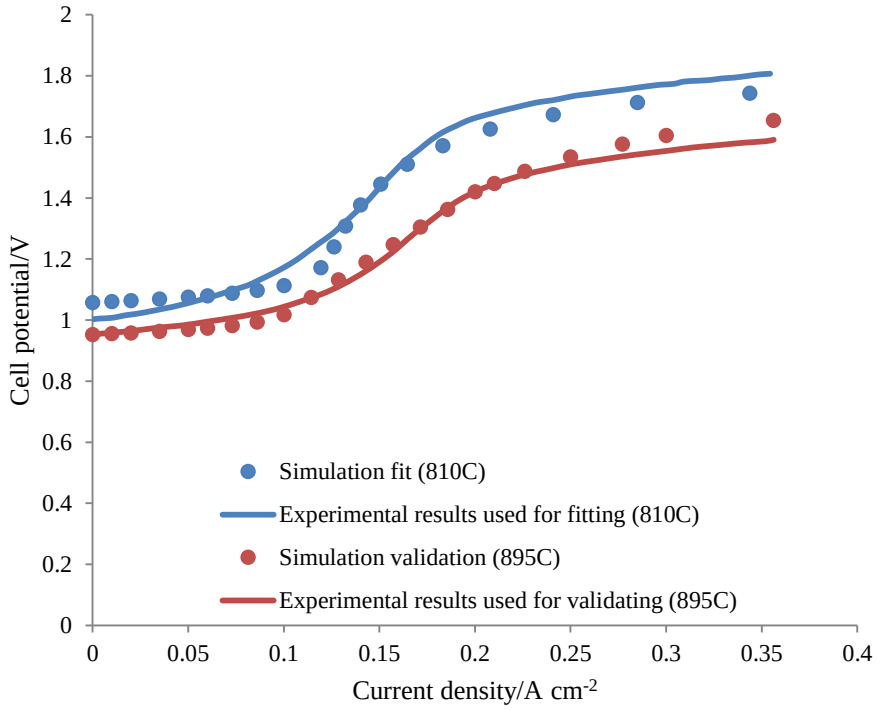

Fig. 3-6 – Fitting and validation curves as compared to experimental results from Schefold et al., fitting curve obtained at 810 °C and validation curve obtained at 895 °C.

In the presented simulation results, there is a certain change of trend. In the fitted curve (810 °C) at low current densities simulation underestimates the performance (i.e., predicts higher potential difference), whereas at high current densities it overestimates the performance. Opposite trend is observed in the validation curve (895 °C). The discrepancy is due to running the fitting case entirely below $p_{O_2} = 10^{-20}$bar, i.e. it uses the fitted electrolyte conductivity properties for all points. The validation case is run partially on the literature conductivity data and partially on the fitted conductivity data. Moreover, in the fit curve, it seems like operation in dominantly ionic conduction mode has little overpotential at all. It is owing to the lack of detailed description of the

experimental cell in (Schefold et al. 2009). The parameters used in the simulation were the same as obtained previously (Stempien et al. 2012). Nevertheless, the exact match in the region above $p_{O_2} = 10^{-20}$ is irrelevant for the purpose of this study.

3.5.3.2 Discussion of the extrapolated electrolyte properties

The electrolyte properties reported in the open literature as compared to the fitted properties are presented in Table 3-1.

Fig. 3-7 shows on the left axis the estimation of short circuit oxygen partial pressure as a function of temperature. The difference between the fitted properties and the literature properties reaches several orders of magnitude. The values based on the literature data is outside of the validated range, the same is the case for the fitted data.

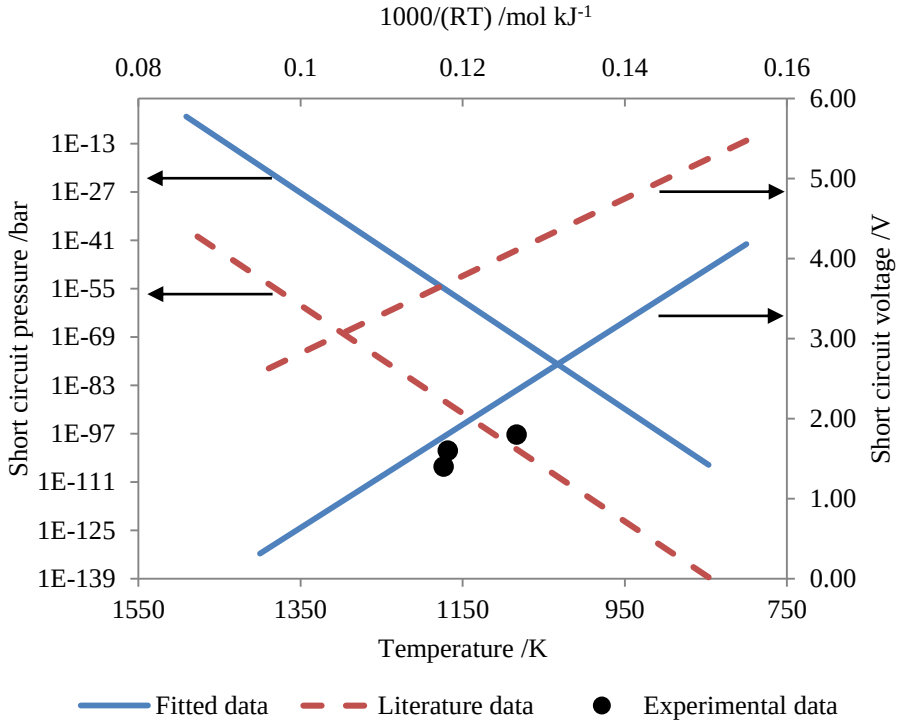

Fig. 3-7 – On the left axis: Short circuit pressure estimation as a function of 1/RT for literature conductivity data (Park & Blumenthal 1989) and fitted conductivity data. On the right axis: Short circuit voltage, as a function of temperature, observed from experiments (Pham & Glass 1998, Schefold et al. 2009), literature conductivity data (Park & Blumenthal 1989) and fitted conductivity data. Points refer to experimental short circuit voltage.

In the range of temperatures 700 – 900 °C the short circuit oxygen partial pressure varies from 10^{-65} to 10^{-31} atm for the fitted data. The value for 800 °C is about 10^{-46} atm.

However, infinitesimal these values may seem, it is important to underline that they correspond to the Faradic efficiency of 0%, and the change between 100% and 0% is expected to occur over a wide range of orders of magnitude. Therefore, the deviation from 100% Faradic efficiency is expected to start at much higher oxygen partial pressures. According to the literature data the change of t_i, and thus the Faradic efficiency, occurs over 15 orders of magnitude at 800 °C, hence starts at 10^{-31} atm. It was highlighted in the previous section that the change in Schefold et al.' experiments was observed to occur over a wider segment. The drop of the Faradic efficiency from 100% to 0%, with use of the fitted data at 800 °C, occurs over roughly 30 orders of magnitude, hence starts at 10^{-16} atm[5]. Luckily, this indicates that drop of the efficiency is not as severe as expected from the literature conductivity data (Park & Blumenthal 1989). However, it starts at much higher oxygen partial pressures.

The short circuit voltage observed in the experimental results of Schefold at al. and Pham & Glass are shown together with the values estimated from fitted and literature data on the right axis of Fig. 3-7. It is seen that fitted data represents the short circuit voltage well.

Interestingly, Schefold et al. (Schefold et al. 2009) suggested that short circuit voltage can be altered by electrolyte thickness adjustment, however, our theoretical consideration yields that it is only a function of temperature. Pham and Glass (Pham & Glass 1998) observed partial oxidation of electrolyte after operating at the short circuit voltage, whereas in Schefold et al. paper (Schefold et al. 2009) it was not observed. Discrepancy may be due to the different simulation setups, i.e. plug flow in Schefold et al. work (Schefold et al. 2009) and constant volume in Pham and Glass work (Pham & Glass 1998). According to Weppner (Weppner 1977), a reduction potential of ZrO_2 doped with 10 moles of Y_2O_3 is 2.32V at 800 °C. If so, one may expect that the operation at short circuit voltage for extended period of time will lead to a permanent reduction of the electrolyte. Schefold et al., however, suggests that the observed short circuit is a "self-defence" mechanism of YSZ against reduction. It seems that plug flow design allows for operation at short circuit potential for extended time without noticeable

[5] Note that the value is inside the range of literature data. Caution is recommended when using the data at the around 10^{-20} atm. In this section, literature data is used up to $5x10^{-20}$ atm, later linear interpolation is done between literature and fitted data.

electrolyte reduction. Nevertheless, the electrolyte is thought to eventually undergo irreversible reduction, if given sufficient time. Similar would be the case for other electrolyte materials, as the behaviour is due to the nature of 'pumping' operation of SOC, rather than properties of material used. Such theoretical observation may be difficult to validate experimentally, due to expected premature failure connected with other high potential difference degradation mechanisms (Chen et al. 2013).

3.5.3.3 Conditions for operating SOEC in dominantly ionic conduction mode. Simple map of oxygen partial pressure for SOEC feedstock chemicals mixture[6]

Fig. 3-8 shows the equilibrium partial pressure of oxygen at 700, 800 and 900 °C and pressure 1 bar. Three feedstock chemicals' mixtures were chosen to represent operating the cell on steam, carbon dioxide, and combination of both. Investigated cases include H_2/H_2O with molar ratio 5/95, H_2/CO_2 with molar ratio 5/95 and $H_2/H_2O/CO_2$ with molar ratio 5/50/45. The calculation is done at the open circuit conditions. Operating the cell at high temperatures gives higher oxygen partial pressures for carbon dioxide electrolysis. Opposite is the case for operation at low temperature. The switch occurs at 827 °C, which is the equilibrium temperature of Water-Gas Shift reaction. Comparing the slope of short circuit pressure as a function of temperature on Fig. 3-7 and feedstock chemicals' oxygen partial pressure on Fig 3-8, it seems that lowering the temperature will decrease the short circuit pressure faster than the feedstock chemicals' oxygen partial pressure. Therefore, lowering the temperature may secure wider operational window for SOEC. It should be noted that the slope of the feedstock chemicals' oxygen partial pressure is expected to decrease with increasing injected current, due to mass transport in the porous electrode and oxygen pumping through the electrolyte. Operation at high current densities will diminish gains associated with lowering the temperature.

[6] To create the fuel map, the mixtures' Gibbs function is minimized and assumption is made on equal rate of reduction of steam and carbon dioxide. The full model is not solved.

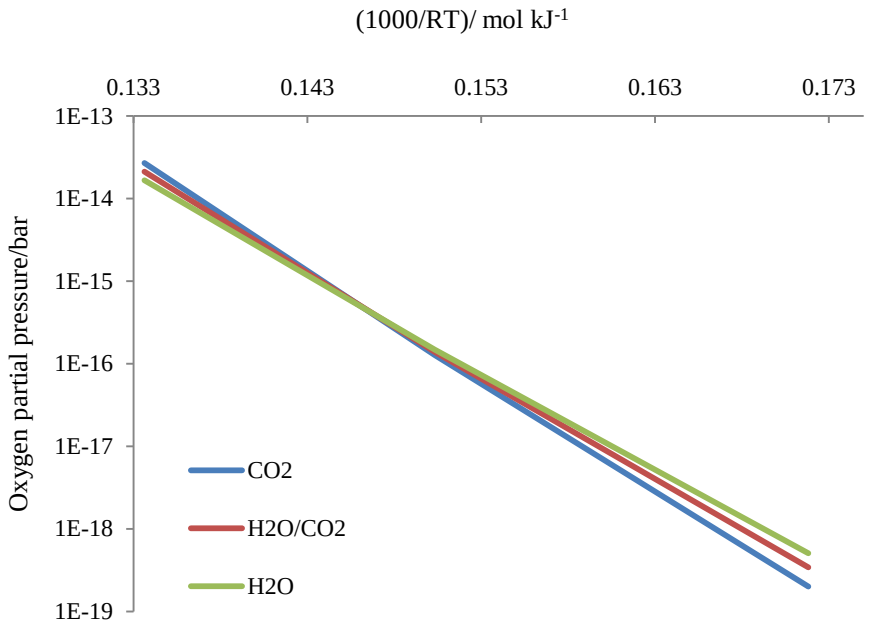

Fig. 3-8 – Equilibrium oxygen partial pressure of different fuel mixtures at OCV conditions. 827 °C is temperature of equilibrium between hydrogen/steam and CO_2/CO mixture. Line at this temperature would be straight.

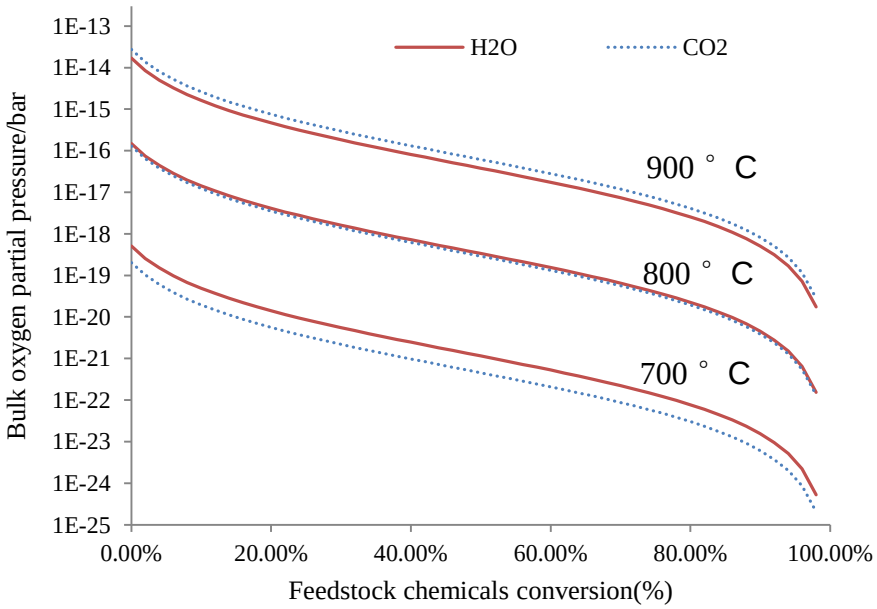

Fig. 3-9 – Exemplary calculation of bulk equilibrium oxygen partial pressure of fuel mixture at 700, 800 and 900 °C. Presented results do not consider partial pressure of oxygen at the interface between electrode and electrolyte, and thus cannot be used directly to calculate transport numbers, or Faradic efficiency. The mixture is being balanced with 5% hydrogen. 827 °C is the temperature at which hydrogen/steam and CO_2/CO mixture is at equilibrium, i.e. non-reacting conditions.

Next the author analyses the effect of feedstock chemicals' conversion on the equilibrium partial pressure of oxygen. Exemplary calculations at 700, 800 and 900 °C as a function of feedstock chemicals' conversion are presented in Fig. 3-9. Again, near 827 °C the curves nearly interlay each other. At feedstock chemicals' conversion of about 90% and 800 °C the cell has $p_{O_2}^{bulk} < 10^{-20}$ and electrolyte's conductivity data is unknown. Similarly, at 700 °C almost entire operation of the cell is in the region outside of the experimentally identified YSZ electrolyte properties. It is important to stress that the reported partial pressure is in the bulk not at the interface, i.e. it does not consider pressure drop due to mass transport through porous electrode and pressure drop due to oxygen transport through the electrolyte. It is expected that the effective pressure at the electrolyte/electrode interface is lower. Therefore, at high fuel utilization, assumption of pure ionic conduction may be invalid.

3.5.3.4 Simulating SOEC operated in excessive polarization conditions or with low feedstock chemicals supply

Results for SOEC simulation operated in excessive polarization conditions are presented in Fig. 3-10. The temperature of operation was set to 810 °C, the ambient pressure to 1 bar and the flow to 50 sccm (83% molar H_2O, 13% molar CO_2, 4% molar H_2). The summary of the simulation parameters used is given in Table 3-2. The presented calculations include the influence of applied electrostatic potential difference on the oxygen partial pressure. Darcy's law was used for fuel electrode to model drop of oxygen partial pressure at high feedstock chemicals' conversion, and thus calculation of concentration loss. The results show that at feedstock chemicals' conversion greater than 80% the Faradic efficiency rapidly drops below 100%. This corresponds well to the data from Fig. 3-9. The consideration of mass transport and electrolyte influence restricted the allowable conversion to 80% from previously expected >90%. Respective surge in potential difference is due to combined effect of concentration loss and switch to mixed conduction in YSZ. It is worth noting that Faradic efficiency is reaching ~5%, not 0%. This is due to a constant supply of steam and carbon dioxide irrespective of polarization. Zero efficiency is expected in the case of finite volume setup, like in the experiments by Pham and Glass. Moreover, in such setup it is expected to observe a drop in conversion due to depletion of the feedstock chemicals at high charge densities (note use of charge, rather than current in this setup). Feedstock chemicals' conversion is calculated from ionic current density and therefore, it departs from linear when ionic transport number

departs from unity. Maximum feedstock chemicals' conversion is achieved simultaneously to short circuit voltage. Increasing injected current density further may result in YSZ reduction and cell failure as described in the previous section.

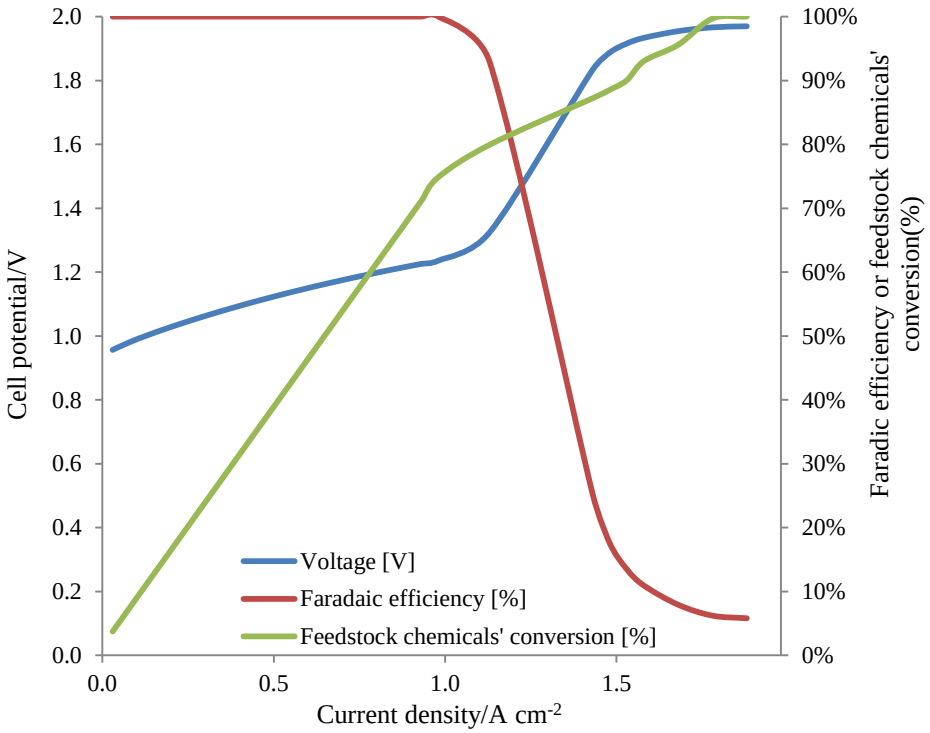

Fig. 3-10 – Exemplary results for SOEC operating at 810 °C in the dominant ionic, mixed and dominant electronic conduction modes. The cell was fed with 83% molar H_2O, 13% molar CO_2 and 4% molar H_2. On the left axis: The continuous line represents the cell potential difference. On the right axis: The dashed line represents Faradic efficiency and the dashed-dotted line represents feedstock chemicals' conversion.

3.5.4 Conclusions

The above chapter theoretically explores the possibility of operating Solid Oxide Electrolyzer Cell based on zirconia electrolyte in conditions with extreme oxygen chemical potential difference. Such circumstances result in decreased Faradic efficiency, hence are not desirable. Moreover, they can occur if the cell works with improper design conditions or is exposed to polarization surge from an intermittent energy source.

A theoretical model is extended from 'standard' model in order to simulate SOEC working in the abnormal conditions, as well as in normal conditions. Material properties required for running the simulation are extrapolated and fitted from the reported

literature data for 8-mol YSZ. Validity of the model is confirmed alongside experimental results. Proposed model can be simplified to a generally accepted form constructed on the assumption of pure ionic conductivity.

Fitted conductivity data is analysed and predictions are made to assure operation with high efficiency. Simple fuel map is reported, showing the allowable design conditions for operating SOEC. Moreover, the assumption of power law exponent for conductivity data is revisited and judged invalid in extremely low oxygen partial pressure gas atmospheres. A correction for the value is suggested.

Sharp increase of potential difference at high current densities in modern electrodes is judged unlikely to be triggered only by the concentration loss. Drop of ionic transport number is suggested as an explanation of the potential difference rise. That is especially reasonable in electrolyte supported cells.

It is shown, that commonly used practice of estimating hydrogen/syngas production rate from Faraday's law cannot be applied unambiguously. Presented model could be used to correctly calculate the electrolysis yield.

Lastly, it is suggested that similar loss mechanism can occur in electrochemical cells based on different electrolyte materials. Proposed model can be modified for simulation of such cells. In case of solid oxide cells no changes are required except the material data. In case of liquid electrolyte cells it is necessary to consider convective term in the Nernst-Planck equation, formula equation (3-84).

3.6 Physical principles of establishment of equilibrium potential in a co-electrolysis Solid Oxide Electrolyzer Cell

This chapter has been published in a modified form as JP Stempien, Q Liu, M Ni, Q Sun, SH Chan. Physical principles for the calculation of equilibrium potential for co-electrolysis of steam and carbon dioxide in a Solid Oxide Electrolyzer Cell (SOEC), Electrochimica Acta, 147, 2014, 490.

3.6.1 Introduction

The Open Circuit Voltage (OCV) is a very important parameter related to the performance of the cell. The OCV reflects the lowest electrical voltage needed for electrolysis reaction or the highest electrical voltage possible to draw from the fuel cell. High values of the OCV are deemed in fuel cells, whereas low are preferred in

electrolyzers. The open circuit voltage of a typical cell is defined by the electrochemical potentials of oxygen on Ni-YSZ/YSZ and LSM-YSZ/YSZ interfaces, i.e. the fuel and air electrodes' interfaces or Triple Phase Boundaries (TPB)[7]. In the literature the calculation of OCV is based on the Nernst equation. However, this equation is hard to use for a reacting (through WGS reaction) gas mixture such as those composed of CO_2, H_2O, CO and H_2 (most common gas mixture for co-electrolysis). In order to circumvent the above issue many authors often assume that the mixture is not reacting, as will be shown in the results section, this assumption is invalid. Moreover, feeding the cell with CO_2 and H_2O creates uncertainty in regard to which of the gases is actually electrolyzed and to what extent. This issue is usually approached by assuming that only H2O is being electrochemically split and CO_2 is being transformed to CO via Reversed Water-Gas shift (RWGS) reaction. (Note that this assumption neglects the benefit of SOEC technology mentioned above).

$$CO_2 + H_2 \rightarrow CO + H_2O \tag{3-96}$$

Stoots et al. developed the first model for co-electrolysis (Stoots et al. 2009). They assumed that the gas mixture is in an equilibrium state via the Water-Gas Shift reaction and then calculated the potential for either CO_2 or H_2O, which were supposed to be equal. Becker et al. (Becker et al. 2012) performed economic analysis of producing liquid fuels via co-electrolysis of CO_2 and H_2O and the Fischer-Tropsch process. They adapted the simplified model of SOEC where they assumed that both CO_2 and H_2O undergo electrochemical reduction, however, they only included H_2O in the calculation of the OCV. The authors based their model on the one from (Stoots et al. 2009). Ni (Ni 2012a, 2012b) calculated the equilibrium potentials for H_2O electrolysis and CO_2 electrolysis separately, based on Nernst equation. During operation, the working potentials for these two electrolysis reactions were assumed the same while their equilibrium potentials were not due to their different overpotential losses. Xie and Xue (Xie & Xue 2012) focused on surface chemistry occurring during co-electrolysis and proposed to use the oxygen conduction reaction to estimate the OCV. Their model required the knowledge

[7] The electrochemically active part of the electrode, where the gas phase, the Ni/LSM phase and YSZ phase meet

of activity of interstitial oxygen, oxygen vacancy and oxygen in air. The authors did not report the value of equilibrium potential. Stempien et al. (Stempien et al. 2012, 2013, 2013) modelled the SOEC for co-electrolysis and the equilibrium potential for H_2O and CO_2 co-electrolysis was weighted by their molar fractions. Li et al. (Li et al. 2013) investigated elementary reactions involved in co-electrolysis, but assumed that only H_2O contributes to the Nernst equation. Recently, several new models analysing co-electrolysis were published (Kazempoor & Braun 2014, 2014, Luo et al. 2014). Kazempoor and Braun assumed that H2O is the only electrochemically active specie, whereas Luo et al. computed the OCV indirectly from the charge balance equation assuming that ratio between H_2O and CO_2 electrolysis is 2.2:1. To the best of our knowledge these are the only publications considering the co-electrolysis, none of them were focused on the calculation of basic characteristic, such as equilibrium potential (OCV).

In this chapter, the models for calculating OCV are summarized and compared with experimental results. Based on the comparison, a simple method is identified for cases with high temperature and low content of CO_2. Furthermore, the author proposes the use of Mixed Potential Theory (MPT) to improve the accuracy of OCV prediction in cases with high CO_2 content or low temperature. The MPT model predicts that the observed OCV is the superposition of potential differences imposed by more than one reaction occurring on the electrochemical interface. To the best of author's knowledge, the MPT model was never used to calculate the equilibrium potential of co-electrolysis. Presented report is the first to consider the calculation of open circuit potential of co-electrolysis SOEC.

3.6.2 Theory

Theoretically, an electrochemical cell can support any reaction performed with use of ions. The requirement is in availability of an electrolyte transporting those ions. Reactions involving splitting of water, carbon oxides, sulphur oxides and nitrogen oxides can be conducted in a solid oxide cell which transports oxygen ions. Electrolytic splitting of water and carbon dioxide is of the most interest for energy industry. The oxygen ion conducting electrolytes are for example YSZ, ScSZ, SDC or GDC.

The reaction occurring in an SOEC can be split into two half reactions assigned to both electrodes. The cathodic half reactions for steam and CO_2 electrolysis are as follows

$$H_2O + 2e^- \rightarrow H_2 + O^= \quad (3\text{-}97)$$

$$CO_2 + 2e^- \rightarrow CO + O^= \quad (3\text{-}98)$$

$$O_2 + 4e^- \rightarrow 2O^= \quad (3\text{-}99)$$

And the anodic reaction is

$$O^= \rightarrow \frac{1}{2}O_2 + 2e^- \quad (3\text{-}100)$$

Assuming that the electrolyte is a pure oxygen-ion conductor[8] the energy barrier required to start the reaction can be calculated from the difference of oxygen electrochemical potential between the Triple Phase Boundary (TPB) of the anode and cathode at the equilibrium condition. The electrochemical potential can be written in general as

$$\bar{\mu} = \mu^0 + RTlna + zF\phi \quad (3\text{-}101)$$

Where μ^0 is the standard chemical potential and can be calculated from the Gibbs energy of specie at given temperature and pressure, *a* is the activity of specie and for the ideal mixtures is equal to the specie partial pressure, ϕ is the inner, Galvani, potential including the contribution from the interface, z is the number of electrons involved in each electrochemical reaction, *R* is the universal gas constant, *T* is the temperature and *F* is the Faraday constant. From the above the inner potential cannot be determined experimentally.

The inner potential is the sum of outer potential (Volta potential, ψ) and surface potential, χ. The inner potential and the surface potential cannot be determined experimentally. Only the difference of the inner potential of two electrodes can be measured and at zero current flow, that is the OCV. The outer potential arises from any free charge on an interface and can be measured with a Kelvin probe. The surface potential arises from the special arrangement of interface and can be further

[8] See our previous publication for discussion of this assumption (previous chapter)

distinguished into two contributions. The above terms are often used to derive the absolute electrode potential which could be in principle used to calculate the equilibrium cell potential. A large research effort in this area can be attributed to Trasatti (Trasatti 1974, 1982, 1986, 1990). A recent review was done by Fawcett (Fawcett 2008).

Conditions for the equilibrium require that the pressure, temperature and electrochemical potential at both electrodes are equal. Thus, one can calculate the difference of Galvani potential (the OCV) resulting from the activities (a) difference as

$$\Delta\phi_{eq}Fz = \mu^0_{cat} - \mu^0_{an} + RTln\left(\frac{a_{cat}}{a_{an}}\right) \tag{3-102}$$

Since the temperature, pressure and specie (oxygen in the case of typical SOEC) is the same on both electrodes $\mu^0_{cat} - \mu^0_{an} = 0$.

Thus, one can write

$$\Delta\phi_{eq} = \frac{RT}{zF}ln\left(\frac{a_{cat}}{a_{an}}\right) \tag{3-103}$$

Equation 3-103 is a form of the Nernst equation and is valid for any non-reacting gas mixture

In case of oxygen ion conductor, it can be written as

$$\Delta\phi_{eq} = \frac{RT}{zF}ln\left(\frac{[O^{\cdot\cdot}_x]_{cat}}{[O^{\cdot\cdot}_x]_{an}}\right) \tag{3-104}$$

where the concentration of oxygen vacancies ($[O^{\cdot\cdot}_x]$) at the cathode site is dependent on a contribution from each of the reactions Equation 3-97 to 3-100. Under the conditions of equilibrium and ideal gas it can be represented by the partial pressure of oxygen on both sides of the cell.

Interestingly, the standard approach is actually to derive the form of Nernst equation from an overall functional reaction of the cell, rather than the electrolyte, e.g. the hydrogen or carbon monoxide production. Thus, most often used form, referred in this section as the standard model, is

$$\Delta\phi_{eq} = \Delta\phi^0 + \frac{RT}{2F} ln\left(\frac{p_{H_2}^{l} p_{O_2}^{\frac{1}{2}}}{p_{H_2O}^{l}}\right) \quad (3\text{-}105)$$

where $\Delta\phi^0$ is the standard equilibrium potential equal to standard chemical potential difference (difference in Gibbs function at standard temperature and pressure) divided by *zF*, power exponents in the partial pressure terms follow from the stoichiometric coefficients of the cell reaction Equation 3-100 (in the case of hydrogen producing cell). The Mixed Potential Theory was first proposed by Fleming (Fleming 1977) to explain the physical principle of nonideal behaviour of YSZ oxygen sensor operated in the gas mixtures of oxygen and CO_2. The work of Fleming unleashed a torrent of research on so-called Non-Nernstian sensors allowing the detection of hydrocarbon combustion products, including CO, CO_2, H_2 and H_2O. Anderson and Graves (Anderson & Graves 1981) later proposed a similar model for YSZ oxygen sensor, but included a chemical kinetics' contribution from electrode boundary layer. The proposed model is not widely used, despite its potential to include electrode kinetics in the calculation of equilibrium potential. Brailsford et al. (Brailsford et al. 1998) (and references therein) proposed a model similar to Fleming's, however, considering more species taking part in the establishing of equilibrium potential. Their model is based on the same physical principles as the Fleming's model. More recently, Wachsman et al. (Wachsman et al. 2001) questioned the universal applicability of the Mixed Potential Theory by giving the example of sensors working without reference electrode, i.e. one chamber sensors (for fuel cell equivalent please see (Hibinio et al. 2000, Nagao et al. 2010)). The authors counter proposed to use Differential Electrode Equilibria theory. Reviews covering the current models used in sensor science can be found in (Lopez-Gandara, et al. 2009, Fergus 2011).

According to the Mixed Potential Theory the measurable potential difference is the superposition of potential differences resulting from reactions Equation 3-97 – 3-99, as described by Equations 3-104 and 3-105. The contribution of each reaction is dependent on the coverage of reactant gas species at the TPB, and the potential difference at equilibrium can be written as

$$\Delta\phi_{eq} = \theta_{O_2}\left[\frac{RT}{4F}\ln\left(\frac{p_{O_2}^{cat}}{p_{O_2}^{an}}\right)\right] + \theta_{H_2O}\left[\frac{\Delta\mu_{H_2O}^0}{2F} + \frac{RT}{2F}\ln\left(\frac{p_{H_2}\sqrt{p_{O_2}}}{p_{H_2O}}\right)\right] + \theta_{CO_2}\left[\frac{\Delta\mu_{CO_2}^0}{2F} + \frac{RT}{2F}\ln\left(\frac{p_{CO}\sqrt{p_{O_2}}}{p_{CO_2}}\right)\right] \quad (3\text{-}106)$$

Where θ_i is the coverage of specie i, and $\Delta\mu^0$ is the standard chemical potential difference of reactions Equation 3-97 and 3-98 and can be calculated from the Gibbs energy difference of respective reaction. The partial pressure of all species is obtained by minimizing the Gibbs energy of initial gas composition, thus the condition for non-reacting gas mixture is met. The coverage of other species, like hydrogen or carbon monoxide also needs to be calculated as it is thought that covering of fuel electrode's TPB with product gas may increase the observed equilibrium potential.

To calculate the coverage of respective specie the author assumes the adsorption process to follow the Langmuir isotherm. The consideration of appropriate adsorption isotherm was recently published by Mocoteguy and Brisse (Mocoteguy & Brisse 2013). In the following work, however, the author assumes that the empty site does not influence the calculation of equilibrium potential and therefore used coverages are relative to other adsorbates only, but not the empty site. Thus, a modified Langmuir adsorption law is used. The coverages are calculated from a following expression.

$$\theta_j = \frac{K_j p_j}{\sum_i K_i p_i} \quad (3\text{-}107)$$

Where K_i represents the adsorption constant of specie i and p_i is the partial pressure of specie i. The adsorption constant is calculated from the kinetic gas theory

$$K_i = K_i^0\, exp\left(\frac{Q_i}{RT}\right) \quad (3\text{-}108)$$

Where Q_i is the enthalpy of adsorption, K_i^0 is the standard adsorption constant, R and T are as defined before.

The values of enthalpy of adsorption and standard adsorption constant reported in the literature are given in Table 3-3.

Table 3-3 – The values of enthalpy of adsorption and standard adsorption constant reported in the open literature.

Specie	Enthalpy of adsorption kJ mol^{-1}	Standard adsorption constant	Source
CO	135.7 – 167.36	$5.127x10^{-13}$ – $3.6x10^{-2}$ or 475 – 1490	(Fleming 1977, Hou & Hughes, 2001)
CO_2	18.828 – 64.852	0.76 – 2.62	(Kester 1974)
H_2O	13.2 – 18.6 or 56 – 113	0.16 – 9.251	(Hou & Hughes 2001)
H_2	13.8 – 19.25 or 86.1 – 112.968	$5.68x10^{-10}$ – 10^{-3}	(Hou & Hughes 2001, Horiuti & Toya 1965)
O_2	83.68 – 439.32	$1.7x10^{-8}$	(Fleming 1977, Malyshev et al. 1977)

The values of enthalpy of adsorption and standard adsorption constant reported in the literature were found for Nickel, except CO_2 where the values are for ruthenium. The range of the values is significant, thus fitting of the data to experiments is required. The large ranges of values are due to multiple experimental set ups resulting in largely different values. The author speculates that the discrepancy may be due to testing different structural types of catalyst.

In previous chapter (chapter 3.5) the author examined the assumption of pure ionic conduction in Solid Oxide Cells and proposed to use a more general formulae incorporating an influence from the electronic conduction under certain conditions. Taking account of those findings one can write

$$\Delta\phi_{observed} \cong OCV = t_i \Delta\phi_{eq} + t_{eh} \frac{RT}{4F} ln\left(\frac{p_{O_2}^{cat}}{p_{O_2}^{SCV}}\right) \tag{3-109}$$

where *t* is the electrolyte's transport number describing the ratio of ionic and electronic conductivity to the total conductivity and $\Delta\phi_{equilibrium}$ is the Equation 3-106.

Inserting formulae Equation 3-106 into 3-109 yields

$$OCV = t_i\theta_{O_2}\left[\frac{RT}{4F}ln\left(\frac{p_{O_2}^{cat}}{p_{O_2}^{an}}\right)\right] + t_i\theta_{H_2O}\left[\frac{\Delta\mu_{H_2O}^0}{2F} + \frac{RT}{2F}ln\left(\frac{p_{H_2}\sqrt{p_{O_2}}}{p_{H_2O}}\right)\right] + t_i\theta_{CO_2}\left[\frac{\Delta\mu_{CO_2}^0}{2F} + \frac{RT}{2F}ln\left(\frac{p_{CO}\sqrt{p_{O_2}}}{p_{CO_2}}\right)\right] + t_{eh}\frac{RT}{4F}ln\left(\frac{p_{O_2}^{cat}}{p_{O_2}^{scv}}\right) \quad (3\text{-}110)$$

Equation 3-110 describes the contribution to open circuit potential in the most general case. It has never been reported previously.

3.6.3 Experimental

Equilibrium potential measurements were done on two types of cell. First cell was a symmetrical Pt|YSZ|Pt and represented a case where equilibrium of half reactions is expected on both electrodes. Second cell was a Ni-YSZ electrode supported cell of configuration Ni-YSZ|YSZ|LSCF-GDC and represented the case of modern SOEC, where lack of half reaction equilibrium on fuel electrode is expected.

Symmetrical Pt cells were prepared by a following method. Yttria-stabilized zirconia (YSZ) electrolyte substrates were prepared from 8 mol% Y_2O_3–ZrO_2 powders (Tosoh, Japan) by a conventional die-pressing process, followed by sintering in air at 1450 °C for 4 h. After surface grinding with sandpaper (180 mesh), the electrolyte substrates had dimensions of 18.2 mm in diameter and 1.0 mm in thickness. Pt paste was applied onto the centre of each side of the electrolyte substrate and subsequently fired at 900 °C for 2 h to form a complete symmetrical Pt cell with an electrode area of 0.5 cm^2.

Ni-YSZ electrode-supported cell's substrates were prepared by a die-pressing process from powders of YSZ, NiO (J.T. Baker, US) and carbon black in a composition of 36, 54 and 10 wt% respectively. The carbon black was used as a pore former. The green Ni-YSZ substrates were then fired at 900 ºC to burn out the carbon black and to increase the mechanical strength of the substrate and subsequently coated with YSZ film using a suspension spray method. The coated Ni-YSZ substrates were co-sintered at 1400 ºC for 3 h to obtain electrolyte/electrode bilayer structures with dense YSZ electrolyte films supported on porous Ni-YSZ electrode substrates. The bilayer structures had dimensions of ca. 18.3 mm in diameter, 0.8 mm in thickness for the Ni-YSZ substrate and 10 μm in thickness for the YSZ film. A paste, which was prepared by mixing LSCF ($La_{0.6}Sr_{0.4}Co_{0.2}Fe_{0.8}O_3$, Nextech, US) powder and GDC ($Gd_{0.1}Ce_{0.9}O_{1.95}$, Nextech, US) powder (50:50 in weight) with appropriate amount of ink vehicle (Nextech, US), was then screen-printed onto the electrolyte side of the bilayer sample and subsequently fired

at 900 °C for 2 h. The active area of the LSCF-GDC electrode was 0.5 cm2. To ensure a good current collection, another layer of Pt paste was painted onto the LSCF-GDC electrode surface followed by firing at 900 °C for 30 min.

Electrochemical characterization of the cell was carried out using an in-house built SOFC/SOEC test station which included sample holder, vertical tubular furnace, humidifier, temperature controllers, gas flow path, mass flow meters and electrochemical measuring system. The cell was mounted to the sample holder with the fuel electrode side sealed using a ceramic paste (Ceramabond 552, Aremco, USA) and the oxygen electrode side exposed to the ambient air. To examine the OCV of the cell under different operation conditions, fuel gases in various compositions of H_2, H_2O, CO_2 and CO were introduced into the fuel electrode chamber at different temperatures with an overall gas flow rate fixed at 50 sccm. The OCV data of the cell were recorded using an Autolab PG30/FRA system (Eco Chimie, Netherlands).

3.6.4 Results and discussion

All the calculations were performed in Aspen HYSYS with Peng-Robinson equation of state (Robinson et al. 1985). The calculation followed the methods described in the theory section.

The measurements of Pt symmetrical cell's OCV performed to aid presented discussion are summarized as circles in Fig. 3-11 (a-c). Lines represent the OCV values as calculated from the standard model equation (3-105) as used in (Stoots et al. 2009, Becker et al. 2012, Ni 2012, 2012, Xie & Xue 2012). Fig. 3-11 (d-f) show the error of used model in percentage terms. As seen, the values are considerably off those experimentally observed. The error ranges from 10% to 20% in relative terms or from 0.1 to 0.16 V in absolute terms. Such discrepancy was not expected for H_2O/H_2 and CO_2/CO mixtures, as these are non-reacting mixtures. An explanation to the findings could be that some oxidation occurs spontaneously at Pt electrodes or concentration of reactant gases at the TPB are different than in the bulk for some other reason.

a

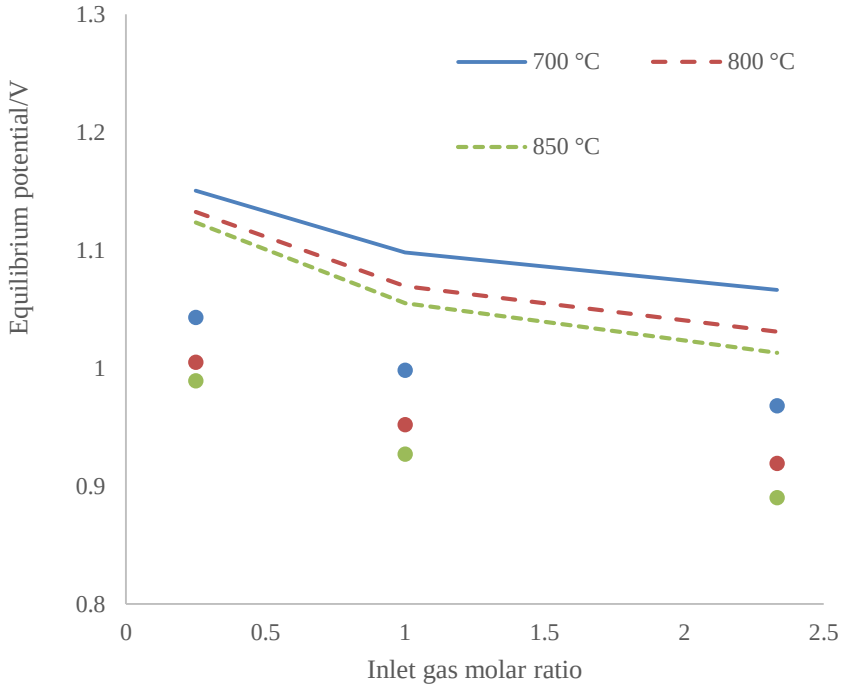
1.3
1.2
1.1
1
0.9
0.8
Equilibrium potential/V
700 °C
800 °C
850 °C
0
0.5
1
1.5
2
2.5
Inlet gas molar ratio

d

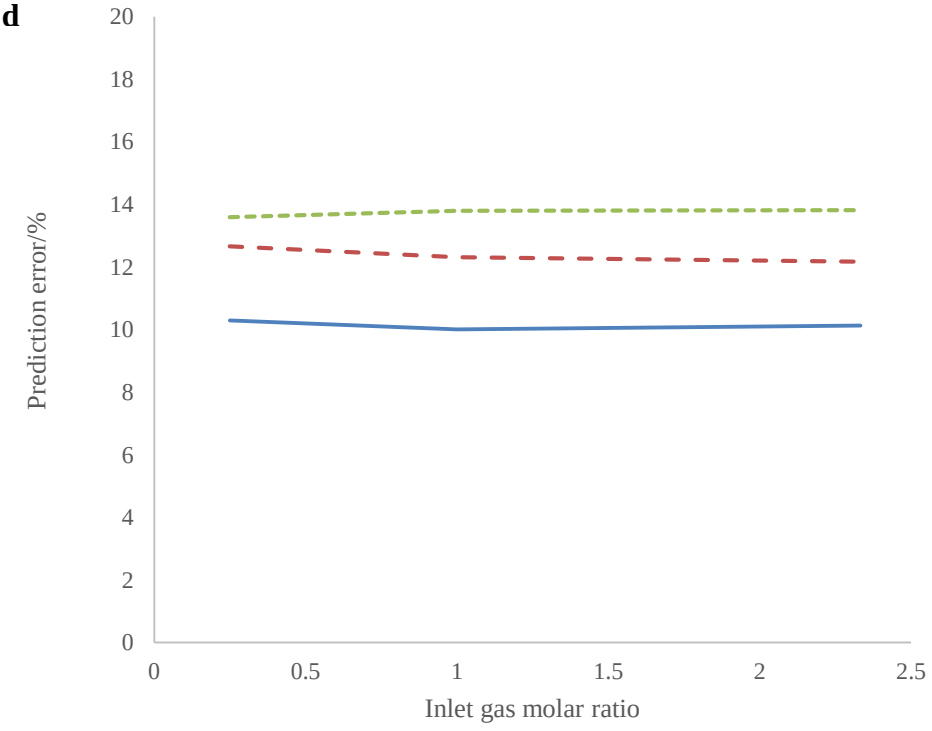
20
18
16
14
12
10
8
6
4
2
0
Prediction error/%
0
0.5
1
1.5
2
2.5
Inlet gas molar ratio

b

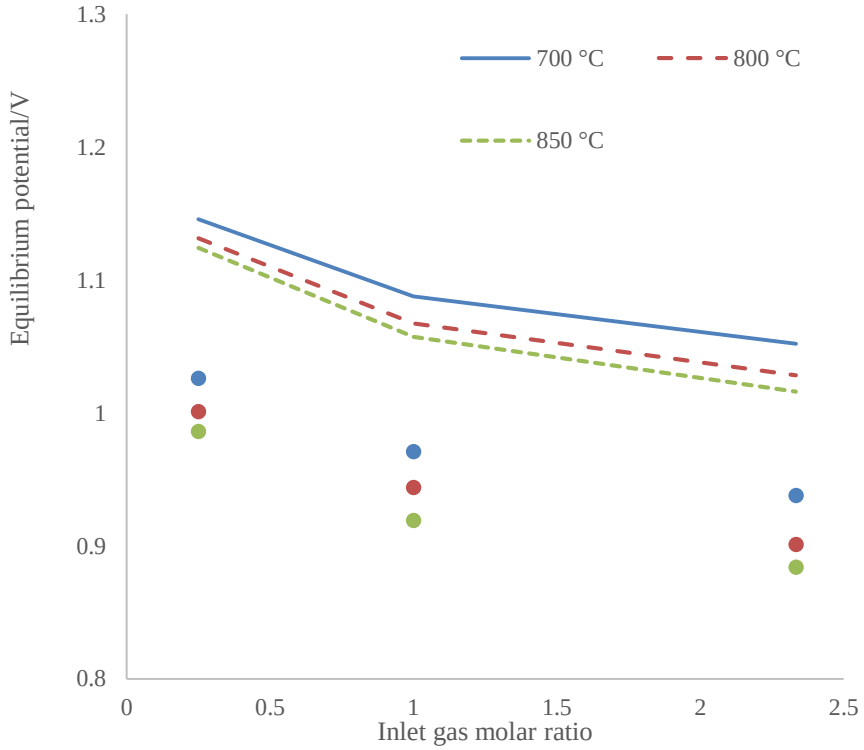
1.3
1.2
1.1
1
0.9
0.8
Equilibrium potential/V
700 °C
800 °C
850 °C
0
0.5
1
1.5
2
2.5
Inlet gas molar ratio

e

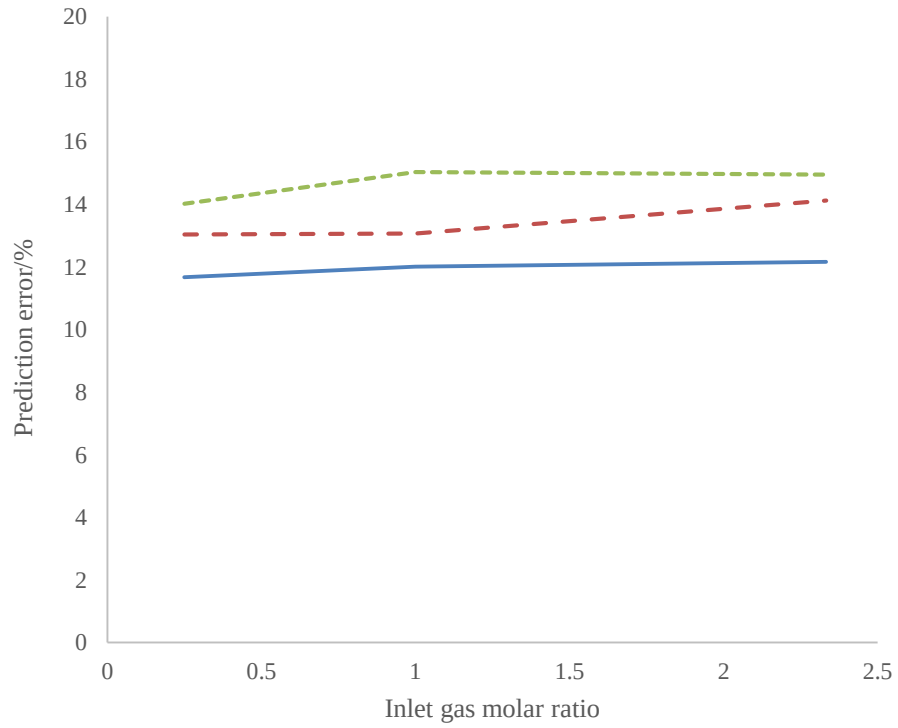
20
18
16
14
12
10
8
6
4
2
0
Prediction error/%
0
0.5
1
1.5
2
2.5
Inlet gas molar ratio

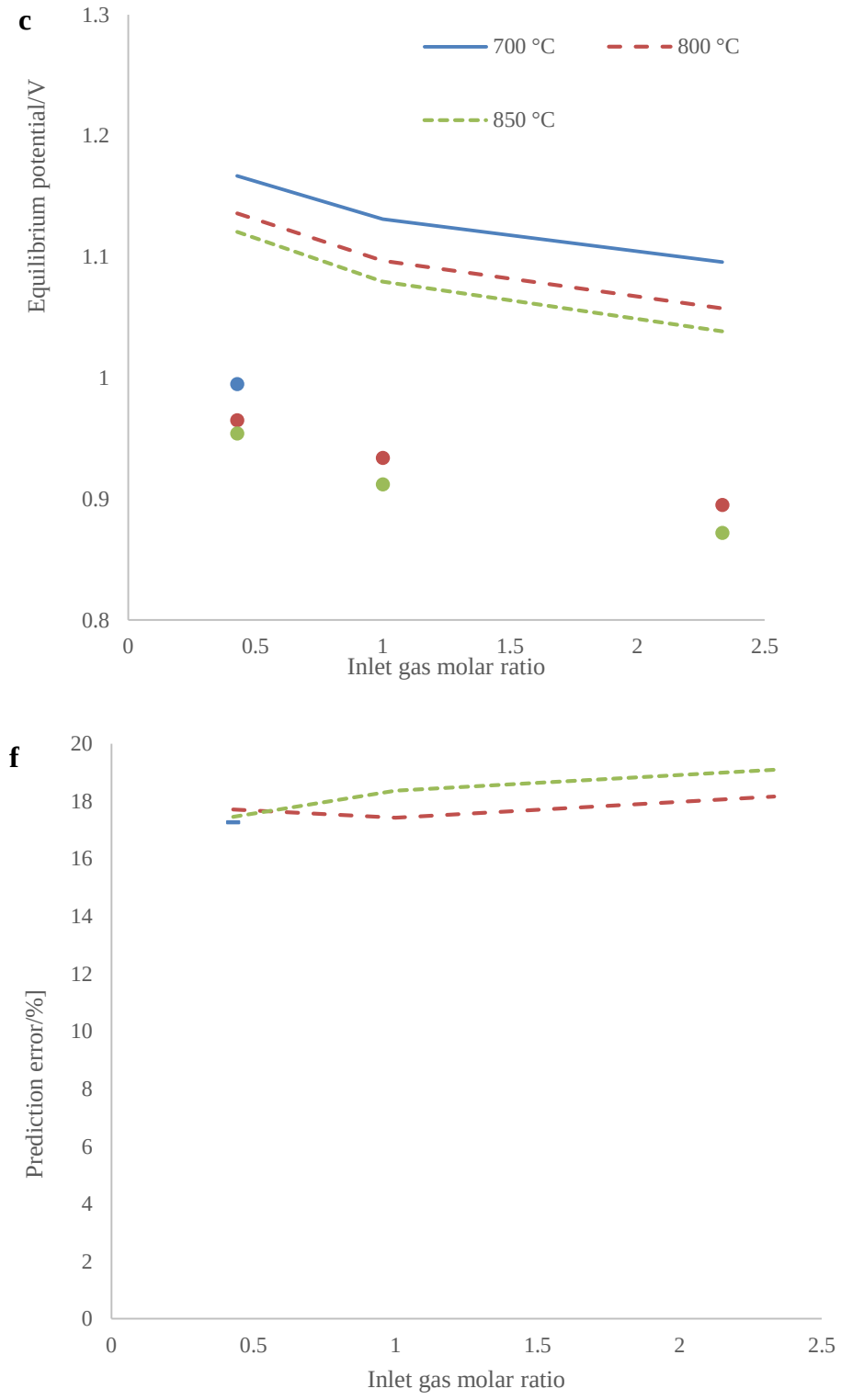

Fig. 3-11 – Comparison of experimentally observed OCV values for Pt-cell (dots) and those calculated with the standard model equation (3-105) (lines) (a-c). Prediction error of the standard model (d-f). a and d refer to CO_2/H_2 mixtures, b and e to H_2O/H_2 mixtures and c and f to CO_2/CO mixtures.

To improve the prediction accuracy, instead of computing the equilibrium potential based on reaction 3-97 or 3-98, the author calculates the equilibrium oxygen partial pressure of the gas mixture and use the Nernst Equation 3-104 to predict the equilibrium potential of reaction 3-99. The author assumes here that the concentration of oxygen interstitial on anode's and cathode's TPBs are equal to the oxygen concentration in the bulk of anode's and cathode's channels. The assumption is valid under the equilibrium conditions. Such approach was recently used for a SOFC modelling by Milewski (Milewski 2012). The results are shown in Fig. 3-12 (a-c) and the method error is shown in Fig. 3-12 (d-f). The values based on oxygen partial pressure are surprisingly close to the experimental values.

In the case of H_2O/H_2 mixtures the error is always below 1%, which can be considered a good match and no further improvement is needed. In other words, reaction 3-97 is much faster than reaction 3-99 and reaction 3-99 is setting the equilibrium value. This is expected in the temperature range above 700 °C for cells with Pt electrodes.

In the case of CO_2/CO gas mixture, the results are only acceptable for temperature above 850 °C. In the case of lower temperature, the error ranges from 1.5 to 4%. Due to experimental difficulties the author could not measure all the OCV values at 700 °C. For an unknown reason at 700 °C the cell did not achieve stable OCV value, the author did not investigate into that. The sole recorded value should be, thus, treated with caution. Nevertheless, it is observed that reaction 3-98 contributes to the mixed potential. In other words, reactions 3-98 and 3-99 are of similar kinetics in the analysed temperature range for a cell with Pt electrodes. Such behaviour is well described in the open literature (Fleming 1977). Simple metal oxide's electrodes and doped perovskite oxide electrodes are described as creating even stronger mixed potential response, i.e. the reaction 3-98 is slower on those electrodes (Hibino et al. 2001).

a

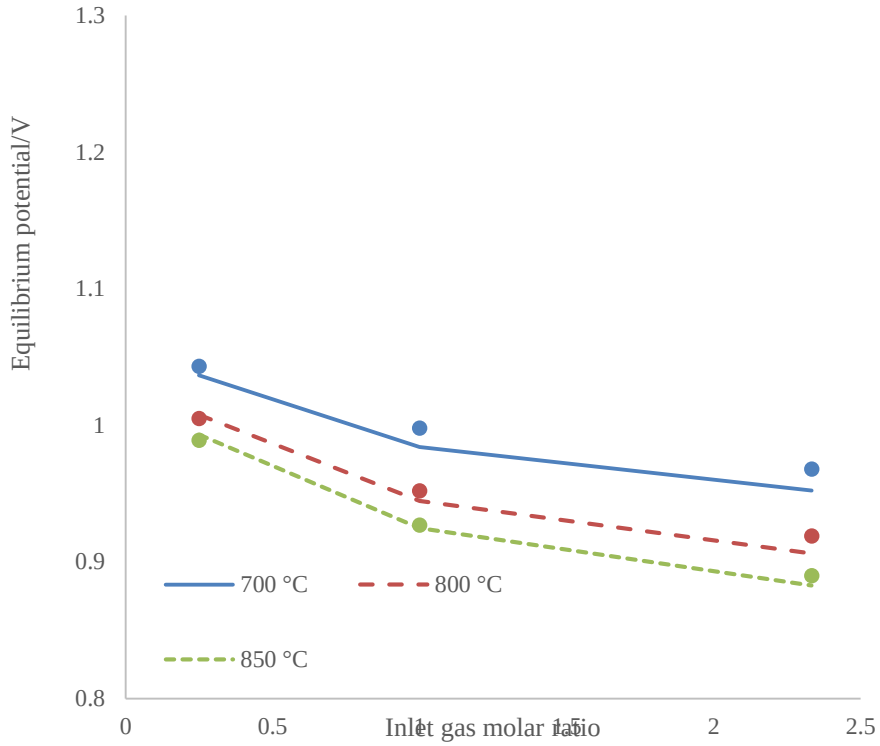
Equilibrium potential/V
1.3
1.2
1.1
1
0.9
0.8
0
0.5
1
1.5
2
2.5
Inlet gas molar ratio
700 °C
800 °C
850 °C

d

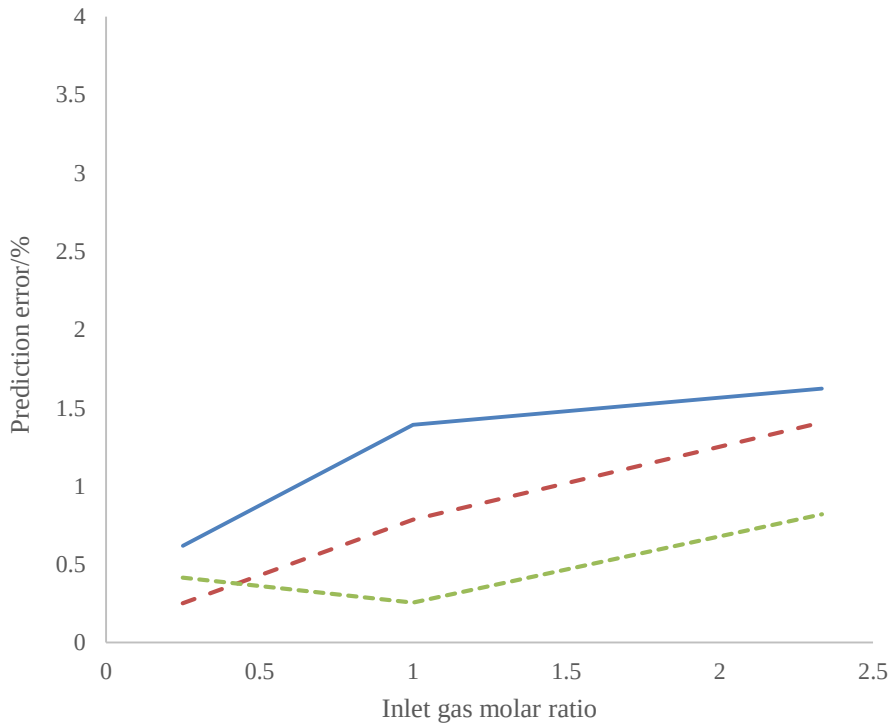
Prediction error/%
4
3.5
3
2.5
2
1.5
1
0.5
0
0
0.5
1
1.5
2
2.5
Inlet gas molar ratio

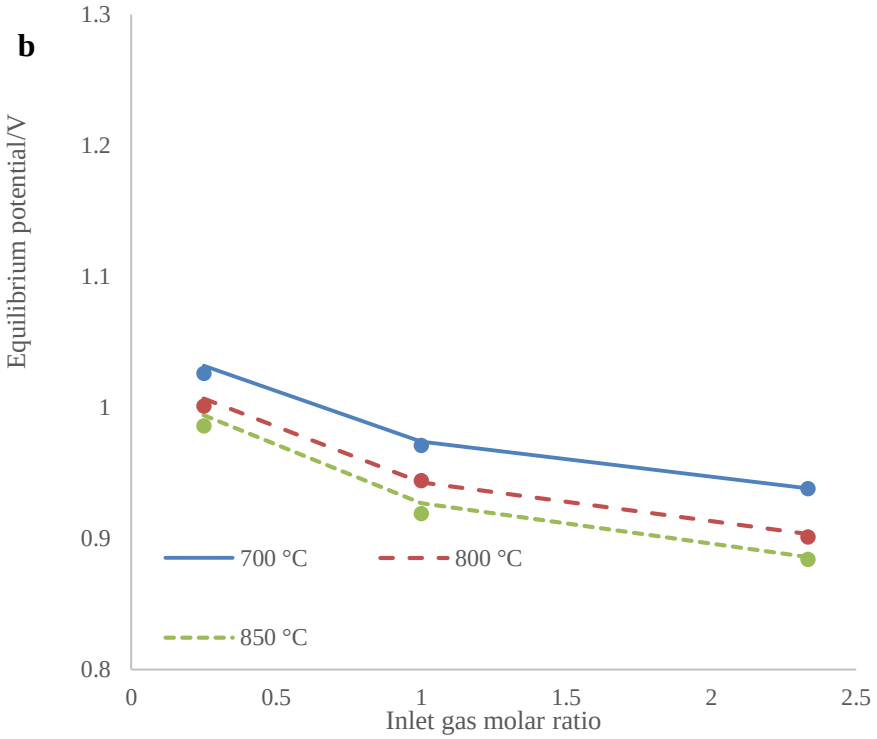
b
Equilibrium potential/V
1.3
1.2
1.1
1
0.9
0.8
0
0.5
1
1.5
2
2.5
Inlet gas molar ratio
700 °C
800 °C
850 °C

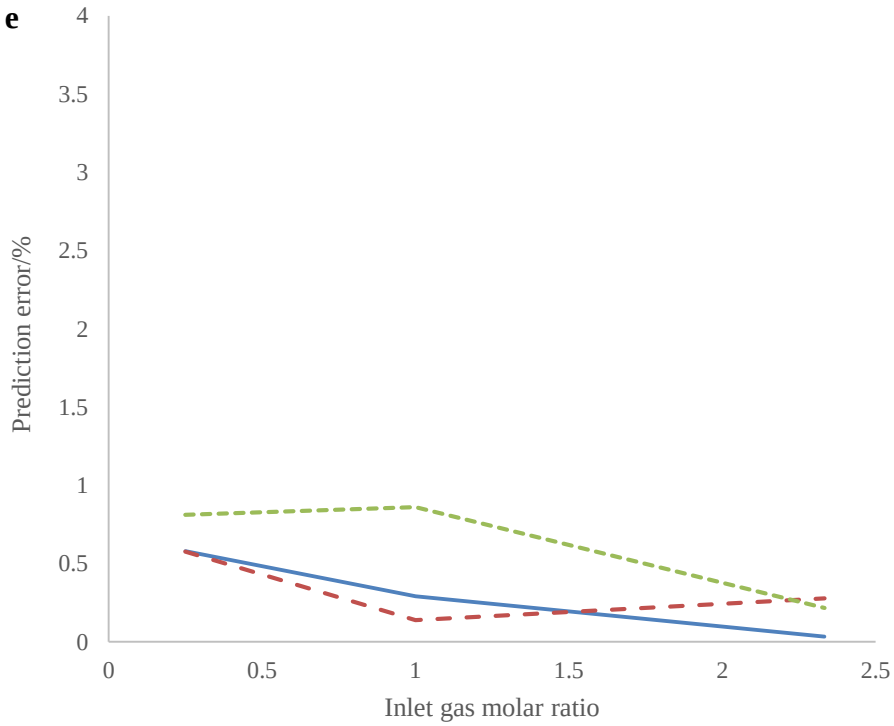
e
Prediction error/%
4
3.5
3
2.5
2
1.5
1
0.5
0
0
0.5
1
1.5
2
2.5
Inlet gas molar ratio

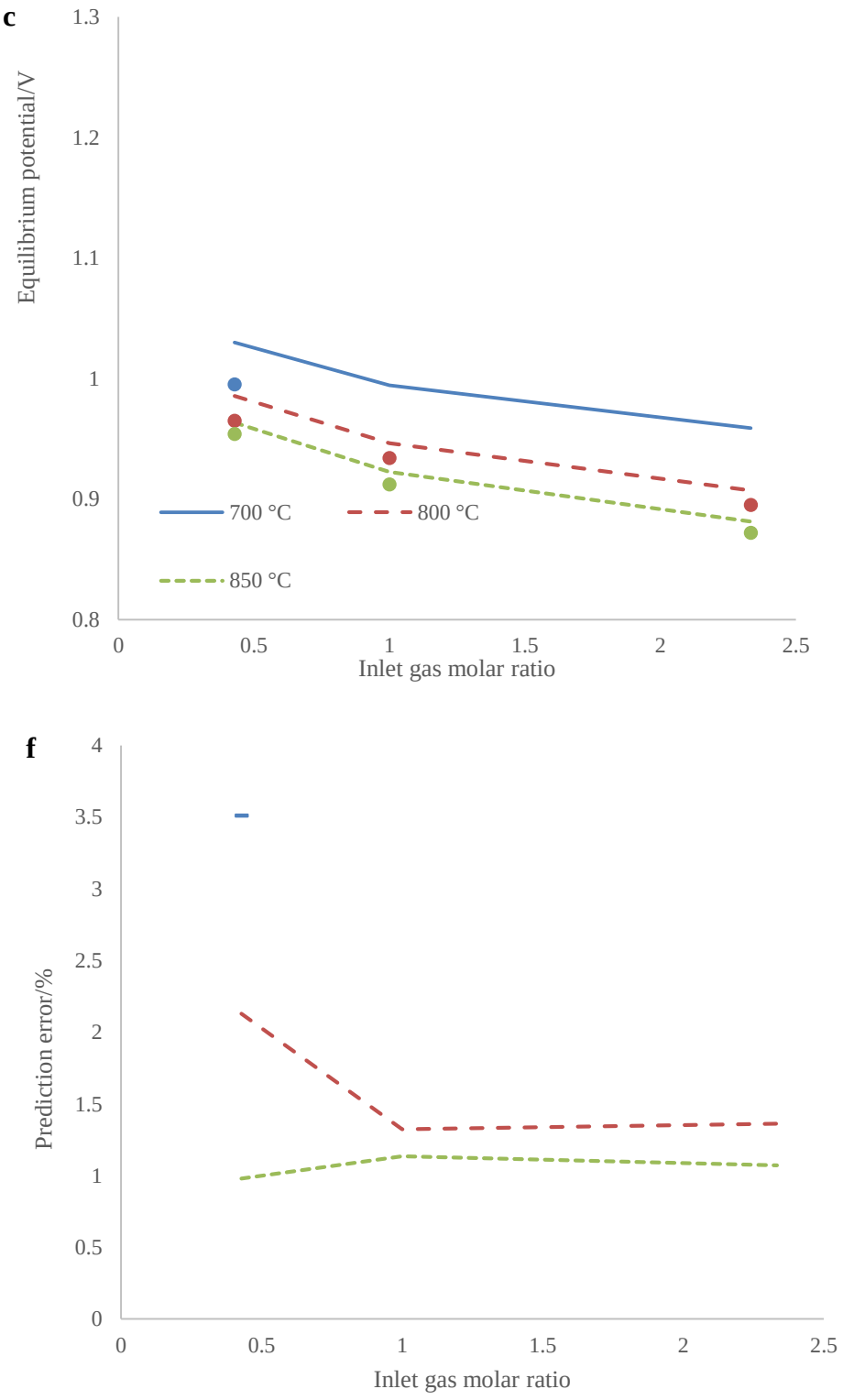

Fig. 3-12 – Comparison of experimentally observed OCV values for Pt-cell (dots) and those calculated with the oxygen partial pressure model equation (3-104) (lines) (a-c). Prediction error of the oxygen partial pressure model (d-f). a and d refer to CO_2/H_2 mixtures, b and e to H_2O/H_2 mixtures and c and f to CO_2/CO mixtures.

In order to compare the model based on oxygen partial pressure with measurements from a state-of-the-art cells composed of Ni-YSZ fuel electrode, the author gathered some of results from our past in-house cell testing. Fig. 3-13 (a-c) compares the standard model, oxygen partial pressure model and the experimental observations conducted at 800 °C for water electrolysis and co-electrolysis with different content of CO_2. It is observed that the discrepancy between the standard model and the measured equilibrium potential values are more visible than in the Pt symmetrical cell case. As stated in above paragraph, it is an expected phenomenon in temperatures below 1000 °C. The error of the oxygen partial pressure method is more visible as well, despite the experiments are conducted in high temperature, Fig. 3-13 (d-f). Interestingly, the lowest discrepancy is observed for the second co-electrolysis experiments with $H_2O/CO_2/H_2$ gas feedstock, however it must be noted that used gas mixtures were very close to stoichiometry (Table 3-4).

Highest discrepancy for the steam electrolysis was observed at gas composition of 97% hydrogen and 3% steam, it was 4%. Analysing Equation 3-110 one may notice that the observed mixed potential is a function of steam coverage. At only 3% steam in the gas stream, the used adsorption model may be not accurate enough. However, more probable explanation is that the actual gas composition could be different than experimentally set or the quality of the YSZ film was not good enough (not dense enough). In the group's lab a bubbler is used to control steam content and hydrogen as a carrier gas for the steam. Perhaps at low steam concentration this method is not very accurate.

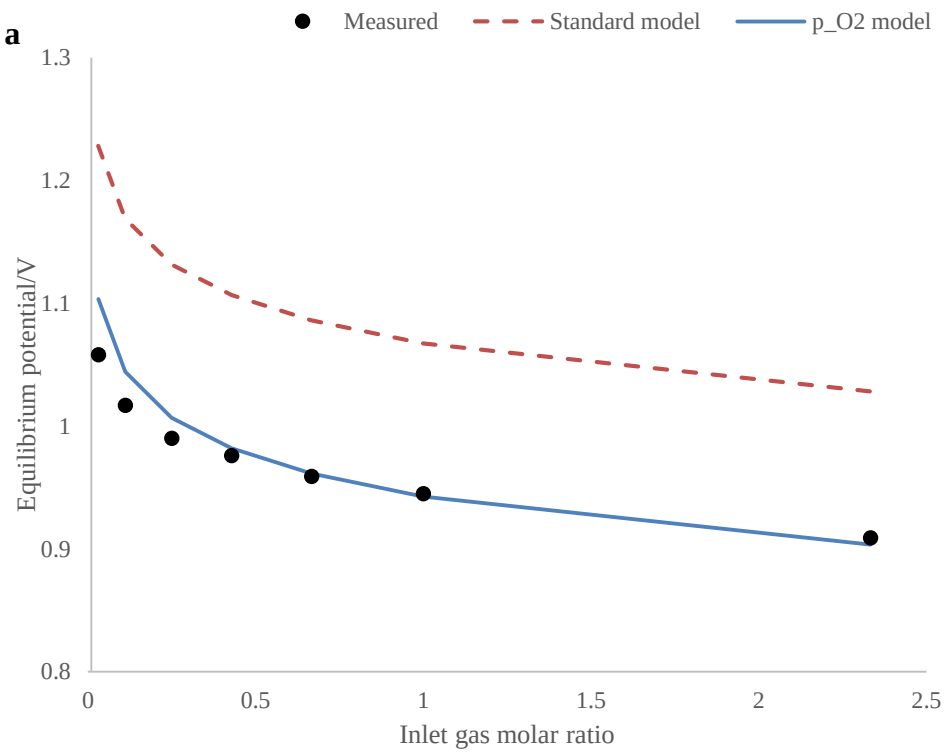
a
Measured
Standard model
p_O2 model
Equilibrium potential/V
1.3
1.2
1.1
1
0.9
0.8
0
0.5
1
1.5
2
2.5
Inlet gas molar ratio

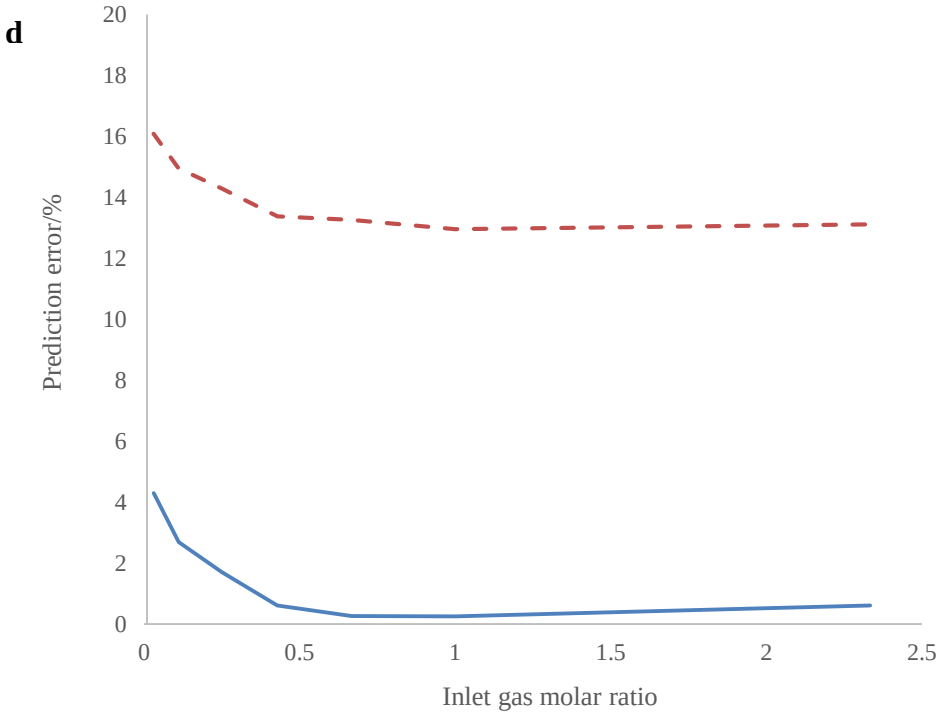
d
Prediction error/%
20
18
16
14
12
10
8
6
4
2
0
0
0.5
1
1.5
2
2.5
Inlet gas molar ratio

b

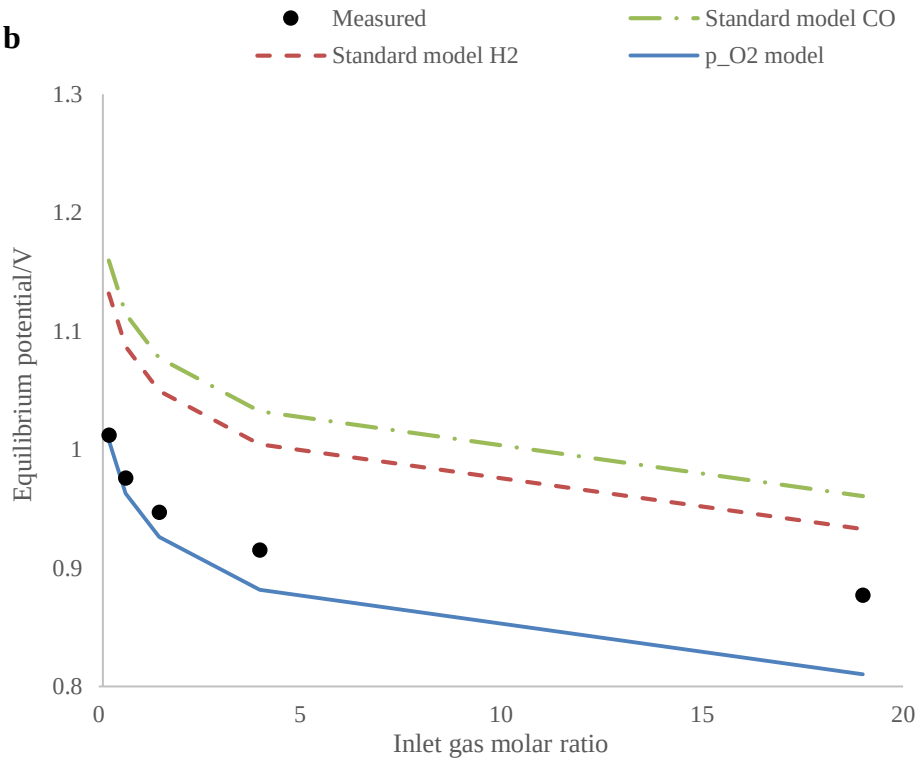
Measured
Standard model CO
Standard model H2
p_O2 model
Equilibrium potential/V
1.3
1.2
1.1
1
0.9
0.8
0
5
10
15
20
Inlet gas molar ratio

e

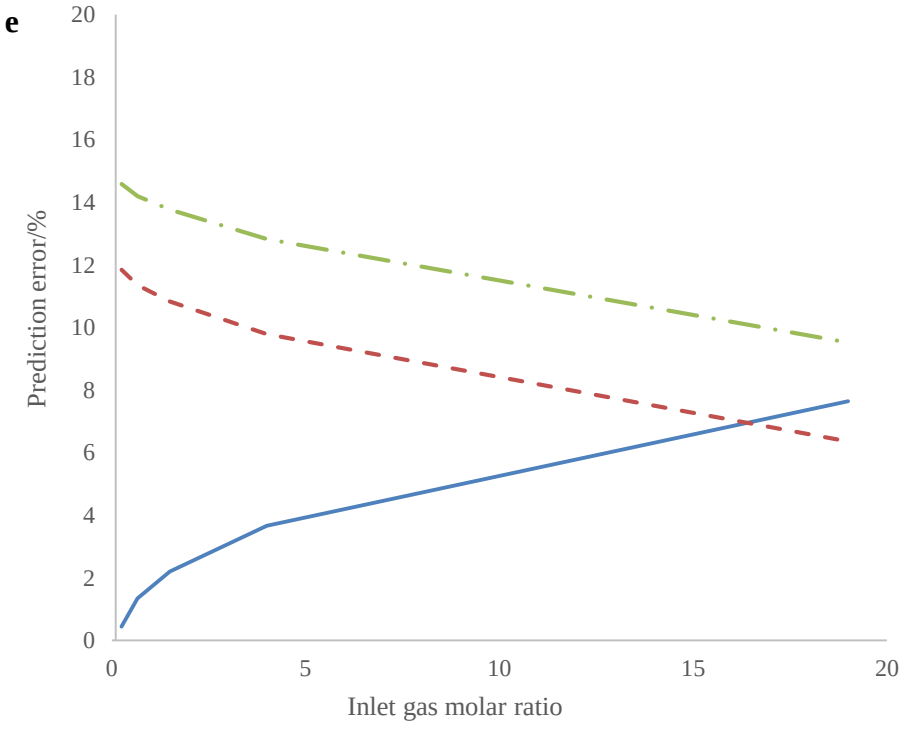
Prediction error/%
20
18
16
14
12
10
8
6
4
2
0
0
5
10
15
20
Inlet gas molar ratio

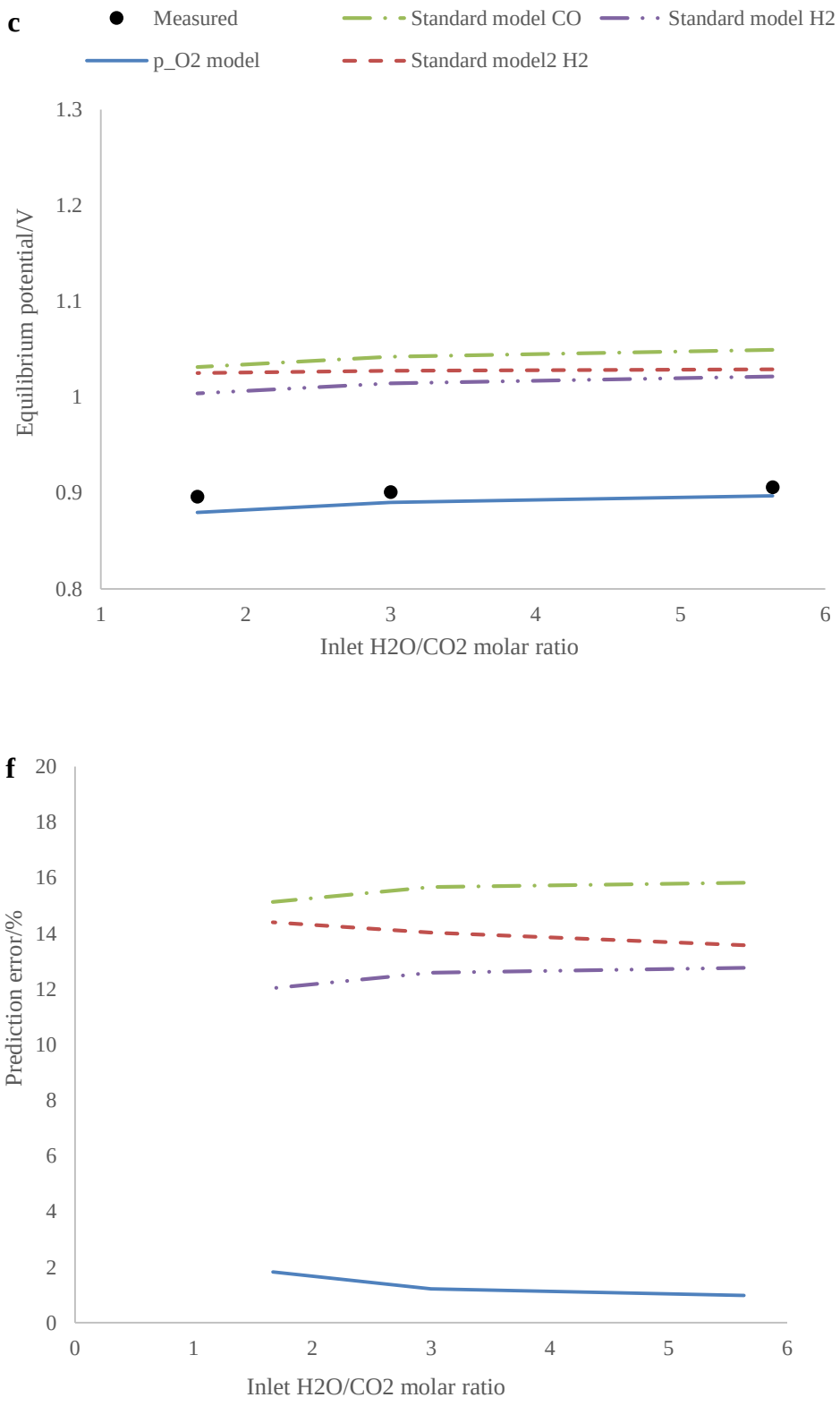

Fig. 3-13 – Comparison of experimentally observed OCV values for Ni-YSZ cell (dots) and those calculated with standard model equation (3-105) and oxygen partial pressure model equation (3-104) (a-c) (lines). Prediction error of the tested models (d-f). a and d refer to H_2O/H_2 mixtures, b and c to CO_2/H_2 mixtures and c and f to $H_2O/CO_2/H_2$ mixtures.

As expected, the results for CO_2/H_2 co-electrolysis of high CO_2 content are difficult to predict. The error of oxygen partial pressure method reaches 8% for inlet gas mixture 95% CO_2 and 5% H_2. Interestingly, the error of the standard model is dropping with increase of CO_2 concentration. This may suggest that reaction 3-98 is similarly fast to reaction 3-99 or 3-97 at high carbon dioxide concentration.

In the second case of co-electrolysis where, all CO_2 H_2O and H_2 are present in the inlet stream, the oxygen partial pressure method seem to be very accurate, with the error below 2% in all investigated cases. This suggests that reaction 3-97 and 3-98 are much faster than reaction 3-99 in this case.

To further investigate the possible influence of mixed ionic/electronic conduction in the electrolyte, the author checked the values of oxygen partial pressure of used gas mixtures at the fuel electrode. Moreover, in order to elucidate the influence of composition in the co-electrolysis cases the results with equilibrated gas compositions, rather than the inlet gas compositions were compared. Non-reacting gas composition is summarized in a table in Table 3-4.

Table 3-4 – Non reacting gas composition used in standard model calculations.

Case	Inlet molar concentration	Non-reacting molar concentration				
		p_{O_2}	p_{CO}	p_{CO_2}	p_{H_2}	$p_{\mathrm{H_2O}}$
Ni-YSZ 800 °C	H_2O: 0.03 H_2: 0.97	3.9×10^{-22}	-	-	0.97	0.03
	H_2O: 0.10 H_2: 0.90	5.1×10^{-21}	-	-	0.90	0.10
	H_2O: 0.20 H_2: 0.80	2.6×10^{-20}	-	-	0.80	0.20
	H_2O: 0.30 H_2: 0.70	7.6×10^{-20}	-	-	0.70	0.30
	H_2O: 0.40 H_2: 0.60	1.8×10^{-19}	-	-	0.60	0.40
	H_2O: 0.50 H_2: 0.50	4.1×10^{-19}	-	-	0.50	0.50
	H_2O: 0.70 H_2: 0.30	2.2×10^{-18}	-	-	0.30	0.70
Ni-YSZ 800 °C	CO_2: 0.20 H_2: 0.80	2.5×10^{-20}	0.16	0.04	0.64	0.16
	CO_2: 0.40 H_2: 0.60	1.7×10^{-19}	0.24	0.16	0.36	0.24
	CO_2: 0.60 H_2: 0.40	8.4×10^{-19}	0.24	0.36	0.16	0.24

Table 3-4 continued

Case	Inlet molar concentration	Non-reacting molar concentration				
		p_{O_2}	p_{CO}	p_{CO_2}	p_{H_2}	$p_{\mathrm{H_2O}}$
Ni-YSZ 800 °C	CO_2: 0.80 H_2: 0.20	5.8×10^{-18}	0.16	0.64	0.04	0.16
	CO_2: 0.95 H_2: 0.05	1.3×10^{-16}	0.05	0.90	0.00	0.05
Ni-YSZ 800 °C	H_2O: 0.62 CO_2: 0.11 H_2: 0.27	3.0×10^{-18}	0.03	0.08	0.24	0.65
	H_2O: 0.57 CO_2: 0.19 H_2: 0.24	4.0×10^{-18}	0.04	0.15	0.20	0.61
	H_2O: 0.50 CO_2: 0.30 H_2: 0.20	6.3×10^{-18}	0.06	0.24	0.14	0.56
Pt 700 °C	H_2O: 0.20 H_2: 0.80	8.8×10^{-23}	-	-	0.8	0.2
	H_2O: 0.50 H_2: 0.50	1.4×10^{-21}	-	-	0.50	0.50
	H_2O: 0.70 H_2: 0.30	7.7×10^{-21}	-	-	0.30	0.70
Pt 800 °C	H_2O: 0.20 H_2: 0.80	2.6×10^{-20}	-	-	0.8	0.2
	H_2O: 0.50 H_2: 0.50	4.1×10^{-19}	-	-	0.50	0.50
	H_2O: 0.70 H_2: 0.30	2.2×10^{-18}	-	-	0.30	0.70
Pt 850 °C	H_2O: 0.20 H_2: 0.80	3.0×10^{-19}	-	-	0.8	0.2
	H_2O: 0.50 H_2: 0.50	4.8×10^{-18}	-	-	0.50	0.50
	H_2O: 0.70 H_2: 0.30	2.6×10^{-17}	-	-	0.30	0.70
Pt 700 °C	CO_2: 0.30 CO: 0.70	9.7×10^{-23}	0.7	0.3	-	-
	CO_2: 0.50 CO: 0.50	5.3×10^{-22}	0.5	0.5	-	-
	CO_2: 0.70 CO: 0.30	2.9×10^{-21}	0.3	0.7	-	-
Pt 800 °C	CO_2: 0.30 CO: 0.70	6.4×10^{-20}	0.7	0.3	-	-
	CO_2: 0.50 CO: 0.50	3.5×10^{-19}	0.5	0.5	-	-
	CO_2: 0.70 CO: 0.30	1.9×10^{-18}	0.3	0.7	-	-

Table 3-4 continued

Case	Inlet molar concentration	Non-reacting molar concentration				
		p_{O_2}	p_{CO}	p_{CO_2}	p_{H_2}	$p_{\mathrm{H_2O}}$
Pt 850 °C	CO_2: 0.30 CO: 0.70	1.1×10^{-18}	0.7	0.3	-	-
	CO_2: 0.50 CO: 0.50	5.9×10^{-18}	0.5	0.5	-	-
	CO_2: 0.70 CO: 0.30	3.2×10^{-17}	0.3	0.7	-	-
Pt 700 °C	CO_2: 0.20 H_2: 0.80	7.1×10^{-23}	0.15	0.05	0.65	0.15
	CO_2: 0.50 H_2: 0.50	8.6×10^{-22}	0.22	0.28	0.28	0.22
	CO_2: 0.70 H_2: 0.30	3.9×10^{-21}	0.19	0.51	0.11	0.19
Pt 800 °C	CO_2: 0.20 H_2: 0.80	2.5×10^{-20}	0.16	0.04	0.64	0.16
	CO_2: 0.50 H_2: 0.50	3.8×10^{-19}	0.25	0.25	0.25	0.25
	CO_2: 0.70 H_2: 0.30	2.0×10^{-18}	0.21	0.49	0.09	0.21
Pt 850 °C	CO_2: 0.20 H_2: 0.80	3.1×10^{-19}	0.16	0.04	0.64	0.16
	CO_2: 0.50 H_2: 0.50	5.3×10^{-18}	0.26	0.24	0.24	0.26
	CO_2: 0.70 H_2: 0.30	3.0×10^{-17}	0.21	0.49	0.09	0.21

In all the cases of Pt symmetrical cell tested at 700 °C, the oxygen partial pressure is below 10^{-20}, however no significant pattern of discrepancy can be observed there, therefore it is concluded that the electrolyte is working in pure ionic conduction mode and thus last term in equation 3-110 is equal to zero. It is expected that same situation occur for Ni-YSZ cell where the lowest oxygen partial pressure is an order of magnitude higher than in the Pt-cell's experiments. Moreover, all the cases with high prediction error have rather high oxygen partial pressure (except the case for CO_2/CO mixture at 700 °C in Pt-cell, however this is thought to be due to the mixed conduction).

Analysing the CO_2/H_2 case, the author can conclude that the change in composition for the measurements with the highest error are very insignificant, thus supporting the requirement for use of MPT model.

Interesting observation can be drawn for the case of H_2O/CO_2/H_2 co-electrolysis, where despite the change in composition, the oxygen partial pressure is changed very little,

accordingly the equilibrium potential is almost unchanged. This suggest that use of co-electrolysis systems may be favourable due to 1) lack of significant mixed potential, 2) no need for strict composition control, from electrical point of view, 3) stable electrolysis process. It seems that content of CO_2 above 25% molar in balanced mixture (for 800 °C it is 30% - 50% in feedstock) will require use of MPT model for the correct prediction of the OCV.

To use the mixed potential theory several parameters needed to be fitted. These are the enthalpy of adsorption and the adsorption constant for all species. As stated before, the author assumed that the only gas causing the mixed potential is CO_2. Furthermore, due to the lack of availability of results at various temperatures, the author did not fit the values of enthalpy of adsorption, but only the adsorption constant for oxygen and carbon dioxide.

Modified Equation 3-110 was used to predict the OCV. The modification included dropping the terms for steam and for mixed ionic/electronic conduction, therefore only the first and the second last part remained.

$$\Delta\phi = \theta_{O_2}\left[\frac{RT}{4F} ln\left(\frac{p_{O_2}^{cat}}{p_{O_2}^{an}}\right)\right] + \theta_{CO_2}\left[\frac{\Delta\mu_{CO_2}^{0}}{2F} + \frac{RT}{2F} ln\left(\frac{p_{CO}\sqrt{p_{O_2}}}{p_{CO_2}}\right)\right] \tag{3-111}$$

The fitting process consisted of estimation of adequate coverage of CO_2 and O_2 required to arrive at the observed OCV values. Based on the known gas composition and assumed adsorption mechanism the ratio of $\frac{K_{O_2}}{K_{CO_2}}$ is estimated. The author noticed that this ratio is not constant in all of the experimental cases. The temperature of all experiments was constant, thus, the variation originates from the standard adsorption constant. According to the kinetic gas theory the standard adsorption constant is equal to

$$K_i^0 = \frac{\sigma\psi^0}{\nu n_s} \tag{3-112}$$

where σ is the condensation coefficient of sticking probability, ψ^0 is the flux of gas molecules at p=1 atm colliding with the unit area of surface per unit time, ν is the frequency of gas molecule vibration and n_s is the number of TPB sites available for adsorption. At least two of those parameters are thought to vary during the experiments. The flux of gas molecules varies as the composition is changed and the total flux is kept

constant. The number of TPB sites available for adsorption varies as other gases (not considered for OCV contribution) may in principle block access for CO_2 or O_2 molecules. The ratio of standard adsorption constant was found to obey following relation (R^2=0.971)

$$\frac{K^0_{O_2}}{K^0_{CO_2}} = 5.588 \times 10^{19}\, exp\left(-8.4564 c_{CO_2} + \frac{Q_{CO_2} - Q_{O_2}}{RT}\right) \quad (3\text{-}113)$$

where c_{CO_2} is the carbon dioxide concentration of balanced, non-reacting gas mixture and $Q_{CO_2} = 18.828\ kJ\ mol^{-1}$, $Q_{O_2} = 439.32\ kJ\ mol^{-1}$.

The comparison of all proposed models against the OCV measurements for Ni-YSZ cell fed with CO_2/H_2 gas mixture is summarized on Fig 3-14 (a, b). It can be seen that the use of the MPT model halved the error of partial oxygen pressure model. Better results could be achieved if adsorption of all the gases is considered.

The maximum error of mixed potential model is at 4%, the average error of the method is 1.24% (R^2=0.8678). The maximum and average error for oxygen partial pressure method is 7.64% and 5.06%, respectively. For the standard model it is 14.58%, 12.97% and 11.84%, 10.03% respectively for CO_2 base and H_2O base. Therefore, the mixed potential model is shown to increase the prediction accuracy of equilibrium potential of the Solid Oxide Electrolyzer Cell.

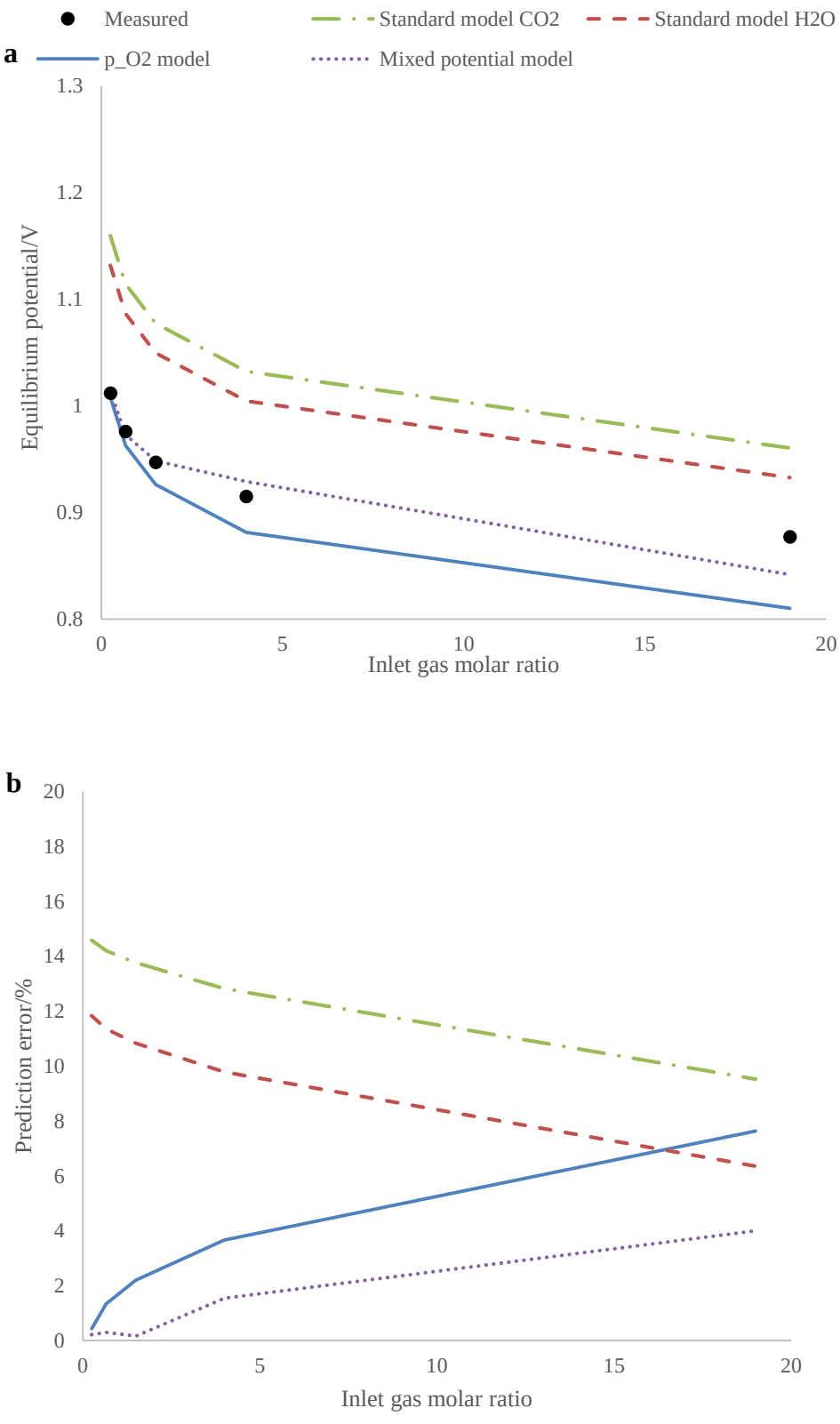

Fig. 3-14 – Comparison of the experimentally observed co-electrolysis OCV values for Ni-YSZ cell (dots) and those calculated by all investigated models (a) (lines). Prediction error for all models (b).

3.6.5 Conclusions

The presented study included the measurements of equilibrium potential (OCV) of a Pt symmetrical cell and a comparison of different methods to predict it. The author concluded that the standard model used in the literature cannot be employed accurately to predict the OCV. However, the model based on oxygen partial pressure is accurate for temperatures above 700 °C for Pt-based cases. The proposed model predicted co-electrolysis OCV well.

Later, the author compared the standard model and oxygen partial pressure model against the OCV measured in Ni-YSZ cells for electrolysis of steam and co-electrolysis of steam and carbon dioxide at 800 °C. It was concluded that the standard model is not accurate enough. The oxygen partial pressure model improved the prediction accuracy, however, the error in cases with large amount of CO_2 in the feed stream was significant. The author proposed to use the MPT model to predict the OCV. After fitting the parameters semi-empirical formula was proposed to calculate the specie coverage which allowed to decrease the prediction error to below 5% for CO_2 concentration of 95%. For lower concentrations the model was accurate to within 99%.

Therefore, it was concluded that the MPT model can be accurately used to predict the OCV of electrolysis and co-electrolysis of the Solid Oxide Electrolyzer Cell with CO_2 content above 25% (at 800 °C). The oxygen partial pressure model is accurate for co-electrolysis with CO_2 content below 25% (at 800 °C). (Lastly, the author proposed a relation between standard adsorption constants of oxygen and carbon dioxide that can be used to predict the OCV at 800 °C for Ni-YSZ based cells (air electrode is assumed to have negligible influence). The predicted values of OCV with use of oxygen partial pressure and MPT (where applicable) models for selected conditions and Ni-YSZ based cells are presented in Table 3-5.

Table 3-5. Values of OCV for selected operating cases of SOEC with Ni-YSZ based fuel electrode.

Temp	Inlet molar concentration	OCV
800 °C	H_2O: 0.03 H_2: 0.97	1.103
	H_2O: 0.10 H_2: 0.90	1.044
	H_2O: 0.20 H_2: 0.80	1.007

Table 3-5 continued

Temp	Inlet molar concentration	OCV
800 °C	H_2O: 0.30 H_2: 0.70	0.982
	H_2O: 0.40 H_2: 0.60	0.961
	H_2O: 0.50 H_2: 0.50	0.943
	H_2O: 0.70 H_2: 0.30	0.903
800 °C	CO_2: 0.20 H_2: 0.80	1.014
	CO_2: 0.40 H_2: 0.60	0.973
	CO_2: 0.60 H_2: 0.40	0.948
	CO_2: 0.80 H_2: 0.20	0.929
	CO_2: 0.95 H_2: 0.05	0.842
800 °C	H_2O: 0.62 CO_2: 0.11 H_2: 0.27	0.897
	H_2O: 0.57 CO_2: 0.19 H_2: 0.24	0.890
	H_2O: 0.50 CO_2: 0.30 H_2: 0.20	0.880
850 °C	CO_2:0.2 H_2:0.8	0.993
	CO_2:0.5 H_2:0.5	0.925
	CO_2:0.7 H_2:0.3	0.883
700 °C	CO_2:0.2 H_2:0.8	1.037
	CO_2:0.5 H_2:0.5	0.984
	CO_2:0.7 H_2:0.3	0.952
850 °C	H_2O:0.2 H_2:0.8	0.994
	H_2O:0.5 H_2:0.5	0.927
	H_2O:0.7 H_2:0.3	0.886
700 °C	H_2O:0.2 H_2:0.8	1.032
	H_2O:0.5 H_2:0.5	0.974
	H_2O:0.7 H_2:0.3	0.938

3.7 Summary of the author's micro-model and the validation

The model reported below has been used in all of the author's systems level studies.

The Solid Oxide Electrolyzer Cell is often modelled by use of overpotentials. These reflect the source of major losses and add up to the equilibrium potential resulting in I-V characteristics of the cell. In this thesis, the author reports a simple kinetic and lumped flow models with the electrochemical overpotential model to characterize the behaviour of the SOEC. The electrochemical model accounts for the effects of temperature, pressure, inlet gas composition and flow on the cell's equilibrium potential and losses related to electrode kinetics (activation loss), electrode microstructure (concentration loss) and electrical properties of constituting materials (ohmic loss). A novel approach

involving simple kinetic expressions is used to quantify the extent of co-electrolysis of CO_2 and H_2O.

Assumptions of the model:

- Steady state,
- Isothermal operation,
- Equilibrium of chemical reactions is always achieved (unless stated otherwise),
- Lumped chemical kinetics model,
- 1D electrochemical model,
- No degradation or structural changes occur in the cell,
- The electrochemical reaction occurs only at the TPB which is located at the interface between electrodes and electrolyte,
- Conductivity of electrodes is much higher than that of electrolyte thus ohmic loss is only considered for electrolyte,
- All of the gases follow Peng-Robinson equation of state,
- Water-Gas Shift reaction always reaches equilibrium,
- All fluxes are equally distributed along perpendicular plane to the charge flow direction,

With an assumed current, the actual potential difference applied is determined by:

$$E = E_0 + \eta_{ohm} + \eta_{act\ an} + \eta_{act\ cat} + \eta_{con\ an} + \eta_{con\ cat} \tag{3-114}$$

where, η_{ohm} is ohmic loss due to electrical resistance, $\eta_{act\ an}$ & $\eta_{act\ cat}$ are activation loss due to charge transfer at the anode and cathode, respectively, $\eta_{con\ an}$ & $\eta_{con\ cat}$ are concentration loss due to slow replenishment of reactants at the anode & cathode, respectively

Electrical current is applied to the SOEC to allow oxygen ions to flow from the fuel electrode to the oxygen electrode through the electrolyte.

The amount of produced syngas is calculated from the Faraday's law:

$$n_{O_2} = \frac{iA}{4F} \tag{3-115}$$

where A is the overall electrolyzer's active area in cm^2 and n_{O_2} is the number of transported oxygen ions through the electrolyte in mol s^{-1}. The amount of oxygen

originating from steam and carbon dioxide is regulated by amount of CO_2/H_2O supplied, reaction rate constants and residence time in the reaction zone of Equations 3-116 and 3-117.

For the SOEC, oxygen ions can be produced through two reaction paths.

$$H_2O + 2e^- \rightarrow H_2 + O^= \quad (3\text{-}116)$$

$$CO_2 + 2e^- \rightarrow CO + O^= \quad (3\text{-}117)$$

The conversion of carbon dioxide and steam to carbon monoxide and hydrogen (syngas) is assumed to follow two steps. First, both gases are electrochemically co-electrolyzed to various extent and later the resulting gas mixture is chemically balanced according to Water-Gas Shift reaction. The Water-Gas Shift reaction is thought to achieve thermodynamic equilibrium on Ni-based fuel electrode at 1073.15 K (equilibrium temperature of WGS is 1100 K). The kinetics of co-electrolysis is modelled by simple reaction rates and the Arrhenius expressions are as follows:

The reaction rates are modelled by Arrhenius equation:

$$k = \gamma exp(-\frac{E_{act}}{RT}) \quad (3\text{-}118)$$

After fitting to experimental data Equation 3-118 takes following forms for steam and carbon dioxide electrolysis, respectively

$$k_{H_2O} = 1.2 \times 10^6 \, exp\left(-\frac{1200}{RT}\right) \quad (3\text{-}119)$$

$$k_{CO_2} = 5 \times 10^5 \, exp\left(-\frac{13068}{RT}\right) \quad (3\text{-}120)$$

3.7.1 Equilibrium potential

The calculation of the equilibrium potential difference (OCV) for co-electrolysis SOEC was discussed in chapter 3.6 and is only briefly described here. The OCV is established as a result of competition between three major electrode electrochemical reactions according to the Mixed Potential Theory (MPT). These reactions are 3-116, 3-117 and

$$O_2 + 4e^- \rightarrow 2O^= \tag{3-121}$$

The MPT states that the resulting observed potential difference is established by the slowest of the above reactions or the superposition of the above if they proceed with similar rates. In chapter 3.6, it was concluded that reaction 3-116 is always fast, while reactions 3-117 and 3-121 have similar rates if large amount (>50%) of carbon dioxide is present in the inlet gas mixture. In this thesis, in all investigated cases, the amount of CO_2 was below the threshold requiring the use of the potential superposition, thus use of the Nernst equation with relation to equilibrium oxygen partial pressures is justified.

$$E_0 = \frac{RT}{4F} ln\left(\frac{[O_x^{\cdot\cdot}]_{cat}}{[O_x^{\cdot\cdot}]_{an}}\right) = \frac{RT}{4F} ln\left(\frac{p_{O_2}^{cat}}{p_{O_2}^{an}}\right) \tag{3-122}$$

where, $[O_x^{\cdot\cdot}]$ is the concentration of interstitial oxygen at the anode/cathode interface (the Triple Phase Boundary, TPB), p_{O_2} is the partial pressure of oxygen in Pa at the TPB (equal to partial pressure in the bulk if the equilibrium is established). *R*, *T* and *F* are universal gas constant, temperature [K] and Faraday constant, respectively. The above formulation includes intrinsic assumption on pure ionic conduction (see chapter 3.5 for the discussion of this assumption). In order to include effects of increased pressure, the author has modified the above formula according to recent report by Henke et al. (Henke et al. 2014). An alternative analysis of high pressure operation of a SOEC was given by Todd et al. (Todd et al. 2014).

$$E_{eq} = \frac{RT}{4F} ln\left(\frac{p_{O_2}^{cat}}{p_{O_2}^{an}}\right) - \frac{RT}{8F} ln\left(\frac{p}{p_{std}}\right) \tag{3-123}$$

where $[O_2]$ is the concentration of oxygen and p_{std} is the standard pressure (101325 Pa).

3.7.2 Ohmic loss

The ohmic losses are the results of cell's resistance to electronic carriers' movement. These include the electrons and ions. The cell's electronic resistance is typically very low, thus the loss due to electron movement is negligible. On a contrary, ionic resistance of electrodes can be significant, however it is being lumped to the one of the electrolyte.

The following formula described the conductivity of the YSZ electrolyte used in this study:

$$\sigma = 1.63 \times 10^2 \, exp\left(-\frac{0.79eV}{kT}\right) \tag{3-124}$$

where σ is the ionic conductivity in S cm^{-1}, eV is the electron-volt, k the Boltzmann constant.

The overpotential resulting from the above conductivity limit is then calculated from:

$$\eta_{ohm} = \frac{i\delta}{\sigma} \tag{3-125}$$

where δ is the electrolyte thickness in cm.

The ohmic loss is calculated with the assumption of pure ionic conduction (see chapter 3.5).

3.7.3 Activation overpotential

The loss resulting from the sluggish electrode kinetics is usually referred to as the activation loss and is often described by the Butler-Volmer equation for electron transfer. The electron transfer process for reactions 3-116, 3-117 and 3-121 is a two-step process for the first two reactions and four-step process for the last reaction. The Butler-Volmer equation describes accurately only a single-step process (single electron transfer) and thus has been criticised to be inaccurate. However, it is the most common tool to describe the reaction kinetics and proved to be good enough to describe the experimental results and the influence of varying gas composition. In this thesis, the author has used the general form of the equation, written as:

$$i = i_0 \left[exp\left(\frac{\alpha z F \eta_{act}}{RT}\right) - exp\left(-\frac{(1-\alpha) z F \eta_{act}}{RT}\right)\right] \tag{3-126}$$

where i is the applied current density in A cm^{-2}, i_0 is the exchange current density in A cm^{-2} and is a function of gas composition, temperature and pressure, z is the number of electrons transferred in a reaction, α is the symmetry factor describing the favoured direction of electron transfer reaction, η is the resulting overpotential in V.

Costamagna et al. (Costamagna et al. 1999) proposed a model of SOFC's electrode based on particle coordination number and percolation theories, this model was later used to relate the electrode's microstructure with observed exchange current density of a fuel cell by (Deng and Petric 2005). Ni et al. (Ni et al. 2007) used this approach to perform a parametric study of SOFC performance. The author of this thesis applied this approach to model the activation overpotential of the SOEC. The approach relates pore and grain size of electrode, the contact angle and porosity with the exchange current density. The resulting formulae for exchange current densities are:

$$i_0^{H_2O} = k_{H_2O} \frac{72\theta[D_p-(D_p+D_s)n]n}{D_p^2 D_s^2(1-\sqrt{1-\theta^2})} \left[\left(\frac{p_{H_2}}{p_{std}}\right)\left(\frac{p_{H_2O}}{p_{std}}\right)\right]^{\kappa} exp\left(-\frac{E_{act,H_2O}}{RT}\right) \quad (3\text{-}127)$$

$$i_0^{CO_2} = k_{CO_2} \frac{72\theta[D_p-(D_p+D_s)n]n}{D_p^2 D_s^2(1-\sqrt{1-\theta^2})} \left[\left(\frac{p_{CO}}{p_{std}}\right)\left(\frac{p_{CO_2}}{p_{std}}\right)\right]^{\kappa} exp\left(-\frac{E_{act,CO_2}}{RT}\right) \quad (3\text{-}128)$$

$$i_0^{O_2} = k_{O_2} \frac{72\theta[D_p-(D_p+D_s)n]n}{D_p^2 D_s^2(1-\sqrt{1-\theta^2})} \left(\frac{p_{O_2}}{p_{std}}\right)^{\kappa} exp\left(-\frac{E_{act,O_2}}{RT}\right) \quad (3\text{-}129)$$

where θ is the contact angle between particles, D_p is the pore size, D_s is the grain size, n is the porosity, k is the pre-exponential factor, E_{act} is the activation energy, R and T are as defined before. The unknown parameters in the above formulae were fitted to match the experimental data.

$$i_0^{H_2O} = 1.82527 \times T p_{H_2}^{-0.1} p_{H_2O}^{0.33} exp\left(-\frac{105.4}{RT}\right) \quad (3\text{-}130)$$

$$i_0^{CO_2} = T p_{CO}^{-0.29} p_{CO_2}^{0.1} exp\left(-\frac{120}{RT}\right) \quad (3\text{-}131)$$

$$i_0^{O_2} = 151.55 \times T p_{O_2}^{0.22} exp\left(-\frac{139.86}{RT}\right) \quad (3\text{-}132)$$

where, all partial pressures are given in bars and temperature in K, and the calculated exchange current density is given in A m^{-2}.

Equations 3-130 and 3-131 are used for the fuel electrode, while Equation 3-132 is used for the air electrode.

3.7.4 Concentration overpotential

The concentration loss is the result of gas starvation due to the diffusion limitation of gas transport in the porous structure of the electrode and the high fuel utilization. In the following thesis, the author uses two separate approaches to describe the loss in the air and the fuel electrodes. The air electrode concentration loss is due to permeation of oxygen through the air electrode and has been described by Ni et al. based on Darcy's law (Ni et al. 2006) as:

$$\eta_{con}^{O_2} = \frac{RT}{4F} ln \left(\frac{\sqrt{\left(p_{O_2}^{bulk}\right)^2 + \frac{iRT\mu\delta_{cat}}{4FB_g}}}{p_{O_2}^{bulk}} \right) \tag{3-133}$$

where μ is the dynamic viscosity of oxygen, B_g is the permeability in m^2 and the superscript bulk refers to the air electrode gas channel.

The loss in the fuel electrode is calculated based on the author's developed empirical formula and the approach of limiting current density. It can be written as follows:

$$\eta_{con} = \frac{RT}{2F} ln \left(\frac{i_L}{i_L - i} \right) \tag{3-134}$$

where i_L is the limiting current calculated as:

$$i_L = \frac{D_{eff} 2F}{S_v \delta_{an}} \chi c_i N_i \tag{3-135}$$

where, D_{eff} is the effective diffusivity (calculated as in Ni et al. 2006), S_v is the cell's active area in cm^2, χ is the reactant's conversion factor, c_i is the reactant specie's concentration, and N_i is the molar flux of feed stream in kg mol $hour^{-1}$.

3.7.5 Cell microstructure parameters

The parameters of the cell used in system level and fundamental level models are summarized in Table 3-6.

Table 3-6 – Summary of cell's parameters.

Active area	16, 81 or 100 cm^2
Materials	Ni-YSZ|YSZ|LSCF-YSZ
Thickness	Fuel electrode (Ni-YSZ): 500 μm Electrolyte (YSZ): 10 μm Air electrode (LSCF-YSZ): 30 μm
Pore diameter	0.5 μm
Porosity	30%
Tortuosity	5

3.7.6 Validation of model

The author fitted the unknown parameters in the model, such as, charge transfer coefficient and reaction kinetics, using the limited data available from the literature (Graves et al. 2011) as well as in-house experimental results. An assumption is made that the charge transfer coefficient does not change with the reactions. This assumption is found to be slightly inaccurate for changes between electrolysis and co-electrolysis. Validation range spans over a temperature range of 800 - 850 °C, mole flux of 625 – 1210 mol h^{-1} m^{-2} without fuel electrode gas recycling considered. Extrapolation of the range by 25% gives a temperature range of ~600 – 1000 °C and mole flux range of ~468 - 1512 mol h^{-1} m^{-2}. By comparison, simulation results covered a temperature range of 500 - 800 °C and mole flux range of 129 - 1289 mol h^{-1} m^{-2}.

The comparison of predicted results against experimental data from (Graves et al. 2011) is shown in Table 3-7 and Fig. 3-15. The predicted results show very good agreement with the data from (Graves et al. 2011).

Table 3-7 – Comparison of predicted feedstock conversion efficiency with data from (Graves et al. 2011).

Case description (Gas composition)	Conversion % Literature	Conversion % Model	Remarks
50% H_2O/50% H_2	68	66.42	air at cathode side
50% CO_2/50% CO	51	48.32	air at cathode side
25%H_2O/ 25%H_2/ 25%CO_2 / 25% CO	59	57.82	air at cathode side

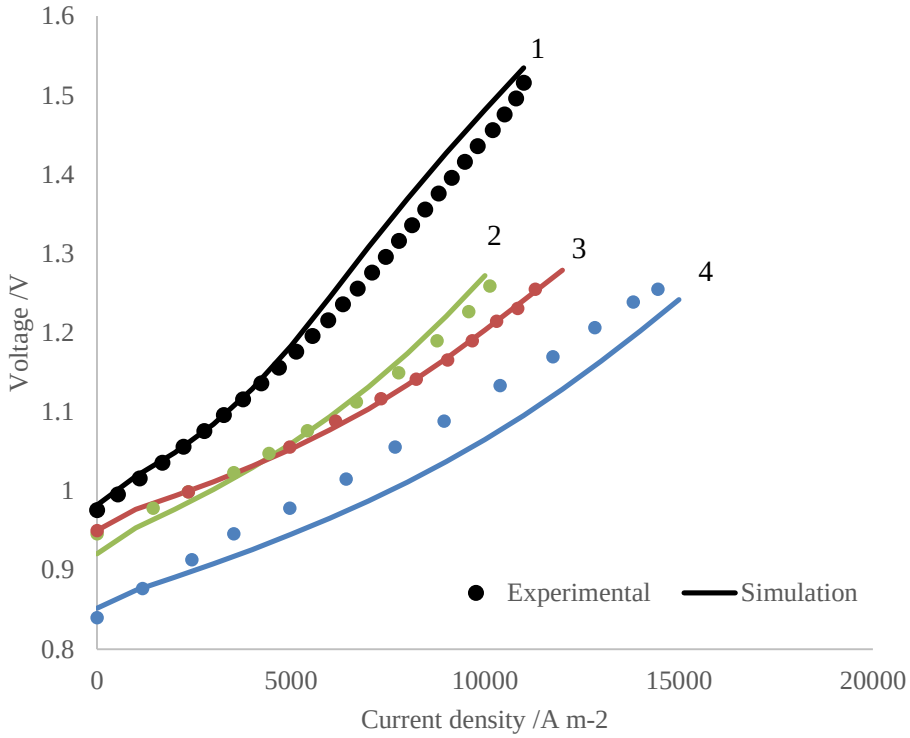

Fig. 3-15 – Comparison of predicted I-V curve for H_2O, CO_2 and co- electrolysis with data from (Graves et al. 2011) and in house data. Curve-1 steam electrolysis 30% H_2O/70%H_2 at 800°C, Curve-2 co-electrolysis (Graves et al. 2011) 25%H_2O/25%H_2/25%CO_2/25%CO 850°C, Curve-3 steam electrolysis (Graves et al. 2011) 50%H_2O/50%H_2 850°C, Curve-4 co-electrolysis (Graves et al. 2011) 45%H_2O/45%CO_2/10%H_2 850°C.

As shown in Fig. 3-15, the predicted results show a reasonably good match with group's own experimental data and it is posited that this model can be used for parametric study.

Chapter 4. Carbon dioxide mitigation system based on Solid Oxide Electrolyzer Cell

Broader context

In the world energy outlook 2014 report compiled by International Energy Agency, it has been unveiled that the global average temperature will increase by 3.5 °C or more if the world continues to delay actions in tackling the climate change brought on by the human activities. The report also pointed out that four-fifths of the total energy-related CO_2 emissions permissible by 2035 are contributed by the existing power plants, buildings and related CO_2-emitting industries. If stringent new action is not forthcoming by 2017, the energy-related industry then in place will generate all the CO_2 emission allowed, leaving no room for additional power plants, factories and other infrastructure unless they are zero-carbon (IEA 2014).

As mentioned in Chapter 1 anthropogenic CO_2 emissions lead to environmental concerns of the world's future. It is a serious problem unique to all nations and only through international cooperation can such a problem be addressed and solved collectively. Approaches involving the capture of CO_2 and its storage in geological formations and ocean or even reacting naturally occurring magnesium and calcium containing minerals with CO_2 to form carbonates as mineral storage, and subsequently used for cement production, have been suggested. However, for those nations with limited land and resources such as Singapore, converting CO_2 to useful material feedstock while reducing the overall carbon footprint would make more logical and economic sense, taking into consideration of the development of novel technologies along the carbon value chain.

Production of syngas from CO_2 and H_2O, i.e., the main components in the flue gas, through electrochemical means is one of the most practical solutions in reducing CO_2 emissions, especially when off-peak power from the fossil power plants or renewable energy such as wind turbines or solar PVs can be tapped from.

Many system studies on solid oxide fuel cell (SOFC) technologies and the integration of SOFC to gas turbines have been conducted in the last decade. These studies were based mainly on the analysis of the thermodynamic system using First Law of Thermodynamics in conjunction with a techno-economical assessment, while some

researchers applying the Second Law of Thermodynamics to analyse the overall plant efficiency by calculating the exergy at each node of the thermodynamic system and the respective exergy destruction in each system component (Oosterkamp et al. 1993, Bedringas et al. 1997, Dincer & Cengel 2001). Literature review on SOEC modelling is limited, especially co-electrolysis modelling (Fu et al. 2010, Ni 2012, Stoots et al. 2009, Ni et al. 2006, Cai et al. 2010). Combinational energy and exergy analysis on SOEC system is also very limited. It is important to know the extent of the losses distribution in the thermodynamic system so that attention can be focused on improvement of a particular system component or process. Such study can provide a basis to establish the relationship between exergy analysis and environmental life-cycle analysis (LCA) (Hardisty et al. 2012).

4.1 Energy and exergy analysis of CO_2 mitigation system

This chapter has been published in a modified form as JP Stempien, OL Ding, Q Sun, SH Chan, Energy and exergy analysis of Solid Oxide Electrolyser Cell (SOEC) working as a CO_2 mitigation device, International Journal of Hydrogen Energy, 37, 2012, 14518.

4.1.1 Introduction

This sub chapter presents a simple model for SOEC system, which is fed with flue gases from a simulated power plant. The system consists of SOEC, heat exchangers and gas separation unit. To prevent nickel from oxidising to nickel oxide in a practical operation, the model considers the recirculation of product gases at the fuel electrode of SOEC. The details of exergy analysis and causes of irreversibility can be found in (Chan et al. 2002, 2005, Cornelissen 1997).

4.1.2 Energy and exergy analysis

4.1.2.1 Energy analysis

The energy balance is the basis for investigating any energy process. It makes the energy analysis possible and forms the base for developing the exergy balance. The analysis of energy balance would unveil the efficiency of energy utilisation in a particular part of the process and allow the comparison of efficiency and the process parameters with the currently achievable values in most of the modern installations. Knowing the differences will help set the priority to rectify issues related to excessive energy consumption or low

efficiency of a particular process. Energy analysis applies the concept of energy conservation with different forms of energy expressed as internal energy, enthalpy, chemical energy, mechanical work, heat, electricity, etc. However, this energy balance approach has some deficiencies as it is unable to differentiate the quality of energy. Accordingly, under pure energy analysis, one cannot tell the difference in heat quality which, however, depends on the heat source temperature, e.g., a 1 MJ of heat produced by a solid oxide fuel cell (SOFC) operating at 800°C versus the same amount of heat produced by a polymer electrolyte membrane fuel cell (PEMFC) operating at 80 °C.

4.1.2.2 Exergy analysis

The exergy concept is thus introduced to overcome limitations of the energy analysis. The exergy expresses the practical value of any substance, and is defined as the maximum ability of this substance to perform useful work relative to the human environment. For this reason, modern approach to the process analysis involves exergies in the equations, which offers a more realistic view on the entire analysis (IEA 2012, Fu et al. 2010, Ni 2012). While the energy analysis is based solely on the First Law of Thermodynamics, the exergy analysis is an approach taking the advantages of both the First and Second Laws of Thermodynamics. Both analyses utilize the material balance in the considered system. Analysis and optimization of any physical or chemical process using the concepts of energy and exergy can provide two different views on the considered process.

In the background of the exergy concept it is assumed that all the common human environment components, available for free in unlimited amounts, are practically valueless and their exergy is defined as zero. However, any matter exists at a particular state (pressure and temperature) with a certain composition, which is not in equilibrium with the environment, will have a certain useful value (exergy), which can be measured as its potential to perform useful work. The exergy can consist of the following components:

- Physical exergy – resulting from the temperature and pressure of a substance measured with respect to the temperature and pressure of the environment,
- Chemical exergy – resulting from the difference in substance composition with respect to the common components of this substance in the environment,
- Potential exergy – resulting from the substance location above the ground level,
- Kinetic exergy – resulting from its velocity relative to the environment.

Very often, under practical engineering considerations, only the thermal exergy, which is the sum of the physical and chemical exergy, is taken into account. In this chapter, only the thermal exergy is considered.

Physical exergy can be calculated using following formula

$$\varepsilon_{ph} = (h_1 - T_0 s_1) - (h_0 - T_0 s_0) \tag{4-1}$$

where subscript zero stands for environmental conditions.

When exergy difference is considered, Equation 4-1 is simplified to

$$\varepsilon_{ph,1} - \varepsilon_{ph,2} = (h_1 - h_2) - T_0(s_1 - s_2) \tag{4-2}$$

Chemical exergy of a mixture can be calculated using

$$\varepsilon_{ch} = \sum_i y_i \overline{\varepsilon_{0i}} + RT_0 \sum_i y_i \, ln(y_i) \tag{4-3}$$

where $\overline{\varepsilon_{0i}}$ is molar chemical exergy of species *i* and can be obtained from Kotas (Kotas 1985).

With the above thermal exergy, the total exergy of a *j-th* stream can be calculated as follows

$$EX_j = \dot{n}_j(\varepsilon_{ph,j} + \varepsilon_{ch,j}) \tag{4-4}$$

The exergy of an electrical power is equal to itself (P_{el}), while exergy of heat delivered is equal to (Kotas 1985)

$$EX_Q = \dot{Q}\left(1 - \frac{T_0}{T}\right) \tag{4-5}$$

The exergy balance is thus expressed as in Perdikaris et al. (Perdikaris et al. 2010)

$$\sum_{IN} EX_j + \sum_{IN} EX_Q + P_{el} - \sum_{OUT} EX_k - \sum_{OUT} EX_Q = I \tag{4-6}$$

where, P_{el} is the exergy input with electrical current, *I* are the irreversibilities

In summary, an energy analysis of the conversion process of energy, which conserves itself totally regardless of its quality, serves rather well for design calculations, whereas the exergy analysis, which takes into consideration the quality of energy and does not obey the conservation, serves mostly for practical estimation and analysis of the process.

4.1.2.3 CO_2 mitigation system model

The modelling of the SOEC system, shown in Fig. 4-1, is performed on the Aspen® Plus HYSYS platform. The software is useful for system analysis and optimization of sub-components. The majority of sub-components, such as, reactors, heaters, and splitters, are modelled using the standard elements found in the software. The electrochemical model of SOEC is created with parameters, constants and equations inserted into a spreadsheet of the software. The electrochemical model considers the products of the chemical reactions, the Nernst potential and polarization losses, the transport of ions, and separation and recirculation of the product gases.

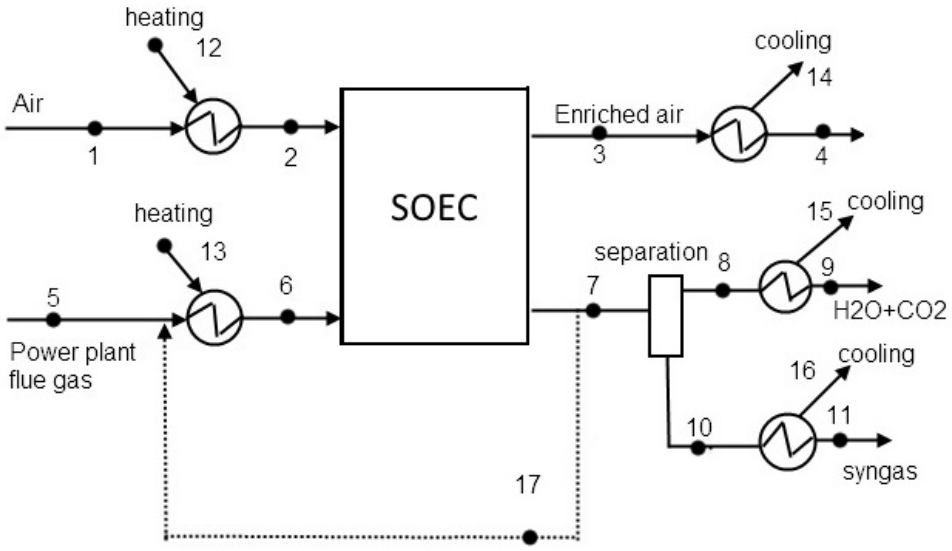

Fig. 4-1 – Schematic of simulated SOEC system.

In this model, it is assumed that the system is perfectly insulated and maintaining at a constant operating temperature at open circuit voltage (OCV) condition. The temperature of SOEC is directly related to the amount of heat generated due to chemical reactions and other polarisation losses within SOEC. The chemical kinetic rates and overpotentials of SOEC are also functions of temperature. It is also assumed that the processes and reactions are all at quasi-equilibrium. Since all the performance related

parameters are dependent on temperature, iterations are performed to compute SOEC temperature, with known thermodynamic state at the inlets of SOEC, until the convergence criteria is met. All energy fluxes are balanced and resulting flux (positive or negative) is applied to increase or decrease temperature of material stream. For the analysis, the CO_2 mitigation system is modelled as a system that converts CO_2 and H_2O from small fraction of the flue gases of a power plant into synthetic gases. It is assumed that the power plant, where flue gases are emitted, is run on pure methane and the combustion is complete. The conditions and assumptions made during the analysis of the CO_2 mitigation system are as follows:

- Electrical efficiency of the power plant is 40%;
- Air excess ratio is 1.1;
- Combustion is complete and perfect;
- Composition of inlet gases to CO_2 mitigation system (before mixing with recycled stream) is as follows: CO_2 = 18%, H_2O = 35%, N_2 = 47% by volume (it is assumed that the oxygen is removed before entering the electrolyzer);
- Temperature of inlet gases is at 110°C;
- Inlet flow rate of the flue gas to SOEC is 200 l h^{-1};
- Inlet flow rate of air to SOEC is 320 l h^{-1};
- Operating temperature of SOEC is 800 °C unless otherwise stated;
- System is capable of recovering 30% of the waste energy from cooling;
- Reference state for exergy calculations is 25°C and 100 kPa;

Key parameters of SOEC are listed in Table 4-1.

Table 4-1 – Parameters of SOEC for CO_2 mitigation system (Ni 2007, 2010).

Active area	81 cm^2
Solid oxide electrolyser cell material	Ni-YSZ/YSZ/LSM (Anode/Electrolyte/Cathode)
Thickness	Support = 500 µm; Anode, Cathode = 12 µm; Electrolyte = 15 µm
Pore diameter (electrode)	3 µm
Grain diameter (electrode)	1.5 µm
Porosity (electrode)	0.4

Table 4-1 continued

Tortuosity (electrode)	5
Ratio of length of grain contact neck to grain size (electrode)	0.7

As seen from the Fig. 4-1, the system consists of 17 control nodes, in which 12 are material streams and 5 are energy/exergy streams.

4.1.3 Results and discussions

Fig. 4-2 shows the respective overpotentials of SOEC model depicted in Fig. 4-1. It can be seen that the activation loss at anode and cathode contributes significantly to the overall overpotential. This indicates that the electrode kinetics for the electrochemical reactions at the anode and cathode are sluggish. This is true as it is well known that the reverse water-gas shift reaction is a slow reaction process.

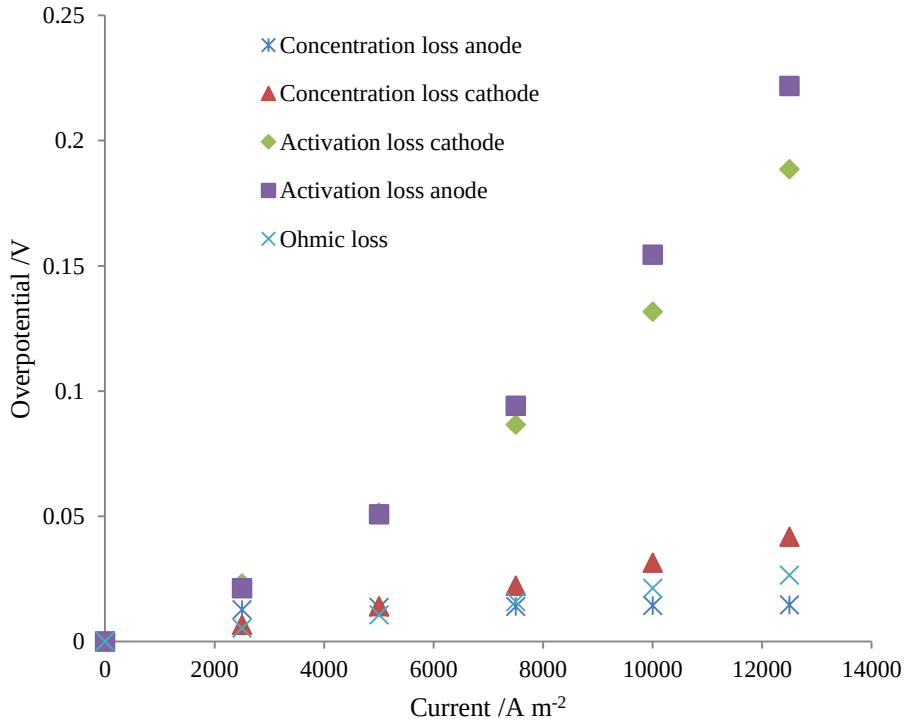

Fig. 4-2 – Analysis of overpotential losses for model result.

Figs. 4-3 – 4-5 show the predicted results at various EGR values under different operating temperatures. It is observed that the performance of SOEC drops when the

recycling ratio is increased for all temperatures under study. The drop of performance is due to the dilution effect on the feedstock (CO_2 and H_2O), which leads to the change in Nernst potential. The results also show that the performance of SOEC decreases with lower operating temperature (as indicated by the higher voltage applied to achieve same current). This can be explained by the increase in overpotentials, which is temperature sensitive. It is noted that typical operating voltage for SOEC is about 1.5 V, which is meant for considerable feedstock conversion with good efficiency at 800 °C. It should also be noted that recycling of product gas is necessary to prevent the oxidation of nickel into nickel oxide in the fuel electrode. For this reason, operating temperature of 800 °C and recycling ratio of 0.1 were selected for the rest of the analysis.

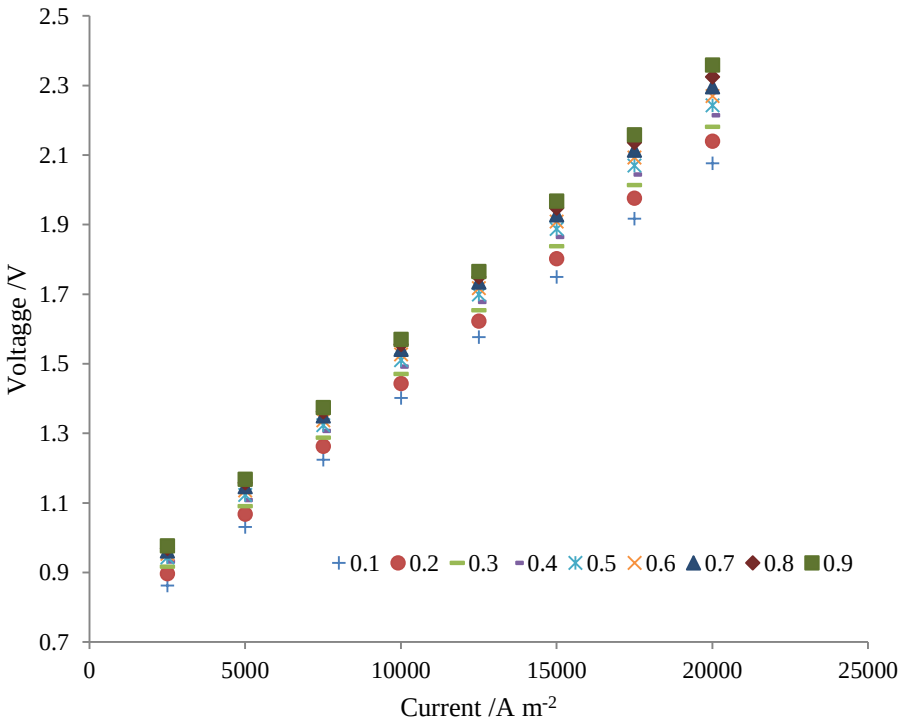

Fig. 4-3 – I-V curves for different recycling ratios at 800 °C.

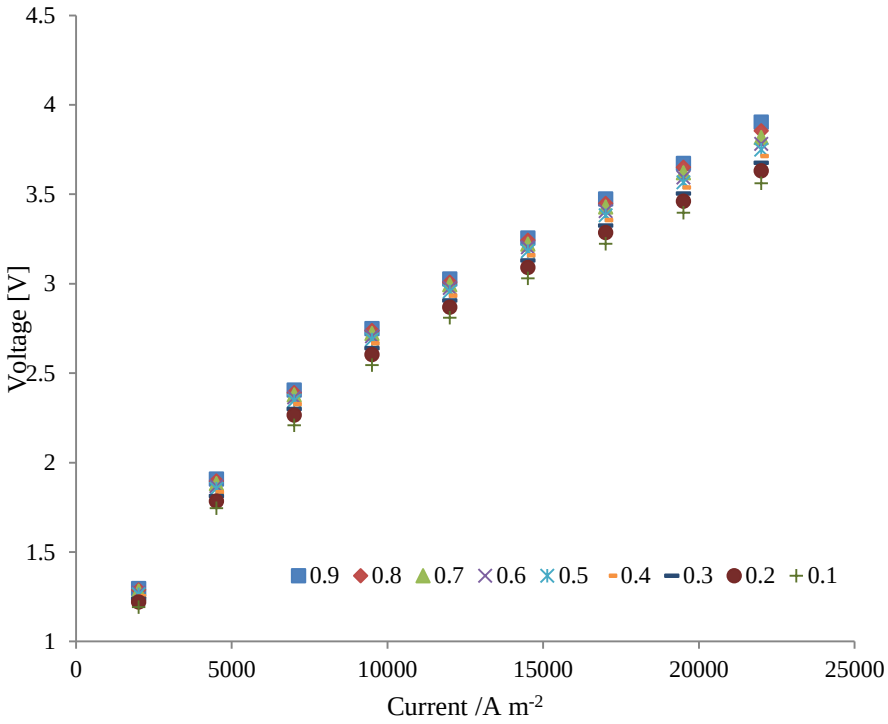

Fig. 4-4 – I-V curves for different recycling ratios at 700 °C.

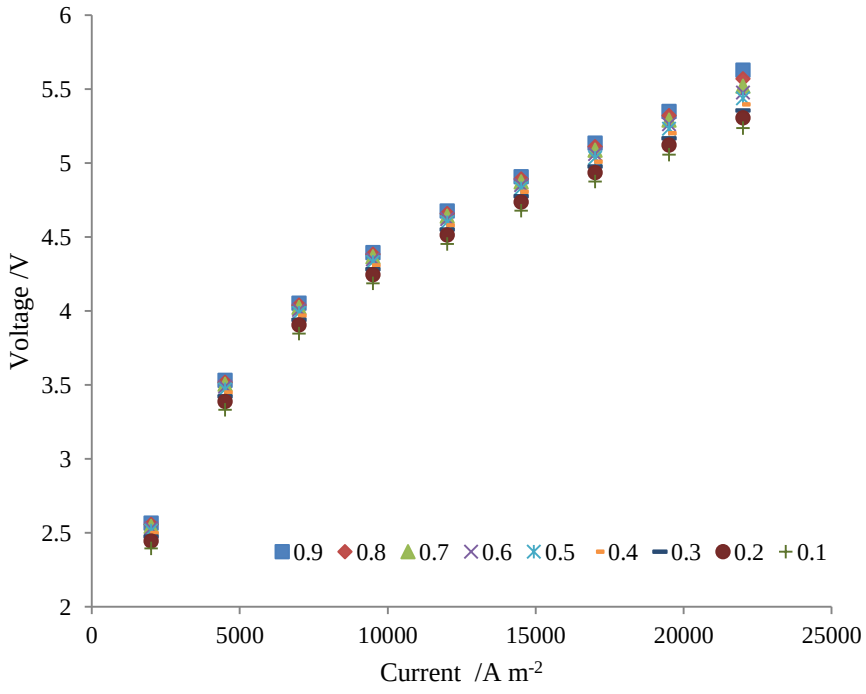

Fig. 4-5 – I-V curves for different recycling ratios at 600 °C.

Fig. 4-6 shows the relation between the voltage and energy efficiency (blue line) of

SOEC (defined as ratio of energy in syngas produced to energy consumed by the device minus 30% waste heat recovered from the product gases). The result shows that the energy efficiency increases with the voltage applied and peaks 50% at 1.37 V, thereafter it drops with increasing voltage. At this optimal operating voltage, SOEC is in a condition where all generated oxygen ions are transported through the electrolyte (maximum feedstock conversion is reached) and, hence, any further increase in voltage will only affect the kinetics of the reactions as it will be converted to heat and increase temperature. This value is also close to so-called thermoneutral voltage (1.29 V for H_2O and 1.46 V for CO_2 at 800 °C) (Stoots et al. 2009).

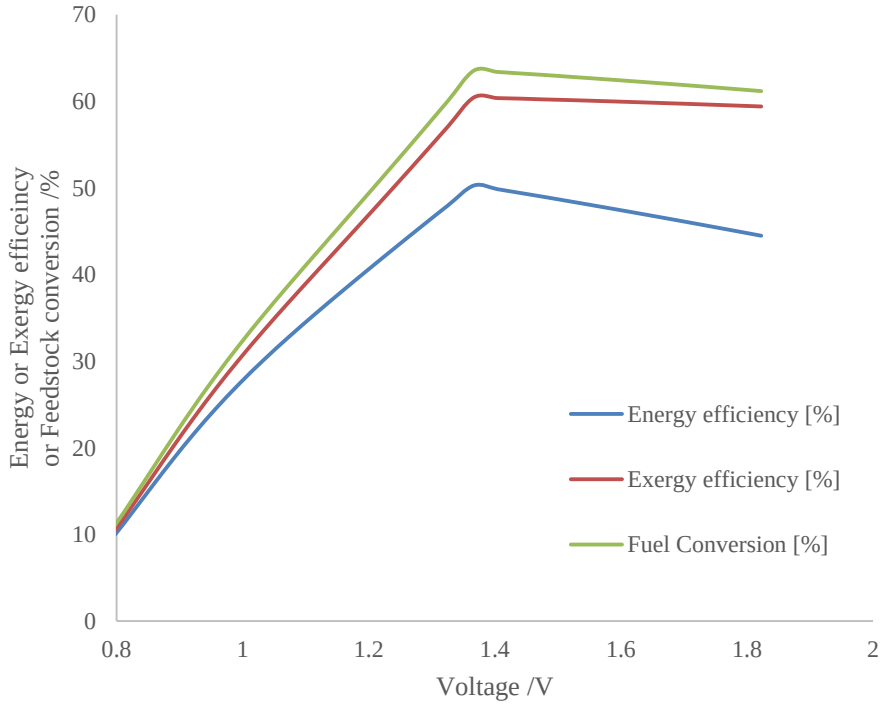

Fig. 4-6 – Relation between the voltage and energy efficiency, exergy efficiency and feedstock conversion for the SOEC operated at 800°C and fed with 18% CO_2, 35% H_2O and 47% N_2, the recycling ratio was set to 0.1 (10%).

The relation between voltage applied and exergy efficiency is shown in Fig. 4-6, red line. From the figure, one can see that the exergy efficiency increases with applied voltage up to 1.37 V before it reaches a plateau at 60%. As explained above, this voltage is where all the generated oxygen ions are transported through the electrolyte and any excess input voltage will be converted to heat.

The relation between feedstock conversion and applied voltage is shown in Fig. 4-6, green line. As expected, the maximum feedstock conversion of 63.5% is achieved at 1.37 V. The drop in feedstock conversion after 1.37 V can be explained by the stronger influence of water-gas shift (WGS) reaction when the temperature of SOEC increases.

Fig. 4-7 depicts the relation between amount of CO_2 converted and the voltage applied. The figure shows that the amount of CO_2 converted increases with applied voltage until 1.37 V. Thereafter, there is a slight decrease in the amount of CO_2 converted. This slight decrease is due to the stronger influence of WGS reaction. At the optimal applied voltage, about 3.5 kmol s^{-1} of CO_2 is converted. For the given inlet conditions 5.288 kmol s^{-1} of CO_2 is produced by the power plant, hence converted is 67.14% of CO_2.

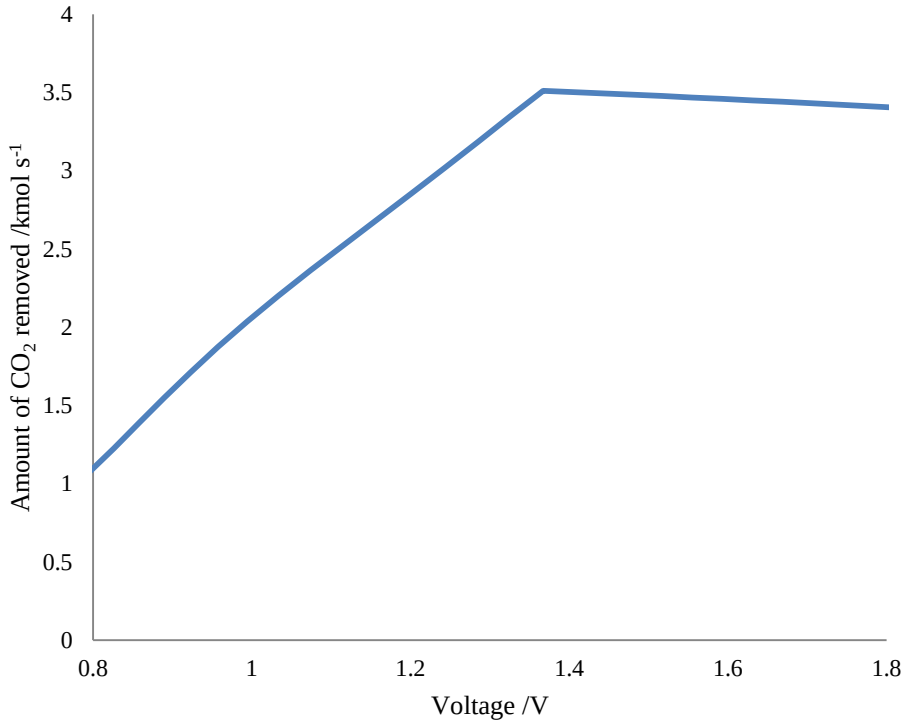

Fig. 4-7 – Relation between amount of CO_2 converted and applied voltage for the SOEC operated at 800°C and fed with 18% CO_2, 35% H_2O and 47% N_2, the recycling ratio was set to 0.1 (10%).

Fig. 4-8 and Fig. 4-9 depict the difference between energy and exergy consumed per kg of CO_2 converted, respectively, under different voltage applied. In Fig. 4-8, the energy consumed per kg of CO_2 converted reduces exponentially with applied voltage until the optimal voltage is reached. Thereafter, the energy consumption increases steadily with voltage applied. The minimum energy required to convert one kg of CO_2 is about 16.5

kJ at 1.37 V. In Fig. 4-9, the exergy consumption per kg of CO_2 converted also reduces exponentially with voltage applied until the optimal voltage is reached. After which, there is almost no change in exergy consumption when further increasing the voltage. The minimum exergy required to convert one kg of CO_2 is about 7.2 kJ at 1.37 V.

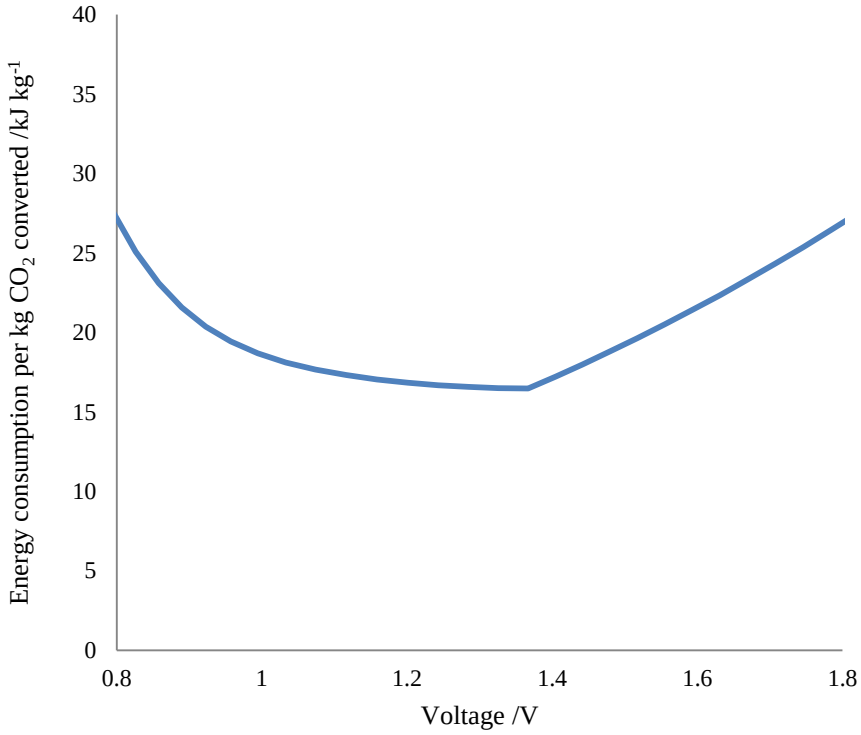

Fig. 4-8 – Relation between energy consumption per kg of CO_2 converted and applied voltage for the SOEC operated at 800°C and fed with 18% CO_2, 35% H_2O and 47% N_2, the recycling ratio was set to 0.1 (10%).

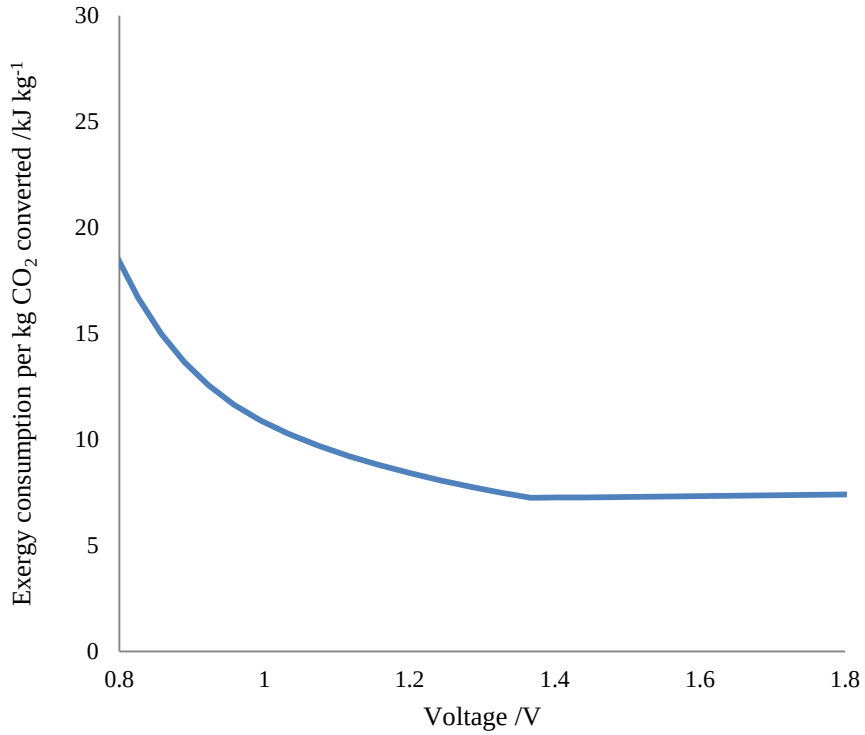

Fig. 4-9 – Relation between exergy consumption per mol of CO_2 converted and applied voltage for the SOEC operated at 800°C and fed with 18% CO_2, 35% H_2O and 47% N_2, the recycling ratio was set to 0.1 (10%).

4.1.4 Conclusion

This section presented analysis of CO_2 mitigation system based on the proposed multi-level model of the electrolyzer. The system consists of SOEC, heat exchangers and gas separation units. Energy and exergy analysis of the CO_2 mitigation system was performed and presented under different conditions. For a given operating condition and assumptions made, it was found that the optimal applied voltage for the SOEC system is 1.37 V. At this optimal value, the system is capable of achieving the energy and exergy efficiencies of 50% and 60 %, respectively. Results showed that at 800°C and voltage 1.37 V (current ~0.7 A cm^{-2}) there was ~63.5% maximum feedstock conversion and ~67% reduction in CO_2 concentration. The corresponding energy and exergy required to convert one kg of CO_2 is 16.4 kJ and 7.2 kJ, respectively. It was also observed that the electrode kinetics of the electrochemical reaction at the anode and cathode are sluggish, which is inevitable due to the slow reverse water-gas shift reaction.

4.2 Parametric study of CO_2 mitigation system

This chapter has been published in a modified version as JP Stempien, Q Sun, SH Chan. Performance of power generation extension system based on solid-oxide electrolyzer cells under various design conditions, Energy, 55, 2013, 647.

4.2.1 Introduction

In the design of a thermodynamic system, one of the important steps is to analyse the behaviour of the system under various design conditions (Stempien et al. 2012, Goplana et al. 2008, Milewski & Miller 2006, Garton et al. 2012, Lawlor 2012). Objective of this chapter is to study the operation of CO_2 mitigation system under various operating conditions of temperature, exhaust gas recycling and mole flux of power plant flue gases to SOEC. Later, the results of the simulation are processed and optimal cases for chosen scenarios are indicated and suggested for the design of a real system.

4.2.2 Simulation set-up

The schematic of the system under study is depicted in Fig. 4-10. It consists of flue gases and air compressors, heat exchanger to recover heat of exhaust from SOEC, electrical heater and extra cooler in case too high temperature is generated inside SOEC. All the balance-of-plant elements were standard Aspen HYSYS modules. If perfect and complete combustion of fuel in the power plant is assumed and nitrogen is treated as inert, then the exhaust flue gas would consist of nitrogen, water vapour and carbon dioxide only. To prevent the fuel electrode from oxidation (by H_2O and CO_2), exhaust gas recirculation (EGR) is necessary to maintain a desired reducing environment for the fuel electrode. The amount of EGR is one of three parameters under analysis in this chapter.

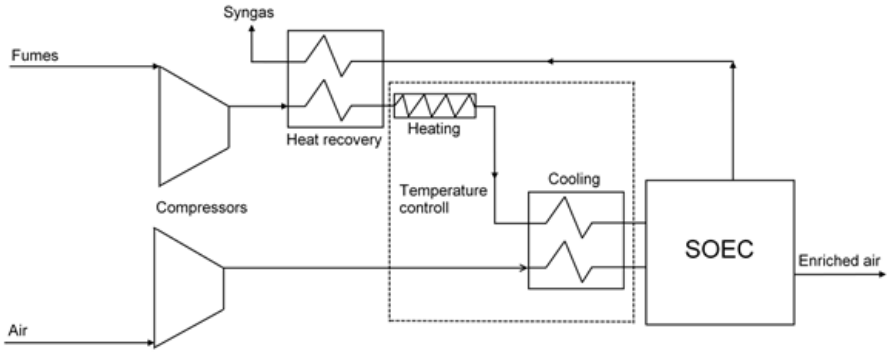

Fig. 4-10 – Schematic of simulated SOEC system #2.

The proposed system is designed for a large-scale implementation; hence the analysis of scaling up effect on the overall system performance is necessary. Molar flux of the flue gas, which is defined as molar flow rate per unit active cell area, is chosen as a parameter for the analysis of the system performance.

Other variable under parametric study is the operating temperature, which would significantly affect the electrochemical performance of the cell.

The values for the three parameters under study are summarized in Table 4-2.

Table 4-2 – Values of temperature, mole flux and EGR used in the parametric study of CO_2 mitigation system.

Temperature °C	Molar flux mol h^{-1} m^{-2}	Percentage of EGR
500	129	0.1 (10%)
600	258	0.2 (20%)
700	516	0.3 (30%)
800	1289	0.4 (40%)
-	-	0.5 (50%)

The performance of the system was assessed using a set of indicators below:

- Electricity consumption W,
- Current density A m^{-2},
- Voltage V,
- Electricity-to-syngas efficiency %,
- Steam conversion %,
- Carbon dioxide conversion %,
- Carbon dioxide conversion efficiency mol kWh^{-1}.

4.2.3 Results and conclusions

Simulation created a vast collection of raw data, especially so when there are many parameters that would affect the desired outcome, causing difficulty in result presentation. One example of messy results presentation is shown in Fig. 4-11. The author would like to underline that this research was first to analyse such specific combination of parameters. Only comparison to previous works can be made based on temperature variation, however, it is considered as trivial and scientifically insignificant, thus it is not part of the study. The obtained results were processed in two ways. First, all results with voltages higher than 1.8 V were removed as they are considered as not realistic. Next, the remaining data was put in descending or ascending order (depending on a case) and extreme values for each simulation were chosen. Exception was given to electricity consumption data. These would allow the prediction of the point where the cell is thermally balanced. For these data series, the switching point between cooling and heating of gas stream was selected for plotting.

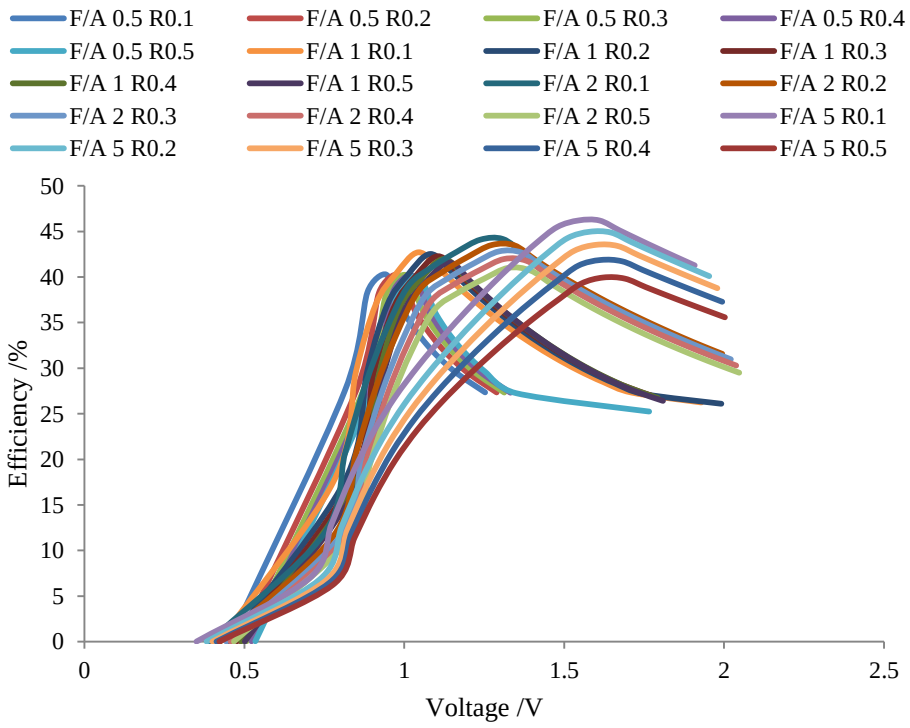

Fig. 4-11 – Efficiency at a constant temperature as a function of voltage, percentage of exhaust gas recycling (EGR) and molar flux – exemplary raw data. F/A stands for flow to cell area (i.e. flux) and R stands for EGR factor.

In Fig. 4-12 to 4-15, the maximum efficiency curves are presented. Highest value of 46.2% is obtained for voltage 1.54 V, EGR 10%, mole flow 1289 mol h^{-1} m^{-2} and temperature 800 °C. At this temperature, the maximum efficiency does not drop below 40%. Acceptable results are also obtained at 700 °C for mole fluxes of 129, 258 and 516 mol h^{-1} m^{-2}. Operation at lower temperature is highly inefficient.

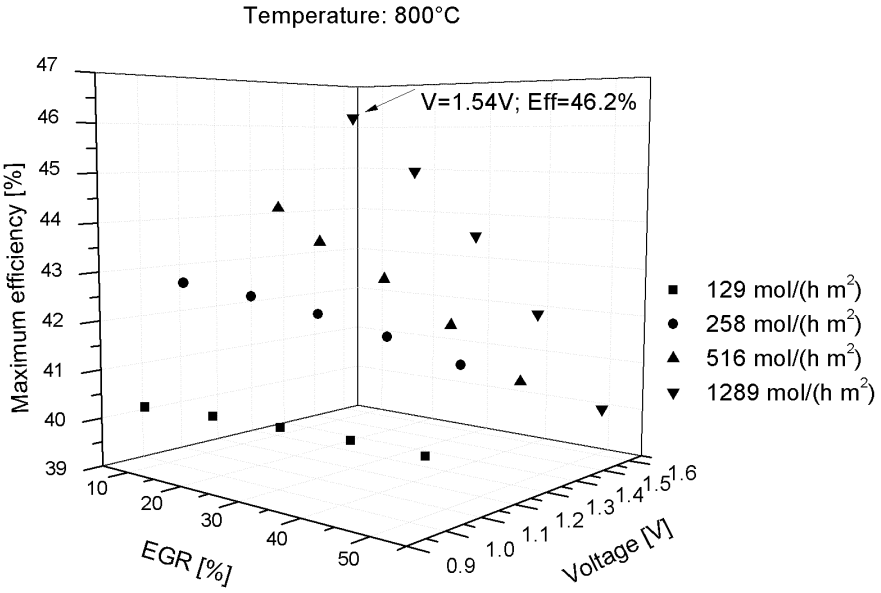

Fig. 4-12 – Maximum efficiency at 800 °C.

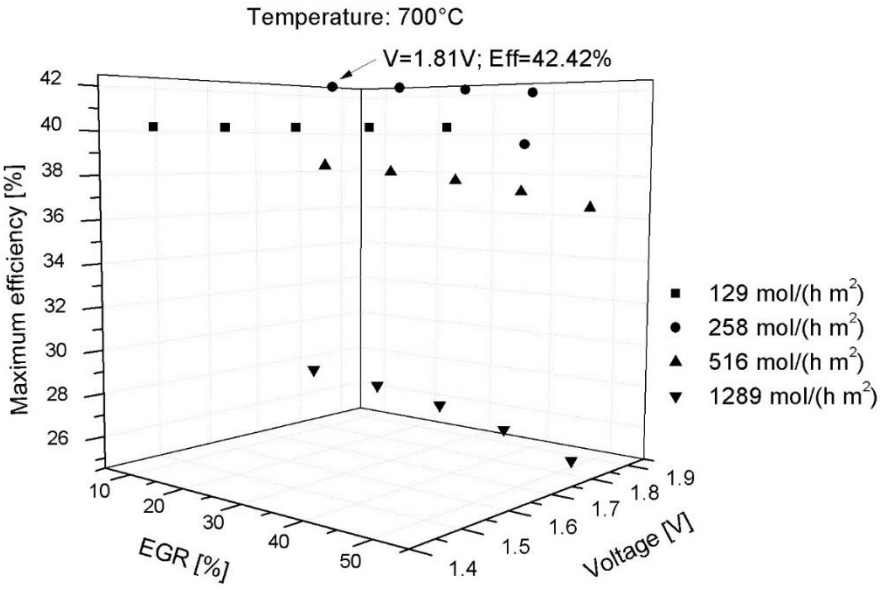

Fig. 4-13 – Maximum efficiency at 700 °C.

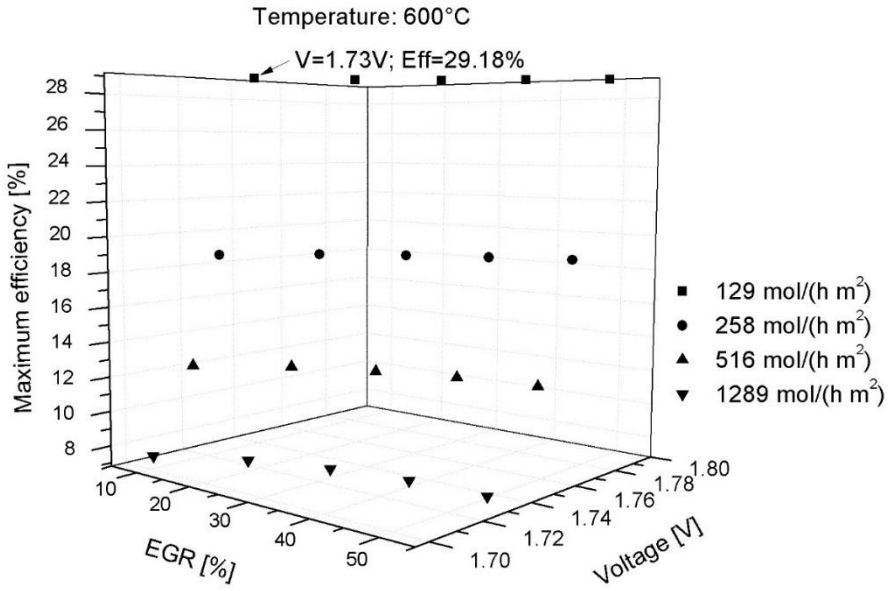

Fig. 4-14 – Maximum efficiency at 600 °C

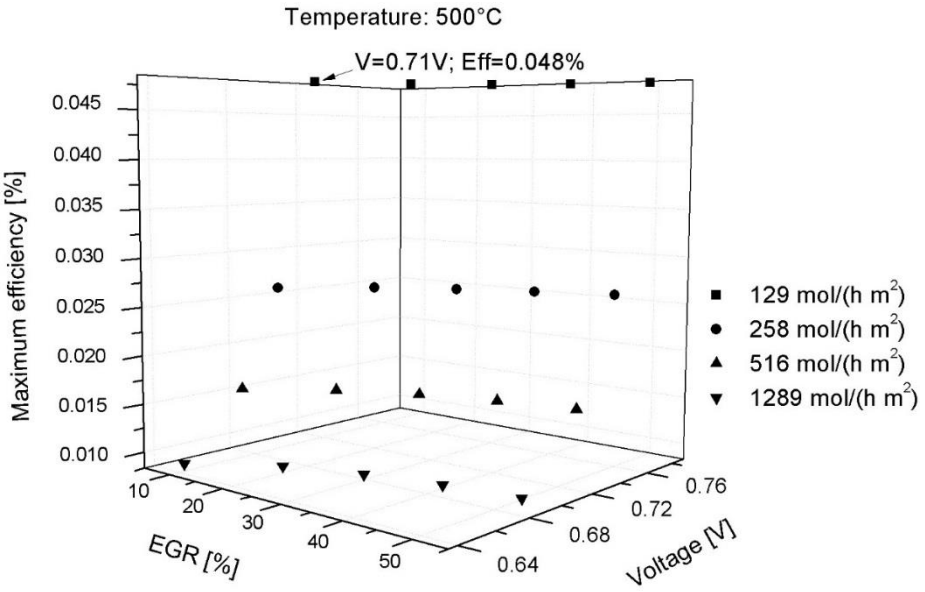

Fig. 4-15 – Maximum efficiency at 500 °C.

Fig. 4-16 and 4-17 present electricity consumption levels at thermally balanced state for different operating conditions at 800 and 700 °C respectively. Increase in power consumption at thermally balanced state is proportional to increase in mole flux. Dropping the temperature from 800 °C to 700 °C causes the drop of electricity

consumption by 250 W or 18%. For 500 and 600 °C thermal balance (flue gases are delivered at 110 °C) of the cell was unable to achieve at voltage below 1.8 V. Cell required heating at all operational conditions.

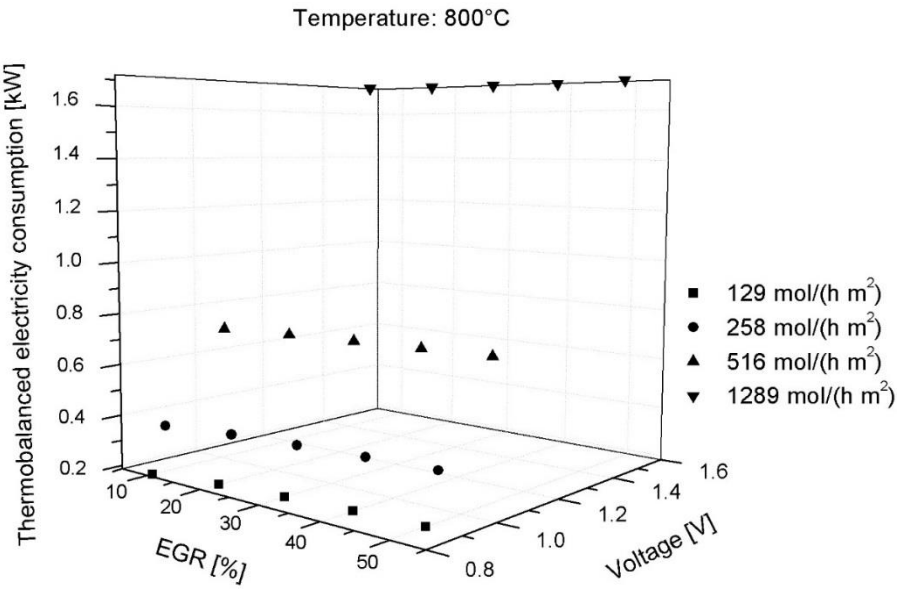

Fig. 4-16 – Electricity consumption for thermally balanced cell at 800 °C.

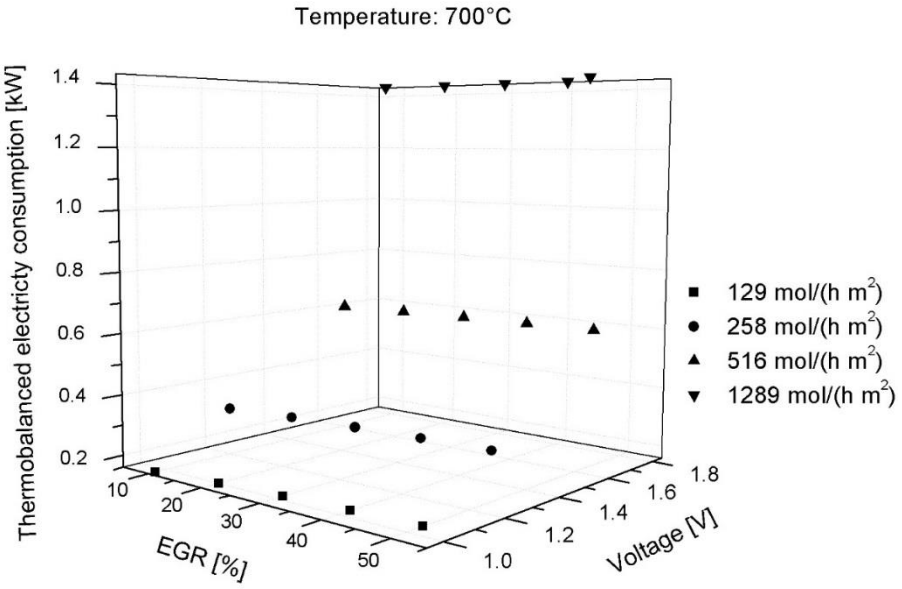

Fig. 4-17 – Electricity consumption for thermally balanced cell at 700 °C.

Fig. 4-18 to 4-21 present the efficiency of CO_2 conversion. Highest value is obtained for

lowest temperature, EGR 40% and lowest mole flux. Each kWh delivered to the cell utilizes 2.57 moles of CO_2. Efficiency of CO_2 removal is inversely proportional to mole flux. Please note that the somewhat low values of operating voltage are due to exhaust gas recycling which in general results in lowering the voltage at current densities close to zero. The revers effect of temperature on cell efficiency and CO_2 removal efficiency can be explained by low heating demand and higher conversion rates at low temperatures and low voltage. Reverse water-gas shift reaction may also play a crucial role. Whereas, the efficiency of SOEC is generally inversely proportional to temperature.

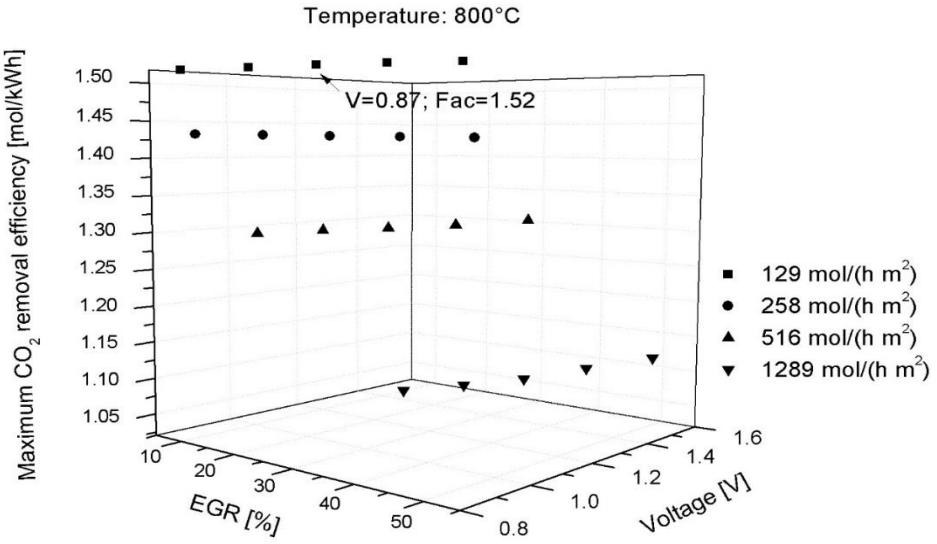

Fig. 4-18 – Maximum CO2 removal efficiency at 800 °C.

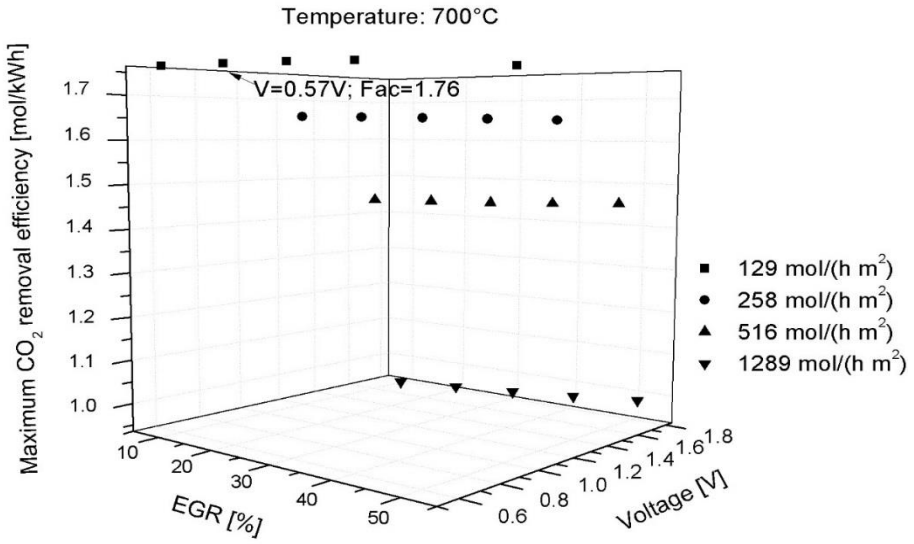

Fig. 4-19 – Maximum CO2 removal efficiency at 700 °C.

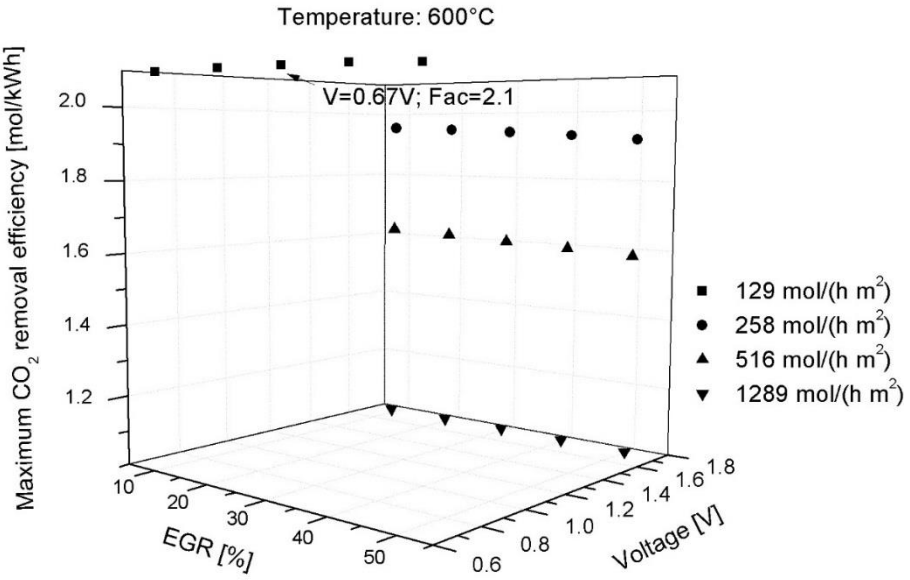

Fig. 4-20 – Maximum CO2 removal efficiency at 600 °C.

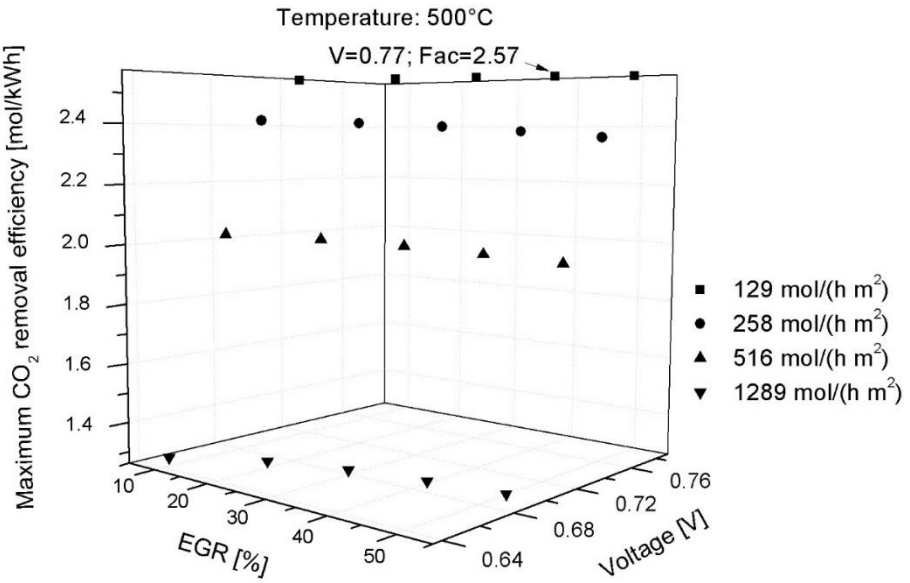

Fig. 4-21 – Maximum CO2 removal efficiency at 500 °C.

In Fig. 4-22 to 4-25 conversion of water vapour is presented. Lowering the temperature and increasing mole flux dramatically reduces conversion of this species. For temperature of 800 °C, only mole fluxes of 129, 258 and 516 mol h^{-1} m^{-2} can guarantee the conversion of over 50% of gas stream. Similarly, this is also true for the case

operating at 700 °C. Operation at lower temperature can give maximum 34.5 and 0.035% conversion at 600 and 500 °C respectively.

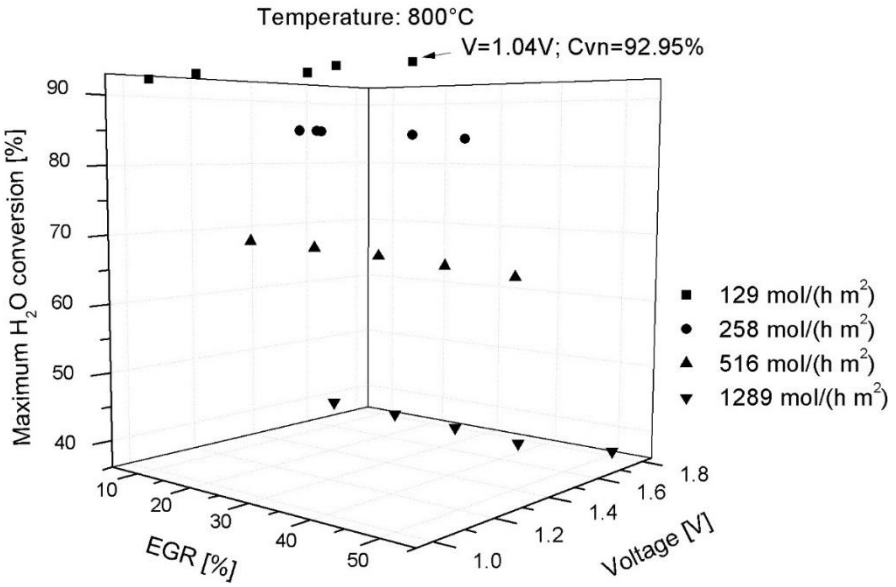

Fig. 4-22 – Maximum H2O conversion at 800 °C.

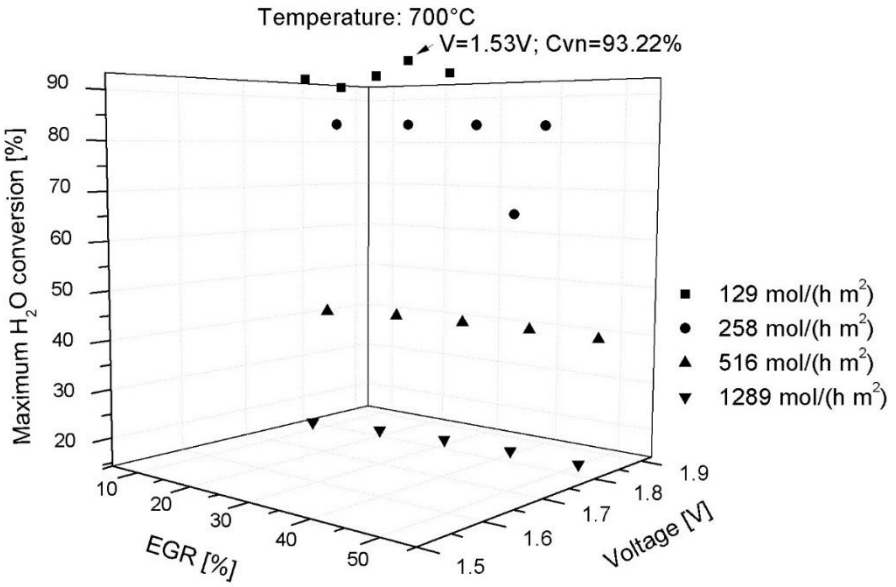

Fig. 4-23 – Maximum H2O conversion at 700 °C.

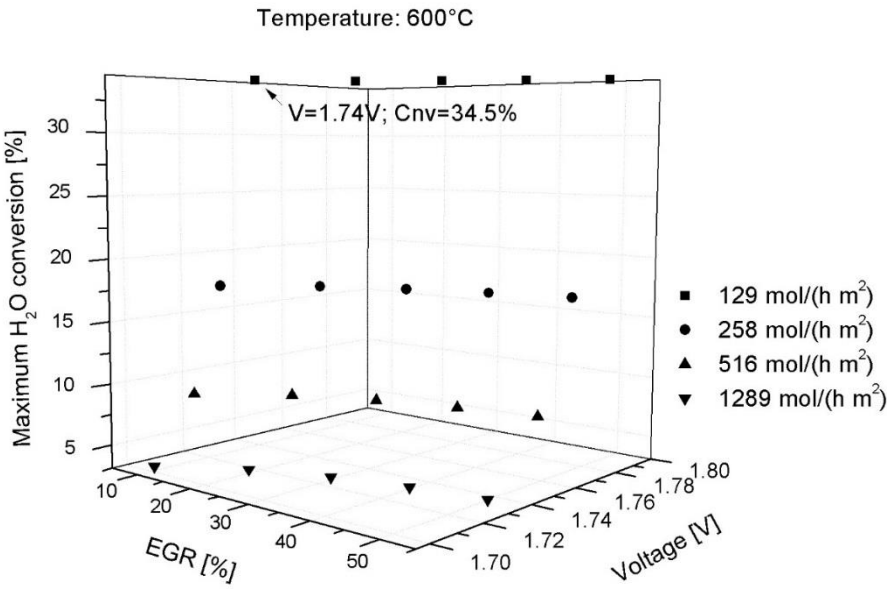

Fig. 4-24 – Maximum H2O conversion at 600 °C.

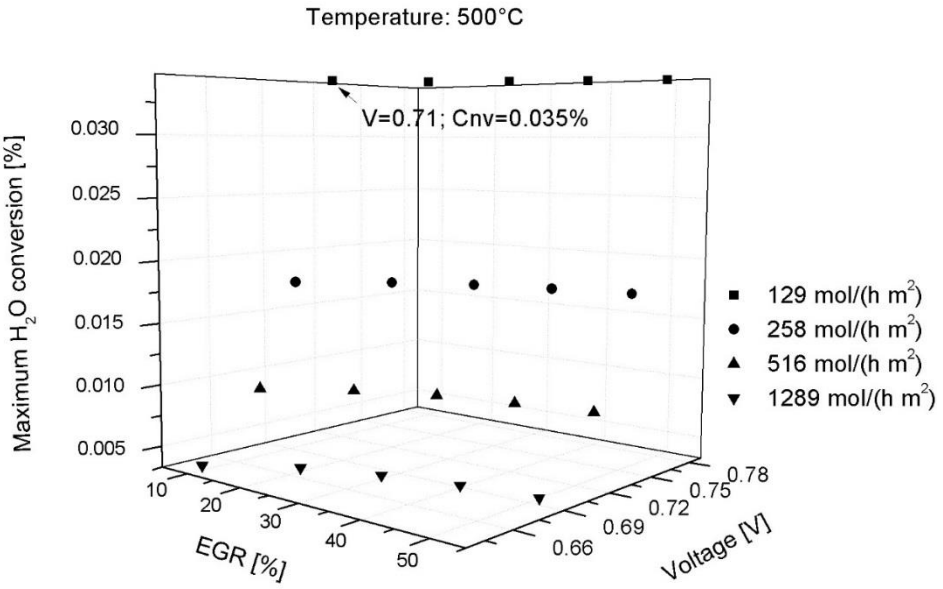

Fig. 4-25 – Maximum H2O conversion at 500 °C.

Fig. 4-26 to 4-29 present the conversion of CO_2. All of the operating conditions guarantee high utilization of CO_2. Only at 500 °C and mole flux of 1289 mol h^{-1} m^{-2}, the conversion drops slightly below 50%.

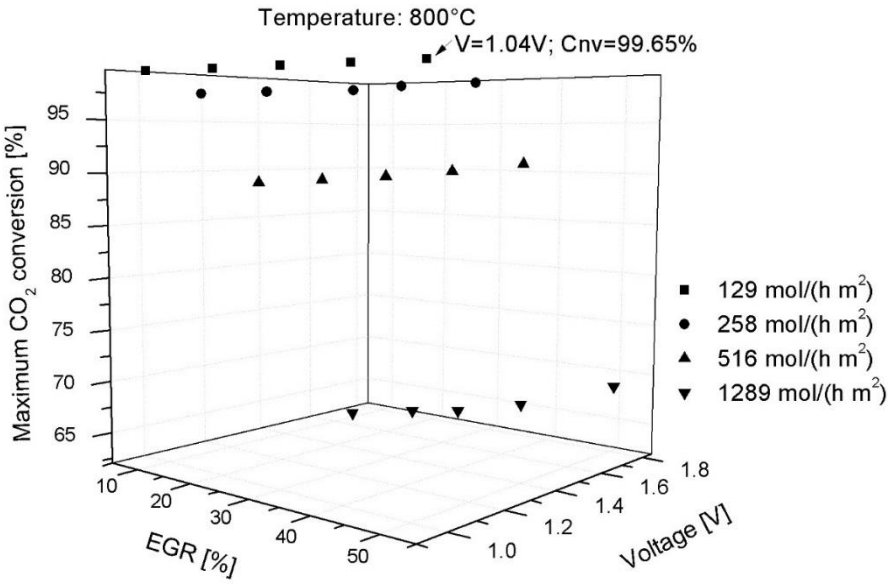

Fig. 4-26 – Maximum CO2 conversion at 800 °C.

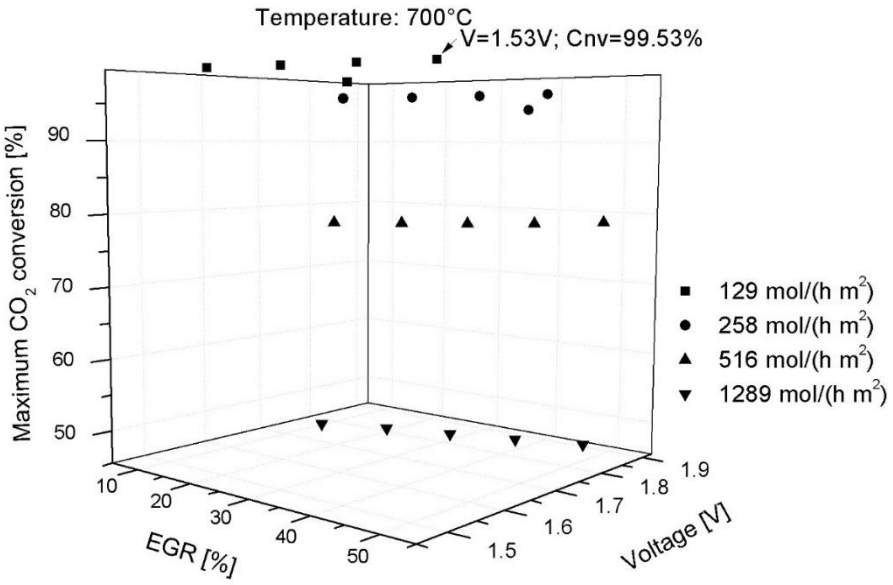

Fig. 4-27 – Maximum CO2 conversion at 700 °C.

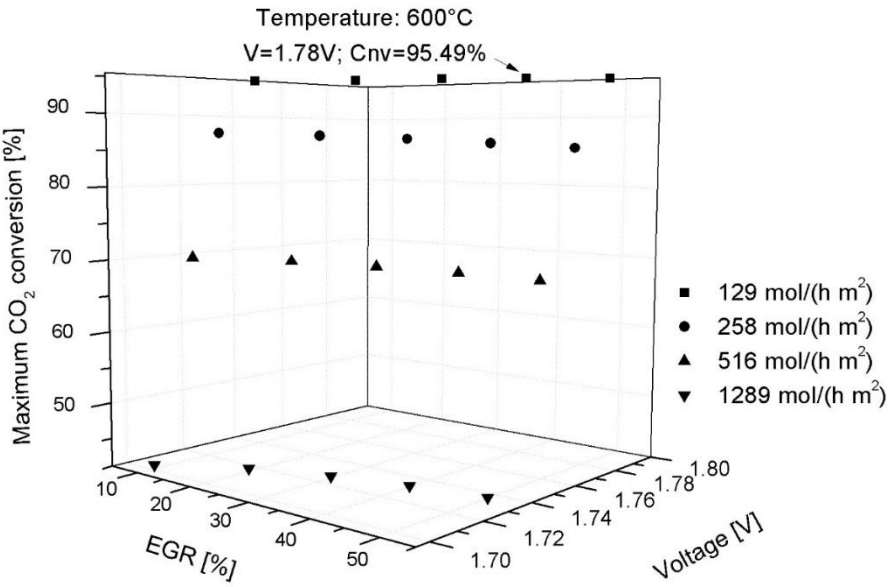

Fig. 4-28 – Maximum CO2 conversion at 600 °C.

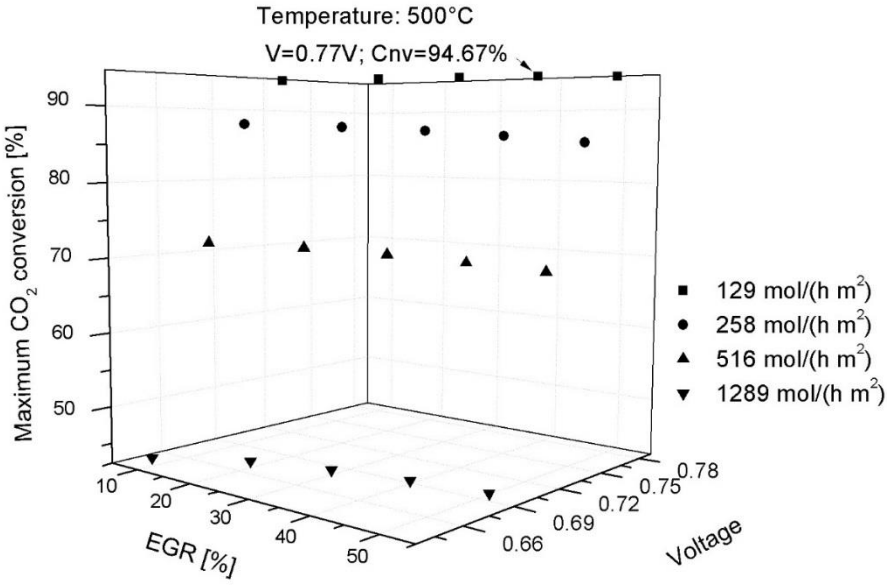

Fig. 4-29 – Maximum CO2 conversion at 500 °C.

Finally, the author has prepared several scenarios for desired system design, i.e.

- Maximum electricity-to-syngas efficiency,
- Maximum H_2O conversion,
- Maximum CO_2 conversion,
- Lowest electricity consumption.

For the scenarios recommendations have been made regarding operating conditions. The recommended design conditions are summarized in table 4-3.

Table 4-3 – Recommended design conditions of CO_2 mitigation system.

Case	Temperature °C	EGR %	Molar flux mol h^{-1} m^{-2}	Voltage V	Corresponding current density A m^{-2}
Maximum electricity-to-syngas efficiency	800	10 – 20	516 – 1289	1.31– 1.54	9000 – 13000
Maximum H_2O conversion	700 – 800	10 – 50	129	0.98 – 1.83	3000 – 5000
Maximum CO_2 conversion	600 – 800	10 – 50	129 – 258	0.94 – 1.89	1000 – 8000
Lowest electricity consumption	700	10 – 50	129	0.97 – 1.04	<1000

Due to aforementioned reasons, the raw data are not presented in this chapter. The following remarks summarize the outcome of the study.

General findings:

- Influence of the temperature on the investigated parameters (electricity-to-syngas efficiency, conversion of steam and carbon dioxide, power consumption, I-V curves, CO_2 conversion efficiency) is far greater than the influence of EGR.
- Influence of mole flux is much greater than the influence of EGR.
- At high mole flux and temperature, the influence of EGR is more pronounced.

Electrochemical performance:

- Elevated temperature enhances the performance of SOEC.
- When increasing the mole flux, fuel utilization drops. Since products of the reaction are recycled (EGR), change of mole flux affects the kinetic state of water-gas shift reaction and gas composition at the cell interface, thus it influences OCV. Increase in mole flux makes OCV higher. Higher mole flux

ensures constant delivery of fresh flue gases (reactants), thus lesser concentration loss and higher overall cell performance.

- EGR has negligible effect on SOEC electrochemical performance.

Electricity consumption:

- Elevated SOEC temperature would lead to lower total polarization loss and hence requires less electrical power input to perform the electrolysis. Such behaviour is directly related to improved energy conversion (electricity to syngas) efficiency of SOEC
- Higher mole flux would lead to higher electricity consumption, which is due to increased energy demand for pumping the gases through the cell as well as higher energy demand for heating.
- EGR (10 – 50%) has negligible effect on electricity consumption.

Electricity-to-syngas conversion efficiency:

- Maximum efficiency is almost invariant with the operating temperature. With decrease of temperature, values of maximum efficiency shift towards higher voltages, which can be explained by lower electrochemical performance of SOEC. The highest value of efficiency corresponds to transition point between electrolyte controlled (ion flow) and electrode controlled regime of operation (kinetics of co-electrolysis reaction).
- Overall electricity-to-syngas conversion efficiency increases with the increase of mole flux. At low temperatures, the increase is less profound than that at high temperatures. Positive influence of the mole flux on the electrochemical performance must be higher than negative influence on higher energy consumption due to compressors work.
- Influence of EGR is somewhat interesting. For mole flux of 516 mol h^{-1} m^{-2} and 1289 mol h^{-1} m^{-2}, increased EGR lowers the efficiency by 3 and 7%, respectively. For low mole fluxes, the trend is opposite albeit slightly. The study revealed that there exist two regions of operation where electrolysis and WGS reaction dominate the processes occurring within the cell. At low mole fluxes electrolysis is dominant process, while at high mole fluxes water-gas-shift (WGS) reaction becomes dominant. The transition occurs between mole fluxes of 258 mol h^{-1} m^{-2} and 516 mol h^{-1} m^{-2}.

CO_2 conversion efficiency:

- At low temperature, performance of CO_2 removal is favourable, which is due to low heating demand and high conversion rate at lower temperature and low voltage. For high mole fluxes and above 700 °C peak value of CO_2 removal efficiency occurs at certain voltage, but it drops significantly with the increase of voltage. The author speculates existence of peak value in whole range of investigated conditions. Further increase in mole flux shifts the peak towards the higher voltages.
- CO_2 removal efficiency is dropping with mole flux. The drop is much greater for low temperatures, than for high temperature. For 800 °C the drop is about 0.5 mol kWh^{-1}, and for 500 °C it is about 1.2 mol kWh^{-1}.
- Influence of EGR on CO_2 removal efficiency depends on the voltage. For low voltages increase in EGR drops the efficiency, while for high voltages the trend is opposite. Transition point occurs at limiting step assigned to oxygen ion transport controlled. This suggests that at some point concentration of gases flips the direction of WGS reaction.

Steam and carbon dioxide conversion:

- H_2O and CO_2 conversion drops with the increase in mole flux. For steam the drop is higher at high temperatures. Opposite is the case for CO_2, hence behaviour can be attributed to WGS reaction.
- Steam conversion at mole flux of 129 mol h^{-1} m^{-2} is decreasing for low voltages when EGR is increasing, at high voltages the trend is opposite. For all other mole fluxes, increase in EGR decreases conversion. For CO_2 conversion at all mole fluxes and at low voltages, increase in EGR decreases the conversion, while at high voltages increase in EGR increases conversion. In general, influence of EGR is more pronounced for higher mole fluxes.
- For low temperature and mole flux, three limiting steps in H_2O and CO_2 conversion can be observed. The authors posit that the first limiting step to be sluggish kinetics of overall process at low voltages, second step can be linked to the transport of oxygen ions through the electrolyte, and last step is due to reaching maximum extent of electrolysis reaction for given thermodynamic state.
- At 500 °C the optimal value of EGR is observed for CO_2 conversion. At molar flux of 258 mol h^{-1} m^{-2} recycling of 20% of product stream results in highest CO_2

conversion. At mole flux of 516 mol h^{-1} m^{-2} at recycling of 40% of product stream lowest CO_2 conversion occurs. Additionally, at low mole fluxes for the whole range of applied voltages increase in EGR increases CO_2 conversion, unlike for higher temperatures. Such behaviour is attributed to reverse water gas shift reaction.

4.3 Chapter summary

In this chapter, an analysis of CO_2 mitigation system was performed. It was concluded that such system is a viable way to reduce direct emissions from power plants. Energy and exergy analysis resulted in estimation of efficiency of such system and later parametric study provided scenarios on how to operate such system based on the desired mode of operation. A recycling of outflow gases in order to provide reducing atmosphere at the fuel electrode was for the first time analysed. Moreover, the two journal papers following from this study were the first to report a co-electrolysis model incorporating microstructure effect on the activation and concentration losses in the co-electrolysis SOEC. Proposed system was first analysed by the author of this thesis.

It is noticed and was later investigated experimentally within the research group that large amount of oxygen in the flue gas stream may, according to theoretical consideration cause a drop in the performance and according to experimental results a critical failure of Ni-based fuel electrode. Thus, it is not recommended to use such system with gas turbine based power plants, were large concentration of oxygen in the exhaust is expected.

Chapter 5. Synthetic, renewable fuel production and energy storage with use of Solid Oxide Electrolyzer Cell

Broader context

Goal 7 in eight "United Nation's Millennium Development Goals" calls to "Ensure Environmental Sustainability". Since the establishment of these goals in year 2001, many scientists explored potential routes of achieving this goal. Much of the research was focused on energy conversion technologies. Few means were identified as possible pathways towards energy sustainability. These include, but are not limited to, biofuels (Chisti 2007), hydrogen energy (Turner 2004), broader introduction of renewable-related energy technologies (Jacobson 2009, Herbert et al. 2007). However, none of these technologies can meet the sustainability goal alone, and hence a well-balanced combination of these energy carriers is expected to make up energy-mix in a long-term future. The most insuperable barrier for reaching the sustainable energy goal is the need for energy infrastructure (Ridjan et al. 2013, 2014, Connolly et al. 2014), which for most of the renewable-related technologies is simply non-existent, e.g. the lack of recharging station for electric vehicles. One of the approaches to tackle this issue is to switch the source of heavily used hydrocarbon energy carriers (66.4%, or 248 x 109 GJ of final energy consumption) from fossil to renewable. Possible technologies are those connected with biofuels and those build around Fischer-Tropsch, methanation or methanol synthesis processes. Production of biofuels has met with considerable criticism over the use of land, change in the structure of natural vegetation and competition with food production business. Use of synthetic fuel production process combined with renewable energy source and CO_2 captured from industrial process or atmosphere greatly reduces the chance of any of the above criticism. Thus, in this chapter focus is placed on the second approach.

Fischer-Tropsch synthesis (FTS) is a catalytic polymerization process first reported in 1924 by Franz Fischer and Hans Tropsch. The scientists described a process of catalytic conversion of syngas (mixture of hydrogen and carbon monoxide) over an iron-based catalyst to form linear hydrocarbon chains of n-paraffins (alkanes) and α-olefins

(alkenes). Fischer-Tropsch process can work over four types of catalyst, iron-, cobalt-, nickel- and ruthenium-based. The first two are the most popular and cheapest (Dry 2002). Several types of reactor designs have been proposed, but the fixed bed and slurry phase are commercially available. The exact mechanism of synthesis is still under studying (Inderwildi et al. 2008, Liu & Hu 2002, Schulz 2013) and most of modelling work is based on semi-empirical formulations with lumped kinetics of CO utilization and simple distribution of products based on Anderson-Schulz-Flory (ASF) model and its variations (Novak et al. 1981, Bos et al. 1989, Zimmerman et al. 1992, Lox & Froment 1993, Jess et al. 1999, Maretto & Krishna 1999, Schulz & Claeys 1999, van der Laan & Beenackers 1999, 2000, Patzlaff et al. 2002, Wang et al. 2003, Ahon et al. 2005, Storsaeter et al. 2006, Teng et al. 2006, Fernandes & Teles 2007, Visconti et al. 2007, Becker et al. 2012, Markvoort et al. 2012, Almeida et al. 2013, Shiva et al 2013, Pour et al. 2014). Majority of the recent publications on Fischer-Tropsch synthesis are devoted to modelling of new types of reactors (Rados et al. 2003, Wang et al. 2003, 2008, Song et al. 2004, Marvast et al. 2005, Masuku et al. 2012, Ghareghashi et al. 2012) or the process analysis (van Vliet et al. 2009, Yu et al. 2010, Bao et al. 2010, Ermolaev et al. 2014, Zhang et al. 2014, Haarlemmer et al. 2014).

In spite of large renaissance in FTS process research and the great potential of this technology, very few of the reports are concerned with making the process more sustainable. Most of the published papers assumed the use of unsustainable natural gas or coal as the feedstock to FTS process. Only a handful of papers proposed the use of renewable power driven H_2O/CO_2 co-electrolysis. In such a system, energy comes from renewable resources while combined with the electrolytic splitting of water and carbon dioxide as a means to recycle carbon and hydrogen atoms as the energy carriers. This idea is very interesting and can be a promising way to achieve sustainability, as such a closed loop system is CO_2 neutral.

Methane is one of the cleanest hydrocarbon fuels, which can be combusted with very high efficiency in a modern internal combustion engine. It is easy to store and there are existing infrastructures for domestic transport and international trade in most of the countries around the world. Methane can be easily produced out of hydrogen and oxides of carbon, such as CO_2 and CO. The simplest chemical pathway to synthesise CH_4 involves equation (5-1) Sabatier and equation (5-2) methanation (reverse of steam-methane reforming, SMR) reactions.

$$CO_2 + 4H_2 \rightarrow CH_4 + 2H_2O \ (\Delta H_{298} = -165 \text{ kJ mol}^{-1}) \quad (5\text{-}1)$$

$$CO + 3H_2 \rightarrow CH_4 + H_2O \ (\Delta H_{298} = -206 \text{ kJ mol}^{-1}) \quad (5\text{-}2)$$

The above reactions are exothermic, thus require only the hydrogen and carbon monoxide/dioxide stream. The required gases can be produced in an environmentally benign and efficient manner by an electrochemical mean through the Solid Oxide Electrolyzer Cell (SOEC).

Similarly, methanol can be easily used as transportation fuel for personal vehicles. It is easy to store and its production is only slightly more difficult than methane (due to larger pressure needed in the reactor). Methanol can be easily produced from CO_2, CO and H_2 mixture

$$3H_2 + CO_2 \rightarrow CH_3OH + H_2O \ (\Delta H_{298} = -49.31 \text{ kJ mol}^{-1}) \quad (5\text{-}3)$$

$$2H_2 + CO \rightarrow CH_3OH \ (\Delta H_{298} = -90.7 \text{ kJ mol}^{-1}) \quad (5\text{-}4)$$

The reactions 5-3 and 5-4 proceed selectively over Copper and Zinc catalysts (Steinberg et al. 1997). Whereas 5-1 and 5-2 over Nickel catalyst.

Production of sustainable methane by using renewable or nuclear electricity, water and carbon dioxide has never been investigated before. Similar analysis was reported on production of Fischer-Tropsch (FT) fuels, methanol or utilization of CO_2 in a traditional FT plant. Steinberg and Dang (Steinberg & Dang 1977) proposed a system to produce synthetic methanol using nuclear energy and carbon dioxide stripped off from air or seawater. They concluded that methanol can be produced at the energy cost of 8.6 – 29.1 kWh kg^{-1} of methanol. Ebbesen et al. (Ebbesen et al. 2009) proposed to use Solid Oxide Electrolyzer and catalytic converter to turn H_2O and CO_2 into synthetic fuels. They reported on experimental investigation of co-electrolysis of H_2O and CO_2 in SOEC and concluded that long term operation of the cell is possible. Graves et al. (Graves et al. 2011) continued the work of Ebbesen et al. performing technology review and economical assessment of recycling CO_2 into synthetic gasoline. They concluded that the cost of electricity is the biggest contributing factor to the final price of the synthetic gasoline. Bierschenk et al. (Bierschenk et al. 2011) analysed theoretically and

experimentally in-situ production of methane from a typical Solid Oxide Cell with a Ni-YSZ fuel electrode. The authors achieved experimentally very low conversion of steam and carbon dioxide to methane (~2% of output composition) at 873.15 K and 1 atm. Nevertheless, they predicted up to ~30% of methane yield at 773.15 K and 10 atm is possible, unfortunately, this was not shown experimentally. Xie et al. (Xie et al. 2011) experimentally investigated production of synthetic methane in-situ in a SOEC with Fe-based catalyst in fuel electrode. The authors concluded that small amounts of methane (2.8% Faradic yield) can be produced over Fe-based catalyst in a FT-like reaction. Li et al. (Li et al. 2013) performed another in-situ experimental study of methane formation in SOEC, reporting small amount of methane produced if steam to carbon dioxide ratio was set to 2 at 923.15 K and atmospheric pressure. The authors suggested that reaction of hydrogen with carbon deposited on the electrode surface is the mechanism of methane formation. Production of methane in a single device offers numerous advantages, however, the methane synthesis proceeds with reasonable reaction rate only at low temperatures (~473.15 K). Thus, it seems more practical to have two-reactor system operated at two different temperatures. Such experimental study was performed by Hoekman at al. (Hoekman et al. 2010). The authors analysed production of methane via Sabatier reaction using renewable hydrogen from a PEM electrolyzer. They have achieved a maximum of 60% CO_2 conversion at hydrogen to CO_2 ratio of 4 to 1 and temperature of 623 K. Becker et al. (Becker et al. 2012) analysed the combined system of SOEC and Co-based FT synthesis to produce hydrocarbon fuels. The authors used a simplified linear model of SOEC combined with simplified lumped model of cobalt-based FTS process with simple Anderson-Schulz-Flory product distribution. The authors predicted 51% of conversion efficiency and the cost of produced gasoline at 4.4 – 15 \$ GGE^{-1} (gallon of gasoline equivalent). However, as the voltage-current relationship of SOEC is highly non-linear, the use of linear model for SOEC in Becker's work could cause considerable errors. Ridjan et al. (Ridjan et al. 2013) realized the importance of transportation sector in the energy market and analysed the feasibility of relying on synthetic fuels in 100% renewable energy system. The authors compared several pathways to produce synthetic fuels and concluded that the use of SOEC combined with renewable energy offers the advantage of grid stabilization and can compete with other technologies, if a SOEC reaches competitive unit price level.

After reviewing the literature on FTS (Novak et al. 1981, Bos et al. 1989, Zimmerman et al. 1992, Lox & Froment 1993, Jess et al. 1999, Maretto & Krishna 1999, Schulz &

Claeys 1999, van der Laan & Beenackers 1999, 2000, Patzlaff et al. 2002, Wang et al. 2003, Ahon et al. 2005, Storsaeter et al. 2006, Teng et al. 2006, Fernandes & Teles 2007, Visconti et al. 2007, Becker et al. 2012, Markvoort et al. 2012, Almeida et al. 2013, Shiva et al 2013, Pour et al. 2014) and SOEC modelling (Stempien et al. 2013, Milewski et al. 2011, Ni et al. 2008), it is clear that a more comprehensive model is required to accurately analyse the combination of the two processes and to explore their potential to a greater extent. As the only existing study in the literature, the simplified linear model cannot correctly predict the influence of varying inlet gas composition, temperature or pressure on the final performance and production of such combined system. Moreover, the use of the ASF distribution to characterise the spectra of produced hydrocarbons from the FT synthesis has been highly criticized. In the past, many authors have proposed more advanced models that include several secondary reactions and a mechanistic approach to the kinetic rate of the process (Novak et al. 1981, Bos et al. 1989, Zimmerman et al. 1992, Lox & Froment 1993, Jess et al. 1999, Maretto & Krishna 1999, Schulz & Claeys 1999, van der Laan & Beenackers 1999, 2000, Patzlaff et al. 2002, Wang et al. 2003, Ahon et al. 2005, Storsaeter et al. 2006, Teng et al. 2006, Fernandes & Teles 2007, Visconti et al. 2007, Becker et al. 2012, Markvoort et al. 2012, Almeida et al. 2013, Shiva et al 2013, Pour et al. 2014). Becker et al.'s work considered the use of cobalt catalysis, which was reported more expensive than iron catalyst investigated in this study. It is, therefore, concluded that combination of SOEC process and FTS process needs to be reassessed with a new and more advanced modelling approach. Complimentary to this analysis studies of SOEC combined with methane, methanol, syngas and hydrogen production are also considered.

Singapore's context

Singapore's electricity generation mix is dominated by natural gas (78%) and complimented by petroleum products (18.4%) and others (mainly waste). Overall efficiency of electricity generation in 2011 was equal to 44% (EMA 2012). The average peak demand in 2011 of 5.4 GW and average annual consumption per capita of above 9000 kWh per capita makes Singapore one of the most energy intensive nations in the world (almost twice that of EU, based on 2008 data) (EEA 2012) and it hosts the first place among countries with similar yearly average temperature (based on own study, however Singapore's economy structure is responsible for bulk of the consumption). The only countries using more electricity per capita are Scandinavian nations and

Iceland (their energy mix is, however, highly sustainable and eco-friendly) (EEA 2012). Moreover, energy consumption in Singapore, like in most developed countries, is growing on average pace of 3.12% per annum (EMA 2012) (Fig. 5-1). An inevitable conclusion is that Singapore will shortly meet need to alter its energy mix. Such statement can be confirmed by recent exemplary roadmap for diversification of Singapore's energy mix (IAEA 2011).

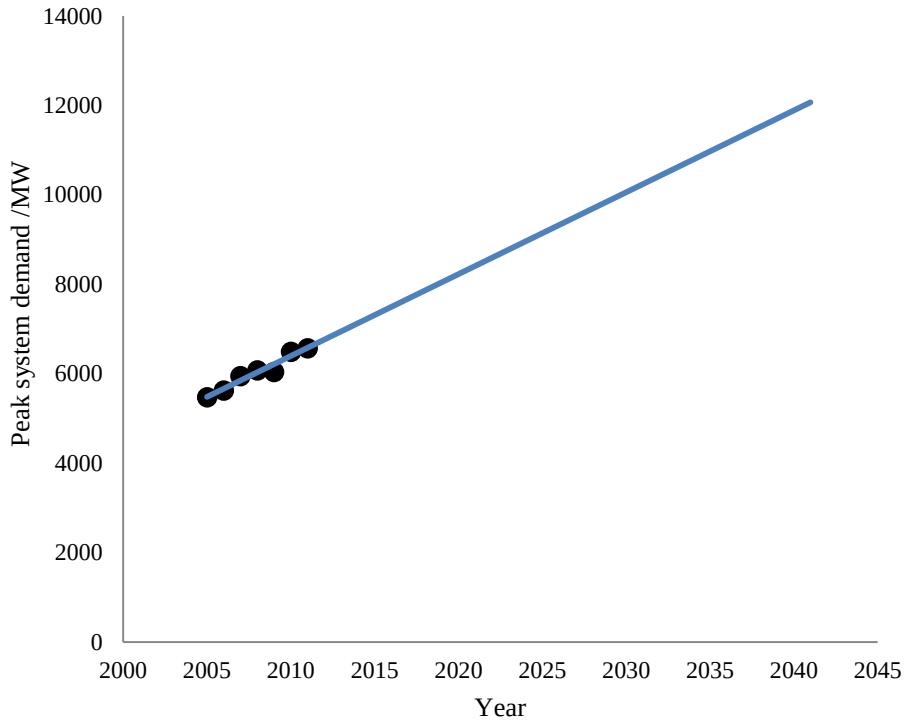

Fig. 5-1 – Projected peak demand growth of Singapore's energy system.

Widely popular move among highly industrialized countries is to invest in wind and solar power (IEA 2012). Those, however, have not been entirely successful due to problem of intermittency of the wind and solar energy (IEA 2012) (Fig. 5-2). Several ideas have been studied regarding harnessing this vast source of energy (Diaz-Gonzales et al. 2012, Albadi & El-Saaday 2010, Gross & Heptonstall 2008, Sovacool 2009, Tian & Zhao 2013). Those include application of flywheels, different kinds of batteries, storing heat in phase change materials or combining wind and water power plants. Furthermore, Singapore's wind resources are still uncharted and based on its weather almanac not very promising. The effort in quantifying the opportunity in harnessing wind energy is nonetheless under way. Especially coastal and offshore wind power are

of interest to Singapore as mentioned by Tiang (Tiang 2012).

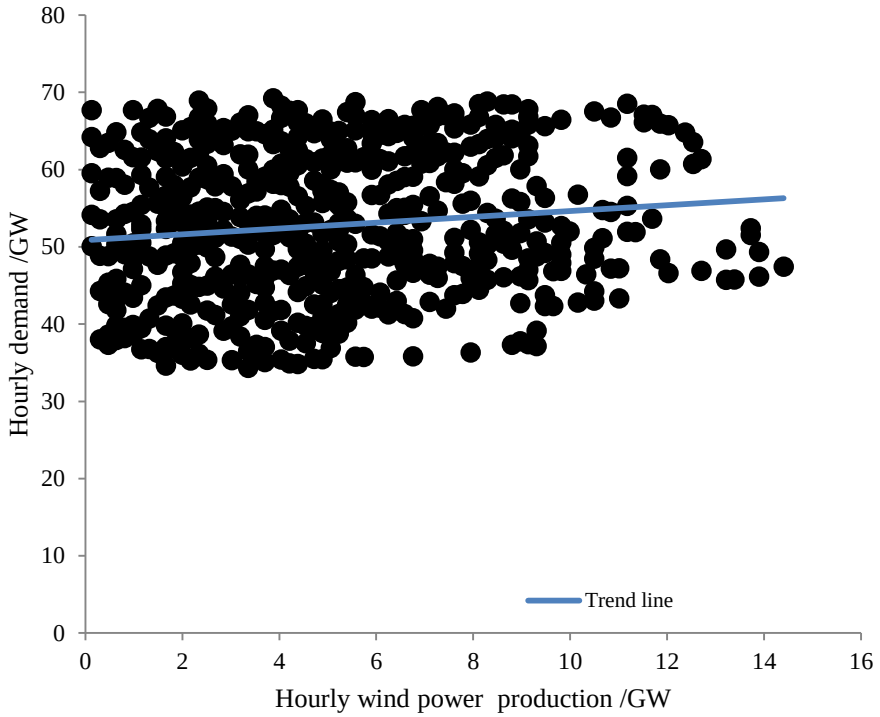

Fig. 5-2 – Intermittency of renewable energy sources (IEA 2012). There is in general no correlation between the demand and supply of electrical energy. Therefore, creating rational for energy storage.

5.1 Study of Singapore's electrical grid balancing and surplus energy storage in form of hydrogen, syngas or methanol

This chapter has been presented in a poster form as JP Stempien, Q Sun, KA Friedrich, SH Chan. Conceptual analysis of Solid Oxide Electrolyzer integration in energy system during 2nd International Conference on Clean Energy Science, April 2014, Qingdao, China.

5.1.1 Introduction

In the following chapter the author presents mathematical simulation and system analysis of three scenarios dealing with possible incorporation of SOEC into Singapore's energy mix. They can be distinguished by two major differences. One is the arrangement of the elements and their connections with SOEC. Second is the output chemical of the

system. In the first case considered the system has the simplest arrangement and yield of electrolyzer is hydrogen. The second case considers incorporation with combined cycle power plant where the cell processes the flue gases of power plant and produces syngas. In the final case similarly to previous SOEC is combined with power plant but the deliverable product, however, is methanol. The two last systems present opportunity to mitigate CO_2 emissions and utilize off peak power. Moreover, in the last case production of methanol poses additional possibilities for reducing fossil fuels use and increasing sustainability and energy security in automotive sector (Bromberg & Cheng 2010). Ridjan et al. (Ridjan et al. 2013) provided interesting study on production of methanol in 100% renewable system and use of SOEC. Naturally the first system is the simplest in processes, while the third is the most complicated, therefore in principal most expensive. Scope of this chapter covers description of the system, its optimisation for a given set criteria and later technical and environmental study of its operation over a chosen period.

5.1.2 SOFC-SOEC model

System in which SOEC is operating is modelled with use of Aspen HYSYS, beside basic model of the cell additional heat exchangers, power plant, power plant flue gases processing and methanol formation reactor are modelled. In all of the scenarios the author assumes that every single SOEC or SOFC is operated in the same conditions and has the same characteristic, thus it is possible to run simulation on single cell and later scale it up to represent real size system. An overview of the three systems is presented on Figs. 5-3 – 5-5. Readers are urged to note that the presented schematics do not show the real configuration of flow patterns (i.e. co-flow, cross-flow or counter-flow), but are arranged to present the layout in a clean manner. Different colours denote different medium in the stream. Dark green is the flue gases of the power plant, dark purple is water or steam, aqua marine is pure CO_2, pink is feedstock composition for SOEC fuel electrode (H_2O and CO_2), brown is fuel electrode gases after electrolysis, orange is fuel electrode gases after methanol formation reaction, khaki is air and air after electrolysis, red is energy (heat and electrical). The simulated power plant is assumed to be combined cycle power plant. Common element in all of the systems, the electrolyzer, is illustrated in Fig. 5-6. Two more colours were used to indicate changes of composition in fuel electrode gas channel due to water gas shift reaction and exhaust gases recycling. Before

electrolysis initial pink colour is getting bluer and after electrolysis it is brighter brown before water gas shift reaction, then after.

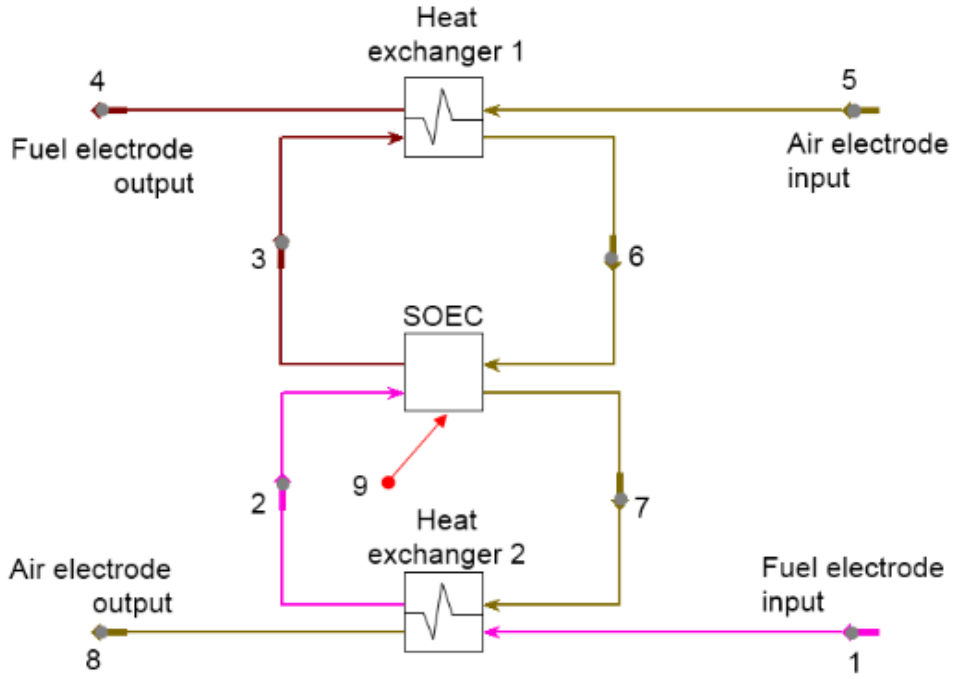

Fig. 5-3 – Schematic of the hydrogen production system.

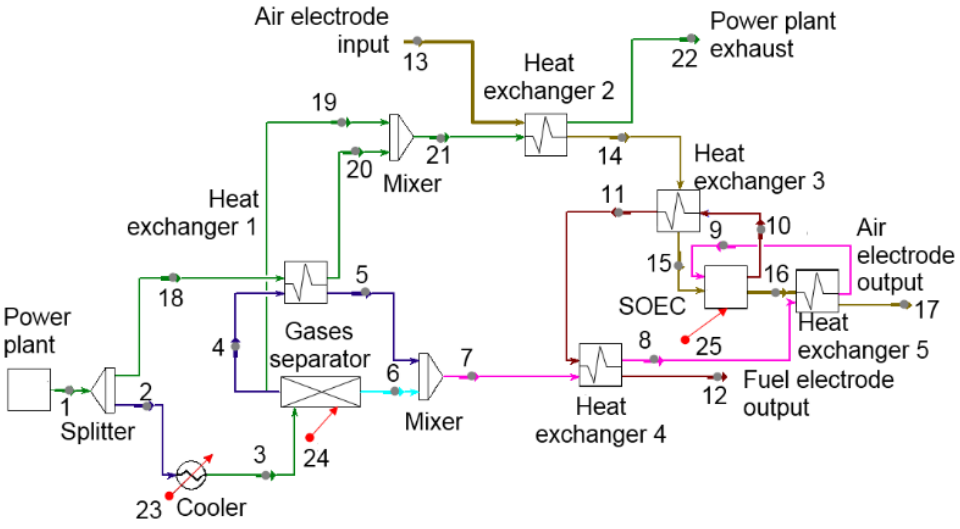

Fig. 5-4 – Schematic of the syngas production system.

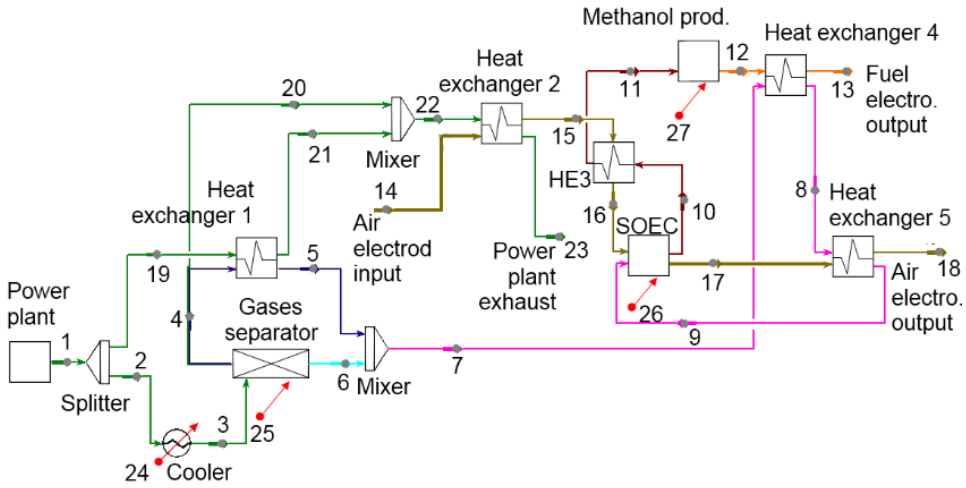

Fig. 5-5 – Schematic of the methanol production system.

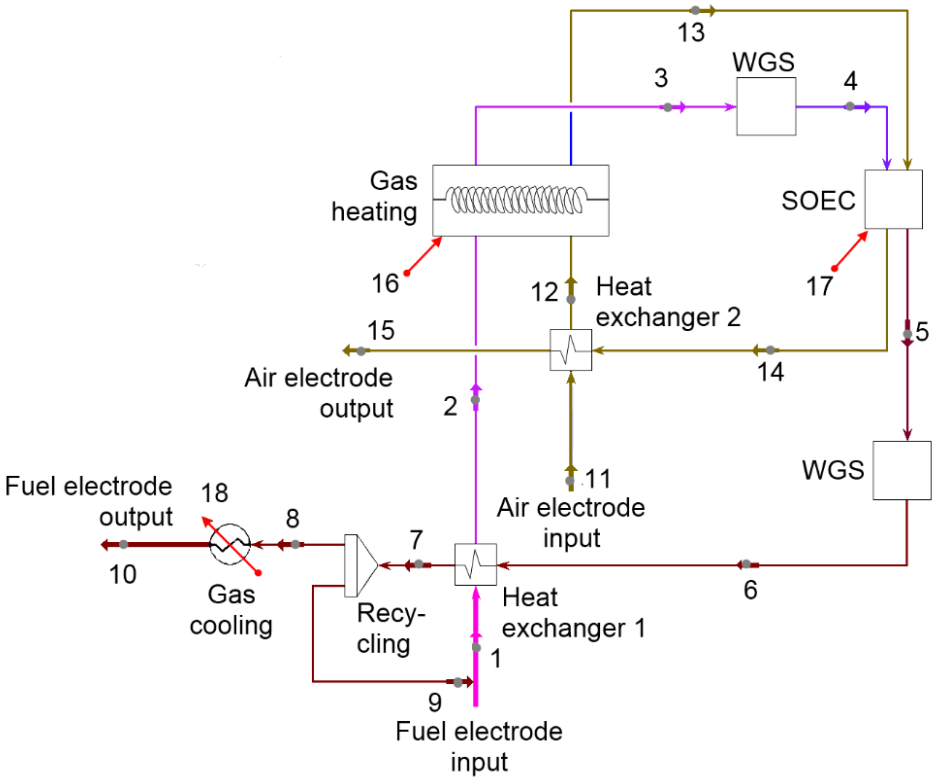

Fig. 5-6 – Schematic of the SOEC.

The SOEC module is made of eight elements (two heat exchangers, one gas cooler, one gas heater, two (reverse) water-gas shift reactor modules and solid oxide cell) and 18 flow streams (15 material flow streams and 3 energy flow streams). There are two main material streams connected via electrolyte membrane, nodes 1 to 10 represent fuel electrode stream and nodes 11 to 15 represent air electrode stream. Fuel electrode mixture after recycling is being heated up via heat exchanger 1, next it is brought to

operating temperature via electric heater. As it was investigated in previous chapters, water-gas shift reaction occurs in the gas channels, therefore before entering cell assembly composition of fuel electrode gas stream is balanced by water-gas shift (WGS) reaction (not applicable in hydrogen scenario). After electrolysis reactions, gases undergo second composition balancing via WGS reaction and are channelled back to heat exchanger 1 to reheat inlet fuel electrode stream. After reheating, the stream is separated and 5 % of outlet stream is recycled to inlet stream in order to improve the reducing atmosphere of fuel electrode. Lastly, the stream is cooled down to output yield temperature. Air stream undergoes similar process path stripped from WGS reactions and exhaust gas recycling. All of the heat exchangers and heaters are standard modules available in Aspen HYSYS.

The hydrogen scenario has the simplest process lay out and additional to SOEC module it has only two heat exchangers. It consists of 9 flow streams, 8 of which are material flow streams and 1 energy flow stream. Heat exchanger 1 is used to recover heat from fuel electrode output stream to heat up the air electrode input stream. Heat exchanger 2 is used to recover heat from air electrode output to heat up the fuel electrode input. Despite its simplicity, this scenario may pose serious problems due to NaCl dissolved in seawater. This salt may influence operation of the system in twofold way. It is known phenomena that during evaporation of seawater layers of salt cover the walls of evaporator, this could happen in heat exchanger responsible for steam formation. If, however, this compound will not deposit on the walls it may be transported inside the electrode and either deposit there and block the pores or decompose to chlorine and sodium and then interfere with electrode operation in an unknown way (group's latest in-house experimental results shows viability of seawater electrolysis).

The syngas scenario is more complex than hydrogen scenario. It consists of 12 elements (heat exchangers, power plant, splitter, separator, mixer, cooler and SOEC module) and 25 flow streams (22 material flow streams and 3 energy flow streams). Initial fuel electrode stream originates at power plant exhaust. Flue gases are split between those processed and unprocessed. Unprocessed stream is used in heat exchangers 1 and 2 to heat up water and air, respectively. Processed stream is first cooled down to condensate steam and then it is separated into three streams: pure water, pure CO_2 and the rest. Reheated water is mixed with CO_2 and passed onwards to heat exchanger 4. The unused part of processed flue gases stream is mixed with unprocessed flue gases stream and emitted to atmosphere. Reheated fuel electrode mixture in stream 5 after heat exchanger

4 is passed to heat exchanger 5 and then to SOEC module. Stream number 10 represents the fuel electrode gas mixture after electrolysis and is passed to recover heat in heat exchanger 3, then 4 and to the final storage. Air electrode stream is first heated by exiting power plant flue gases via heat exchanger 2. Next, it gains temperature from electrolysed fuel electrode stream via heat exchanger 3 and is channelled to SOEC module. After the electrochemical reaction, air electrode stream is giving its heat to fuel electrode inlet stream via heat exchanger 5 and then is passed to final storage or atmosphere. All of the heat exchangers and heaters are standard modules available in Aspen HYSYS.

The methanol scenario has the most complex process layout. It consists of 13 elements (same as in syngas scenario plus methanol production module) and 27 flow streams (23 material flow streams and 4 energy flow streams). The initial preparation of fuel electrode mixture is the same until stream 7, where it is passed though heat exchanger 4. In the methanol case the heat to stream 7 is passed from products methanol formation reaction from stream 12. Later, similar to previous case, it recovers heat from the air electrode output via heat exchanger 5 and is passed to SOEC module. After electrolysis fuel electrode stream 10 heats up air electrode stream 15 via heat exchanger 3 and is later passed to methanol production module. After formation of methanol stream 12 is used in heat exchanger 4 and passed to final storage in stream 13. The air electrode stream is the same as in syngas scenario. All of the heat exchangers and heaters are standard modules available in Aspen HYSYS.

Similar to the first case in the second and third purity of inlet chemicals composition is an issue. Exhaust gases of power plant are known to consist of wide spectra of constituent, the major being CO_2, N_2, H_2O. Except those the mixture includes particulate matters of different size (PM), sulphur oxides (SOx) and nitrogen oxides (NOx). Hydrogen sulphide (part of natural gas composition) can be especially dangerous to SOEC electrodes (Cheng et al. 2007). In the author's group, however, electrode material able to cope with small amount of H_2S in gas mixture was developed (Ge et al. 2011). Another dangerous gas on fuel electrode is oxygen. Large amount of oxygen on Nickel-based electrode can oxidize the metal and thus make it catalytically inert and underperforming. Our group's preliminary study showed that even small amounts of oxygen in fuel electrode channel is terminal to the cell and must be avoided at all cost.

Optimization of the system for methanol and syngas product was done with following criteria:

- Total electricity consumption of the system does not exceed the production from

given power plant,

- Energy storage efficiency is sufficiently high and yield of output chemical is high. To obtain an optimum of combination of these two, a mathematical product of these is used as final criterion.
- Energy storage efficiency is defined as

$$\eta_{storage} = \frac{\frac{P_{CCPP} - P_{SOEC}}{\dot{n}_{CH_4} LHV_{CH_4} - \dot{n}_{output} LHV_{output}}}{\eta_{CCPP}} \quad (5\text{-}5)$$

where, P_{ccpp} is the power output of combined cycle power plant, P_{SOEC} is the power requirement of solid oxide electrolyzer cell, $\dot{n}_{CH_4}$ is the molar flow of methane to power plant, LHV_{CH_4} is the lower heating value of methane, $\dot{n}_{output}$ is the molar flow of SOEC output chemical, LHV_{output} is the lower heating value of SOEC output chemical, η_{CCPP} is the efficiency of combined cycle power plant.

Since hydrogen production by SOEC using offshore wind energy is not related to fossil power plant, but to the wind turbine, it requires different optimization criterion, i.e., yield of hydrogen and thermal efficiency of the SOEC system. To obtain optimal of combination of two above the maximum value of a mathematical product is taken as final criterion.

In the first case, the author analyses SOEC combined with an off-shore wind turbine. In order to draw the possible scenarios, the author assumed that the performance of the cell working with seawater is not different from that working on pure water. In the second case, SOEC is linked to a combined cycle power plant and the output fuel is syngas. In this approach authors adopted daily variation in power demand to be utilized by SOEC/SOFC pair. The idea is to increase overall efficiency of power generation by stabilizing, thus increasing low efficiency production of combined cycle power plant and adopting high efficiency SOEC/SOFC pair to cover peak demand. The system uses the excess power in off-peak time to convert the greenhouse gases from the fossil power plant to syngas, therefore decreasing environmental impact in twofold, i.e., by increasing global efficiency and by narrowing the range and amount of pollutants (SOFC is thought to emit CO_2 and H_2O only). Additionally, if in the future, fossil fuel power plant is substituted with wind or solar energy one can imagine SOEC as a buffer between

intermittent wind or solar energy and demand driven consumption of electricity. In such respect, it gives a base for transformation to carbon neutral or even non-carbon energy generation. The last case is slight modification of the previous. Instead of gaseous form of energy output, it is a liquid methanol. This case, in principle, is more expensive due to additional requirement for gas-to-liquid (GTL) installation. Nevertheless, it has all the benefits of producing liquid fuel for automotive application

Due to lack of official data for wind statistics in Singapore, the author used the estimates depicted in Figs. 5-7 and 5-8 in the first case of study. Fig. 5-7 presents data for daily variation of offshore wind speed. These data were extracted from water sport enthusiast's website (Windfinder.com). Fig. 5-8 presents statistically processed data used in wind energy potential assessment. Slight mismatch between average wind speed predicted in Fig. 5-8 for March and that obtained in Fig. 5-7 may be due to too small sample size for the creation of Fig. 5-7 or weather anomalies. No better data is available at the moment. Both of the sources claimed to use data from Changi weather station. Second and third cases use data from Energy Market Authority, Singapore's energy market regulatory body (EMA 2012). An hourly demand for electricity is presented in Fig. 5-9.

Average energy from horizontal axis wind power turbine was calculated based on Weibull function wind distribution (Barthelmie et al. 2009). A typical Weibull probability density function with scale parameter fixed at 2 (Rayleigh probability density function) was used to predict how many hours a year wind is blown at particular speeds depicted in Fig. 5-10. Due to low average wind speed, the author chose specific design of blades with pitch angle set at 18° proposed by Singh and Ahmed (Singh & Ahmed 2013). Heier (Heier 1998) reported formula to calculate mechanical power extraction from wind. It is assumed that mechanical to electrical conversion is 90%.

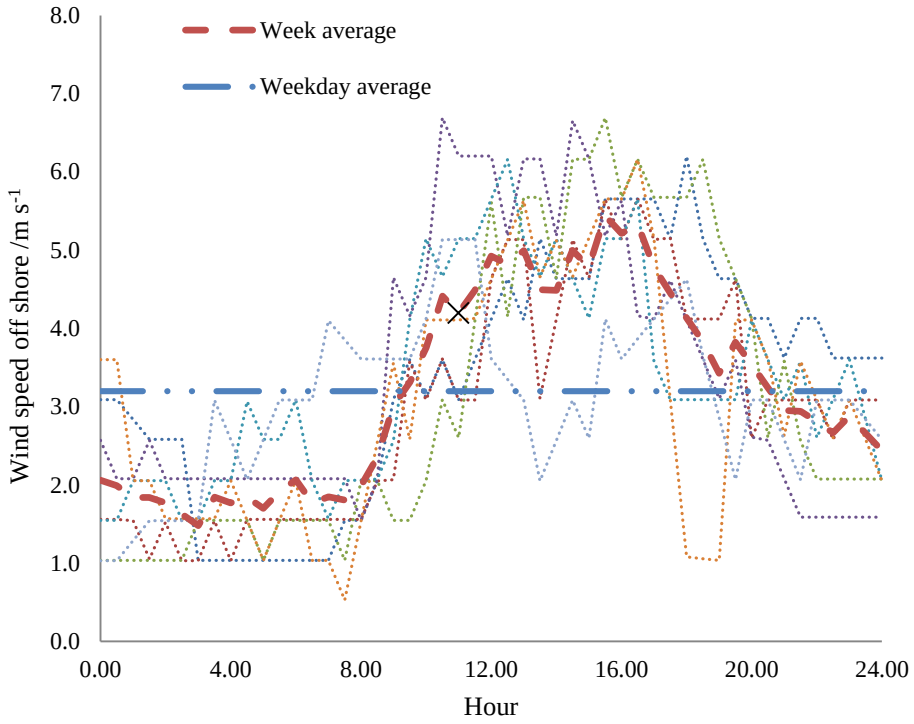

Fig. 5-7 – Wind speed graph, hourly over the week 01.03.13 – 07.03.13, hourly average of the week and weekday average (WindFinder.com) measured at ground level. Dotted lines represent wind speed of each separate day during the measurement period.

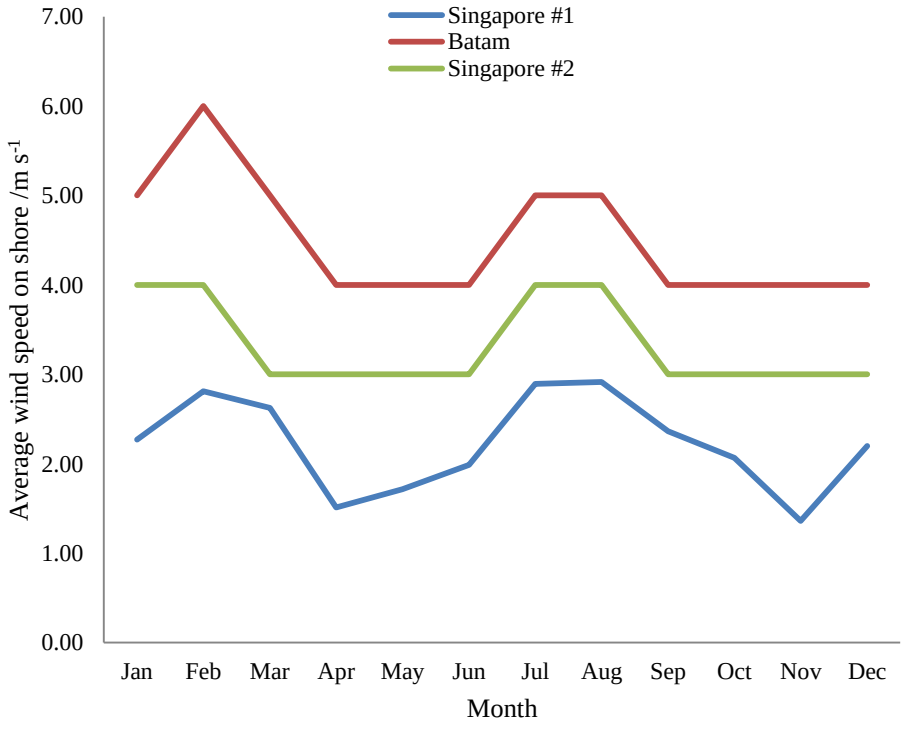

-1

Fig. 5-8 – Monthly average wind speed (Windfinder.com, Lee et al. 2011).

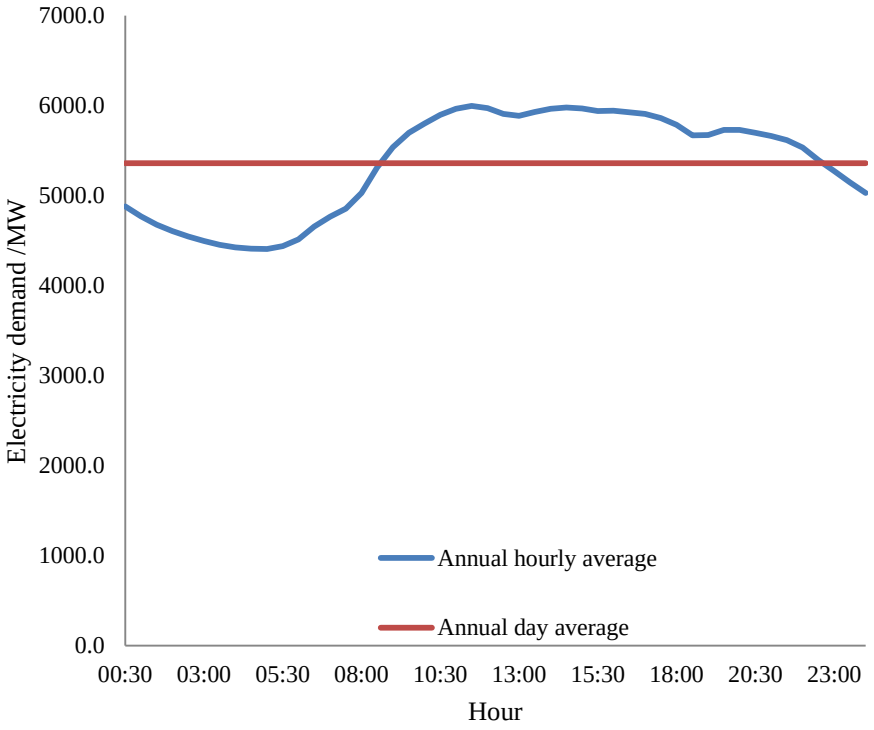

Fig. 5-9 – Hourly demand for electricity averaged over random weeks of each month between February 2012 and February 2013 (EMA 2012).

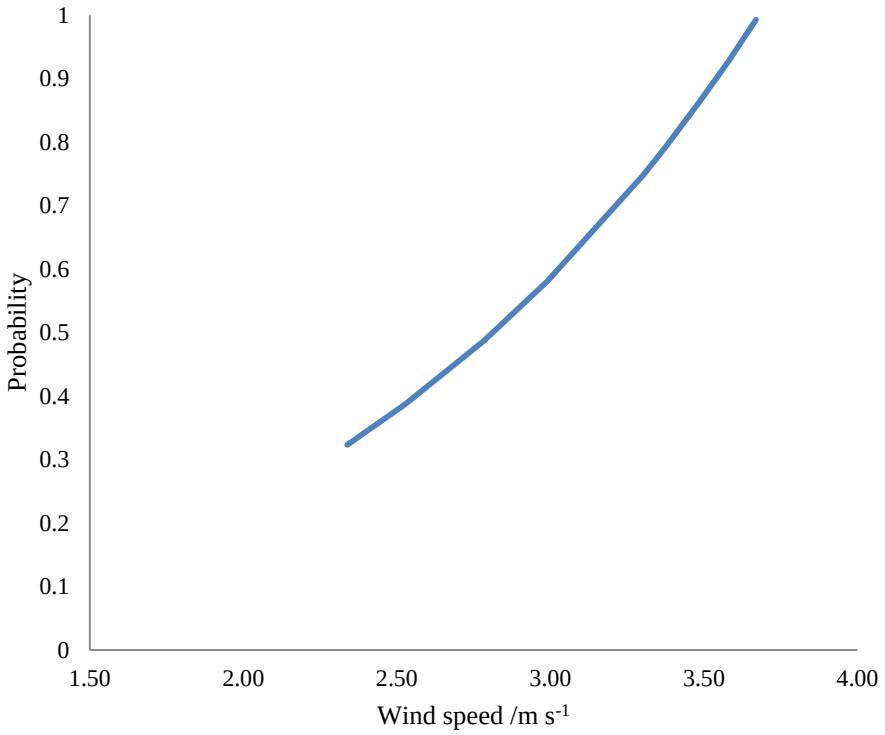

Fig. 5-10 – Cumulative probability of wind blowing at particular wind speed.

5.1.3 Results

5.1.3.1 Technical assessment

First step in analysing opportunities in producing hydrogen from seawater using offshore wind turbine energy is to assess the potential amount of energy available from offshore wind in Singapore. Figs. 5-7 and 5-8 present statistical data for Singapore over a day and over a year, respectively. Since only on-shore data are available at the moment, the author has to use data from neighbouring Indonesian island Batam, which is not far from Singapore. Yearly probability density function of a wind speed was calculated using average value of Singapore and Batam statistic (3.9 m s^{-1}).

Cumulative representation of wind speeds starting from cut-in speed of the wind turbine studied by Singh and Ahmed is presented in Fig. 5-10. Wind speed allowing operation of wind turbine with Singh and Ahmed blade is achievable in Singapore for 5909 hours a year. Note that an optimal speed (6.5 m s^{-1}) identified by Singh and Ahmed can never be achieved in Singapore, hence low performance is anticipated. Using wind turbine blade with radius of 1 meter (the same as Singh an Ahmed) calculations were done with formula from (Heier 1998). Resulting electricity production per annum in Singapore's offshore wind turbine from 1 meter radius blade is roughly 3.8 kWh a^{-1}. Additional calculations were done for blade radius of 5 and 10 meters. The annual electricity production, including results extrapolated to blade radius of 100 meters, is presented in Fig. 5-11. Results for single small wind turbine is not satisfactory, however contemporary turbines tend to have much higher blade radius (e.g. Vestas V164-8.0 MW has 164 m diameter), nevertheless they also have higher optimal speeds (11 m s^{-1}) and cut-in speeds (4 m s^{-1}). Annual amount of hydrogen produced from single wind turbine of rotor blade radius equal to 1 meter is roughly 11 MJ or ~0.1 kg at STP conditions (equivalent to about 100 km range in a hydrogen powered vehicle). If that value is sized up to more typical wind turbine design of blade radius 80 m, yearly hydrogen production is at level 629 kg a^{-1} per single wind turbine.

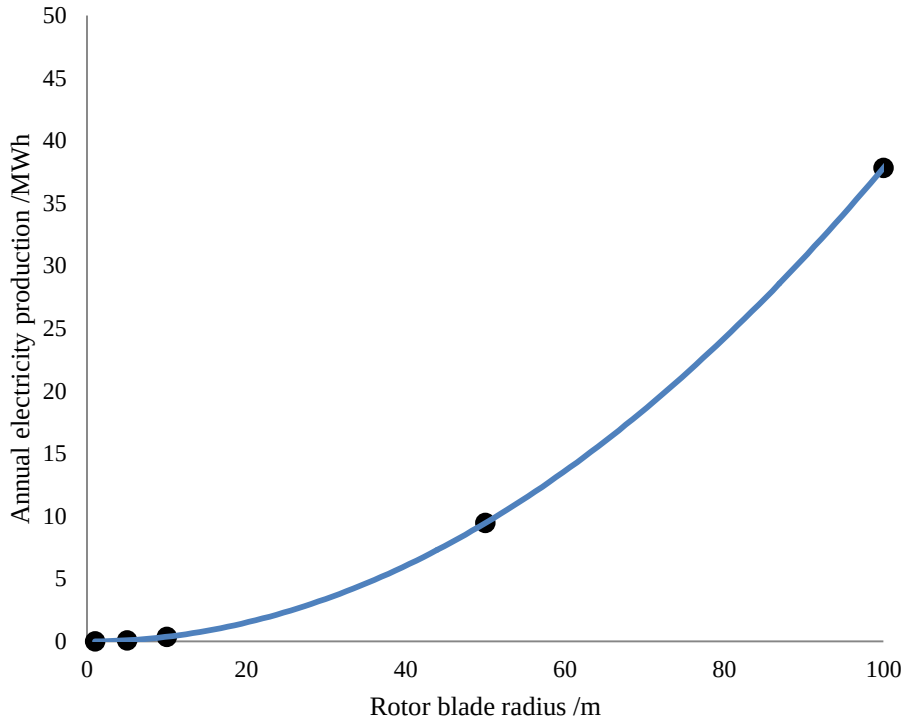

Fig. 5-11 – Predicted annual electricity production from single off-shore wind turbine in Singapore.

Authors would like to note that elevation of the measurement point from ground level to 80 m can double the predicted wind speed (Lee et al. 2011), hence increase performance and lower investment costs.

Table 5-1 – Operational parameters at design conditions of hydrogen producing system.

Parameter	Value
Thermal efficiency LHV based %	79.39
EEET LHV based %	108.31
Feedstock gases conversion %	83.11
Cell voltage V	1.17
Cell current density A m^{-2}	0.55
Cell area cm^2	81.00
Cell total current A	44.55
Hydrogen produced (LHV based) kJ	202.79

In order to allow this research to be utilized if higher wind speeds resource is identified

Fig. 5-12 presents exact value of derivative of power extraction function with wind speed assuming second order polynomial fitting of coefficient of power (Cp) factor changes with wind speed. As seen wind speed has major influence on system performance. The peak of power extraction is achieved at about 20 m/s for given blade design.

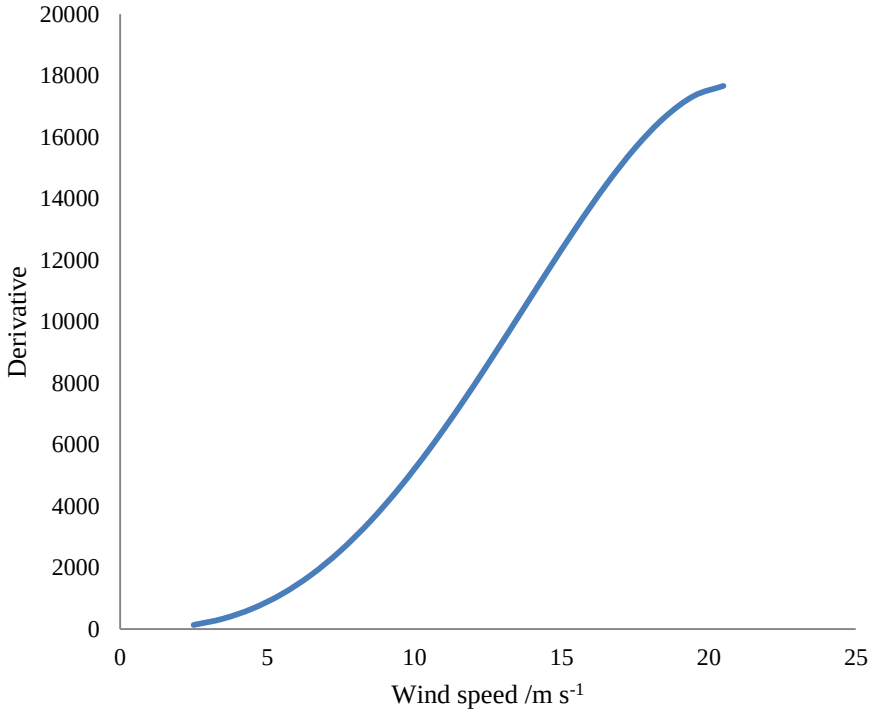

Fig. 5-12 – Derivative of power extraction from wind with respect to wind speed.

In the second and third case one major assumption is made that combining SOEC with combined cycle plant will increase overall efficiency of electricity generation through stabilizing the load of thermal part[9] and use of highly efficient SOEC (in fuel cell mode) to generate peak hours' electricity.

Analysing Fig. 5-9 one notices that average daily peak demand over last year was 5360 MW. This line separates region of operation into two domains, SOEC (below the average line) and SOFC (above average line). Duration of the SOEC period is on average of 10 hours, while for SOFC it is 14 hours. Luckily those domains are continuous allowing for easy implementation of SOCs.

[9] In general, efficiency of a conventional power plant is a function of load. The maximum is achieved when running at design point load.

As an initial modernization of power generation system the author suggests applying SOCs only to 10% of Singapore's power generation (i.e. on average 53.6 MW of capacity would be affected). In the case of producing syngas maximum SOEC power would be roughly 9.5 MW and for SOFC 6.4 MW, that translates into initial construction of 380 SOCs (255 working in dual mode at 25 kW per stack). Loading diagram for such system is presented in Fig. 5-13. Positive numbers represent electrolyzer mode, while negative fuel cell mode.

The author estimated that if no gain is achieved due to stabilizing of thermal power plant load, efficiency of transforming syngas to electricity would have to average 83% over considered period in order to meet the peak demand with no extra energy input. Nevertheless, increase in electricity production efficiency is anticipated, however it is impossible to calculate or even estimate the gain based on data possessed by the author. In spite of difficulty encountered, the author has estimated what gain in efficiency is required in order to make the investment financially sound. Results are presented in Fig. 5-14. It can be seen that gain of only 0.4 percentage point (p.p.) justifies investment of 300 SGD per solid oxide cell stack. Operating parameters of the system are presented in Table 5-2 and details of analysis are presented in Table 5-3.

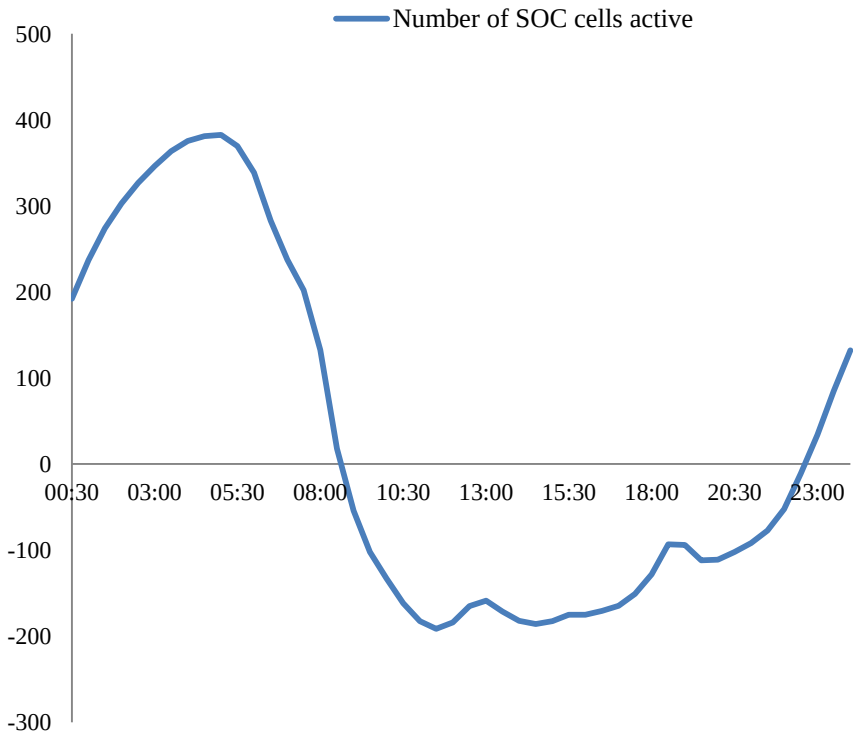

Fig. 5-13 – Loading diagram of SOCs working with 1% of Singapore's power plants and

yielding syngas.

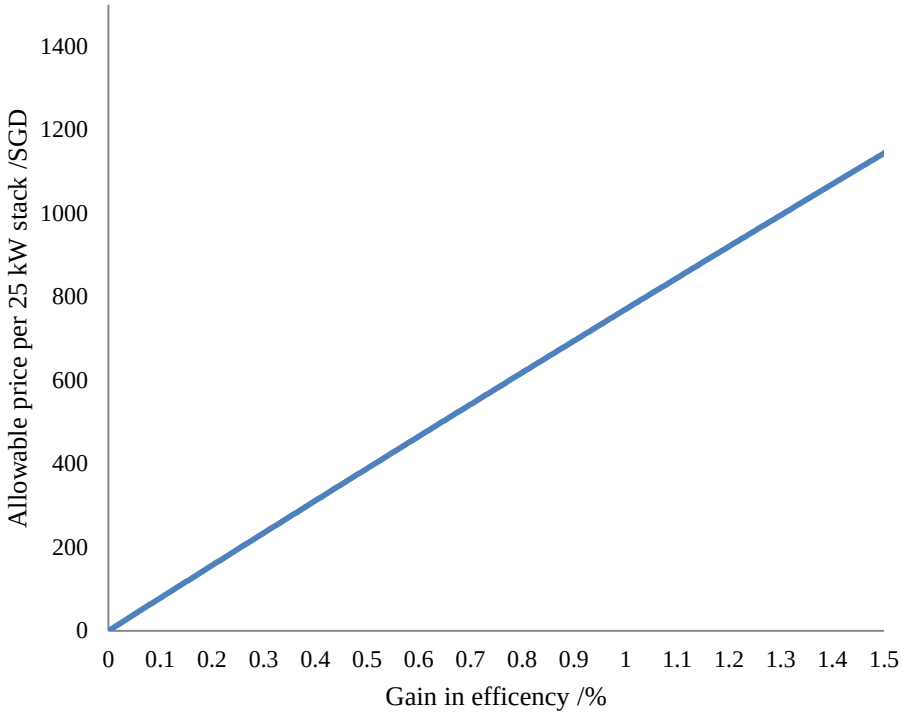

Fig. 5-14 – Allowable price per 25 kW stack (in SGD) as function of efficiency gain.

Table 5-2 – Operational parameters at design conditions of syngas producing system.

Parameter	Value
Thermal efficiency LHV based %	89.04
EEET LHV based %	133.17
Fumes conversion %	57.63
Cell voltage V	1.00
Cell current density A cm^{-2}	0.25
Cell area cm^2	100.00
Cell total current A	25
Syngas produced (LHV based) W	33.20
Energy storage efficiency %	90.03

Table 5-3 – Details of analysis of syngas production case.

Parameter	Value	Unit
Maximum power for SOEC	9.536	MW
Maximum power for SOFC	6.357	MW
Operation time for SOEC	10.0	Hr
Operation time for SOFC	14.0	Hr
Average power for SOFC	4.464	MW
Average power for SOEC	6.25	MW
Total SOFC energy	62.4953	MWh
Total SOEC energy	62.4953	MWh
Maximum number of SOEC cells	383	Units
Maximum number of SOFC cells	255	Units
Average number of SOEC cells	251	Units
Average number of SOFC cells	179	Units
Minimum number of SOEC cells	18	Units
Minimum number of SOFC cells	15	Units
Total syngas production	83.2	MWh
Total energy requirement during reversed period	62.5	MWh
Energy produced from syngas if used in combined cycle power plant	41.6	MWh
Electricity production efficiency required to satisfy SOFC period demand	83.06	%
Natural gas price SGD GJ^{-1}	4.4	SGD GJ^{-1}

Methodology for analysis of methanol production system is exactly the same as the one used for syngas. Difference lies in figures and in the fact that methanol production system will be in principle more expensive (more components required). Operating parameters of the system are presented in Table 5-4. Investment level from Fig. 5-14 is valid for this case. Details of analysis are presented in Table 5-5. Due to more complex process outline its efficiency is generally lower, this results in lower yield of output fuel and additionally increases investment costs. Additionally, more SOFC cells are required to satisfy high demand period as shown in Fig. 5-15. In this scenario one cell produces only 20 W of methanol which is 40 MWh day^{-1}. It is assumed that SOFC can transform

methanol directly to electricity with the same efficiency as operating on syngas. However, amount of energy to synthesise methanol is higher than energy to create syngas, hence overall number of SOCs working as fuel cell is higher, in this case, than those working as electrolyzer.

Table 5-4 – Operational parameters at design conditions of methanol producing system.

Parameter	Value
Thermal efficiency (LHV based) %	61.16
EEET LHV based %	68.39
Fumes conversion %	40.77
Cell voltage V	1.00
Cell current density A cm^{-2}	0.25
Cell area cm^2	100.00
Cell total current A	25
Methanol produced (LHV based) W	20.43
Energy storage efficiency %	83.62

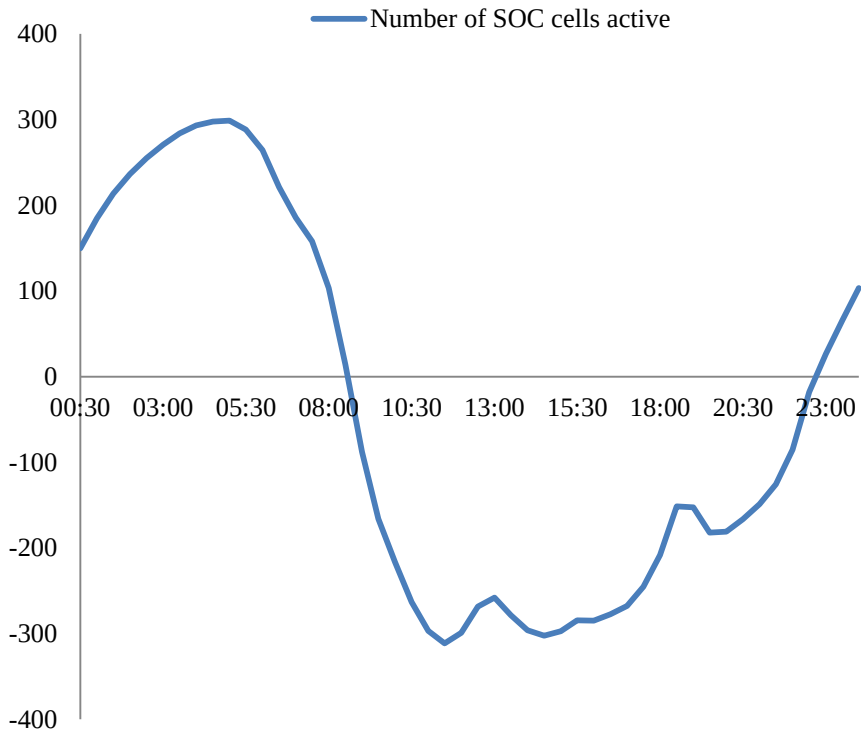

Fig. 5-15 – Loading diagram of SOCs working with 1% of Singapore's power plants and yielding methanol.

Table 5-5 – Details of analysis of methanol production case.

Parameter	Value	Unit
Maximum power for SOEC	9.536	MW
Maximum power for SOFC	6.357	MW
Operation time for SOEC	10.0	Hr
Operation time for SOFC	14.0	Hr
Average power for SOFC	4.464	MW
Average power for SOEC	6.25	MW
Total SOFC energy	62.4953	MWh
Total SOEC energy	62.4953	MWh
Maximum number of SOEC cells	299	Units
Maximum number of SOFC cells	311	Units
Average number of SOEC cells	196	Units
Average number of SOFC cells	219	Units
Minimum number of SOEC cells	18	Units
Minimum number of SOFC cells	15	Units
Total methanol production	40.0	MWh
Total energy requirement during reversed period	62.5	MWh
Energy produced from methanol if used in combined cycle power plant	20.0	MWh
Electricity production efficiency required to satisfy SOFC period demand	255.49	%
Natural gas price SGD GJ^{-1}	4.4	SGD GJ^{-1}

5.1.3.2 Environmental assessment

Environmental assessment of the first case is rather difficult to quantify in numerical terms and thus it is made here qualitatively. Producing hydrogen from wind energy is in principle environmentally benign. Moreover, if one replaces existing infrastructure of hydrogen production based dominantly on Steam Methane Reforming (SMR) with wind energy hydrogen production, it can be expected that the carbon footprint would be reduced significantly. Additionally, if direct use of sea water is possible, it also increases the global availability of drinkable water (if hydrogen is oxidized to water in the later

application).

Negative impacts of this technology on environment are those related to wind farms in general, i.e. sound pollution or creating dangerous environment for birds. This technology specific threat to environment can only be caused by increased salinity of water. It is however outside the scope of this study.

In the second scenario, one can predict the decrease in pollutants emissions (including CO_2) due to increased efficiency of power plant. Additional decrease of emission is possible if SOFC is employed in electrochemical conversion of syngas to electricity. Fig. 5-16 presents reduction of the CO_2 emissions due to the use of SOFCs assuming contributing to 1% of Singapore's total power demand. The anticipated total efficiency of SOFC is about 80%, which can contribute to roughly 0.4% reduction in CO_2 emissions. Fig. 5-17 presents reduction in pollutants emissions due to increased efficiency of modernized power plants. Complete substitution of power plants in Singapore with fuel cells would result in 50% reduction in pollutants emissions (or 100% reduction if the exhaust of fuel cell is captured and recycled back to fuel) as well as narrowing of spectra of pollution constituents to CO_2 and steam only. Additionally, if those cells are fed with hydrogen, emitted carbon dioxide would be replaced with steam. Negative impacts of combining SOCs with power plants are so far unknown.

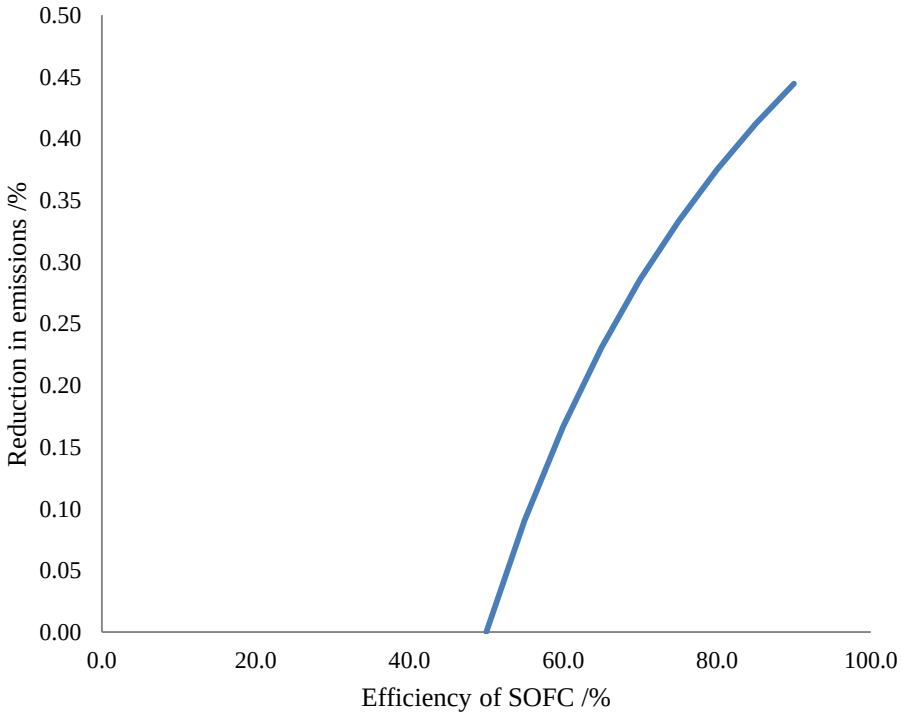

Fig. 5-16 – Reduction in CO_2 emissions due to use of SOFC with 1% of Singapore's total capacity.

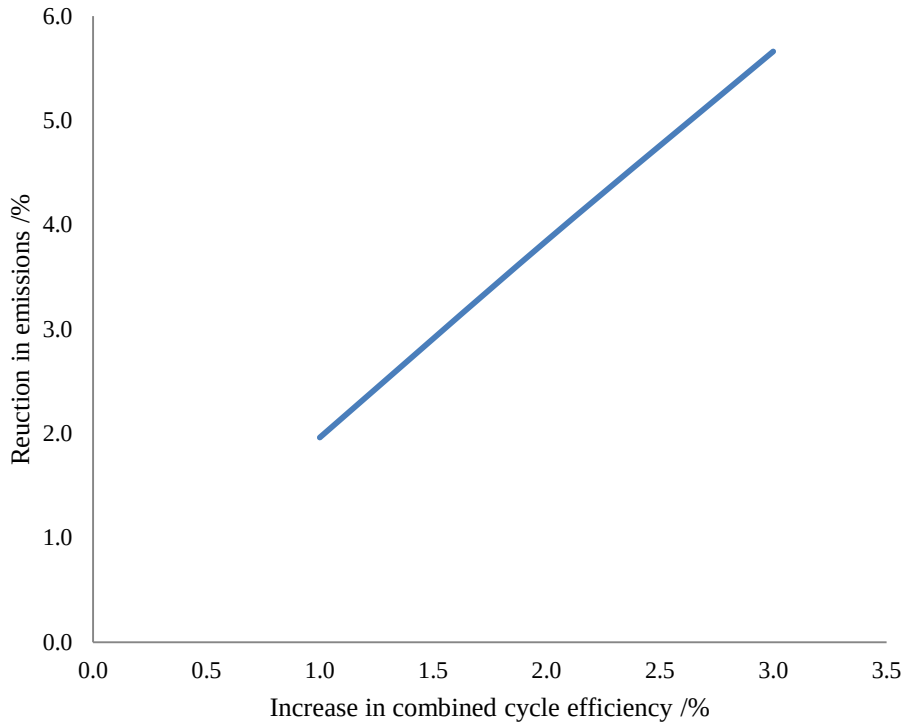

Fig. 5-17 – Reduction in CO_2 emissions due to increased combined cycle efficiency.

The last scenario has slightly less impact on environment, due to lower feedstock chemicals conversion one can predict lower emissions reduction of roughly 20%. Additionally, fuel cells running on hydrocarbon fuels showed reduced efficiencies (Milewski & Lewandowski 2009), hence benefits from using SOFC will also be mitigated.

5.1.4 Conclusion

In this chapter, three cases of application of Solid Oxide Cells (SOCs) in Singapore's energy mix were presented. First and the most futuristic case predicted use of offshore wind power (non-existent in Singapore) combined with solid oxide electrolyzer to produce hydrogen out of seawater. Second and third cases are easier to implement and base on combination of Singapore's combined cycle power plant and solid oxide electrolyzer and fuel cell, given the oxygen in fuel electrode channel issue is solved. The output of second scenario is the syngas, while in the third case the authors predict production of methanol. In order to make it possible to analyse different scenarios, the author collated data for wind statistic in the first scenario. The second scenario required

gathering and processing the data from Singapore's Energy Market Authority regarding consumption of electrical energy.

Specific systems were technically described in details supported by diagrams and charts with design condition parameters. The author has proposed design condition for those systems in order to achieve optimal operational parameters, i.e. thermal efficiency, output chemical yield and energy storage efficiency. Technical summary of analysed systems is presented in Fig. 5-18. It is seen from the diagram that among all chosen characteristics, the second scenario seems to be the most feasible one, with hydrogen scenario came to the second place and methanol scenario as last.

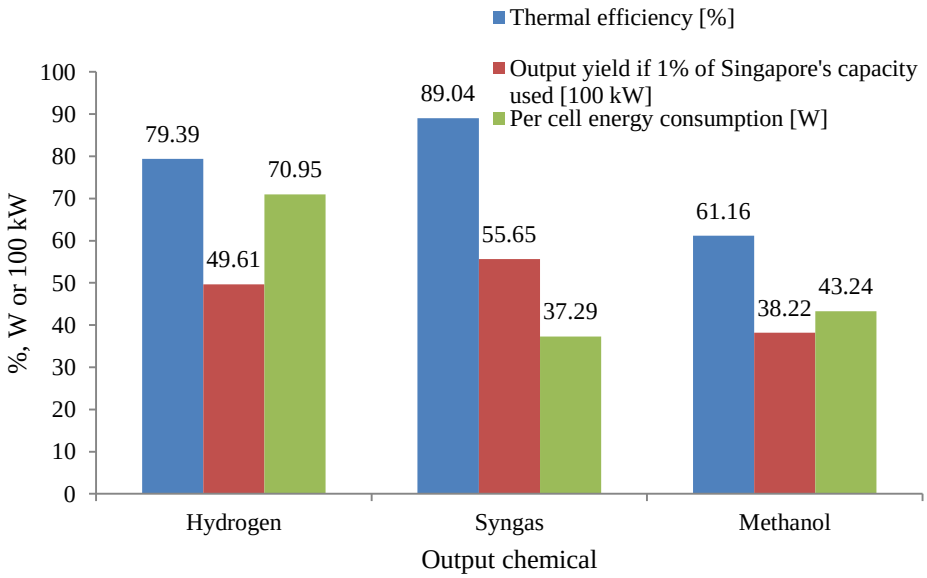

Fig. 5-18 – Technical summary of proposed systems.

The most immediate results in environmental aspects are most favourable for syngas yielding system. Similar results, offset by 20%, can be achieved by methanol system. First scenario remained undefined in quantitative respect. However, it posed interesting opportunities for creating sustainable energy mix and new business opportunities.

Following technical, environmental and scarcely presented economical evaluation, the most favoured system for immediate application is described by second scenario. Initial small scale application provides positive gains with respect to environment, it is financially viable, technologically sound and scientifically most interesting.

5.2 Production of renewable and sustainable hydrocarbon fuels in combined Fischer-Tropsch and Solid Oxide Electrolyzer processes

This chapter has been published in a modified form as JP Stempien, M Ni, Q Sun, SH Chan. Thermodynamic analysis of combined Solid Oxide Electrolyzer and Fischer-Tropsch processes, Energy, 81, 2015, 682.

5.2.1 Introduction

In this chapter, an accurate SOEC model is integrated with FTS process to analyse the system efficiency and product distribution. Contrary to Becker et al. (Becker et al. 2012) work, the highly non-linear characteristics of the voltage-current relationship of SOEC is fully considered and modelled. The in-house developed SOEC model is able to account for changes in reactant gas composition, temperature and pressure of operation. The model of FTS was based on highly regarded model proposed by van der Laam (van der Laam 1999). The model described the operation of FTS plant based on commercial Fe-Cu-K-SiO_2 catalyst in a Fixed Bed reactor. The model used to describe product distribution, α-Olefin Re-adsorption Product Distribution Model, combined influence from olefin re-adsorption and variation in chain growth probability stemming from increasing physisorption strength and increasing solubility of product hydrocarbon in FT-wax[10] with increasing chain length. The model was validated for operation in pressure range of 0.4 – 8 MPa, H_2/CO feed ratio 0.25 – 4.0 and space velocity of 0.5 – 2 x 10-3 Nm^3 $kgcat^{-1}$ s^{-1} at a constant temperature of 523 K. The analysis included the thermodynamic analysis of syngas production from steam and carbon dioxide and the catalytic conversion of syngas to hydrocarbon. A product upgrade part was not considered and the combined process was a once-through without unreacted gases, or light hydrocarbons recycling. No water knock-out was included in the model, however, the inhibiting effect of water content is considered. The proposed process was optimized to obtain the highest energy efficiency and the highest yield of heavy paraffins desired in operation of such plant as a raw material for diesel and other chemicals production. Optimization parameters included temperature of co-electrolysis, H_2O/CO_2 ratio,

[10] FT-wax is gathering in the catalysis bed pores

applied current density, the SOEC stack size (i.e. number of cells), reactant gas flow rate, the FTS pressure, the FTS temperature and cases of pressurized and the atmospheric operation of SOEC. Several strategies of energy recovery and heat recuperation were compared for process optimization. Obtained results were compared against those reported by Becker et al.

5.2.2 Theory

5.2.2.1Fischer-Tropsch Synthesis model

In the simulation, the author adopts the model developed by van der Laam (van der Laam 1999) for iron-based catalyst. The model incudes lumped kinetics of syngas utilization and kinetics of WGS reaction. The product distribution is the modified version of the ASF distribution. The distribution does not include production of oxygenates and acids. The product distribution is described in terms of selectivity with the following equations for first, second and n-th order of paraffins and olefins.

$$m_{CH_4} = t_p^1 \theta_1 \tag{5-6}$$

$$m_{C_2H_6} = t_p^2 \alpha_2 \theta_1 \tag{5-7}$$

$$m_{C_2H_4} = \frac{t_o^2}{1+k_R^2} \alpha_2 \theta_1 \tag{5-8}$$

$$m_{C_nH_{2n+2}} = \theta_1 \prod_{i=2}^{n} \alpha_i \tag{5-9}$$

$$m_{C_nH_{2n}} = \frac{t_o}{1+k_R e^{cn}} \theta_1 \prod_{i=2}^{n} \alpha_i \tag{5-10}$$

Above equations are subject to the normalization condition that the sum of m over n is equal to unity, $\sum_n m_n = 1$. θ_1 is used as a fitting parameter to match with experimental distribution.

In the above formulations, t_p is the pseudo reaction constant of paraffin formation, θ_1 is the surface fraction of alkyl with one carbon atom, α is the probability of chain growth, t_o is the pseudo reaction constant of olefin formation, k_R is the pseudo kinetic constant for the olefin re-adsorption, c is a constant depending on the exponential increase of

physisorption and solubility with chain length, *n* is the carbon number. The values of selectivity parameters are summarized in Table 5-6, in which the partial pressures are given in MPa.

Table 5-6 – Summary of selectivity parameters for Fischer-Tropsch process.

t_{p1}	6.62
t_{p2}	1.59
k_{R2}	12.58kRe2c
c	0.29
k_R	$3.32\times10^{-4}\ \frac{p_{H_2}^{1.4}\,p_{CO}^{-0.49}}{\phi/W}$
t_o	$6.1686\,p_{H_2}^{-0.5}$
p	$13.8\,p_{H_2}^{-0.47}\,p_{CO}^{0.43}$

The kinetics of the FTS process is described by two Langmuir-Hinshelwood-Hougen-Watson type reaction rates

$$R_{FT} = \frac{kp_{CO}p_{H_2}}{\left(1+ap_{CO}+bp_{H_2O}\right)^2} \tag{5-11}$$

$$R_{CO_2} = \frac{k_w p_{CO} p_{H_2O} - k_{wr} p_{CO_2} p_{H_2}}{\left(1+K_1 p_{CO}+K_2 p_{H_2O}\right)^2} \tag{5-12}$$

The first equation describes the extent of FTS reaction, while the second equation describes the extent of WGS reaction. The above kinetic Equation 5-11 is to lump all produced hydrocarbons into one. In the simulation, the author chose n-dodecane ($C_{12}H_{26}$) as the lumping hydrocarbon. Parameters used in the reaction rates are summarized in Table 5-7, where the partial pressures are given in kPa. Note that the units kgmol m^{-3} s^{-1} kPa^{-2} are converted from mol kg^{-1} s^{-1} MPa^{-2} and kPa^{-1} from MPa^{-1} in order to match with the requirements of employed simulation software. Change of kg^{-1} to m^{-3} is based on including catalyst loading of the reactor.

Table 5-7 – Summary of Fischer-Tropsch process kinetic parameters.

k	0.4565x109 kgmol m^{-3} s^{-1} kPa^{-2}
a	0.125x103 kPa^{-1}
b	7x103 kPa^{-1}
k_w	14.5326x109 kgmol m^{-3} s^{-1} kPa^{-2}
k_{wr}	1.1054x1011 exp(-1.7235x104/RT) kgmol m^{-3} s^{-1} kPa^{-2}
K_1	2.1x103 kPa^{-1}
K_2	24.19x103 kPa^{-1}

5.2.2.2 SOEC-FT process model

In the study, the author analyses a simple combination of electrolyzer unit with FTS reactor. The author sizes the electrolyzer unit in order to produce amount of syngas equal to the one used in validation experiment of van der Laam (van der Laam 1999). The author then analyses 16 variants of SOEC operation, 20 variants of FTS operation and 5 cases of process operation, which are summarized in Tables 5-8 – 5-10. Varying parameters in SOEC include current density, temperature, steam/carbon dioxide ratio and number of cells used in the electrolyzer unit (reactant gas flux).

Table 5-8 – SOEC parameters analysed in SOEC-FTS case.

Case	Current density A cm^{-2}	Temperature K	H_2O/CO_2 ratio	Reactant gas flux kgmol h^{-1} cm^{-2}	#SOEC
I	0.5	1073.15	2	$0.15x10^{-4}$	288
II	1	1073.15	2	$0.15x10^{-4}$	288
III	0.5	973.15	2	$0.15x10^{-4}$	288
IV	1	973.15	2	$0.15x10^{-4}$	288
V	0.5	1073.15	1	$0.15x10^{-4}$	288
VI	1	1073.15	1	$0.15x10^{-4}$	288
VII	0.5	973.15	1	$0.15x10^{-4}$	288
VIII	1	973.15	1	$0.15x10^{-4}$	288
IX	0.5	1073.15	2	$0.3x10^{-4}$	144

Table 5-8 continued

Case	Current density A cm^{-2}	Temperature K	H_2O/CO_2 ratio	Reactant gas flux kgmol h^{-1} cm^{-2}	#SOEC
X	1	1073.15	2	$0.3x10^{-4}$	144
XI	0.5	973.15	2	$0.3x10^{-4}$	144
XII	1	973.15	2	$0.3x10^{-4}$	144
XIII	0.5	1073.15	1	$0.3x10^{-4}$	144
XIV	1	1073.15	1	$0.3x10^{-4}$	144
XV	0.5	973.15	1	$0.3x10^{-4}$	144
XVI	1	973.15	1	$0.3x10^{-4}$	144

In the FTS process, operational pressure, temperature and flow of reactant gases are varied.

Table 5-9 – FTS parameters analysed in SOEC-FTS case.

Case	Pressure MPa	Temperature K	Flow kgmol h^{-1}	#SOEC
A	1.5	523	0.432	288
B	1	523	0.432	288
C	2	523	0.432	288
D	1.5	573	0.432	288
E	1	573	0.432	288
F	2	573	0.432	288
G	1.5	473	0.432	288
H	1	473	0.432	288
I	2	473	0.432	288
J	1.5	523	0.216	288
K	1	523	0.216	288
L	2	523	0.216	288
M	1.5	573	0.216	288
N	1	573	0.216	288
O	2	573	0.216	288
P	1.5	473	0.216	288

Table 5-9 continued

Case	Pressure MPa	Temperature K	Flow kgmol h^{-1}	#SOEC
R	1	473	0.216	288
S	2	473	0.216	288
F1	2	573	0.5	334
F2	2	573	0.6	400

After choosing the optimal parameters for the SOEC and FTS parts of the process, the author compares a few alternative ways of arranging the combined process. These included the use of heat recuperation from hot gases outlets to heat up the reactant gases, operating SOEC in pressurized and atmospheric variant and driving the compressor with energy recovered from turbines.

Table 5-10 – Parameters of combined process analysed in SOEC-FTS case.

Case	Description
Process-1	Heat recuperation
Process-2	Heat Joule utilization
Process-3	Turbine energy drives compressors
Process-4	Atmospheric operation of SOEC
Process-5	Enhanced heat recuperation in atmospheric SOEC

The analysed cases are all once-through and no recirculation is used. In each case, SOEC is fed with 5% hydrogen to provide reducing atmosphere at the fuel electrode. The scheme of the process is presented in Fig 5-19. This figure presents only the base case with no heat recuperation or the atmospheric operation of SOEC. Black arrows depict the material flows, while red arrows depict the energy flows. Compressors, turbines and heaters/chillers are represented by standard thermodynamic symbols. All of the balance-of-plant elements are standard modules available in Aspen HYSYS.

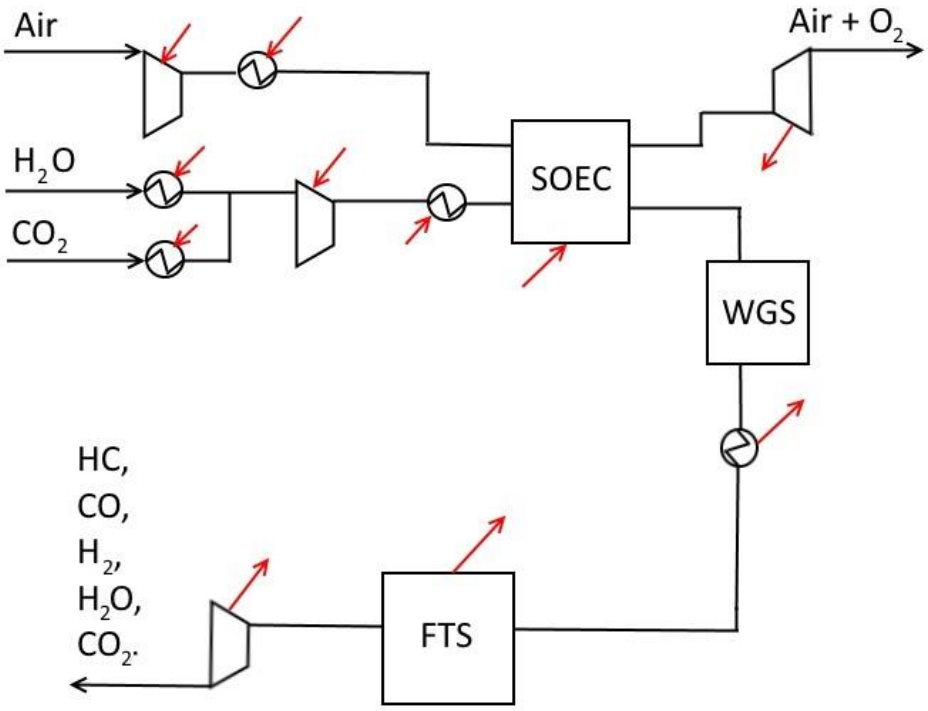

Fig. 5-19 – Scheme of SOEC-FT process.

5.2.3 Results and discussion

Models of the SOEC and FTS are implemented in Aspen HYSYS® V7.2 platform. Peng-Robinson equation of state (Robinson et al. 1985) is employed to calculate species' thermodynamic properties. The author chose four performance indicators to describe proposed system, i.e.,

- Energy stored in hydrocarbons,
- Syngas-to-hydrocarbon conversion efficiency,
- SOEC electricity-to-hydrocarbon conversion efficiency,
- Total (overall) conversion efficiency.

An additional indicator is the product distribution, with high content of heavy paraffins being favourable.

To calculate the amount of energy stored in paraffins and olefins, following empirical formulae for LHV kJ mol^{-1} are used

$$LHV_{paraffins} = 608.44n + 213.31 \quad (5\text{-}13)$$

$$LHV_{olefins} = 604.93n + 113.83 \quad (5\text{-}14)$$

All efficiencies are calculated based on LHV of respective chemicals. In all of the analysed cases, the electrolyzer works in exothermic mode, thus the electricity-to-syngas efficiency of SOEC is equal to its total conversion efficiency. Note that reported voltage is below the thermoneutral value, however due to heat generation in the system, exothermic operation is achieved at a lower voltage.

Operating SOEC in exothermic mode requires cooling of the electrolyzer. This is typically done by increasing the air flow. However, in pressurized operation of the stack, such approach may be too costly, due to increased compressor power. In a typical FTS process, the reactor is being cooled by water, hence it may be reasonable to engineer water cooled SOEC in order to simplify such combined process and ensure high overall efficiency.

5.2.3.1 Model validation

The validation of SOEC model was presented in chapter 3 and is omitted here. The validation of distribution model for FTS process is presented in Fig. 5-20. The validation of FTS kinetic model can be found in van der Laam's PhD thesis (van der Laam 1999).

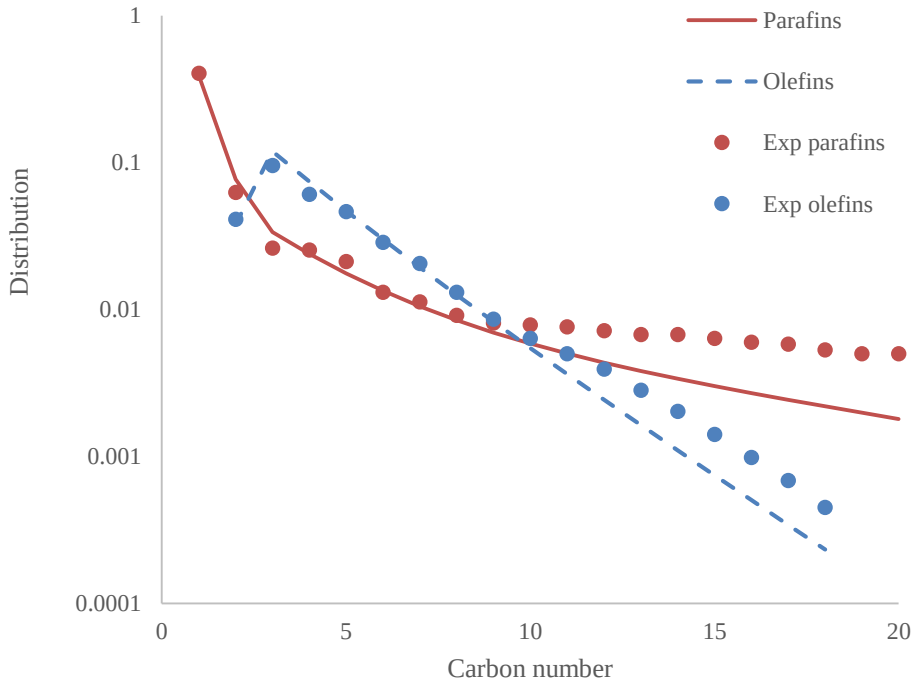

Fig. 5-20 – Validation of distribution model with the experimental data reported in (van der Laam 1999).

It can be seen in Fig. 5-20 that the model predicts the experimental conditions well,

albeit slight underestimation at high carbon numbers. The SOEC model was validated at 1073.15 K and atmospheric pressure for a wide range of inlet gas compositions and feed gas flux of 0.6 – 1.2 kgmol h^{-1} cm^{-2}. The materials used in the cell were typical for SOEC, i.e. Ni-YSZ|YSZ|LSCF-YSZ, which is fuel electrode-supported. Whereas the FTS model was validated for operation in pressure range of 0.4 – 8 MPa, H_2/CO feed ratio of 0.25 – 4.0 and space velocity of 0.5 – 2 x 10^{-3} Nm^3 $kgcat^{-1}$ s^{-1} at a constant temperature of 523 K. The catalyst loading was 8.2105 kg m^{-3} (2.34 g in 285 cm^3 reactor). In the course of analysis, the operating temperature of both SOEC and FTS are varied, despite not being validated at different temperatures. However, used formulae include the effects of temperature on model outputs. Also, the applied SOEC flux is slightly lower than in the case of model validation. The author could not validate the model with the experimental data of SOEC working with high flux (high reactant conversion) due to general trend of studying low conversions in laboratory testing. Nevertheless, the used validation parameters were close enough to industrially relevant conditions.

5.2.3.2 Optimization of SOEC process

The first part of proposed process analysis is to optimize the electrolysis unit. The author analyses 16 cases of varying temperature, applied current, the ratio of reactant gases and the number of cells in the electrolyzer unit. The cases are summarized in Table 5-9 in the previous section. The results of the comparison are presented in Fig. 5-21 and 5-22.

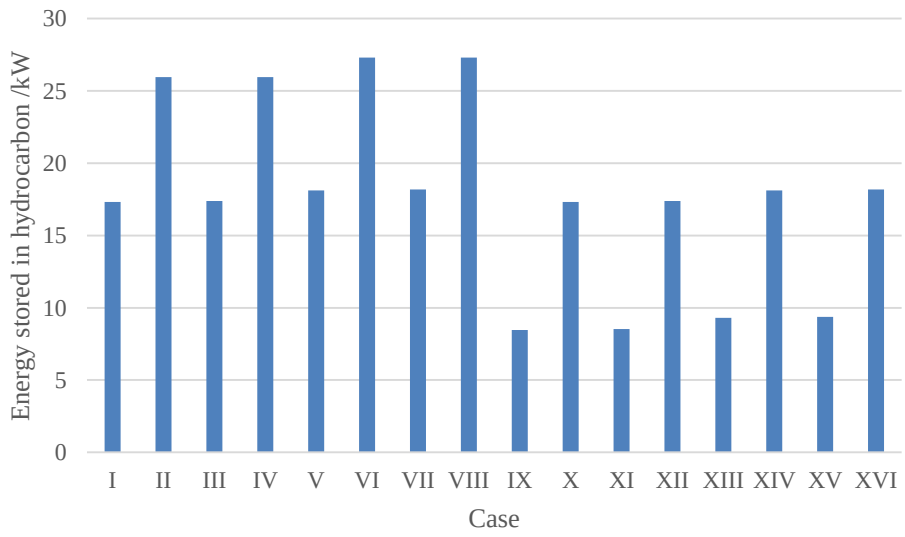

Fig. 5-21 – Optimization of SOEC process for high amount of energy stored in hydrocarbons.

In Fig. 5-21, it can be seen that two parameters are most influential on the amount of energy that is stored in the form of hydrocarbons. The first is the molar flux of the reactant gases, which is inversely-proportional to the conversion of these gases (the flux defines the time of residence in the reaction zone). The second is the applied current density, which is directly proportional[11] to the conversion of reactant gases through the Faraday's law. High current and low molar flux result in high conversion, hence high amount of energy stored in form of hydrocarbons. Care should be given to the choice of these parameters as it is known that high current density may facilitate degradation of the cell. Moreover, low molar flux, thus high reaction rate, will increase the temperature inside the cell and will require extensive thermal management of the unit. The second issue is somewhat less important as it is expected to self-regulate itself through the following mechanism: increased rate of reaction causes temperature rise, this in turn causes overpotential reduction at a constant current density, which will lower generated Joule heat and, in turn, lower the electrolyzer's temperature.

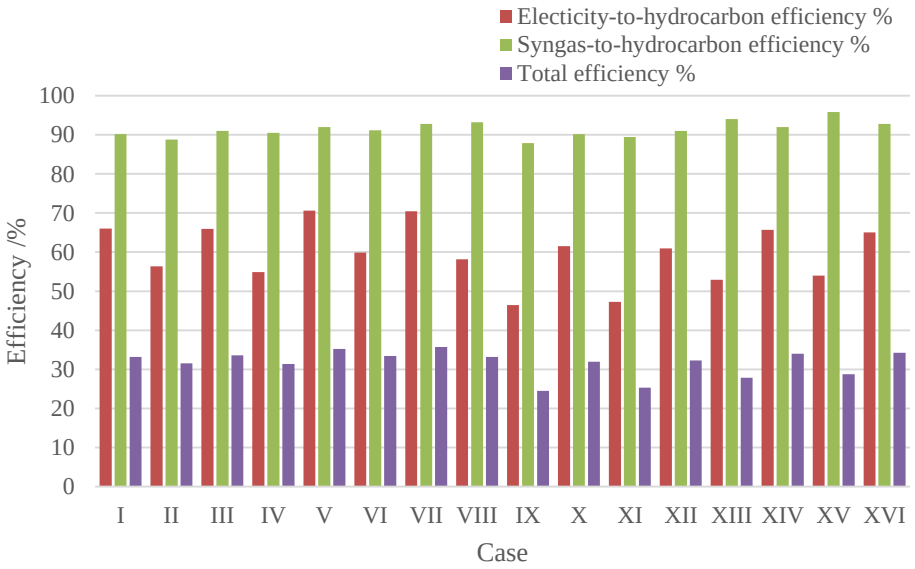

Fig. 5-22 – Optimization of SOEC process for high conversion efficiency.

Fig. 5-22 shows that the impact of SOEC operating conditions on the conversion efficiency of the system is limited. Generally, higher molar fluxes result in lower conversion efficiency and increased current density causes reduced conversion

[11] The proportionality holds until 100% conversion, passed respective current density there is no relation between the two

efficiency as well. The effect of operating conditions on conversion efficiency is limited to variation of few percent of overall efficiency and ~15% of SOEC efficiency.

Table 5-11 – Operational parameters of optimized SOEC unit in SOEC-FTS case.

Parameter	Value
Current density	1 A cm^{-2}
Voltage	1.255 V
#SOEC	288
Inlet gas composition	CO_2=0.475/H_2O=0.475/H_2=0.05
Temperature	1073.15 K
Flux	0.15 x 10^{-4} kgmol h^{-1} cm^{-2} [12]

From the above 16 cases, the author first identifies those with the highest amount of energy stored in form of hydrocarbon, which will allow one to minimize the size of the plant for a given product yield. Cases II, IV, VI and VIII are further analysed. Out of these, case VI offers the highest efficiency, and lowest operational cost, thus is preferred for further optimization. Resulting optimized SOEC case operates with parameters as summarized in Table 5-11.

Product weight distribution of the optimized case is presented in Fig. 5-23. The process is highly selective (>60%wt) towards paraffins with high carbon numbers, which is a desired effect in FTS process. Heavy hydrocarbons can be cracked into lighter products or used as reactants for chemical's production. Light hydrocarbons are usually recycled back to the reactor. However, in this simulation, the author neither considers "upgrading" nor recycling of the products.

[12] cm refers to total active area of electrolyzer unit

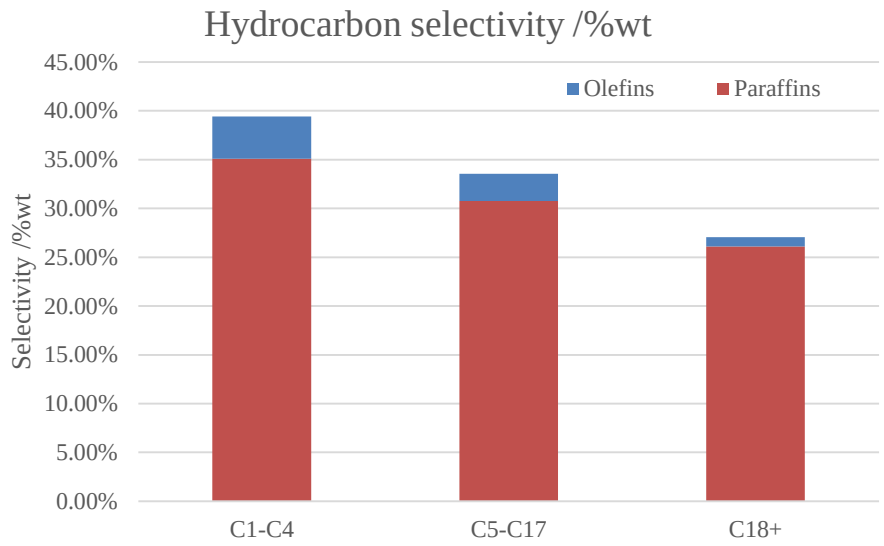

Fig. 5-23 – Weight distribution of FTS products.

5.2.3.4 Optimization of FTS process

The second part of this analysis is to optimize the FTS process' parameters. The author analyses 20 cases of varying pressure, temperature and reactants flow on the performance of the SOEC-FT process. These cases are summarized in Table 5-10 of the previous section. The results of comparison are presented in Figs. 5-24, 5-25 and 5-26.

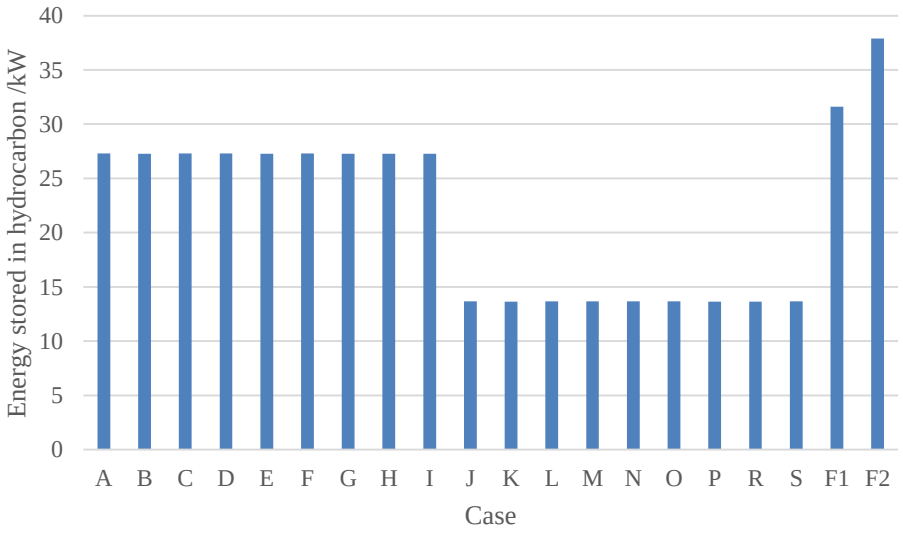

Fig. 5-24 – Optimization of FTS process for high amount of energy stored in hydrocarbons.

From Fig. 5-24 it is seen that cases with the low flow of reactant gases (J – S) result in halving the amount of energy stored in hydrocarbons and are thus disregarded. In this part of the optimization process the molar flow of reactant gases to the electrolyzer was

halved, while keeping the size of it unchanged (unlike in the case of SOEC optimization, where the flow was constant and number of cells adjusted, the author referred to it as changing the flux). Thus, the opposite effect to previously observed is due to very similar conversions of the reactant gases at both flows (the size of the SOEC unit was chosen to deliver high conversion in the base case of 0.15 x 10^{-4} kgmol h^{-1} cm^{-2}). Cases J to S store less energy simply due to lower amount of reactant gases available for conversion, while conversion in cases A-I and J-S is alike high. It is noted that adequate sizing of both reactors is required for optimal operation of the combined process.

Analysing efficiencies of remaining processes (Fig. 5-25) it is impossible to distinguish between effects of changing FTS conditions in cases A to I. Thus, the author introduced additional parameter, the product weight distribution, depicted in Fig. 5-26. Processes with the lowest share of light hydrocarbons are chosen for further optimizing (C, F and I). Such approach allows for limiting the required recycling and thus lowers the cooling requirements and plant cost. Out of these three processes, F has the highest overall efficiency and is chosen for further optimization.

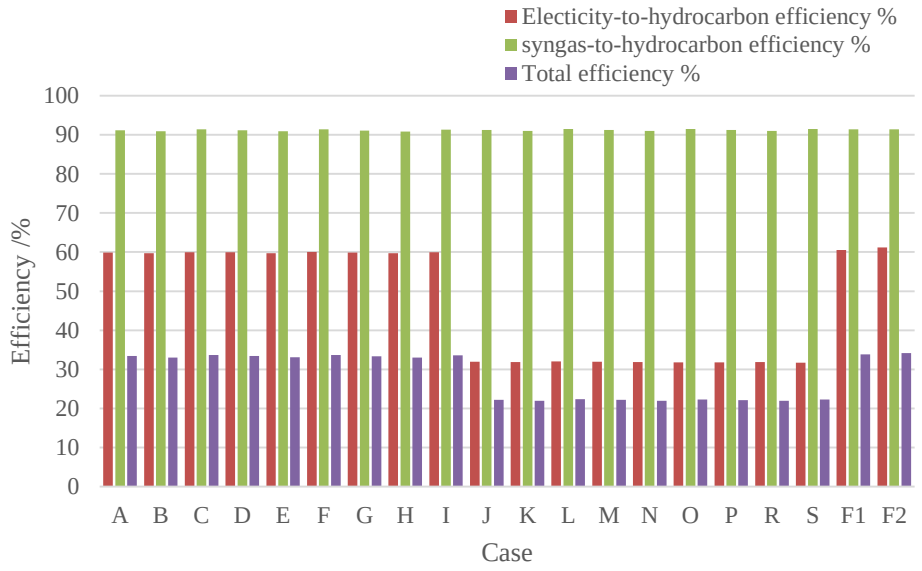

Fig. 5-25 – Optimization of FTS process for high conversion efficiency.

It can be noted in Fig. 5-26 that increasing the flow of reactant gases is directly proportional to the amount of energy stored in hydrocarbons, thus the author decided to run two extra cases with increased flow (F1 and F2), while keeping the constant flux. Despite the overall efficiency of the process is increased with higher flow, the tested cases are more selective towards light hydrocarbons and thus they are disregarded for further analysis.

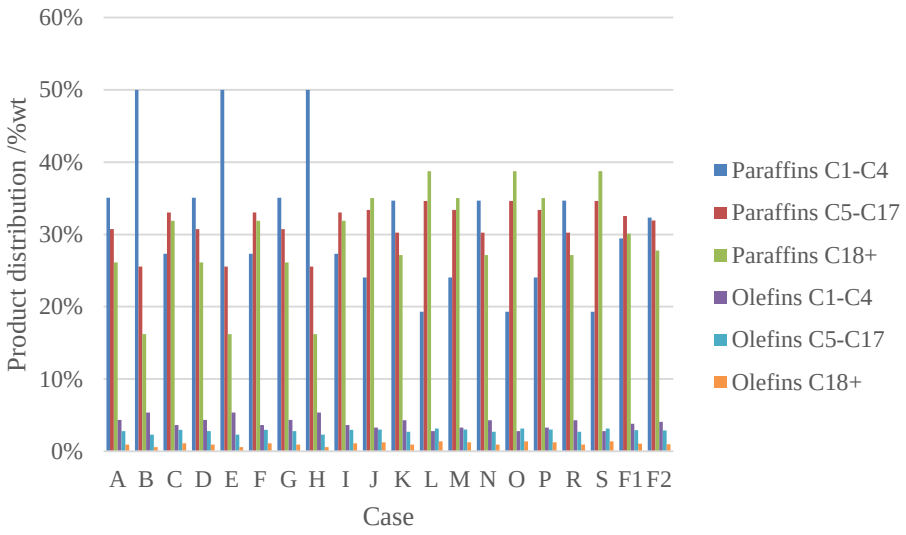

Fig. 5-26 – Optimization of FTS process for high yield of heavy paraffins.

Case F is chosen for further analysis. The summary of the optimized FTS process parameters are given in Table 5-12.

Table 5-12 – Operational parameters of optimized FTS reactor in SOEC-FTS case.

Parameter	Value
Pressure	2 MPa
Temperature	573 K
Reactants flux	1.5 x 10^{-3} kgmol h^{-1} cm^{-2} or 1.846 x 10^{-2} kgmol h^{-1} kg^{-1} [13]

Product weight distribution of the optimized process is presented in Fig. 5-27. As can be seen optimized process dropped the selectivity towards light hydrocarbons by ~10% and increased selectivity towards heavy hydrocarbons by ~6% and ~3% for mid distillate. The overall effect is highly desired.

[13] For meaning of cm refer to footnote 12. kg refers to used catalyst mass in the reactor.

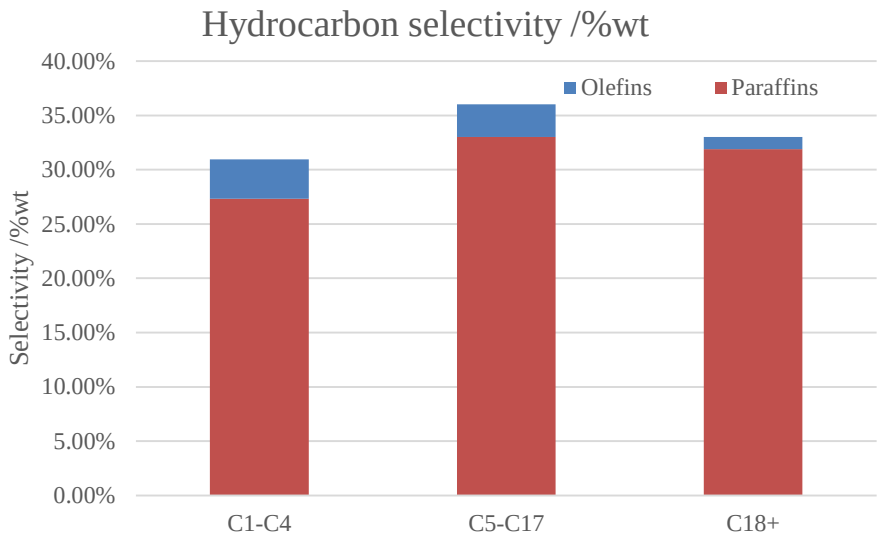

Fig. 5-27 – Weight distribution of FTS products.

5.2.3.5 Combined process optimization

In the last part of the optimization process the author aims at employing several techniques capable of increasing energy utilization and heat recuperation. The author has identified sources of highest energy losses as the air electrode high temperature outflow, the fuel electrode high temperature outflow and mismatch between the temperature of SOEC and FTS processes. The energy recovered from these streams are used to heat up water stream and heat up compressed gas stream to SOEC. Moreover, running high temperature processes at high pressure largely reduces possibilities of heat recuperation (due to increased work of compressing hot gasses). Thus, it was decided to compare the case of atmospheric operation of SOEC with pressurized operation. In the former case, much more extensive heat recovery is possible. Note that Process-1, which was the base case for the previous two optimization steps, is somewhat unrealistic, as it excluded Joule heat generated by SOEC from the energy balance of the system. The reason to separate this energy stream was due to simplified optimization procedure. Cases Process-2 to Process-5 all include realistic heat balance of the system. In the analysis, the author did not include energy required for pumping cooling water through FTS reactor and SOEC unit, however an estimate of required energy suggests it to be only a small fraction of the total Balance-of-Plant, thus can be neglected. Comparison of all 5 cases is presented in Fig. 5-28 and Fig 5-29.

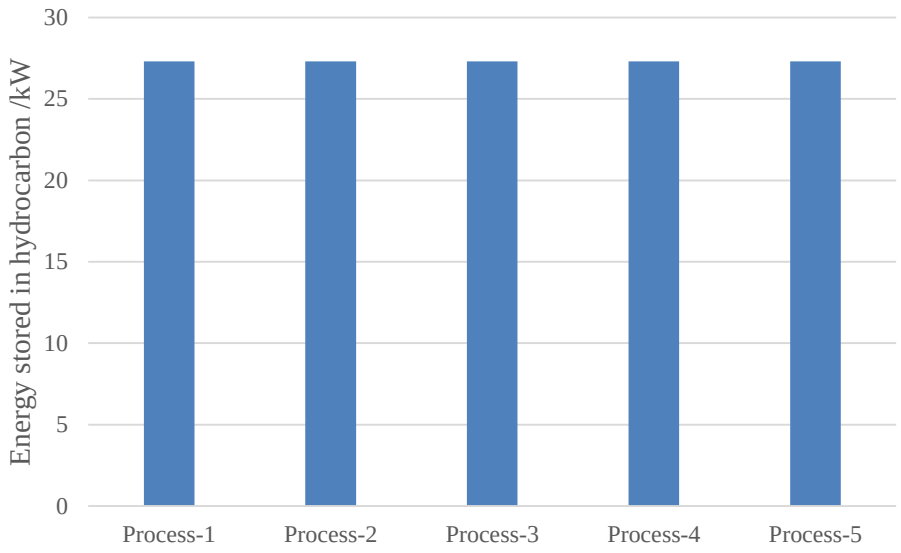

Fig. 5-28 – Optimization of SOEC-FT process for high amount of energy stored in hydrocarbons.

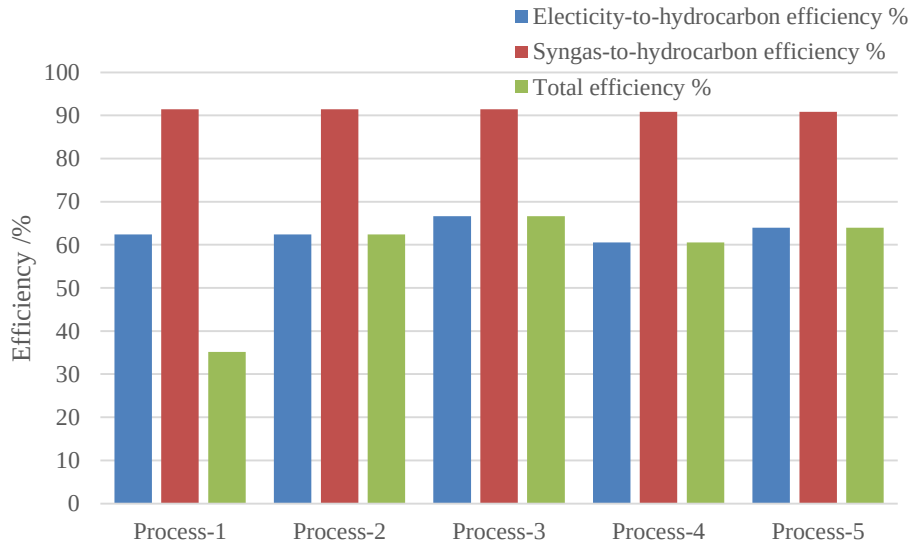

Fig. 5-29 – Optimization of SOEC-FT process for high conversion efficiency.

Fig. 5-28 shows that running the SOEC on atmospheric pressure has no effect on the amount of energy stored in hydrocarbons. Fig. 5-29 shows that in all realistic cases the efficiency of combined process is above 60%, which is 9% higher than values reported by Becker et al. (Becker et al. 2012). Process-3 is chosen as optimal pressurized case and has highest efficiency of all cases (66.67%). Process-5 is the highest efficiency (63.95%) atmospheric SOEC case. Decision on running the combined process' electrolyzer unit as pressurized or atmospheric should be based on consideration of a few facts. Firstly, little research is available on such pressurized operation of SOEC.

Secondly, designing the system with the recycling loop seems to be easier if the whole system operates at the same pressure level. Thirdly, it has been shown that pressurized system has higher efficiency, despite employing smaller number of heat exchangers (two as compared to four in atmospheric case), thus presents lowered initial plant cost. Interestingly, it has been noticed that increasing the system pressure enhances the efficiency, opposite was observed by previous authors. Becker et al. limited their process optimization to analysing two variants of FTS pressure only. Here presented model was validated for industry relevant conditions of reactant flux, pressure and flow. Previous authors analysed somewhat lower levels of applied pressure.

5.2.4 Conclusions

In this chapter, the author has revisited the idea of combining Solid Oxide Electrolyzer Cell process with Fischer-Tropsch Synthesis process. The SOEC replaces syngas production unit of a typical FTS process. The author analysed the combined system from the thermodynamic point of view, optimizing several key parameters in order to obtain high yield of heavy paraffins at highest possible efficiency. The electrolyzer unit was modelled with our in-house developed model validated over a wide range of operating conditions. Used parameters were fitted to a typical cell made of Ni-YSZ fuel electrode, YSZ electrolyte and LSCF-YSZ air electrode. The model accounted for influence of temperature, pressure and reactant gas composition and flux on the observable open circuit potential, activation and concentration losses, as well as syngas yield and composition. The model included the WGS reaction. The FTS reactor was modelled according to procedure described by van der Laam. The model equations were describing the commercially available fixed bed reactor using commercially available iron-based catalyst. The model was validated within the range of industrially relevant conditions and proved to be very accurate. The model did not include production of oxygenates and acids. Both models were solved using Aspen HYSYS® chemical package with Peng-Robinson equation of state.

The optimized system worked with pressurized SOEC at 2 MPa constant pressure throughout the process. The electrolyzer unit operated at 1073 K, whereas the FT reactor operated at 573K. The molar flux of reactant gases was set to 0.15×10^{-4} kgmol h^{-1} cm^{-2} (SOEC area based) or 1.846×10^{-2} kgmol h^{-1} kg^{-1} (FTS catalysis loading based). No product upgrading was considered, the process operated as once-through pass and no

recycling of light hydrocarbons or unreacted gases was analysed. Excluding energy required to pump cooling water through the FTS reactor and exothermic electrolyzer unit, the overall efficiency reached 66.67%. Almost 31% of the produced hydrocarbons were in the carbon number range 1 to 4 with the ratio of saturated to unsaturated of 7.5. Slightly over 36% of produced hydrocarbons were in the carbon number range 5 to 17 and their paraffin to olefin ratio was 11. Remaining 33% were the heavy hydrocarbons with ratio of alkanes to alkenes of 28. All product shares were given on the weight basis. Obtained results were compared against a recent report by Becker et al. on combination of the above processes. The previously reported data included much simplified model equations and resulted in somewhat lower efficiency (51% LHV-based) and different trend of process efficiency with changing pressure. The current author extended the analysis to incorporate effects of reactant feed composition and flux and the temperatures of operation of both processes. Moreover, the cases of atmospheric and pressurized operation of the electrolyzer unit were compared.

To the best of the author's knowledge results presented in this report are describing correct behaviour of such combined system at industrially relevant conditions. It is, however, underlined that experimental validation of such combined process is required in order to clarify the observed, contradictory trends of pressure effect.

5.3 Renewable and sustainable methane production with use of Solid Oxide Electrolyzer

This chapter has been published in a modified form as JP Stempien, M Ni, Q Sun, SH Chan. Production of sustainable methane from renewable energy and captured CO_2 with use of Solid Oxide Electrolyzer: A thermodynamic assessment, Energy, 82, 2015, 714.

5.3.1 Introduction

In this chapter, the author employs an in-house developed SOEC model and a thermodynamic model to analyse a combined SOEC-CH_4 system for production of sustainable methane. The employed SOEC model has been validated satisfactorily with several experimental studies. It is able to account for the effect of applied current, temperature, pressure, gas flow rate and composition on the syngas composition, yield and production efficiency. The thermodynamic model for methane production includes Sabatier, methanation and Water-Gas Shift reactions. Although, methanol can be

synthesized from the same feed gases, it is not within the scope of this study, as it was investigated in section 5.1. Simulated models of chemical reactions are based on equilibrium constants implemented on Aspen HYSYS v.7.2 platform, which can be found in the literature. It is generally believed that methane synthesis reactions achieve equilibrium easily, thus no kinetic modelling is required. Nevertheless, the author has analysed several cases based on kinetic modelling of methanation as reported in (Sehested et al. 2005), arriving at the same conclusion. In this study, the author investigated the effects of pressure, temperature, applied current (voltage), feedstock steam-to-carbon dioxide ratio (SCR) on several system's key performance indicators (KPI). It should be noted that the author did not attempt to optimise the overall energy conversion efficiency in this study as it is a trade-off between economic and technical analysis, which is not the objective of present study. Contrarily, the author focuses on electrical energy conversion efficiency, which is indicative of the optimal value of overall energy conversion efficiency.

5.3.2 Methane synthesis reactor model

The reactions occurring in the methanation reactor are Sabatier reaction equation (5-1), the methanation reaction equation (5-22) and the Water-Gas Shift reaction equation (3-28). The author assumed that all reactions reach their equilibrium in no time. This assumption is valid for high enough hydrogen to carbon ratio (Sehested et al. 2005). It has been confirmed that this assumption is valid by comparing the results of the equilibrium thermodynamic model and the kinetic model based on kinetic expression given by Sehested et al. (Sehested et al. 2005).

The equilibrium constant of reaction 5-1 was reported by Ohya et al. (Ohya et al. 1997) and can be written as:

$$lnK(T) = 45.787 + 1.772 \times 10^{4}T^{-1} - 8.103\, ln(T) + 3.282 \times 10^{-3}T - 5.618 \times 10^{-8}T^{2} \quad (5\text{-}15)$$

The equilibrium constant for reaction 5-2 was taken from Aspen HYSYS® reaction library and can be written as:

$$lnK(T) = 20.55 + 2.292 \times 10^{4}T^{-1} - 7.195\, ln(T) + 2.949 \times 10^{-3}T \quad (5\text{-}16)$$

Similarly, the equilibrium constant for reaction 3-30 was taken from Aspen HYSYS® reaction library and can be written as:

$$lnK(T) = -12.11 + 5.319 \times 10^{4}T^{-1} + 1.012\, ln(T) + 1.144 \times 10^{-4}T \qquad (5\text{-}17)$$

Other possible reactions that may occur are the methanol formation reactions 5-3 and 5-4.

However, the reactions 5-3 and 5-4 proceed selectively over Copper and Zinc catalysts (Steinberg et al. 1997), whereas the reactions 5-1, 5-2 and 3-28 proceed selectively over Nickel catalyst (Sehested et al. 2005, Xu & Froment 1989). Moreover, the pressure range for the methanol synthesis is an order of magnitude higher than that of methane.

More discussion on methane synthesis reactions can be found in the literature (Hoekman et al. 2010, Sehested et al. 2005, Ohya et al. 1997, Xu & Froment 1989).

The thermodynamic analysis of the system included varying of parameters:

- Applied current density;
- Operating temperature of methane synthesis reactor;
- Pressure of the system (single pressure level was analysed);
- Initial ratio of steam to carbon dioxide fed to the electrolyzer.

The pressure has shown some effect on the electrolyzer, whereas the other three remaining parameters would affect the operation of both electrolyzer and the fuel conversion process of the system.

A few parameters are calculated to characterise the key performance of the proposed system, these include:

- Electrical energy conversion efficiency in %;
- Overall energy conversion efficiency in %;
- Amount of energy stored in methane in $Nm^3\ h^{-1}$; and
- CO_2-to-CH_4 conversion in %.

Several other parameters are calculated but not reported for the clarity of the presentation, these are:

- Amount of energy stored in methanol in $Nm^3\ h^{-1}$;
- Cell voltage in V
- Hydrogen-to-carbon monoxide ratio of syngas from SOEC; and
- Steam and carbon dioxide conversion to hydrogen and carbon monoxide, respectively.

The author underlines that the overall conversion efficiency is a function of system layout and degree of heat recovery. In the following study, the author did not attempt to optimize the system layout thus the predicted values are only indicative. Contrarily, the focus is on electrical energy conversion efficiency, which is indicative of the optimal value of overall energy conversion efficiency. The geometric and intrinsic parameters of the cell under study are summarized in Table 5-13.

Table 5-13 – Summary of geometric and intrinsic parameters of electrolyzer in SOEC-CH_4 case.

Active area:	100 cm^2 x 154 cell or 1.54 m^2
Materials:	Ni-YSZ|YSZ|LSCF-YSZ
Thickness:	Fuel electrode (Ni-YSZ): 500 μm
Electrolyte (YSZ):	10 μm
Air electrode (LSCF-YSZ):	30 μm
Pore diameter:	0.5 μm
Porosity:	30%
Tortuosity:	5

5.3.4 Results and discussion

The model equations were implemented and solved using Aspen HYSYS® with Peng-Robinson equation of state. The proposed system is a single-pass with no recycling or gases separation. The schematic of the proposed system is presented in Fig. 5-30, while the HYSYS representation in Fig 5-31. All of the balance-of-plant elements are the standard modules of Aspen HYSYS. No special settings were used for BoP elements.

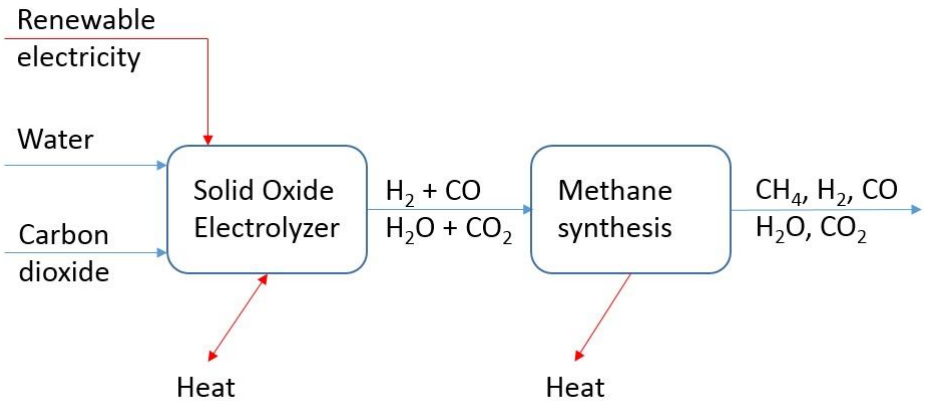

Fig. 5-30 – Schematic of the modelled system (Blue arrows indicate combined material and energy streams, red arrows indicate energy streams).

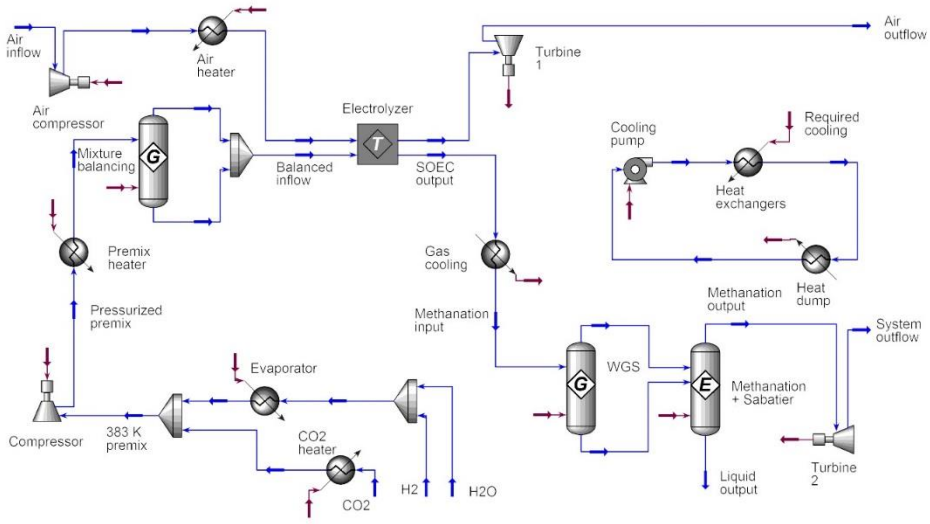

Fig. 5-31 – Representation of the modelled system under Aspen HYSYS® platform (Red arrows represent energy streams, blue arrows correspond to material and energy streams).

In the analysed system, feed gasses (H_2O, CO_2 and 5%mol H_2 are preheated to evaporate water and then compressed before entering the electrolyzer. The air channel (79% N_2 and 21% O_2) gases of the electrolyzer are also compressed. Past the electrolyzer unit, the air channel gases are decompressed through Turbine 1 and the energy is used to drive the compressors. Compressed fuel channel gases are passed to the methane synthesis reactor. After converting to the final mixture, the liquid component, if any, is being knocked out while the remaining gases are decompressed through Turbine 2, which is connected to a compressor. Additionally, energy requirement for cooling of the excess heat generated from the electrolyzer and the methane synthesis reactor is included. The methane synthesis reactions are highly exothermic and thus require water cooling. In the proposed system, cooling of the SOEC has been considered. In this study, only air cooled systems are investigated, which can be quite energy consuming as the amount of air required for cooling is several times higher than that of fuel channel gas flow (Udugawa et al. 2008).

In the presented study, the author analysed the effects of pressure, temperature, current density and steam to carbon dioxide ratio (SCR) on the key performance indicators (KPI) of the system. The ranges of investigated parameters are 1 – 10 bar for pressure, 473.15 – 1073.15 K for methanation temperature (electrolyzer operates at constant 1073.15 K), 0.5 – 1.5 A cm^{-2} for current density and 0.5 – 8 for steam to carbon dioxide ratio.

The current-voltage characteristics of the electrolyzer are depicted in Fig. 5-32. The best

predicted performance is at low SCR and high pressure, while the predicted value of Area Specific Resistance (ASR) is 0.2187 Ω cm^2. The worst performance is predicted at high SCR ratio and low pressure, the calculated ASR value is 0.2784 Ω cm^2. As can be seen in the Fig. 5-32, the effect of SCR is superior to that of the pressure. The superior impact of SCR is due to its relation with open circuit potential via the Nernst equation. The fuel reactant gases conversion ranges from 35% at low current density to 100% at high current density.

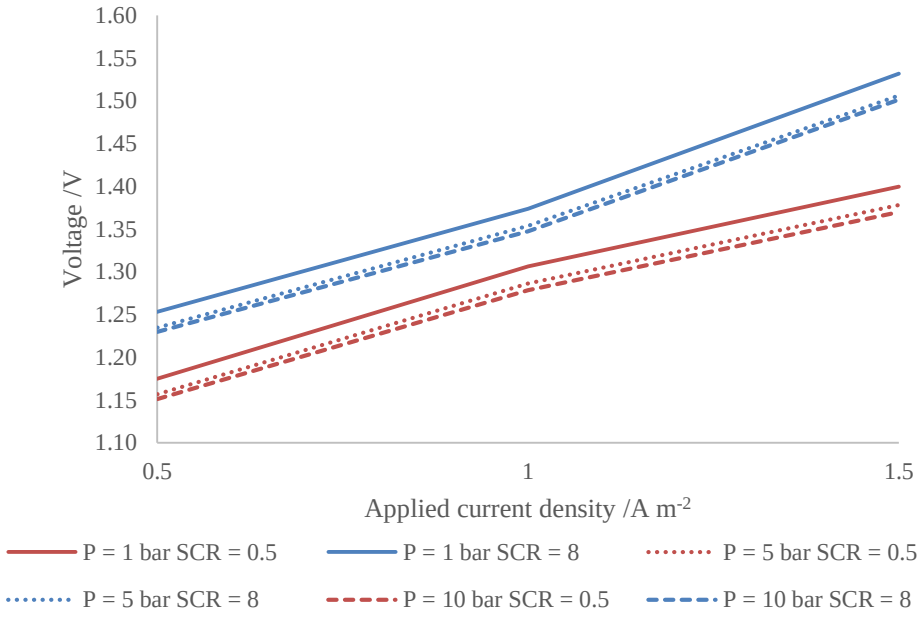

Fig. 5-32 – The current-voltage characteristic of the electrolyzer (Green lines: SCR 0.5, red line: SCR 8; Solid lines: 1 bar, dotted lines: 5 bar; and the dash-dot lines: 10 bar).

The effect of the investigated parameters on the maximum electricity to methane conversion efficiency and overall energy conversion efficiency is presented in Fig. 5-33. The highest value of electrical energy conversion efficiency achieved in this study is 81.08% under the current density of 0.5 A cm^{-2} and SCR of 7. The corresponding pressure is 3 bar and the methane synthesis temperature 473.15 K. The maximum value of electrical efficiency is not a strong function of applied current density, however it generally drops with increase in applied current density. At high current density, a value of 71.64% in electrical efficiency can be achieved. It can be seen that increasing the applied current density brings the electrical energy conversion efficiency closer to the overall energy conversion efficiency, this is simply due to greater amount of Joule heat generated in the system and resulting lower need of external heat supply.

The highest value of overall energy conversion efficiency achieved in this study is 60.87%

and is obtained at 1.5 A cm^{-2} and SCR of 2.5. The corresponding pressure is 10 bar and temperature of 473.15 K. The difference between the overall efficiency and electrical efficiency at 1.5 A cm^{-2} is a mere 10%, whereas at low applied current density it reaches 40%. It seems that less system optimization effort would be needed for operating at high applied current density. Moreover, due to higher syngas production in this case equation (3-115), such system would be considerably smaller. However, the maximum value of conversion efficiency in the case of low applied current density is higher and this value is a weak function of applied SCR. This is an important feature given that steam is relatively easier to obtain than CO_2. Thus, it is case-specific to conclude which mode of operation is more favourable. Running the system at high current would result in smaller system size, with lesser need for heat recovery, however it can result in faster performance degradation and is generally achieving lower efficiency. Low current operation can achieve higher efficiency, and is more flexible towards initial steam to carbon dioxide ratio, however, the system would have to be three times larger to achieve same amount of methane yield as the high current case and will require extensive heat recuperation to obtain reasonable overall energy conversion efficiency.

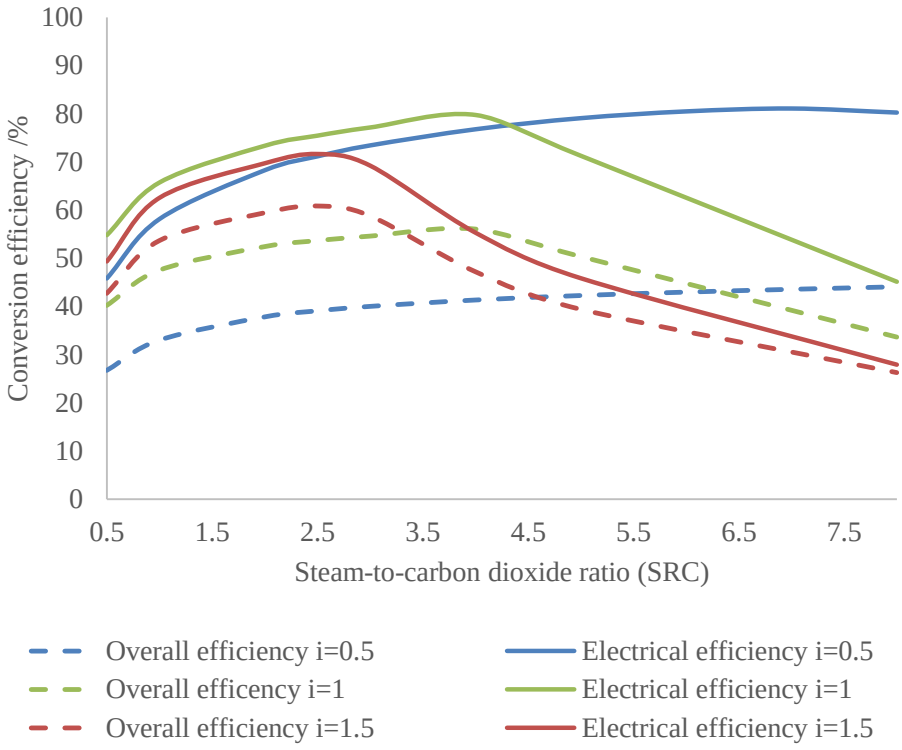

Fig. 5-33 – Effect of the applied current density and SCR on the maximum electricity to methane conversion efficiency (Green lines: 0.5 A cm^{-2}, blue lines: 1 A cm^{-2}, red lines: 1.5 A cm^{-2}, Solid lines: electrical energy conversion efficiency, dotted lines: overall energy conversion efficiency).

To explain the hump on the conversion efficiency graph at medium and high current density, the author refers to the Fig. 5-34, which presents the gases conversion and energy storage in methane. As can be seen, the location of the hump in the conversion efficiency graph coincides with the same occurrence in the energy storage graph. It is generally known that increasing the SCR can enhance the conversion of carbon dioxide to methane (Hoekman et al. 2010). However, after achieving 100% conversion, further increase will have an adverse effect due to insufficient number of carbon atoms in the gas mixture. It can be concluded from Fig. 5-33 and 5-34 that SCR is an important parameter in the system optimization and need to be kept under strict control.

The maximum amount of energy stored in methane varies from ~0.4 to ~1.6 $Nm^3\ h^{-1}\ m^{-2}$ depending on the applied current density. The correlation is positive and follows from the reactant gases conversion in the electrolyzer unit. At low current density only 35 % of feedstock steam/CO_2 is converted to syngas, whereas at the high current density the number approaches 100 %.

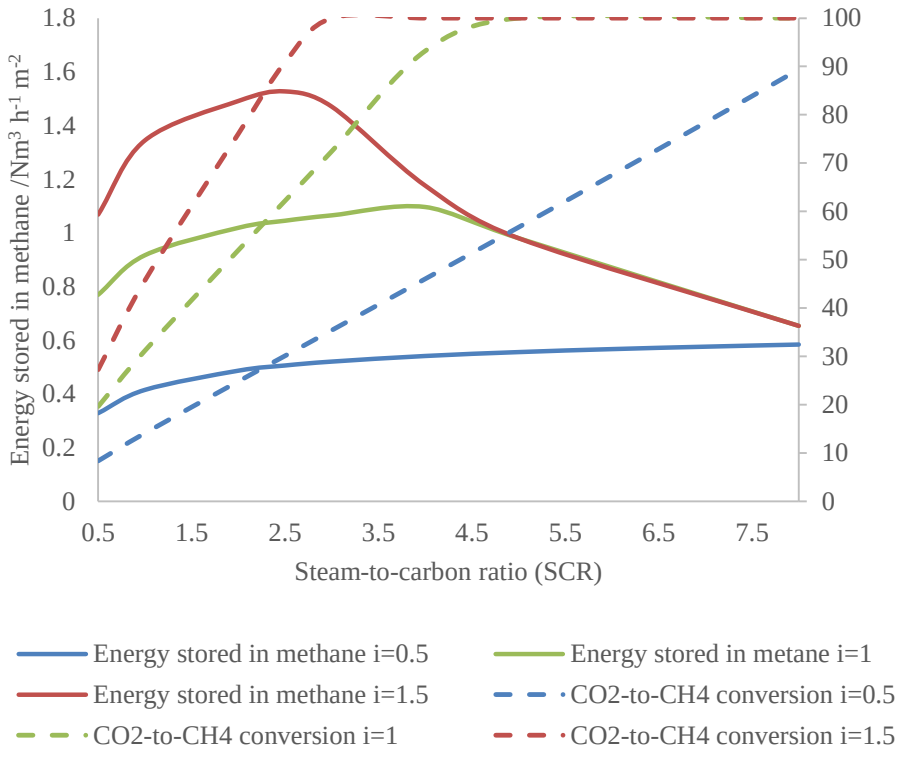

Fig. 5-34 – Effect of applied current and SCR on the maximum energy storage and CO_2-to-CH_4 conversion (Green lines: 0.5 A cm^{-2}, blue lines: 1 A cm^{-2}, red lines: 1.5 A cm^{-2}; Solid lines: maximum amount of energy stored in methane, dotted lines: maximum CO_2-to-CH_4 conversion).

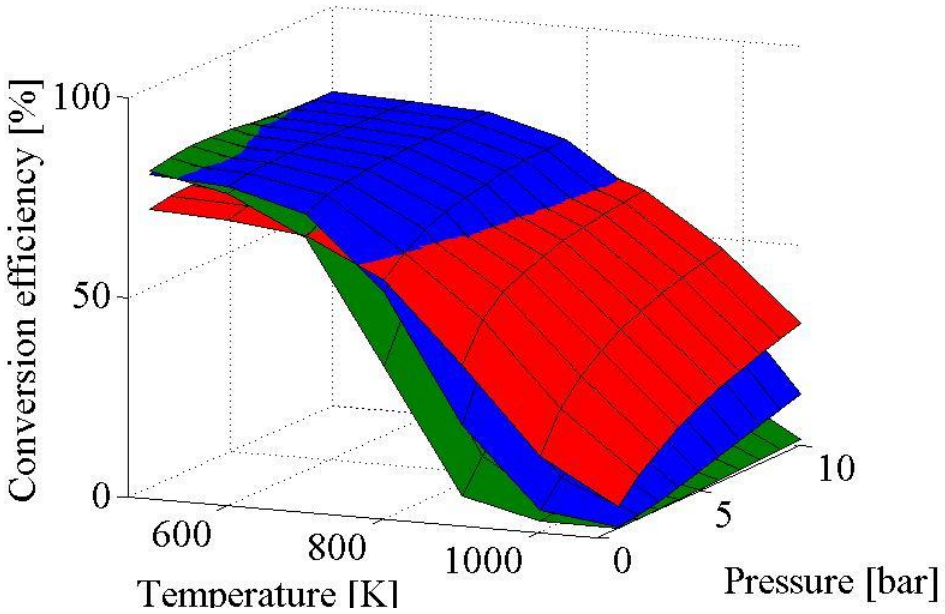

Fig. 5-35 – Effects of temperature and pressure under the maximum electrical energy conversion efficiency (Green surface: 0.5 A cm^{-2} and SCR 7, Blue surface: 1 A cm^{-2} and SCR 4; Red surface: 1.5 A cm^{-2} and SCR 2.5)

The influence of pressure and temperature on the maximum electrical energy conversion efficiency is presented in Fig. 5-35. As expected, at high temperature the predicted efficiency is very low. High temperature favours the reverse direction of the reactions 5-1 and 5-2, i.e. the steam reforming. In general, in the whole investigated pressure range and below 700 K the conversion efficiency is above 70%. In this study, the pressure exhibits some effect on the electrolyzer, it has no effect on chemical equilibrium for methanation, Sabatier and WGS reactions.

Fig. 5-36 further clarifies that pressure has no effect on the methanation part of the process. The effect of the temperature is similar to that under the maximum conversion efficiency. For temperatures below 700 K, the plateau region of amount of energy stored in methane is achieved for each applied current density. Below that temperature, the amount of energy stored in form of methane is a direct function of applied current density and could be related by some form of Faraday's law (assuming that conversion in the methanation reactor is unaffected). In other words, the production of syngas in the electrolyzer dictates the whole process.

The maximum amount of energy stored in methane is ~1.52 $Nm^3\ h^{-1}\ m^{-2}$ of SOEC and is achieved at the highest applied current density. The lowest maximum amount of energy stored in methane is 0.58 $Nm^3\ h^{-1}\ m^{-2}$ of SOEC and is achieved at the lowest

applied current density.

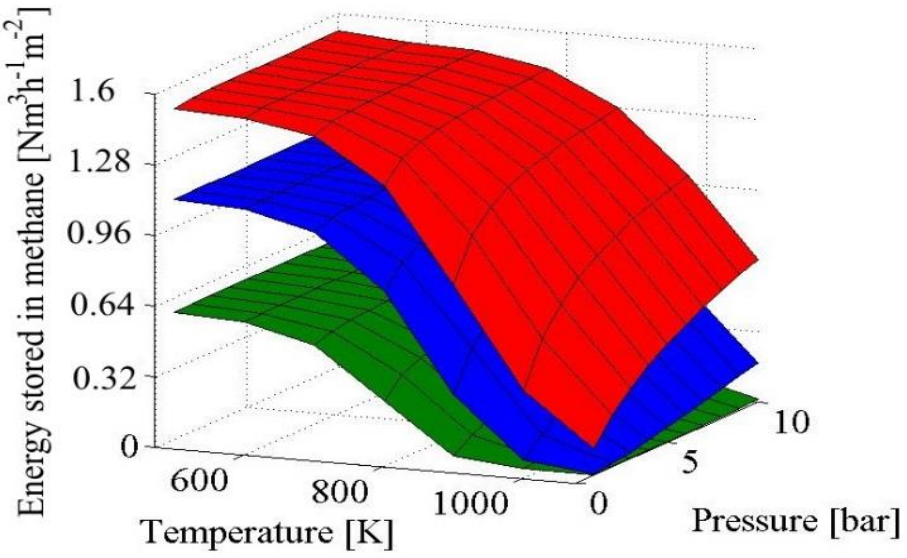

Fig. 5-36 – Effects of temperature and pressure under the maximum amount of energy stored in the methane (Green surface: 0.5 A cm^{-2} and SCR 8, Blue surface: 1 A cm^{-2} and SCR 4, Red surface: 1.5 A cm^{-2} and SCR 2.5)

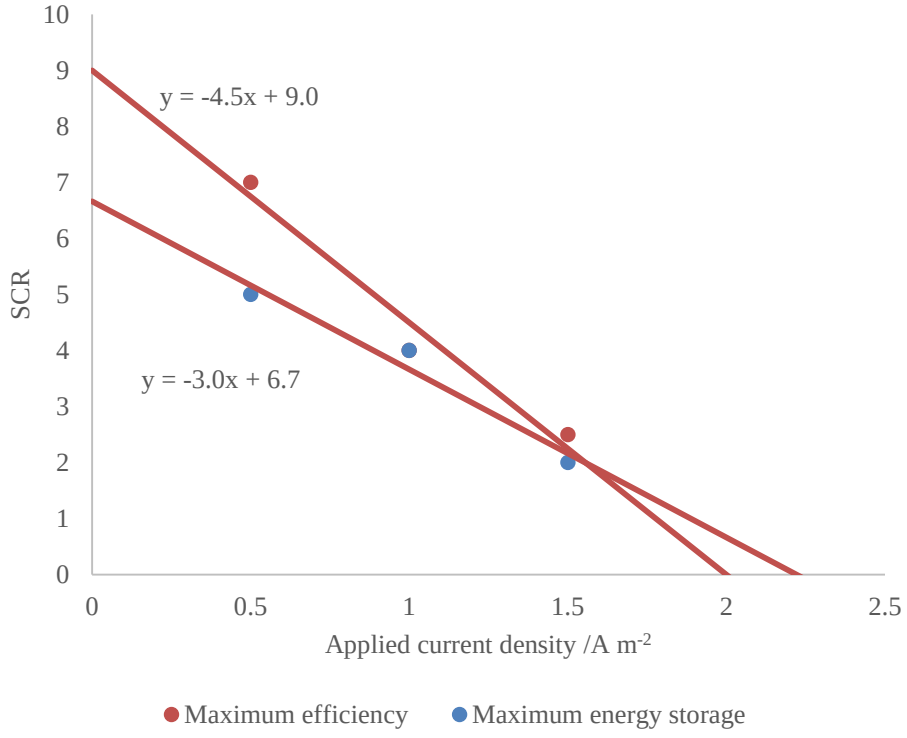

Fig. 5-37 – Relationship between SCR and applied current density (Red squares: maximum electrical energy conversion efficiency, red line: fitted trend line to red crosses; Green circles: maximum amount of the energy stored in methane, green line: fitted trend line to red circles).

From Fig. 5-33 and 5-34, it is seen that increasing the applied current density shifts the optimal value of SCR, and this phenomenon is further analysed in Fig. 5-37. At low applied current only part of feed gases are converted to syngas in the electrolyzer, further hydrogen-to-carbon ratio shift occurs via the WGS reaction at high applied current density, almost all steam and carbon dioxide are converted to syngas inside the electrolyzer, thus WGS reaction cannot proceed in the methane synthesis reactor. As a result, the optimum SCR must be achieved right after the gases leave the electrolyzer. This value is actually a reflection of optimal syngas composition for methane formation. Slightly higher values of SCR corresponding to the maximum efficiency at low applied current are due to lower energy requirement of the electrolyzer fed with gases with high steam content. At high current densities, the effect of gas composition on electrolyzer electricity consumption is less visible and being traded-off by gains in the methanation reactor.

5.3.5 Conclusion

In this study, the author analysed production of sustainable/ renewable methane gas from water and carbon dioxide feed using renewable energy. The analysed system consists of a Solid Oxide Electrolyzer Cell (SOEC) and an ex-situ methane synthesis reactor including Methanation, Sabatier and Water-Gas shift reactions. To simplify the study, the author considered a simple flow-through operation with no recycling and heat recuperation.

The analysis included varying applied current density, pressure and initial ratio of steam to carbon dioxide fed to the electrolyzer. In conjunction with pressure variations of SOEC, the author varied the pressure of the methane synthesis reactor and its temperature. The temperature of SOEC was kept constant at 1073.15 K. To assess the influence of the above parameters on the system performance, the author observed the electrical energy conversion efficiency, overall energy conversion efficiency, amount of energy stored in methane and CO_2-to-CH_4 conversion.

The author concluded the study with following remarks:

- Applied current density affects the amount of produced syngas and thus the amount of produced methane via the Faraday's law,
- Operating at low current density, i.e. with gases conversion below 100% promotes the WGS reaction in the methane synthesis reactor. At low applied

current densities higher steam to carbon dioxide ratios are deemed to achieve optimal hydrogen to carbon ratio in the synthesis reactor,

- At high applied current densities there exist well defined optimal value of SCR resulting in highest efficiency and methane production. At low applied current densities, the effect of SCR is mitigated due to overall low conversion of steam and carbon dioxide. The process is controlled by WGS reaction of methane synthesis reactor,
- Temperature has significant negative effect on the efficiency and methane storage at T > 700K. Below this temperature, the methane synthesis reactions are close to stoichiometric equilibrium, thus the temperature has minor effect,
- Effect of the pressure on the system performance is confined to affecting the electrolyzer. High pressure operation increases the open circuit potential and need of energy for gases compression. However, it lowers the overpotential losses,
- The maximum electrical energy conversion efficiency ranges from 71.64% at 1.5 A cm^{-2} to 81.08% at 0.5 A cm^{-2}. The maximum amount of stored energy in methane varies from 0.58 $Nm^3 h^{-1} m^{-2}$ of SOEC at 0.5 A cm^{-2} to 1.52 $Nm^3 h^{-1} m^{-2}$ of SOEC] at 1.5 A cm^{-2}. The system can achieve 100% CO_2 conversion at 1 A cm^{-2}. The maximum overall energy conversion efficiency varied from 44.07% at low applied current density to 60.87% at high applied current density.

5.4 Chapter summary

In this chapter, the author analysed systems aimed at producing the synthetic fuels, energy storage and intermittency mitigation. Analysed systems envisaged production of hydrogen, syngas, methanol, methane and Fischer-Tropsch fuels. All of the investigated systems can achieve satisfactory conversion efficiency and can be adopted in the industry. The author notes that the easiest system to implement would be the syngas production system, the systems producing hydrocarbon fuels have, in general lower efficiency and require additional reactor to convert the syngas to the desired output. The case for production of hydrogen requires additional storage systems for hydrogen which are in general price and not very effective. The contents of this chapter were published as two journal papers and one international conference poster.

Chapter 6. Conclusions, recommendations and outlook for the energy sector

6.1 Conclusions

A brief conclusion from this thesis is presented below. The more detailed information is included in each chapter's conclusion section.

Several fundamental aspects of operation of Solid Oxide Electrolyzer Cell were reviewed in this thesis and resulted in a proposed new model of the electrolyzer. Effects of electrode microstructure on activation overpotential, operation under extreme oxygen chemical potential difference and co-electrolysis were investigated and state-of-the-art model of the electrolyzer was proposed. Such defined model, incorporating effects of temperature, pressure, gas flow and composition and cell geometry and microstructure was applied to model several energy conversion systems design to mitigate some of the current issues of energy sector, i.e. CO_2 emissions, renewable energy intermittency, production of synthetic, renewable hydrocarbon fuels (comprising majority of end-use energy carrier) and grid balancing. The author's contribution to the discipline is confined to chapters 3 through 5.

Chapter 3 presents the state-of-the-art modelling knowledge on SOEC and author's contribution to the discipline. The author's contribution is described in somewhat more detail following the published articles in international peer-reviewed journals. Exact derivation of models of equilibrium potential and extreme oxygen chemical potential difference model are included.

A system design to mitigate CO_2 emissions from a power plant was designed, analysed and optimized in chapter 4. Depending on operating conditions, maximum efficiency of energy conversion was predicted to be ~50% and maximum exergy efficiency was of similar magnitude (with no heat recovery). Reduction of ~70% of CO_2 is viable.

Synthetic fuels production was analysed in chapter 5 in conjugation with renewable intermittency mitigation and grid balancing. Production of hydrogen, syngas, methanol, methane and Fischer-Tropsch fuels was analysed and energy conversion efficiencies ranging from 61% to 89% were predicted, where the lower value relates to methanol and the higher to hydrogen production. Conversion of almost 100% CO_2 is viable in

such systems and is only a question of proper process design.

6.2 Major achievements

Major achievements of this thesis are summarized in point format for clarity of presentation.

- Formulation and validation of equilibrium potential model for co-electrolysis SOEC,
- Formulation and validation of extreme oxygen chemical potential difference model of SOEC,
- Formulation and validation of co-electrolysis SOEC model incorporating effects of microstructure on cell's performance,
- Formulation, design, analysis and optimization of CO_2 mitigation system based on SOEC,
- Formulation, design, analysis and optimization of synthetic fuels production system based on SOEC,
- Technical and environmental analysis of introduction of SOEC in Singapore as grid balancing, intermittency mitigation and energy storage solution.

6.3 Recommendations

One of the biggest issues preventing from clarifying the fundamentals of Solid Oxide Electrolyzer operation is the discrepancy between the modelled and real systems. One of the big research topics thus is related to inclusion of 2D and 3D structures. Novel modelling techniques must be mastered allowing to simulate the detailed reaction kinetics on complex 3D structures. This must be complemented by development of more comprehensive measurement and validation tools.

The synthetics fuels production technologies are almost century old and the theoretical data to model these reactions is limited. Another important research area in the field covered in this thesis pertains to updating the understanding of chemistry behind synthetic fuels production. Particularly interesting seem the inclusion of kinetic data for synthetic fuel production and further elucidation of Fischer-Tropsch reaction mechanism. It seems valuable to design an experimental study to validate the findings of the optimized models at a reasonable scale.

6.4 Outlook

Solid oxide electrolyzer is set to be tested as one of the Power-to-gas technologies during Energy Research Institute at NTU's Renewable Integrator Demonstrator – Singapore (REIDS) project. This is one of the major consequences spurring from this thesis.

Despite endless efforts and funds poured into SOEC projects, the technology is still far from commercial, more R&D and demonstration efforts will be seen in the next 5-10 years. Research into sustainable and cheap mass production methods will be seen in private and public R&D centres. Energy carriers other than electricity are needed to effectively drive the growth. SOEC can make HC fuels sustainable and bring hydrogen economy to reality.

REFERENCES

ACHENBACH, E. 1994. Three-dimensional and time-dependent simulation of a planar solid oxide fuel cell stack, *Journal of Power Sources*, 49, 333.

AHON, V. R., COSTA JR, E. F., MONTEAGUDO, J. E. P., FONTES, C. E., BISCAIA JR, E. C., LAGE, P. L. C. 2005. *Chemical Engineering Science*, 60, 677.

AKBAR, S., DUTTA, P., LEE, C. 2006. *International Journal of Applied Ceramic Technology*, 3, 302.

ALBADI, M. H., EL-SAADANY, E. F. 2010. Overview of windo power intermittency impacts on power systems, *Electrical Power Sytems Research*, 80, 627.

ALMEIDA, L. C., SANZ, O., MERINO, D., ARZAMENDI, G., GANDIA, L. M., MONTES, M. 2013. *Catalysis Today*, 215, 103.

ANDERSON, A. B., VAYNER, E. 2006. Hydrogen oxidation and proton transport at the Ni-zirconia interface in solid oxide fuel cell anodes: Quantum chemical predictions, *Solid State Ionics*, 177, 1355.

ANDERSON, J. E., GRAVES, Y. B., 1981. Steady-State Characteristics of Oxygen Concentration Cell Sensor Subjected to nonequilibrium Gas Mixtures, *Journal of The Electrochemical Society*, 128, 294.

ANDERSSON, M., YUAN, J., SUNDEN, B. 2013. Grading the Amount of Electrochemical Active Sites along the Main Flow Direction of an SOFC, *Journal of The Electrochemical Society*, 160, F1.

APPLEBY, A. J. 1996. Fuel cell technology: status and future prospects. *Energy*, 21, 521.

Aspen HYSYS ®, http://www.aspentech.com/hysys/.

BAO, B., EL-HALWAGI, V. S., ELBASHIR, N. O. 2010. *Fuel Processing Technology*, 91, 703.

BARTHELMIE, R. J., PRYOR, S. C., FRANDSEN, S. T. 2009. Climatological and meteorological aspects of predicting offshore wind energy, In: GAUDOSI, G., TWIDELL, J. (Eds). Offshore wind power, *Multi-Science publishing Co. Ltd.*, 43.

BECKER, W. L., BRAUN, R. J., PENEV, M., MELAINA, M. 2012. Prodcution of Fischer-Tropsch liquid fuels from high temeprature solid oxide co-electrolysis units, *Energy*, 47, 99.

BEDRINGAS, K. W., ERTESVAG, I. S., BYGGSTOYL, S., MAGNUSSEN, B. F. 1997. Exergy analysis of a solid-oxide fuel cell (SOFC) systems, *Energy*, 22, 403.

BERTEI, A., THOREL, A.S., BESSLER, W. G., NICOLELLA, C. 2012. Mathematical modeling of mass and charge transport and reaction in a solid oxide fuel cell with a mixed ionic conduction, *Chemical Engineering Science*, 68, 606.

BESSLER, W. G. 2005. A new computational approach for SOFC impedance from detailed electrochemical reaction-diffusion models, *Solid State Ionics*, 176, 997.

BESSLER, W. G., GEWIES, S., VOGLER, M. 2007. A New Approach for Elementary-Kinetic Modeling of Internal-Reforming SOFCs, *ECS Transactions,* 7, 1801.

BESSLER, W. G., GEWIES, S., VOGLER, M. 2007. A new framework for physically based modeling of solid oxide fuel cells, *Electrochimica Acta*, 53, 1782.

BESSLER, W. G., VOGLER, M., STOERMER, H., GERTHESEN, D., UTZ, A., WEBER, A., IVERS-TIFFEE, E. 2012. Model anodes and anode models for understanding the mechanism of hydrogen oxidation in solid oxide fuel cells, *Physical Chemistry Chemical Physics*, 12, 13888.

BESSLER, W. G., WARNATZ, J., GOODWIN, D. G. 2007. The influence of equilibrium potential on the hydrogen oxidation kinetics of SOFC anodes, *Solid State ionics*, 177, 3371.

BIEBERLE, A., GAUCKLER, L. J. 2002. State-space modeling of the anodic SOFC system Ni, H_2-H_2O|YSZ, *Solid State Ionics,* 146, 23.

BIEBERLE, A., MEIER, L. P., GAUCKLER, L. J. 2001. The Electrochemistry of Ni Pattern Anodes Used as Solid Oxide Fuel Cell Model Electrodes, *Journal of the Electrochemical Society*, 148, A646.

BIERSCHENK, D. M., WILSON, J. R., BARNETT, S. A. 2011. High efficiency electrical energy storage using a methane-oxygen solid oxide cell, *Energy and Environmental Science*, 4, 944.

BOS, A. N. R., BORMAN, P. C., KUCZYNSKI, M., WESTERTERP, K. R. 1989, *Chemical Engineering Science*, 44, 2435.

BRAILSFORD, A. D., YUSSOUFF, M., LOGOTHETIS, E. M. 1998. A first principle model of metal oxides gas sensor for measuring combustibles, *Sensors and Actuators B*, 49, 93.

BRITISH PETROLEUM, 2014 BP statistical review of world energy 2014.

BROENSTED, J. N., LAEREBOG, H. 1943. I Fysik Kemim 2nd ed., *Munksgaerd*, 1943.

BROMBERG, L., CHENG, W. K. 2010. Methanol as an alternative transportation, *Available from: www.afdc.energy.gov/afdc/pdfs/mit_methanol_white_paper.pdf*, USA.

BROOK, R. T. In: HEUER, A. H., HOBBS, L .W. (eds.). 1981. Science and Technology of Zirconium III, *American Ceramic Society*.

BROWN, J. T. 1986. High-temperature solid-oxide fuel cells (SOFCs), *Energy,* 1, 209.

CAI, Q., LUNA-ORTIZ, E., ADJIMAN, C. S., BRANDON, N. P. 2010. The Effects of Operating Conditions on the Performance of a Solid Oxide Steam Electrolyser: A Model-Based Study, *Fuel Cells*, 10, 1114.

CHAN, S. H., CHEN, X. J., KHOR, K. A. 2002. An electrolyte model for ceramic oxygen generator and solid oxide fuel cell, *Journal of Power Sources*, 111, 320.

CHAN, S. H., CHEN, X. J., KHOR, K. A. 2004. Cathode Micromodel of Solid Oxide Fuel Cell, *Journal of The Electrochemical Society,* 151, A164.

CHAN, S. H., HO, H. K., DING, O. L. 2005. Analysis of a simple solid oxide fuel cell system with gas dynamic in afterburner and connecting pipes, *Fuel Cells*, 5, 25.

CHAN, S. H., KHOR, K. A., XIA, Z. T. 2001. A complete polarization model of a solid oxide fuel cell and its sensitivity to the change of cell components thickness, *Journal of Power Sources*, 93, 130.

CHAN, S. H., LOW, C. F., DING, O. L. 2002. Energy and exergy analysis of simple solid-oxide fuel-cell power systems, *Journal of Power Sources*, 103, 188.

CHAN, S. H., XIA, Z. T. 2001. Anode Micro Model of Solid Oxide Fuel Cell, *Journal of The Electrochemical Society*, 148, A388.

CHEDDIE, D. 2012. Integration of a solid oxide fuel cell into a 10 MW gas turbine power plant, *Energies*, 3, 754.

CHEN, M., LIU, Y. –L., BENTZEN, J. J., ZHANG, W., SUN, X., HAUCH, A., TAO, Y., BOWEN, J. R., HENDRIKSEN, P. V. 2013. *Journal of The Electrochemical Society*, 160, F883.

CHEN, X. J., CHAN, S. H., KHOR, K. A. 2004. Simulation of a composite catode in solid oxide fuel cells, *Electrochimica Acta,* 49, 1851.

CHENG, Z., ZHA, S., LIU, M. 2007. Influence of cell voltage and current on sulphur poisoning behaviour of solid oxide fuel cells, *Journal of Power Sources*, 25, 688.

CHISTI, Y. 2007. *Biotechnology Advances*, 25, 294.

CHOI, H. –W., BERSON, A., PHAROAH, J. G., BEALE, S. B. 2011. Effective transport properties of the porous electrodes in solid oxide fuel cells,

Proceedings of the Institution of Mechanical Engineers, Part A: Journal of Power and Energy, 225, 183.

CHRONEOS, A., YIDLIZ, B., TARANCON, A., PARFITT, D., KILNER, J. A. 2011. *Energy and Environmental Science*, 4, 2774.

CONNOLLY, D., MATHIESEN, B. V., RIDJAN, I. 2014. *Energy*, dx.doi.org/10.1016/j.energy.2014.05.104.

CORNELISSEN, R. L. 1997. Thermodynamics and sustainable development – the use of exergy analysis and the reduction of irreversibility. PhD, *University of Twente*, The Netherlands.

COSTAMAGNA, P., COSTA, P., ANTONUCCI, V. 1998. Micro-modelling of solid oxide fuel cell electrodes, *Electrochimica Acta,* 43, 375.

COSTAMAGNA, P., COSTA, P., ARATO, A. 1998. Some more considerations on the optimization of cermet solid oxide fuel cell electrodes, *Electrochimica Acta,* 43, 967.

CUMMING, D. J., TAYLOR, R., MANEROVA, J., SINCLAIR, D. C., HARDACRE, C., ELDER, R. H. 2013. *In-situ* Monitoring of Solid Oxide Electrolysis Cells, *ECS Transactions*, 58, 207.

DAMEN, K., VAN TROOST, M., FAAIJ, A., TURKENBURG, W. 2006. A comparison of electricty and hydrogen production systems with CO_2 capture and storage. Part A: Review and selection of promising conversion and capture technologies. *Progress in Energy and Combustion Science*, 32, 215.

DAR, Y. R., VIJAY, P., TADE, M. O., DATTA, R. 2012. Topological analysis of hydrogen oxidation reaction kinetics at Ni/YSZ anode of the solid oxide fuel cell, *Journal of Electroanalytical Chemistry*, 677-680, 15.

DEMIN, A., GORBOVA, E., TSIAKARAS, P. 2007. High temeprature electrolyzer based on solid oxide co-ionic electrolyte: A theoretical model, *Journal of Power Sources*, 171, 205.

DENG, X., PETRIC, A. 2005. Geometrical modeling of the triple-phase-boundary in solid oxide fuel cells, *Journal of Power Sources*, 140, 297.

DIAZ-GONZALES, F., SUMPER, A., GOMIS-DELLMUNT, O., VILLAFAFILA-ROBLES, R. 2012. A review of energy storage technologies for wind power applications, *Renewable and Sustainable Energy Reviews*, 16, 2154.

DILLIG, M., KARL, J. 2012. Thermal management of high temeprature solid oxide electrolyser cell/fuel cell systems, *Energy Procedia*, 28, 37.

DINCER, I., CENGEL, Y. 2001. Energy, entropy and exergy concepts and their roles in thermal engineering, *Entropy*, 3, 116.

DOENITZ, W., DIETRICH, G., ERDLE, E., STREICHER, R. 1988. Electrochemical high temeprature technology for hydrogen production or direct electricity generation. *International Journal of Hydrogen Energy*, 13, 283.

DOENITZ, W., ERDLE, E. 1985. High-temperature electrolysis of water-vapor – status of development and perspectives for application. *International Journal of Hydrogen Energy*, 10, 291.

DOENITZ, W., ERDLE, E., STREICHER, R. 1990. In *Electrochemical Hydrogen Technologies. Electrochemical production and combustion of hydrogen.* WENDT, H. (ed), Elseveir, Amsterdam.

DOENITZ, W., SCHMIDBERGER, R. 1982. Concepts and Design for Scaling Up High Temperature Water Vapor Electrolysis, *International Journal of Hydrogen Energy*, 7, 321.

DOENITZ, W., SCHMIDBERGER, R., STIENHEIL, E., STREICHER, R. 1980. Hydrogen production by High Temeprature Electrolysis of Water Vapor, *International Journal of Hydrogen Energy*, 5, 55.

DRY, M. E. 2002. *Catalyst Today*, 71, 227.

DUMORTIER, M., SANCHEZ, J., KEDDAM, M., LACROIX, O. 2012. Energy transport inside a three-phase electrode and application to a proton-conducting solid oxide electrolysis cell, *International Journal of Hydrogen Energy*, 38, 2610.

DUMORTIER, M., SANCHEZ, J., KEDDAM, M., LACROIX, O. 2012. Theoretical considerations on the modelling of transport in a three-phase electrode and application to a proton conducting solid oxide electrolysis cell, *International Journal of Hydrogen Enenrgy,* 37, 11579.

DUMORTIER, M., SANCHEZ, J., KEDDAM, M., LACROIX, O. 2014. Analytical calculation of transfer across a cermet for solid oxide fuel cells and electrolyzers, *Journal of Power Sources,* 248, 703.

EBBESEN, S. D., JENSEN, S. H., HAUCH, A., MOGENSEN, M. B. 2014. High Temperature Electrolysis in Alkaline Cells, Solid Proton Conducting Cells, and Solid Oxide Cells, *Chemical Reviews*, dx.doi.org/10.1021/cr5000865.

EBBESEN, S., MOGENSEN, M. 2009. Electrolysis of carbon dioxide in solid oxide electrolysis cells, *Journal of Power Sources*, 193, 349.

ELIKAN, L., MORRIS, J. P., WU, C. K. 1972. Development of Solid Oxide Electrolyte

Carbon Dioixde and Water Reduction System for Oxygen Recovery, *NASA contractor report NASA CR-2014*, Washigton, D.C. 1972.

ENERGY MARKET AUTHORITY. 2012. Energising our nation. Singapore energy statistics 2012, Singapore.

ERDLE, E., DOENITZ, W., SCHAMM, R., KOCH, A. 1990. In *Hydrogen Energy Progress VIII: Proceedings of the 8th World Hydrogen Energy Conference*. TAKAHASHI, P. K., VEZIROGLU, T. N. (eds), Pergamon, New York, US.

ERDLE, E., GROSS, J., MEYRINGER, V. 1986. In *Proceedings of 3rd International Workshop*. BECKER, M. (ed.), Springer-Verlag, Heidelberg.

ERMOLAEV, I. S., ERMOLAEV, V. S., MORDKOVICH, V. Z. 2014. *Industrial and Engineering Chemistry Research*, 53, 2758.

EUROPEAN ENVIRONMENT AGENCY. 2012. Electricity consumption per capita in 2008, Denmark.

FARJAH, E., BORNAPOUR, M., NIKNAM, T., BAHMANIFIROUZI, B. 2012. Plecemnt of combined heat, power and hydrogen production fuel cell power plants in a distribution network, *Energies*, 5, 790.

FAWCET, W. R. 2008. The Ionic Work Function and its Role in Estimating Absolute Electrode Potentials, *Langmuir*, 24, 9868.

FERGUS, J. W. 2011. Sensing mechanism of non-equilibrium solid-electroyte-based chemical sensors, *Journal of Solid State Chemistry*, 15, 971.

FERNANDES, F. A. N., TELES, U. M. 2007. *Fuel Processing Technology*, 88, 207.

FERRERO, D., LANZINI, A., SANTARELLI, M., LEONE, P. 2013. A comperative assessment on hydrogen production from low- and high-temeprature electrolysis, *International Journal of Hydrogen Energy*, 38, 3523.

FLEIG, J. 2003. Solid Oxide Fuel Cell Cathodes: Polarization Mechanisms and Modeling of the Electrochemical Performance, *Annual Reviews in Materials Research*, 33, 361.

FLEMING, W. J. 1977. Physical Principles Governing Nonideal Behavior of the Zirconia Oxygen Sensor, *Journal of The Electrochemical Society*, 124, 21.

FU, Q., MABILAT, C., ZAHID, M., BRISSE, A., GAUTIER, L. 2010. Syngas production *via* high-temeprature steam/CO_2 co-electrolysis: an economic assessment, *Energy and Environmental Science*, 3, 1382.

GAHLEITNER, G. 2013. Hydrogen from renewable electricity: An international review of power-to-gas pilot plants for stationary applications, *International Journal of*

Hydrogen Energy, 38, 2039.

GARCIA-CAMPRUBI, M., IZQUIERDO, S., FUEYO, N. 2014. Challenges in the electrochemical modelling of solid oxide fuel and elextrolyser cells, *Renewable and Sustainable Energy Reviews*, 33, 701.

GARTON, J.G., LAWLOR, V., OLABI, A.G., HOCHENAUER, C., ZAUNER, G. 2012. Water droplet accumulation and motion in PEM (proton exchange membrane) fuel cell mini-channels, *Energy*, 39, 63.

GE, X., ZHANG, L., FANG, Y., ZENG, J., CHAN, S. H. 2011. Robust solid oxide cells for alternate power generation and carbon conversion, *RSC Advances*, 1, 715.

GEWIES, S., BESSLER, W. G., SONN, V., IVERS-TIFFEE, E. 2007. Experimental and Modeling Study of the Impedance of Ni/YSZ Cermet Anodes, *ECS Transactions*, 7, 1573.

GHAREGHASHI, A., GHADER, S., HASHEMIPOUR, H. 2013. *Journal of Industrial and Engineering Chemistry*, 19, 1811.

GOODWIN, D. G., ZHU, H., COLCLASURE, A. M., KEE, R. J. 2009. Modeling Electrochemical Oxidation of Hydrogen on Ni-YSZ Pattern Anodes, *Journal of The Electrochemical Society*, 156, B1004.

GOPLANA, S., MOSLEH, M., HARTVIGSEN, J. J., MCCONNEL, R. D. 2008. Analysis of self-sustaining recuperative solid oxide electrolysis systems, *Journal of Power Sources*, 185, 1328.

GORSKI, A., YURKIV, V., STARUKHIN, D., VOLPP, H. –R. 2011. H_2O chemisorption and H_2 oxidation on yttria-stabilized zirconia: Density functional theory and temperature-programmed desorption studies, *Journal of Power Sources*, 196, 7188.

GRAVES, C. R. 2012. Recycling CO_2 into Sustainable Hydrocarbon Fuels: Electrolysis of CO_2 and H_2O, PhD Thesis, Columbia University.

GRAVES, C. R., EBBESEN, S. D., MOGENSEN, M. 2011. Co-electrolysis of CO_2 and H_2O in solid oxide cells: performance and durability, *Solid State Ionics*, 192, 398.

GREENPEACE. 2012. Energy [r]evolution: a sustainable world energy outlook.

GREW, K. N., PERACCHIO, A. A., JOSHI, A. S., IZZO JR, J. R., CHIU, W. K. S. 2010. Characterization and analysis metchods for the examination of the heterogenous solid oxide fuel cell electrode mictrostructure. Part 1: Volumetric measurments of the heterogenous structure, *Journal of Power Sources*, 195, 7930.

GRONDIN, D., DESEURE, J., BRISSE, A., ZAHID, M., OZIL, P. 2010. Simulation of a high temperature electrolyzer, *Journal of Applied Electrochemistry,* 40, 933.

GRONDIN, D., DESEURE, J., OZIL, P., CHABRIAT, J. –P., GRONDIN-PEREZ, B., BRISSE, A. 2011. Computing approach of cathodic process within solid oxide electrolysis cell: Experiments and continuum model validation, *Journal of Power Sources,* 196, 9561.

GRONDIN, D., DESEURE, J., OZIL, P., CHABRIAT, J. –P., GRONDIN-PEREZ, B., BRISSE, A. 2013. Solid oxide electrolysis cell 3D simulation using artificial neural network for cathodic process description, *Chemical Engineering Research and Design,* 91, 134.

GROSS, R., HEPTONSTALL, P. 2008. The cost and impacts of intermittency: An ongoing debate: "East is East, and West is West, and never the twain shall meet.", *Energy Policy,* 36, 4005.

GUAN, Y., LI, W., GONG, Y., LIU, X., ZHANG, X., CHEN, J., GELB, J., YUN, W., XIONG, Y., TIAN, Y., WANG, H. 2011. *Journal of Power Sources,* 196, 1915.

HAARLEMMER, G., BOISSONNET, G., PEDUZZI, E., SETUER, P. –A. 2014. *Energy*, 66, 667.

HARDISTY, P., CLARK, T., HYNES, R. 2012. Life cycle greenhouse gas emissions from electricity generation: a comperative analysis of Australian energy sources, *Energies*, 5, 872.

HAUCH, A., EBBESEN, S., JENSEN, S., MOGENSEN, M. 2008. Highly efficient high temperature electrolysis, *Journal of Materials Chemistry*, 18, 2331.

HAWKES, G. L., O'BRIEN, J. E., STOOTS, C. M., HERRING, J. S., SHAHNAM, M. 2005. CFD Model of a Planar Solid Oxide Electrolysis Cell for Hydrogen Prodction from Nuclear Energy, *The 11th International Topical Meeting on Nuclear Reactor Thermal-Hydroaulics*, France, 2005.

HAWKES, G., O'BRIEN, J., STOOTS, C., HAWKES, B. 2009. 3D CFD model of a multi-cell high-temperature electrolysis stack, *International Journal of Hydrogen Energy,* 34, 4189.

HECHT, E. S., GUARAV, K. G., ZHU, H., DEAN, A. M., KEE, R. J., MAIER, L., DEUTSCHMANN, O. 2005. Methane reforming kinetics within a Ni-YSZ SOFC anode support, *Applied Catalysis A: General*, 295, 40.

HEIER, S. 1998. Grid integration of wind energy conversion system, *John Wiley & Sons Ltd.*, UK.

HENKE, M., WILLICH, C., WESTNER, C., LEUCHT, F., KALLO, J., BESSLER, W. G., FRIEDRICH, K. A. 2013. A validated multi-scale model of a SOFC stack at elevated pressure, *Fuel Cells*, 13, 773.

HERBERT, G. M. J., INIYAN, S., SREEVALSAN, E., RAJAPANDIAN, S. 2007. *Renewable and Sustainable Energy Reviews*, 11, 1117.

HERNANDEZ-PACHECO, E., SINGH, D., HUTTON, P. N., PATEL, N., MANN, M. D. 2004. A macro-level model for determining the performance characteristics of solid oxide fuel cells, *Journal of Power Sources*, 138, 174.

HERTZ, J. L., TULLER, H. L. 2007. Measurment and finite element modeling of triple phase boundary-related current constriction in YSZ, *Solid State Ionics*, 178, 915.

HIBINO, T., HASHIMOTO, A., KAKIMOTO, S., SANO, M. 2001. Zirconia-Based Potentiometric Sensor Using Metal Oxide Electrodes for Detection of Hydrocarbons, *Journal of The Electrochemcial Society*, 148, H1.

HIBINO, T., WANG, S., KAKIMOTO, S., SANO, M. 2000. One-chamber solid oxide fuel cell canstructed from a YSZ electrolyte with a Ni anode and LCM cathode, *Solid State Ionics*, 127, 89.

HJALMARSSON, P., SUN, X., LIU, Y. –L., CHEN, M. 2014. Durability of high performance Ni-yttria stabilized zirconia supported solid oxide electrolysis cells at high curren density, *Journal of Power Sources*, 262, 316.

HOEKMAN, S. K., BROCH, A., ROBBINS, C., PURCELL, R. 2010. *International Journal of Greenhouse Gas Control*, 4, 44.

HOLTAPPELS, P., DE HAART, L. G. J., STIMMING, U. 1999. Reaction of Hydrogen/Water Mixtures on Nickel-Zirconia Cermet Electrodes. I. DC Polarization Characteristics, *Journal of The Electrochemcial Society*, 146, 1620.

HOLTAPPELS, P., DE HAART, L. G. J., STIMMING, U. 1999. Reaction of Hydrogen/Water Mixtures on Nickel-Zirconia Cermet Electrodes. II. AC Polarization Characteristics, *Journal of The Electrochemcial Society*, 146, 2976.

HOLZER, L., WIEDENMANN, D., MUENCH, B., KELLER, L., PRESTAT, M., GASSER, PH., ROBERTSON, I., GROBETY, B. 2013. The influence of constrictivity on the effective transport properties of porous layers in electrolysis and fuel cells, *Journal of Material Science*, 48, 2934.

HORIUTI, J., TOYA, T. 1965. Theoretical isotherm of hydrogen adsorption on nickel (I), *Journal of The Research Institute for Catalyst Hokkaido University*, 12, 76.

HOU, K., HUGHES, R. 2001. The kinetics of methane steam reforming over a Ni/α-

Al_2O catalyst, *Chemical Engineering Journal,* 82, 311.

INDERWILDI, O. R., JENKINS, S. J., KING, D. A. 2008. *The Journal of Physical Chemistry C Letters,* 112, 1305.

INGRAM, D. B., LINIC, S. 2009. *Journal of The Electrochemical Society,* 156, B1457.

INTERNATIONAL ATOMIC ENERGY AGENCY. 2011. Singapore's Energy Landscape and Future Developments, *IAEA Workshop on Advanced Nuclear Reactor Technology for Near Term Deployments*, Singapore.

INTERNATIONAL ENERGY AGENCY, 2012 World Energy Outlook – 2012 Edition.

INTERNATIONAL ENERGY AGENCY, 2014 Key World Energy Statistics – 2014 Edition.

INTERNATIONAL ENERGY AGENCY, IEA Energy Technology Essentials: Hydrogen Production & Distribution – Edition 2007.

INTERNATIONAL ENERGY AGENCY. 2012. The Impact of Wind Power on European Natural Gas Markets, France.

INTERNATIONAL PANEL ON CLIMATE CHANGE, Climate Change 2007: The Physical Science Basis – 2007 Edition.

INTERNATIONAL PANEL ON CLIMATE CHANGE, Climate Change 2014: Impacts, Adaptaion, and Vulnerability. Summary for Policymakers – 2014 Edition.

INTERNATIONAL PANEL ON CLIMATE CHANGE, IPCC Fifth Assessment Report: Climate Change 2013 (AR5) – 2013 Edition.

IORA, P., CHIESA, P. 2009. High efficiency process for the production of pure oxygen based on solid oxide fuel cell-solid oxide electrolyzer technology, *Journal of Power Sources*, 190, 408.

IORA, P., TAHER, M. A. A., CHIESA, P., BRANDON, N. P. 2010. A novel system for the production of pure hydrogen from natural gas based on solid oxide fuel cell – solid oxide electrolyzer, *International Journal of Hydrogen Energy,* 35, 12680.

IORA, P., TAHER, M. A. A., CHIESA, P., BRANDON, N. P. 2012. A one dimensional solid oxide electrolyzer-fuel cell stack model and its application to the analysis of a high efficiency system for oxygen production, *Chemical Engineering Science,* 80, 293.

ISHIHARA, T., JIRATHIWATHANKUL, N., ZHONG, H. 2010. Intermediate temperature solid oxide electrolysis cell using $LaGaO_3$ based perovskite electrolyte, *Energy and Environmenal Science*, 3, 1382.

JACOBSEN, T., MOGENSEN, M. 2008. The course of Oxygen Partial Pressure and

Electric Potentials across an Oxide Electrolyte Cell, *ECS Transactions*, 13, 259.

JACOBSON, M. Z. 2009. *Energy and Environmental Science*, 2, 148.

JANARDHANAN, V. M., DEUTSCHMANN, O. 2006. CFD analysis of a solid oxide fuel cell with internal reforming: Coupled interactions of transport, heterogenous catalysis and electrochemical processes, *Journal of Power Sources*, 162, 1192.

JENSEN, S. H., HAUCH, A., KNIBBE, R., JACOBSEN, T., MOGENSEN, M. 2013. Modeling Degradation in SOEC Impedance Spectra, *Journal of The Electrochemical Society*, 160, F244.

JEON, D. H. 2009. A comprehensive CFD model of anode-supported solid oxide fuel cells, *Electrochimca Acta*, 54, 2727.

JESS, A., POPP, R., HEDDEN, K. 1999. *Applied Catalysis A: General*, 186, 321.

JIANG, S. P., BADWAL, S. P. S. 1997. Hydrogen Oxidation at the Nickel and Platinum Electrodes on Yttria-Tetragonal Zirconia Electrolyte, *Journal of The Electrochemcial Society*, 144, 3777.

JIANG, S. P., BADWAL, S. P. S. 1999. An electrode kinetics study of H_2 oxidation on Ni/Y_2O_3-ZrO_2 cermet electrode of the solid oxide fuel cell, *Solid State Ionics*, 123, 209.

JIN, X., XUE, X. 2010. Computational fluid dynamics analysis of solid oxide electrolysis cells with delaminations, *International Journal of Hydrogen Energy*, 35, 7321.

JIN, X., XUE, X. 2010. Mathematical modeling analysis of regenerative solid oxide fuel cells in switching mode conditions, *Journal of Power Sources*, 195, 6652.

KAKAC, S., PRAMUANJAROENKIJ, A., ZHOU, X. Y. 2007, A review on numerical modeling of solid oxide fuel cells, *International Journal of Hydrogen Energy*, 32, 761.

KAZEMPOOR, P., BRAUN, R. J. 2014. Model validation and performance analysis of regenerative solid oxide cells: Electrolytic operation, *International Journal of Hydrogen Energy,* 39, 2669.

KAZEMPOOR, P., BRAUN, R. J. 2014. Model validation and performance analysis of regenerative solid oxide cells: Reversible operation, *International Journal of Hydrogen Energy,* 39, 5955.

KEANE, M., FAN, H., HAN, M., SINGH, P. 2014. Role of initial microstructure on nickel-YSZ cathode degradation in solid oxide electrolysis cells, *International Journal of Hydrogen Energy*, doi:10.1016/j.ijhydene.2014.09.057

KENNOUCHE, D., CHEN-WIEGART, Y. –C. K., CRONIN, J. S., WANG, J., BARNETT, S. A. 2013. Three-Dimensional Microstructural Evolution of Ni-Yttria-Stabilized Zirconia Solid Oxide Fuel Cell Anodes at Elevated Temperatures, *Journal of The Electrochemical Society*, 160, F1293.

KESTER, F. L. 1974. Hydrogenation of Carbon Dioxide over a Supported Ruthenium Catalyst, *American Chemical Society, Division of Fuel Chemistry*, 19, 146.

KIM, J., JI, H. –I., DASARI, H. P., SHIN, D., SONG, H., LEE, J. –H., KIM, B. –K., JE, H. –J., LEE, H. –W., YOON, K. J. 2013, Degradation mechanism of electrolyte and air electrode in solid oxide electrolysis cells operating at high polarization, International Journal of Hydrogen Energy, 38, 1225.

KINGERY, W. D., PAPPIS, J., DOTY, M. E., HILL, D. C. 1959. *Journal of The American Ceramic Society*, 42, 393.

KLEIS, J., JONES, G., ABILD-PEDERSEN, F., TRIPKOVIC, V., BLIGAARD, T., ROSSMEISL, J. 2009. Trends for Methane Oxidation at Solid Oxide Fuel Cell Conditions, *Journal of The Electrochemical Society,* 156, B1447.

KOTAS, T. J. 1985. The exergy method of thermal plant analysis, *Anchor Brendon Ltd.*, Tiptree, Essex.

LAGUNA-BERCERO, M. A. 2012. Recent advances in high temperature electrolysis using solid oxide fuel cells: A review, *Journal of Power Sources*, 203, 4.

LAURENCIN, J., KANE, D., DELETTE, G., DESEURE, J., LEFEBVRE-JOUD, F. 2011. Modelling of solid oxide steam electrolyser: Impact of the operating conditions on hydrogen production, *Journal of Power Sources,* 196, 2080.

LAWLOR, V. 2012. Highlighting of critical experimental data for SOFC modeling that is missing from the literature and potential of N-IR thermography for SOFC study, *Journal of Fuel Cell Science and Technology*, 9, 1.

LAWLOR, V., GREISSER, S., BUCHINGER, G., OLABI, A. G., CORDINER, S., MEISSNER, D. 2009. Review of the micro-tubular solid oxide fuel cell: part I. Stack design issues and research activities, *Journal of Power Sources*, 193, 387.

LAY-GRINDLER, E., LAURENCINC, J., DELETTE, G., AICART, J., PETITJEAN, M., DESSMOND, L. 2013. Micro modelling of solid oxide electrolyser cell: From performance to durability, *International Journal of Hydrogen Energy*, 38, 6917.

LEE, J. H., HYUN-GOO, K., WAN-HO, J., SEONG-WOOK, Y. 2011. Wind Mapping

of Singapore by WindSim, *WindSim 2011 Annual User Meeting.*

LI, C., SHI, Y., CAI, N. 2010. Elementary reaction kinetic model of an anode-supported solid oxide fuel cell fueled with syngas, *Journal of Power Sources*, 195, 2266.

LI, W., SHI, Y., LUO, Y., CAI, N. 2013. Elementary reaction modeling of CO_2/H_2O co-electrolysis cell considering effects of cathode thickness, *Journal of Power Sources*, 243, 118.

LI, W., WANG, H., SHI, Y., CAI, N. 2013. *International Journal of Hydrogen Energy*, 38, 11104.

LIU, Z. –P., HU, P. 2002. *Journal of American Chemical Society Communications*, 124, 11568.

LOPEZ-GANDARA, C., RAMOS, F. M., CIRERA, A. 2009. YSZ-Based Oxygen Sensors and the Use of Nanomaterials: A Review from Classical Models to Current Trends, *Journal of Sensors,* dx.doi.org/10.1155/2009/258489.

LOX, E. S., FROMENT, G. F. 1993. *Industrial and Engineering Chemistry Research*, 32, 71.

LUO, Y., SHI, Y., LI, W., CAI, N. 2014. Comprehensive modeling of tubular solid oxide electrolysis cell for co-electrolysis of steam and carbon dioxide, *Energy*, dx.doi.org/j.energy.2014.04.019.

MALYSHEV, E. M., PANKRATIEV, D., RYNDIN, A., TURKOV, V. M. 1977. Heat of Oxygen Adsorption on Nickel Catalyst, *Reaction Kinetics Catalysis Letters*, 7, 115.

MANAGE, M. N., HODGSON, D., MILLIGAN, N., SIMONS, S. J. R., BRETT, D. J. L. 2011. A techno-economic appraisal of hydrogen generation and the case for solid oxide electrolyser cells, *International Journal of Hydrogen Energy*, 36, 5782.

MARETTO, C., KRISHNA, R. 1999. *Catalysis Today,* 52, 279.

MARKVOORT, A. J., VAN SANTEN, R. A., HILBERS, P. A. J., HENSEN, E. J. M. 2012. *Angewandte Chemie International Edition*, 51, 9015.

MARVAST, M. A., SOHRABI, M., ZARRINPASHNE, S., BAGHMISHEH, G. 2005. *Chemical Engineering and Technology*, 28, 78.

MASUKU, C. M., MA, W., HILDEBRANDT, D., GLASSER, D., DAVIS, B. H. 2012. *Fluid Phase Equilibria*, 314, 38.

MATSUZAKI, Y., YASUDA, I. 2000. Electrochemical Oxidation of H_2 and CO in a H_2-H_2O-CO-CO_2 System at the Interface of a Ni-YSZ Cermet Electrode and YSZ

Electrolyte, *Journal of The Electrochemical Society*, 147, 1630.

MCKELLAR, M. G., SOHAL, M. S., STOOTS, C. M., MULLOTH, L., LUNA, B., ABNEY M. B. 2010. Mathematical Analysis of High-Temperature Co-Electrolysis of CO_2 and O_2 production in a Closed-Loop Atmosphere Revitalization System, *NASA contractor report DE-AC07-05ID14517*, Report for NASA research centre.

MENDYBAEV, R. A., BECKETT, J. R., STOPLER, E., GROSSMAN, L. 1998. *Geochimica et Cosmochimica Acta*, 62, 3131.

MILEWSKI, J. 2012. A Mathematical Model of SOFC: A proposal, *Fuel Cells*, 12, 709.

MILEWSKI, J., LEWANDOWSKI, J. 2009. Solid oxide fuel cell fuelled by biogases, *Archives of Thermodynamics*, 30, 3.

MILEWSKI, J., MILLER, A. 2006. Influences of the type and thickness of electrolyte on solid oxide fuel cell hybrid system performance, *Journal of Fuel Cell Science and Technology*, 3, 396.

MILEWSKI, J., SWIRSKI, K., SANTARELLI, M., LEONE, P. 2011. Advanced Methodes of Solid Oxide Fuel Cell Modeling, *Springer*.

MINH, N. Q., TAKAHASHI, T. 1995. Science and Technology of Ceramic Fuel Cells, *Elsevier*, Amsterdam, 1995.

MITTERDORFER, A., GAUCKLER, L. J. 1999. Identification of the reaction mechanism of the Pt, O_2(g)|yttria-stabilized zirconia system. Part I: General framework, modelling, and structural investigation, *Solid State Ionics*, 117, 187.

MITTERDORFER, A., GAUCKLER, L. J. 1999. Identification of the reaction mechanism of the Pt, O_2(g)|yttria-stabilized zirconia system. Part II: Model implementation, parameter estimation, and validation, *Solid State Ionics*, 117, 203.

MITTERDORFER, A., GAUCKLER, L. J. 1999. Reaction kinetics of the Pt, O_2(g)|c-ZrO_2 system: precursos-mediated adsorption, *Solid State Ionics*, 120, 211.

MIZUSAKI, J., TAGAWA, H., SAITO, T., YAMAMURA, T., KAMITANI, K., HIRANO, K., EHARA, S., TAKAGI, T., HIKITA, T., IPPOMMATSU, M., NAKAGAWA, S., HASHIMOTO, K. 1994. Kinetic studies of the reaction at the nickel pattern electrode on YSZ in H_2-H_2O atmospheres, *Solid State Ionics*, 70/71, 52.

MOCOTEGUY, P., BRISSE, A. 2013. A review and comprehensive analysis of degradation mechanisms of solid oxide electrolysis cells, *Intenrational Journal*

of Hydrogen Energy, 38, 15887.

MUKHERJEE, J, LINIC, S. 2007. First-Principle Investigations of Electrochemical Oxidation of Hydrogen at Solid Oxide Fuel Cell Operating Conditions, *Journal of the Electrchemical Society*, 154, B919.

NAEFE, H. 1997. *Journal of The Electrochemical Society*, 144, 3922.

NAGAO, M., TAKAHASHI, M., HIBINO, T. 2010. Separator-free fuel cell stacks operating in a mixture of hydrogen and air, *Energy & Enviroment Science*, 3, 1934.

NAM, J. H., JEON, D. H. 2006. A comprehensive micro-scale model for transport and reaction in intermediate temperature solid oxide fuel cells, *Electrochimica Acta*, 51, 3446.

NASRALLAH, M. M., DOUGLASS, D. L. 1974. *Journal of The Electrochemical Society*, 121, 255.

NECHACHE, A., CASSIR, M., RINGUEDE, A. 2014. Solid oxide electrolysis cell analysis by means of electrochemical impedance spectroscopy: A review, *Journal of Power Sources,* 258, 164.

NELSON, G. J., CASSENTI, B. N., PERACCHIO, A. A., CHIU, W. K. S. 2012. Two-dimensional charge transfer and space charge effects in exteneded surface solid oxide fuel cell electrodes, *Journal of Power Sources*, 205, 48.

NELSON, G. J., PERACCHIO, A. A., CHIU, W. K. S. 2011. Analytical investigations of varying cross section microstructures on charge transfer in solid oxide fuel cell electrodes, *Journal of Power Sources*, 196, 4695.

NERNST, W. 1899. Ueber die Elektrolytische Leitung Fester Koerper bei sehr Hohen Temperaturen. *Zeitschrift fuer Elektrochemie*, 6, 41.

NERNST, W. 1899. Ueber Wasserstoffentwicklung. *Zeitschrift fuer Elektrochemie*, 6, 37.

NERNST, W. 1889. *Zeitscrift fuer physikalische Chemie, Stoechiometrie und Verwandtschaftslehre*, 4, 129.

NI, M. 2010. Modeling of a solid oxide electrolysis cell for carbon dioxide electrolysis, *Chemical Engineering Journal*, 164, 246.

NI, M. 2012. 2D thermal modeling of solid oxide electrolyzer cell (SOEC) for syngas production by H_2O/CO_2 co-electrolysis, *International Journal of Hydrogen Production*, 37, 6389.

NI, M. 2012. An electrochemical model for syngas production by co-electrolysis of H_2O

and CO_2, *Journal of Power Sources*, 202, 209.

NI, M., LEUNG, M. K. H., LEUNG, D. Y. C. 2006. A modeling study on concentration overpotentials of a reveresible solid oxide fuel cell, *Journal of Power Sources*, 163, 460.

NI, M., LEUNG, M. K. H., LEUNG, D. Y. C. 2006. An Electrochemical Model of a Solid Oxide Steam Electrolyzer for Hydrogen Production, *Chemical Engineering and Technology*, 29, 636.

NI, M., LEUNG, M. K. H., LEUNG, D. Y. C. 2007. Energy and exergy analysis of hydrogen production by solid oxide steam electrolyzer plant, *International Journal of Hydrogen Energy*, 32, 4648.

NI, M., LEUNG, M. K. H., LEUNG, D. Y. C. 2007. Mathematical modeling of the soupled transport and electrochemical reactions in solid oxide steam electrolyzer for hydrogen production, *Electrochimica Acta*, 52, 6707.

NI, M., LEUNG, M. K. H., LEUNG, D. Y. C. 2007. Micro-scale modelling of solid oxide fuel cells with micro-structurally graded electrodes, *Journal of Power Sources*, 168, 369.

NI, M., LEUNG, M. K. H., LEUNG, D. Y. C. 2007. Parametric study of solid oxide fuel cell performance, *Energy Conversion and Management*, 48, 1525.

NI, M., LEUNG, M. K. H., LEUNG, D. Y. C. 2007. Parametric study of solid oxide steam electrolyzer for hydrogen production, *International Journal of Hydrogen Production*, 32, 2305.

NI, M., LEUNG, M. K. H., LEUNG, D. Y. C. 2008. Technological development of hydrogen production by solid oxide electrolyzer cell (SOEC), *International Journal of Hydrogen Energy*, 33, 2337.

NICHOLSON, W. & CARLISLE, A. 1800. Account of the new electrical or galvanic aparatus of Sig. Alex. Volta, and experiments performed with the same *Nicholson's Journal of Natural Philosophy, Chemistry and the Arts*, 4, 179.

NIELSEN, J., HJELM, J. 2014. Impedance of SOFC electrodes: A review and a comprehensive case study on the impedance of LSM:YSZ cathodes, *Electrochimica Acta*, 115, 31.

NOREN, D. A., HOFFMAN, M. A. 2005. Clarifying the Butler-Volmer equation and related approximations for calculating activation losses in solid oxide fuel cell models, *Journal of Power Sources*, 152, 175.

NOVAK, S., MADON, R. J., SUHL, H. 1981. *The Journal of Chemical Physics*, 74,

6083.

O'BRIEN, J. E., MCKELLAR, M. G., STOOTS, C. M., HERRING, J. S., HAWKES, G. L. 2009. Parametric study of large-scale production of syngas via high-temeprature co-electrolysis, *International Journal of Hydrogen Energy,* 34, 4216.

O'BRIEN, J. E., STOOTS, C. M., HAWKES, G. L. 2005. Comparison of a One-Dimensional Model of a High-Temperature Solid-Oxide Electrolysis Stack with CFD and Experimental Results, *2005 ASME International Mechanical Engineering Congress and Exposition,* USA, 2005.

OHYA, H., FUN, J., KAWAMURA, A., ITOH, K., OHASHI, H., AIHARA, M., TANISHO, S., NEGISHI, Y. 1997. *Journal of Membrane Science,* 131, 237.

OOSTERKAMP, P. F., GOORSE, A. A., BLOMEN, L. J. M. M. 1993. Review of an energy and exergy analysis of a fuel cell system, *Journal of Power Sources*, 41, 239.

PARK, J. –H., BLUMENTHAL, R. N. 1989. *Journal of The Electrochimical Society*, 136, 2867.

PATTERSON, J. W., BOGERN, E. C., RAPP, R. A. 1971. *Journal of The Electrochemical Society,* 19, 229.

PATYK, A., BACHMANN, T. M., BRISSE, A. 2013. Life cycle assessment of H_2 generation with high temeprature electrolysis, *International Journal of Hydrogen Energy*, 38, 3865.

PATZLAFF, J., LIU, Y., GRAFFMANN, C., GAUBE, J. 2002. *Catalysis Today,* 71, 381.

PENNER, S. S., APPLEBY, A. J., BAKER, B. S., BATES, J. L., BUSS, L. B., DOLLARD, W. J. 1995. Commercialization of fuel cells, *Energy*, 20, 331.

PERDIKARIS, N., PANAPOULOS, K. D., HOFMANN, P., SPYRAKIS, S., KAKRAS, E. 2010. Design and exergetic analysis of a novel carbon free tri-generation system for hydrogen, power and heat production from natural gas, based on combined solid oxide fuel and electrolyser cells, *International Journal of Hydrogen Energy*, 35, 2446.

PETERS, R., DEJA, R., BLUM, L., PENNANEN, J., KIVIAHO, J., HAKALA, T. 2013. Analysis of solid oxide fuel cell system concepts with anode recycling, *International Journal of Hydrogen Energy,* 38, 6809.

PETIPAS, F., BIRSSE, A., BOUALLOU, C. 2013. Model-based behaviour of a high temeprature electrolyser system operated at various loads, *Journal of Power Sources,* 239, 584.

PETIPAS, F., BIRSSE, A., BOUALLOU, C. 2014. Beneits of external heat sources for high temeprature electrolyser systems, *Intenrational Journal of Hydrogen Enenrgy,* 39, 5505.

PHAM, A. Q., GLASS, R. S. 1998. *Electrochimica Acta,* 43, 2699.

PIETROWSKI, M. J., DE SOUZA, R. A., FARTMANN, M., TER VEEN, R., MARTIN, M. 2013. *Fuel Cells,* 13, 673.

POUR, A. N., KHODABANDEH, H., IZADYAR, M., HOUSAINDOKHT, M. R. 2014. *Reaction Kinetics, Mechanisms and Catalysis*, 111, 29.

PRIMDAHL, S., MOGENSEN, M. 1997. Oxidation of hydrogen on Ni/Yttria-Stabilized Zircona Cermet Anodes, *Journal of The Electrochemical Society*, 144, 3409.

RADOS, N., AL-DAHHAN, M. H., DUDUKOVIC, M. P. 2003. *Catalysis Today,* 79-80. 211.

RASHKEEV, S. N., GLAZOFF, M. V. 2012. Atomic-scale mechanisms of oxygen electrode delamination in solid oxide electrolyzer cells, *International Journal of Hydrogen Energy*, 37, 1280.

RIDJAN, I., VAN MATHIESEN, B., CONNOLLY, D. 2014. Synthetic fuel production costs by means of solid oxide electrolysis cells, *Energy*, doi: 10.1016/j.energy.2014.04.002

RIDJAN, I., VAN MATHIESEN, B., CONNOLLY, D., DUIC, N. 2013. The feasibility of synthetic fuels in renewable energy systems, *Energy*, 57, 76.

ROBINSON, D. B., PENG, D. –Y. S., CHUNG, Y. –K. 1985. The Development of The Peng – Robinson Equation and its Application to Phase Equilibria in a System Conteining Methanol, *Fluid Phase Equilibria*, 24, 25.

ROSSMEISL, J., BESSLER W. G. 2008. Trends in catalytic activity for SOFC anode materials, *Solid State Ionics,* 178, 1694.

SCHEFOLD, J., BRISSE, A., ZAHID, M. 2009. *Journal of The Electrochemical Society*, 156, B897.

SCHOULER, E. J. L. 1983. Relation between solid oxide electrolyte surface properties and electrode reaction kinetics, *Solid State Ionics*, 9 & 10, 945.

SCHULZ, H. 2013. *Catalysis Today*, 214, 140.

SCHULZ, H., CLAEYS, M. 1999. *Applied Catalysis A: General*, 186, 91.

SEHESTED, J., DAHL, S., JACOBSEN, J., ROSTRUP-NIELSEN, J. R. 2005. *Journal of Physical Chemistry B*, 109, 2432.

SHI, J., XUE, X. 2011. Inverse approach to quantify multi-physicochemical properties of porous electrodes for solid oxide fuel cells, *Electrochimica Acta*, 56, 8718.

SHI, Y., LI, C., CAI, N. 2011. Experimental characterization and mechanistic modeling of carbon monoxide fueled solid oxide fuel cell, *Journal of Power Sources*, 196, 5526.

SHI, Y., LUO, Y., CAI, N., QIAN, J., WANG, S., LI, W., WANG, H. 2013. Experimental characterisation and modeling of the electrochemical reduction of CO_2 in solid oxide electrolysis cells, *Electrochimica Acta*, 88, 644.

SHISHKIN, M., ZIEGLER, T. 2008. The Oxidation of H_2 and CH_4 on an Oxygen-Enriched Yttria-Stabilized Zirconia Surface: A Theoretical Study Based on Density Functional Theory, *Journal of Physical Chemistry C*, 112, 19662.

SHISHKIN, M., ZIEGLER, T. 2009. Oxidation of H_2, CH_4 and CO Molecules at the Interface between Nickel and Yttria-Stabilized Zirconia: A Theoretical Study Base on DFT, *Journal of Physical Chemistry C*, 113, 21667.

SHISHKIN, M., ZIEGLER, T. 2010. Hydrogen at the Ni/Yttria-Stabiilized Zirconia Interface: A Study Based on Density Functional Theory, *Journal of Physical Chemistry C*, 114, 11209.

SHIVA, M., ATASHI, H., TABRIZI, F. F., MIRZAEI, A. A., ZARE, A. 2013. *Fuel Processing Technology*, 106, 631.

SINGH, R. K., AHMED, M. R. 2013. Blade design and performance testing of a small wind turbine rotor for low wind speed applications, *Renewable Energy*, 50, 812.

SINGHAL, S. C., KENDALL, K. 2003. High-temperature Solid Oxide Fuel Cells: Fundamentals, Design, and Applications, *Elsevier*, Amsterdam, 2003.

SONG, H. –S., RAMKRISHNA, D., TRINH, S., WRIGHT, H. 2004. *Korean Journal of Chemical Engineering*, 21, 308.

SOVACOOL, B. K. 2009. The intermittency of wind, solar, and renewable electricity generators: Technical barrier or rhetorical excuse?, *Utilities Policy*, 17, 288.

SPACIL, H. S., TEDMON JR, C. S. 1969, Electrochemical Dissociation of Water Vapor in Solid Oxide Electrolyte Cells. I. Thermodynamics and Cell Characteristics, *Journal of the Electrochemical Society*, 116, 1618.

SRIDHAR, K. R., BLANCHARD, J. A. 1999. *Sensors and Actuators B*, 59, 60.

SRIDHAR, K. R., IACOMINI, C. S., FINN, J. E. 2004. Combined H_2O/CO_2 Solid Oxide Electrolysis for Mars In Situ Resurce Utilization, *Journal of Propulsion and Power*, 20, 892.

STEINBERG, M., DANG, V. –D. 1977. *Energy Conversion*, 17, 97.

STEMPIEN, J. P., DING, O. L., SUN, Q., CHAN, S. H. 2012. *International Journal of Hydrogen Energy*, 37, 14518.

STEMPIEN, J. P., LIU, Q., NI, M., SUN, Q., CHAN, S. H. 2014. *Electrochimica Acta*, 147, 490.

STEMPIEN, J. P., SUN, Q., CHAN, S. H. 2013. *Energy*, 55, 647.

STEMPIEN, J. P., SUN, Q., CHAN, S. H. 2013. Solid Oxide Electrolyzer Cell Modeling: A Review, *Journal of Power Technologies*, 93, 216.

STEMPIEN, J. P., SUN, Q., CHAN, S. H. 2014. *Electrochimica Acta*, 130, 718.

STOOTS, C. M., O'BRIEN, J. E., HERRING, J. S., HARTVIGSEN, J. J. 2009. Syngas Production via High-Temeprature Coelectrolysis of Steam and Carbon Dioixde, *Journal of Fuel Cell Science and Technology*, 6, 011014-1.

STORSAETER, S., CHEN, D., HOLMEN, A. 2006. *Surface Science*, 600, 2051.

SUKESHINI, A. M., HABIBZADEH, B., BECKER, B. P., STOLTZ, C. A., EICHHORN, B. W., JACKSON G. S. 2006. Eectrochemical Oxidation of H_2, CO, and CO/H_2 Mixtures on Patterned Ni Anodes on YSZ Electrolytes, *Journal of the Electrochemical Society*, 153, A705.

SUNDE, S. 1997. Calculations of impedance of composite anodes for solid oxide fuel cells, *Electrochimica Acta*, 42, 2637.

SUNDE, S. 2000. Simulations of Composite Electrodes in Fuel Cells, *Journal of Electroceramics*, 5, 153.

SUWANWARANGKUL, R., CROISET, E., FOWLER, M. W., DOUGLAS, P. L., ENTCHEV, E., DOUGLAS, M. A. 2003. Performance comaprison on Fick's, dusty-gas and Stefan-Maxwell models to predict the concentration overpotential of a SOFC anode, *Journal of Power Sources*, 122, 9.

SYNODIS, M. J., PORTER, C. L., VO, N. M., RESZKA, A. J. L., GROSS, M. D., SNYDER, R. C. 2013. A model to predict percolation threshold and effective conductivity of infiltrated electrodes for solid oxide fuel cells, *Journal of The Electrochemical Society,* 160, F1216.

TENG, B. –T., CHANG, J., ZHANG, C. –H., CAO, D. –B., YANG, J., LIU, Y., GUO, X. –H., XIANG, H. –W., LI, Y. –W. 2006. *Applied Catalysis A: General*, 301, 39.

TIAN, Y., ZHAO, C. Y. 2013. A review of solar collectors and thermal energy storage in solar thermal applications, *Applied Energy*, 104, 538.

TIANG, K. J. 2012. Keynote at the Off-Shore Renewable Energy Conference, Singapore.

TRASATTI, S. 1974. The concept of absolute electrode potential an attempt at a calculation, *Electroanalytical Chemistry and Interfacial Electrochemistry*, 52, 313.

TRASATTI, S. 1982. The concept and physical meaning of absolute electrode potential. A reassessment, *Journal of Electroanalytical Chemistry*, 139, 1.

TRASATTI, S. 1986. The absolute electrode potential: An explenatory Note, *Pure & Applied Chemistry*, 58, 955.

TRASATTI, S. 1990. The absolute electrode potential – the end of story, *Electrochimica Acta*, 35, 269.

TSATSARONIS, B., KAPANKE, K., MARIGORTA, A. M. B. 2008. Exergoeconomic estimates for a novel zero-emission process generating hydrogen and electric power. *Energy*, 33, 321.

TURNER, J. A. 2004. *Science, 305, 972.*

UDAGAWA, J., AGUIAR, P., BRANDON, N. P. 2007. Hydrogen production throug steam electrolysis: Model-based steady state performance of a cathode-supported intermediate temeprature solid oxide electrolysis cell, *Journal of Power Sources,* 166, 127.

UDAGAWA, J., AGUIAR, P., BRANDON, N. P. 2008. Hydrogen production through steam electrolysis: Control strategies for a cathode-supported intermediate temeprature solid oxide electrolysis cell, *Journal of Power Sources*, 180, 354.

UDAGAWA, J., AGUIAR, P., BRANDON, N. P. 2008. Hydrogen production through steam electrolysis: Model-based dynamic behaviour of a cathode-supported intermediate temeprature solid oxide electrolysis cell, *Journal of Power Sources,* 180, 46.

UHM, S., KIM, Y. D. 2014, Electrochemical conversion of carbon dioxide in a solid oxide electrolysis cell, *Current Applied Physics*, 14, 672.

USSEGLIO-VIRETTA, F., LAURENCIN, J., DELETTE, G., VILLANOVA, J., CLOETENS, P., LEGUILLON, D. 2014. Quantitive microstructure characterization of a Ni-YSZ bi-layer coupled with simulated electrode polarisation, *Journal of Power Sources,* 256, 394.

VAN DER LAAM, G. P. 1999. Kinetics, Selectivity and Scale Up of the Fischer-Tropsch Synthesis, PhD Thesis, University of Groningen.

VAN DER LAAN, G. P., BEENACKERS, A. A. C. M. 1999. *Industrial and Engineering*

Chemistry Research, 38, 1277.

VAN DER LAAN, G. P., BEENACKERS, A. A. C. M. 2000. *Applied Catalysis A: General*, 193, 39.

VAN VILET, O. P. R., FAAIJ, A. P. C., TURKENBURG, W. C. 2009. *Energy Conversion and Management*, 50, 855.

VAN ZEGHBROECK, B. 2011. Principles of Semiconductor Devices, *published online*, ch 2.7.

VEST, R. W., TALLAN, N. M., TRIPP, W. C. 1964. *Journal of The American Ceramic Society*, 47, 635.

VIRKAR, A. V. 2007. A model for solid oxide fuel cell (SOFC) stack degradation, *Journal of Power Sources*, 172, 713.

VIRKAR, A. V. 2010. Mechanism of oxygen electrode delamination in solid oxide electrolyzer cells, *International Journal of Hydrogen Energy*, 35, 9527.

VIRKAR, A. V., LIM, H. –T., TAO, G. 2014. Failure of solid oxide fuel cells by electrochemically induced pressure, *Procedia IUTAM*, 10, 328.

VISCONTI, C. G., TRONCONI, E., LIETTI, L., ZENNARO, R., FORZATTI, P. 2007. *Chemical Engineering Science*, 62, 5338.

VOGLER, M., BESSLER, W. G. 2009. The Role of Interstitial Hydrogen Species in Ni/YSZ Patterned Anodes: A 2D Modeling Study, *ECS Transactions*, 25, 1957.

VOGLER, M., BIEBERLE-HUETTER, A., GAUCKLER, L., WARNATZ, J., BESSLER, W. G. 2009. Modelling Study of Surface Reactions, Diffusion, and Spillover at a Ni/YSZ Patterned Anode, *Journal of the Electrochemical Society*, 156, B663.

WACHSMAN, E. D., JAYAWEERA, P. 2001. in : WACHSMAN, E. D., WEPPNER, W., TRAVERSA, E., LIU, M., VANYSEK, P., YAMAZOE, N. (Eds), Solid State Ionic Devices II – Ceramic Sensors, *The Electrochemical Society Proceedings Series*, Pennington, NJ, 298.

WACHSMAN, E. D., MARLOWE, C. A., LEE, K. T. 2012. *Energy and Environemntal Science*, 5, 5498.

WAGNER, C. 1933. *Zeitschrift fuer physicalische chemie B*, 21, 25.

WANG, Y. –N., MA, W. –P., LU, Y. –J., YANG, J., XU, Y, -Y., XIANG, H. –W., LI, Y, -W., ZHAO, Y. –L., ZHANG, B. –J. 2003.*Fuel*, 82, 195.

WANG, Y. –N., XU, Y. –Y., LI, Y. –W., ZHAO, Y. –L., ZHANG, B. –J. 2003. *Chemical Engineering Science*, 58, 867.

WANG, Y., FAN, W., LIU, Y., ZENG, Z., HAO, X., CHANG, M., ZHANG, C., XU, Y., XIANG, H., LI, Y. 2008. *Chemical Engineering and Processing,* 47, 222.

WEISSBART, J., RUKA, R. 1962. A Solid Electrolyte Fuel Cell. *Journal of The Electrochemical Society*, 109, 723.

WEISSBART, J., SMART, W. H. 1967. Study of Electrolytic Dissociation of CO_2-H_2O Using a Solid Oxide Electrolyte, *NASA contractor report CR-680*, Report for NASA research centre.

WEPPNER, W. 1977. *Journal of Electroanalytical Chemistry*, 84, 339.

WILLIFORD, R. E., CHICK, L. A. 2003. Surface diffusion and concentration polarization on oxide-supported metal electrocatalyst particles, *Surface Science*, 547, 421.

WINDFINDER.COM, Real time wind & weather report: Singapore Changi, *available from: www.windfinder.com/report/wind/singapore_changi/.*

WORLD BANK, CO_2 Emissions (kt) – 2014 Edition.

WORLD BANK, Gender Statistics – 2014 Edition.

XIE, K., ZHANG, Y., MENG, G., IRVINE, J. T. S. 2011. *Energy and Environemntal Science*, 4, 2218.

XIE, Y., XUE, X. 2012. Modeling of solid electrolysis cell for syngas generation with detailed surface chemistry, *Solid State Ionics*, 224, 64.

XIE, Y., XUE, X. 2012. Multi-scale electrochemcial reaction anode model for solid oxide fuel cells, *Journal of Power Sources*, 209, 81.

XU, J., FROMENT, G. F. 1989. *ALChE Journal*, 35, 88.

YAO, W., CROISET, E. 2014. Modelling and Ni/Yttria-Stabilized-Zirconia pattern anode experimenal validation of a new charge transfer reaction mechanism for hydrogen electrochemical oxidation on solid oxide fuel cell anodes, *Journal of Power Sources*, 248, 777.

YU, G. –W., XU, Y. –Y., HAO, X., LI, Y. –W., LIU, G. –Q. 2010. *Fuel,* 89, 1070.

YUAN, D., KROEGER, F. A.1969. *Journal of The Electrochemical Society*, 116, 594.

YURKIV, V., GORSKI, A., BESSLER, W.G., VOLPP, H. –R. 2012. Density functional theory study of heterogenous CO oxidation over an oxygen-enriched yttria-stabilized zirconia surface, *Chemical Physics Letters*, 543, 213.

YURKIV, V., STARUKHIN, D., VOLPP, H.-R., BESSLER, W. G. 2011. Elementary Reaction Kinetics of the CO/CO_2/Ni/YSZ Electrode, *Journal of the Electrochemcial Society*, 158, B5.

YURKIV, V., UTZ, A., WEBER, A., IVERS-TIFFEE, E., VOLPP, H. –R., BESSLER W. G. 2012. Elementary kinetic modeling and experimental validation of electrochemical CO oxidation on Ni/YSZ pattern anodes, *Electrochimica Acta*, 59, 573.

ZHAN, Z., KOBSIRIPHAT, W., WILSON, J. R., PILLAI, M., KIM, I., BARNETT, S. A. 2009. *Energy and Fuels*, 23, 3089.

ZHANG, C., JUN, K. –W., HA, K. –S., LEE, Y. –J., KANG, S. C. 2014. *Environmental Science and Technology,* dx.doi.org/10.1021/es501021u.

ZHANG, H., SU, S., CHEN, X., LIN, G., CHEN, J. 2013. Configuration design and performance optimum analysis of a solar-driven high temperature steam electrolysis system for hydrogen production, *International Journal of Hydrogen Energy,* 38, 4298.

ZHANG, H., WANG, J., SU, S., CHEN, J. 2013. Electrochemical performance characteristics and optimum design strategies of a solid oxide electrolysis cell system for carbon dioxide reduction, *International Journal of Hydrogen Energy,* 38, 9609.

ZHU, H., KEE, R. J. 2003. A general mathematical model for analyzing the performance of fuel-cell membrane-electrode assemblies, *Journal of Power Sources*, 117, 61.

ZHU, H., KEE, R. J. 2006. Modeling Electrochemical Impedance Spectra in SOFC Button Cells with Internal Methane Reforming, *Journal of The Electrochemical Society,* 153, A1765.

ZHU, H., KEE, R. J., JANARDHANAN, V. M., DEUTSCHMANN, O., GOODWIN, D. G. 2005. Modeling Elementary Heterogenous Chemistry and Electrochemistry in Solid-Oxide Fuel Cells, *Journal of The Electrochemical Society*, 152, A2427.

ZHU, H., KROMP, A., LEONIDE, A., IVERS-TIFFEE, E., DEUTSCHMANN, O., KEE, R. J. 2012. A Model-Based Interpretation of the Influence of Anode Surface Chemistry on Solid Oxide Fuel Cell Electrochemical Impedence Spectra, *Journal of The Electrochemcial Society*, 159, F255.

ZIMMERMAN, W., BUKUR, D., LEDAKOWICZ, S. 1992. *Chemical Engineering Science*, 47, 2707.